THE UNIVERSITY OF LIVERPOOL

DEPARTMENT OF ELECTRICAL ENGINEERING AND ELECTRONICS

COMPUTER AIDED ANALYSIS, MODELLING AND EXPERIMENTAL ASSESSMENT OF PERMANENT MAGNET SYNCHRONOUS MACHINES WITH RARE EARTH MAGNETS

by

Farid B. Chaaban

Thesis submitted in accordance with the requirements of the University of Liverpool for the degree of

Doctor in Philosophy

June 1989

ABSTRACT

The work presented in this thesis concentrates on the computer aided analysis, modelling, and experimental assessment of permanent magnet synchronous machines which utilise a newly developed high- energy neodymium iron boron magnet for their field excitation.

This work can be divided into two main parts. In the first part trends and development of CAD techniques are highlighted and computer packages used in the work are briefly described. Properties and characteristics of the new neodymium magnets relative to the other available types are investigated. In order to assess the advantages of these magnets, the performance of a high- field machine using ferrites, samarium cobalt, and neodymium magnets are compared. In addition a prototype machine with skewed magnets and canned rotor is described.

The second part considers an accurate equivalent circuit model for a rare earth permanent magnet machine. For this purpose the equivalent circuit parameters such as leakage and synchronous reactance, winding resistance, and core loss are determined using both computational and experimental methods. The proposed model is shown to give a good prediction of the machine performance. The sensitivity of each of the machine parameters on the model accuracy is also tested.

ACKNOWLEDGEMENT

I wish to express my thanks and sincere gratitude to everyone who contributed in making this thesis possible particularly:

- My Supervisor, Prof. K. J. Binns, for his continuous encouragement, advice, and ideas during the course of this research.

- Dr. P. H. Mellor, Co- supervisor, for his invaluable guidance and useful suggestions at every stage of the work.

- The staff in the Department of Electrical Engineering and Electronics in particular the Machine Group for their useful comments and helpful discussion.

- The technical staff in the electrical workshop and machine laboratory who were always of great assistance.

- The Hariri Foundation, represented by their London Coordinator Miss Mona Knio, for their sponsorship to this work and their moral support.

- Finally, all my friends and colleagues in and outside the department for making my time in Liverpool enjoyable. I can not mention them all individually, but I hope they will accept this acknowledgement.

to my beloved family

TABLE OF CONTENTS

LIST OF PRINCIPAL SYMBOLS

Symbol	Description	Unit
A	magnetic vector potential	A
B	magnetic flux density	T
B_r	residual flux density	T
d	diameter	mm
E	electro- motive force	V
F_t	tangential electromagnetic stress	N
f	frequency	Hz
g	air gap width	mm
H	magnetic field intensity	A/m
H_c	coercivity	A/m
I	electric current	A
J	current density	A/m^2
j	operator	-
K_d	distribution factor	-
K_p	pitch factor	-
K_{sk}	skewing factor	-
K_{st}	stacking factor	-
L	inductance	H
l	length	mm
M_a	armature mmf	A
N	conductors per slot	-
P	power	W
p	pole pairs	-
r	radius	mm

R	electric resistance	Ω
T	torque	N.m
T_C	Curie temperature	°c
t	time	sec
V	voltage	V
W	energy	W
Z	impedance	Ω
X_S	synchronous reactance	Ω
τ	pole pitch	deg.
δ	load angle	deg.
θ	power factor angle	deg.
α	skewing angle	deg.
ω	speed of rotation	rpm

Subscripts

d	direct- axis component
q	quadrature- axis component
i	internal value

CHAPTER ONE

INTRODUCTION

1.1 Introduction

1.2 Advantages of permanent magnet machines

1.3 Development of computer- aided design

1.4 Effects of computers on the manufacturing process

1.5 Scope of the work

Figures 1.1 - 1.2

CHAPTER ONE

INTRODUCTION

1.1 Introduction

The development of permanent magnet (PM) synchronous machines with line- starting capability or inverter-driven has gained a great momentum in the last decade. Machines with permanent magnet excitation have established an important role in many applications including machine tool drives used in textile and glass industries, electro-mechanical propulsion in electric vehicles and recently in robotics and computer drives. The various configurations of permanent magnet machines can be classified according to the method of commutation (brushed or brushless), stator design (slotted or slotless), type of magnetic material (ceramic, ferrite, or rare earth), and the positioning of the magnets (interior , peripheral, etc..). Permanent magnet motors for use with constant-frequency supplies require a cage bar winding for self-starting as well as for other purposes. On the other hand an inverter- driven motor with a shaft- position sensor may not need the cage bar since it is expected to be always in synchronism.

This development in permanent magnet machines has gained a greater potential in the eighties due to two major factors:

1- The recent announcement of neodymium iron boron magnets (NdFeB), a cobalt- free magnetic material which has excellent magnetic properties and a higher energy product than the presently available rare- earth cobalt, but at much lower cost.

2- The rapid development in Computer- Aided Analysis (CAA) software including packages and programs that solve the electromagnetic fields using numerical methods like finite element and finite difference method, (1,2,8). This advanced technology allows new variants and concepts of permanent magnet machines to be developed. A preview of this technology and its impact on machine design and production is described later in this introductory section.

1.2 Advantages of permanent magnet machines

PM machines have attractive operating characteristics which are not easily achievable for induction motors or for synchronous machines with a field winding using the same frame size, (3,4,14). Some of these characteristics are:

a- From the view points of energy requirements and cost, the assessment of magnetic material for field excitation is particularly economical since it leads to volume reduction of 40% for ferrite magnets and up to 75% when powerful rare- earth magnets are employed. An illustration of the volume reduction is shown in Fig.1.1. Also with reduced volume the rotor acceleration at a given power is increased.

b- There is no rotor copper loss due to the slip as in induction motors nor is there a field winding as found in conventional synchronous machines. This enhances the thermal capability thus giving a more efficient and more reliable machine.

c- Whereas the reluctance motor derives its excitation from the supply thus giving relatively low power factor, the high- field excitation provided by the magnets enables the machine to operate at a power factor close to unity, or at leading power factor.

d- Possibility of precise synchronous operation regardless of the supply voltage and load variations.

e- Smooth brushless operation especially at high speeds with easy maintenance.

1.3 Development of computer- aided design

Computer- aided design is barely 20 years old, yet in recent years it is transforming the working practices of designers in many industries specially in electrical engineering and electronics and has become a huge world-wide industry in itself. Its single historical origin is believed to be the revolutionary system SKETCHPAD developed at the Massachusetts Institute of Technology (MIT) in 1962. This system had for the first time graphical interaction with the computer, via the medium of display screen and light pen. It was limited to two- dimensional modelling but later three- dimensional models were created so they could be displayed from different viewpoints. The logical next step was to link the CAD of a component di-

rectly to its manufacture in what has become known as CADCAM (Computer- Aided Design and Computer- Aided manufacture). The latest step was the development of a great variety of separate computer programs or packages for carrying out the analyses of the device by testing its performance and modifying its parameters according to the results of these tests. Hence these programs could be referred to as Computer- Aided Analysis (CAA). Also the development of interactive computer display technology has made possible the computer- aided draughting system which is now one of the most widespread uses of computers in design. These computer based draughting packages use an interactive display terminal and a plotter to replace the drawing board. Some of these packages are used throughout this work and are discussed in detail later in this thesis.

Because of the high cost of computers in the 1960's the first commercial users of CAD/CAA were the big car and aerospace companies and large electronics firms. In the 1970's this technique expanded into many other applications with the rapid decrease in expense and increase in processing power of the computer equipment. Nowadays new graphic packages can make an ordinary personal computer outperform dedicated workstations and microcomputers, at a fraction of the cost, (6,7,10). Moreover, new ideas are being developed to prepare the new generation of CADCAM that will make it a more effective tool for present users and more attractive to new comers. Recently new "sizing

software" packages are being reported, (8,9). These packages appear to go beyond the simple analysis and assist the designer in the choice of the optimum design parameters.

1.4 Effect of computers on the manufacturing process.

The graph in Fig.1.2 represents the variation of the cost- effectiveness with each of the three main phases of the design and manufacturing process,i.e. the design, the production and the maintenance phase.

In the old traditional procedure, before the utilisation of computers, an engineering designer and in particular one involved in machines would create a new machine design according to certain theoretical requirements of its performance. Often a new design may in fact be only a modification of an existing one. The production phase that follows may become extremely expensive because it is often necessary to build, test, and modify the device before it finally matches the requirements. This sometimes may lead to scrapping the whole prototype and building a new one. The optimum design is the one that would satisfy a whole array of requirements and constraints. Once the new machine is built the cost- effectiveness will drop to cover the maintenance of this machine during its economical life cycle.

After the involvement of computers in the machine design the curve of the cost- effectiveness has changed very

significantly. The peak of the cost is concentrated in the design phase where besides the usual theoretical calculations a lot of computing time is required. Using the suitable package the designer is now able to test his device analytically and to make modifications even without constructing it. The advent of computer packages allows the construction of more complex analytical models. Devices are simulated and evaluated at a much more refined design stage thereby moving the requirement for device construction even further along the design path. Once the optimum design is obtained the prototype is built in the production phase where the expenses will be lower. The maintenance of the new machine or device will be lower than that of the old procedure because all the parameters are chosen carefully to make the machine operate at optimum conditions. Special care is given to these parts of the machine that will be under any kind of stress. Good thermal design for example improves the reliability of electrical and electronic equipment and significantly reduces life- cycle cost, (6).

1.5 Scope of the work

The aim of the work presented in this thesis is the analysis, modelling, and experimental assessment of rare earth permanent magnet synchronous machines. Effects of the magnetic material as well as different design aspects on the machine performance are discussed. The modelling is based on the determination of the machine parameters and the inclusion of the core loss in the equivalent cir-

cuit. It should be emphasised that throughout this work experimental measurements are subsequently confirmed by computational results and vice versa.

The characteristics of permanent magnets are discussed in Chapter two with special emphasis on the properties of the new NdFeB magnetic material. A review of the techniques for improving its thermal properties is also discussed.

Chapter three is devoted to the description of the finite element programs that are used in this work. The accurate computation of the synchronous torque using different methods is also discussed. In addition two computer graphic systems are also described which are used in the building of solid models of different machines.

Chapter four consists of two parts. In the first part a comparison of the synchronous performance of a permanent magnet machine with different magnetic material is provided. Tests at different supply frequencies and different operating conditions are carried out. In the second part the characteristics of the machine with interior (buried) magnets are compared to those having the magnets mounted on the periphery of the rotor core.

In Chapter five a novel design of a six- pole rotor with NdFeB magnets is discussed. The aspects of a number of new design parameters, such as skewing the magnets and canning the rotor, and their effects on the machine performance are investigated.

Chapter six is concerned with the determination of the machine parameters. New methods are proposed to find the equivalent circuit elements both experimentally and by finite element analysis. In both cases the effect of saturation is taken into consideration. The discussion also involves the analysis and calculation of losses in high-field machines.

The machine equivalent circuit parameters, as determined in Chapter six, are used in Chapter seven to develop a mathematical model for a high- field PM machine. This model is derived from a modified phasor diagram in which the core loss is represented and its effect on the machine performance has been considered.

Finally, in Chapter eight, promising applications of PM machines with high- energy magnets are previewed. The discussions and conclusions of the thesis are drawn together. In particular the details of the design aspects and the accurate modelling of the machine which is being developed are highlighted. Suggestions for further research are also presented.

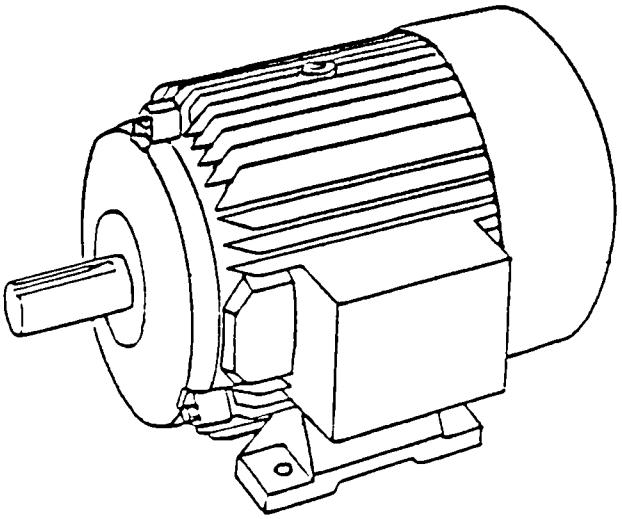

a.

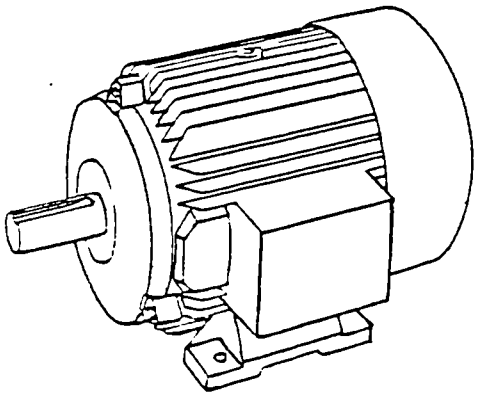

b.

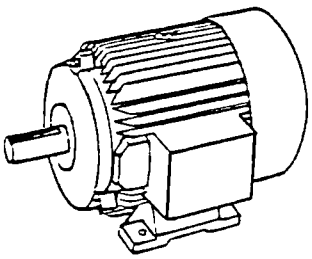

c.

a... conventional synchronous machine
b... PM machine with ferrite magnets
c... PM machine with rare earth magnets

Fig.1.1 Illustration of the approximate volume reduction of machine caused by utilisation of magnets for field excitation.

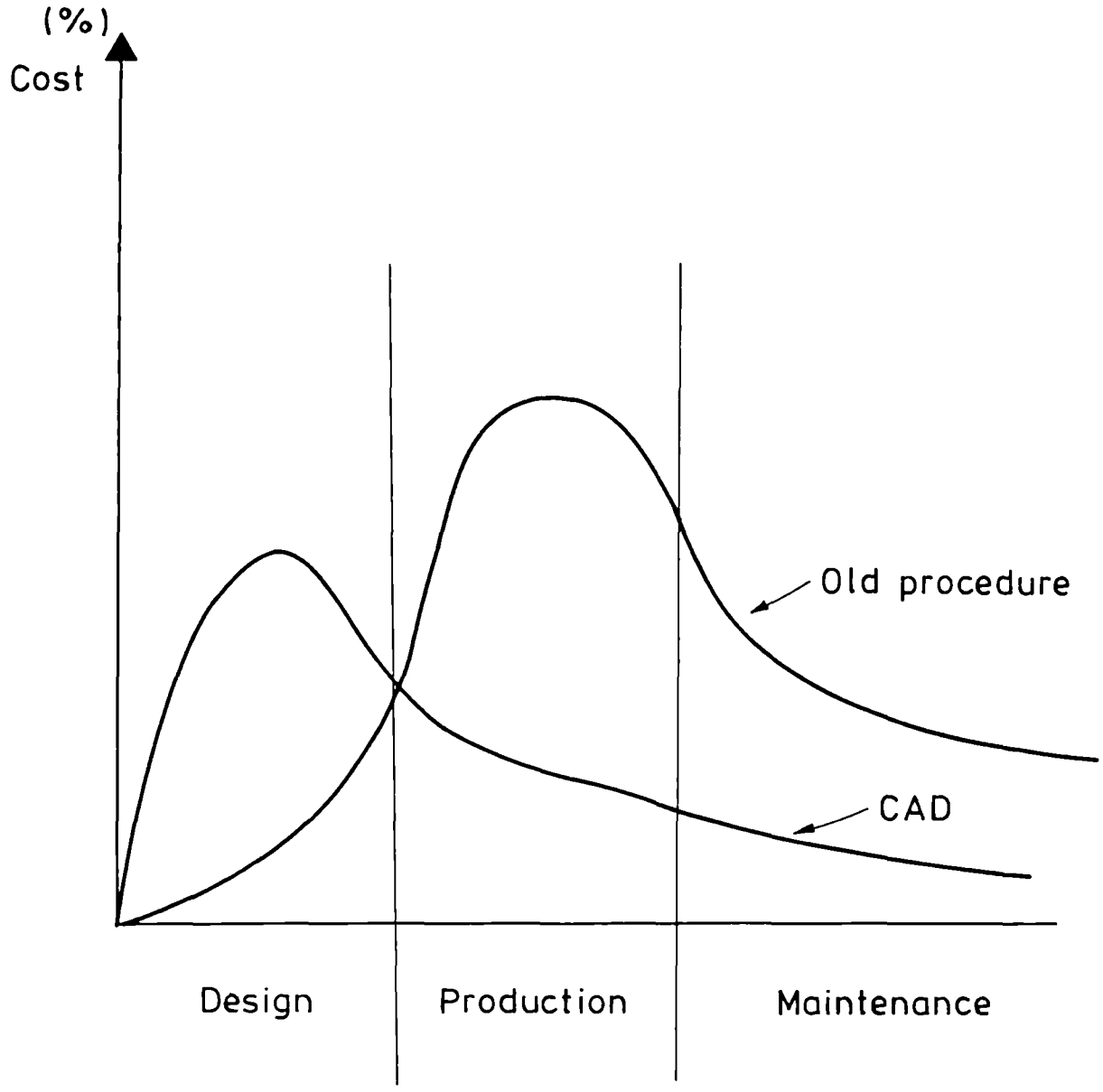

Fig.1.2 Effect of CAD on the cost- effectiveness of the manufacturing process.

CHAPTER TWO

PHYSICAL AND MAGNETIC PROPERTIES OF A NEW FAMILY OF NON- COBALT RARE EARTH MAGNETIC MATERIALS.

CHAPTER TWO

PHYSICAL AND MAGNETIC PROPERTIES OF A NEW FAMILY OF NON- COBALT RARE EARTH MAGNETIC MATERIALS.

2.1 Introduction

Developments in permanent magnets have taken place in quantum steps with the introduction of rare earth magnetic materials which are defined as a group of materials containing a magnetically active rare earth transition metal like samarium. The advances in the development of these magnetic materials, and the requirements for high- efficiency machines have aroused widespread interest in the utilisation of these magnets in a.c and d.c drives. It was demonstrably clear that the rare earth magnets could be used to up- rate conventional drives including those using induction and reluctance motors. Some motor designs with rare earth magnets (14,15) produce up to 50% more torque than other drives having comparable dimensions. However, despite their promise, the cost of these magnets has been found to be too high for large- scale applications. In the late 70's a cobalt crisis took place and that led to a movement to reduce the dependance on this strategic material and to find a non- cobalt magnet with the same desirable properties, (16,20).

In 1983 two firms, Sumitomo Special Metals in Japan and Colt Crucible in the USA announced the development of sintered commercial magnets based on ferrite, neodymium, and boron with energy product up to 320 KJ/m^3. In the short interval since then many other magnet producers have developed and produced these new magnets. The cost of the neodymium iron boron (NdFeB) magnets is currently comparable with that of the samarium cobalt because of the high fabrication cost, which is about 75% of the total cost of the magnet. It is believed that the cost will go down and neodymium magnets can be produced in large volumes when demand justifies it. New techniques have been developed to produce the new magnets with a wide variety of specification (17,18,19). It is now generally recognised that these new magnets will be of great importance for a large number of applications, especially in electric machines. However, the low Curie temperature of 320°C results in a greater reversible temperature coefficient and a rapid decrease in the coercivity with increase in operating temperature. This limits the magnets operation to temperatures below 150°C. Systematic studies are being carried out to improve the thermal properties, thus producing new alloys with better thermal properties (21,22,26). When magnet material developers provide cost- effective neodymium magnets with high operating temperatures and magnet users implement appropriate motor designs, ultimate success can be assured.

2.2 Properties of permanent magnet materials

The magnetic properties of every permanent magnet material are represented by a hysteresis loop such as that shown in Fig.2.1 which gives the relationship between the magnetic flux density 'B' and the magnetising force 'H'. The ratio of B to H involves the permeability 'μ'. The hysteresis loop of each material varies according to its physical and magnetic properties. When a piece of ferromagnetic material is subjected to a magnetising field, the flux density inside the material will increase until the slope of the curve approaches the value of the permeability of free space 'μ_o' at relatively high values of H where saturation takes place, point "a" in Fig. 2.1. If the magnetising field is steadily reduced to zero the induction will not follow the original magnetisation curve but will lag behind the magnetising force and the residual flux density or remanence will remain. When a relatively strong field is applied in the opposite direction so that the flux is reduced to zero, the field strength is called the coercive force or coercivity. Further increase in the demagnetising field will eventually saturate the specimen with the magnetising direction reversed till it reaches point "b" in Fig.2.1. It should be noted that the remanence B_r and coercivity H_c, as quoted in the manufacturers catalogues, are the values obtained after the material has been driven beyond point "a" well into saturation.

In a permanent magnet, the field strength measured at the magnet surface has a direction opposite to that of the induction inside the magnet; with positive induction the field strength is negative. The operating range of the magnetic material will therefore be in the second quadrant of the hysteresis loop referred to as the demagnetisation curve. This is in contrast to electromagnets in which both the induction and magnetising force have the same direction, with their range consequently in the first quadrant. The main characteristics of this second quadrant operation are the remanence B_r, the coercivity H_c, the maximum energy product $(BH)_{max}$, and the recoil permeability of the curve as shown in Fig.2.2. These characteristics have the following features:

1- Residual flux density ' B_r ' determines the maximum flux density that the magnet can pass.

2- Coercive force ' H_c ' gives a first order measure of the magnet's resistance against demagnetisation during starting, short circuit etc...

3- The maximum energy product $(BH)_{max}$ is the indicator of the maximum stored energy in the magnet. The optimum operating point of the magnet is normally close to this value. The maximum energy product is established by plotting the product of BH for a number of points as a function of the flux density. A simpler way to locate the $(BH)_{max}$ without the necessity to plot additional curves is to draw a straight line between the point with coordinates (B_r,H_c) and the origin, this line will intersect the

demagnetisation curve at the point of maximum energy as shown in Fig.2.2.

4- Recoil permeability: Magnets working under conditions such as high opposing field (short circuit) are said to work under recoil conditions. Such phenomena occur when the magnet is subjected to a demagnetising condition showing opposing field , then the working point will follow the major loop down to point "x" as illustrated in Fig.2.2. When the demagnetising field is reduced the working point will move to "y" but along a different trajectory. Therefore varying the demagnetising force will cause the operating point to follow a minor loop. In practice this loop can be very narrow and is a straight line with a slope equal to μ_r termed the recoil permeability if the characteristic is linear. It may be shown that the recoil permeability is nearly equal to the slope of the major hysteresis loop at point B_r.

An important property of high- field permanent magnets is the linearity of the demagnetisation curve. When materials with such curves are subjected to demagnetisation field within the linear range, the recoil characteristic is nearly identical with the demagnetisation curve and there is no loss in residual magnetism. The relative permeability of such materials is very close to unity (1.05 for the rare earth magnets). Rare earth magnets generally exhibit such characteristics allowing them to be magnetised before final assembly. Ferrites and alnico magnets with non- linear characteristics are magnetised

after assembly otherwise they must be keepered to retain strength. Fig.2.3 represents the demagnetisation curves as well as the (BH) plots for different classes of magnets.

Although there exist several grades of alnico with emphasis on the remanence (alnico 8) or coercivity (alnico 5) these alloys are characterised by their high remanence and low coercivity and above all their non- linear characteristic. Their mechanical properties are inconvenient because the magnetic hardness is accompanied by extreme mechanical hardness and brittleness, (20,31). The cost of the alnicos is much less than the rare earth magnets and much more than the ferrites. Ferrite magnets, also referred to as ceramic, are generally characterised by lower remanence but higher coercivity with demagnetisation curves closer to linearity. This makes them less vulnerable to demagnetising fields and sometimes they can be magnetised before assembly. Ferrite magnets are the cheapest of all kinds shown in Fig.2.3, and this makes them so far the most widely- used magnets especially in the electrical machine industry.

In the last decade a new class of magnets has been developed, combining a relatively high remanence of the alnico type materials with coercivities greater than those of ferrites. These materials are formed by the combination of rare earth elements with compounds like iron, nickel and cobalt. Samarium cobalt, one of the most useful

combinations, has a maximum value of energy product about three to four times that achievable with alnico. Its demagnetisation curve deviates from linearity at very low values of Br at high demagnetising field. However, for practical applications a recoil permeability of value close to unity (1.05) can be used throughout the second quadrant. The cost of these magnets is relatively high and so its applications have been restricted to small magnets where small size and weight are important requirements.

In addition to the four parameters discussed above the important physical quantities are normally concerned with the Curie temperature at which the material losses its magnetic properties, namely the maximum permissible temperature, density, machinability, thermal expansion and conductivity, irreversible and reversible temperature coefficients.

2.3 Properties of NdFeB magnets

The excellent properties of Nd- Fe- B alloys have been investigated by many researchers (15,23,24) and it is now generally recognised that these new alloys will be of great importance in a wide variety of applications, particularly in electric motors. Table 2.1 and the demagnetisation curves of Fig.2.3 illustrate very clearly the superiority of these magnets among other available types. In the early stages of production the cost per unit volume of the NdFeB magnets has been comparable to that of the rare earth cobalt magnets. This is changing

rather quickly as properties are improving and more activity in raw material development is occurring.

The main characteristics of these magnets are:

- higher coercivity
- higher remanence
- higher energy product
- more ductile material which is less prone to chipping or breaking which makes handling much easier
- lower density that enables lighter- weight applications, (25).

Another important factor is the relative abundance of the constituent elements, especially in comparison with those of the Sm- Co magnetic materials. These magnets, however, have a low Curie temperature (320°C) and a rapid decrease in the coercivity with increase in temperature which limits their applications to some extent. Corrosion- free magnets are yet to be developed, however reduced corrosion resistance could be avoided by coating the magnet. Several coating types are being applied, the choice of which is dependent on the needs.

2.4 Effect of temperature on magnetic properties

The coercive force of the neodymium magnet falls with increasing temperature. Figure 2.4 shows the drop of coercivity and remanence with the increasing temperature, the temperature dependence of these magnets is illustrated in Fig.2.5. The loss that occur with rising temperature

falls into three categories: reversible, irreversible and irrecoverable.

a- Reversible losses, expressed in terms of temperature coefficient of remanence, are higher for NdFeB magnets (0.13%K) than for $SmCo_5$ magnets. Also the reversible coefficient, which gives a measure of the change in strength of the magnet with temperature, is higher for NdFeB (H_cJ= -0.6%/K).

b- Irreversible losses, recoverable by remagnetisation, are caused by elemental parts of the magnet becoming demagnetised by thermal agitation. The extent to which this occurs depends upon the magnetic working point and upon temperature. Stabilisation of the magnet at a few degrees above the expected operating temperature is effective against additional irreversible losses.

c- Irrecoverable losses, that can not be recovered by remagnetisation, are caused by metallurgical changes within the magnet such as oxidation and corrosion.

Extensive investigations are provided to improve the magnetic properties of the neodymium magnets. Recently several companies have announced the development of NdFeB magnets with higher operating temperature, (21,27,29). In general there are several strategies to enhance the magnetic characteristics, the detailed analysis of these strategies are beyond the aim of this thesis. These strategies are:

1- To raise the Curie temperature by partial substi-

tution of the iron by cobalt which results in a better temperature behaviour. Nevertheless the coercivity drops very sharply due to this substitution and this can be only explained by assuming a different microstructure compared to the pure NdFeB magnets. Magnets manufacturers at the same time tend to avoid the use of cobalt because of the volatility of its price as discussed earlier.

2- To increase the coercivity by partial substitution of the neodymium by a heavy rare- earth element like dysprosium (Dy) or terbium (Tb). This, however, causes a reduction of the saturation magnetisation and consequently a reduction of the energy product.

3- Another possibility is the substitution of non-magnetic elements such as aluminium (Al) and silicon (Si). All these elements increase the coercivity but the responsible mechanism is yet to be cleared. More studies are carried out to get a better understanding of the role of these elements especially Al in Nd- Fe- B based magnets.

In conclusion, the amount of Al, Co and boron in the NdFeB system has to be carefully optimised to obtain magnets with higher Curie temperature, good intrinsic coercivity and low temperature coefficient. Higher Co content is desirable for raising the Curie temperature, but it does not lead to better temperature coefficients due to the formation of other phases. Efforts are underway to identify those low T_c and low magnetisation minor phases existing in the high Co content NdFeCoB alloys.

A new magnetic alloy of NdFeCoBAl has been identified as having higher Curie temperature with large intrinsic coercive force, (19,27).

2.5 Application of NdFeB magnets

Rare earth magnets are generally available in block, disc, ring and segment shapes suitable for a wide range of applications such as motors, actuators (focusing, voice coil motors), audio frequency transducers (ear phones), mechanical applications (separators, bearings) and others. One of the new significant fields for application is the classification of airborne asbestos where the most commonly encountered asbestos types would orientate in the strong magnetic fields of neodymium magnets, (33). The orientation characteristics are sufficiently different thus enabling the different fibres types to be distinguished and magnetically classified. In the electric drives field, where quick response, light weight, and large continuous and peak torque are required, the neodymium magnets offer the opportunity for the best designs. The brushless motor construction with NdFeB magnets allows for an improvement in the material utilisation and results in a greater volumetric efficiency. The power rating is increasing and the torque and speed can also increase. The new magnet also make possible a new kind of brushless motor with a toothless armature which provides more space for the stator windings with higher flux density, despite an air gap larger than normally found in small d.c motors.

2.6 Conclusion

The properties of neodymium iron boron magnets in relation to other magnetic materials are discussed. NdFeB magnets have, among other properties, higher coercivity, higher remanence, and higher energy product which could be very advantageous in various applications. These characteristics, together with relatively low cost per unit weight, make these magnets almost ideal for use in rotating machines. However their wide range application is machine industry is still limited because of the low Curie temperature and the rapid decrease in the coercivity with increasing temperature, (high reversible coefficient). Several techniques to improve the thermal properties especially the Curie temperature are highlighted.

Material	NdFeB	$SmCo_5$	Ferrite	Alnico-5
B_r (T)	1.1	0.85	0.38	1.26
H_c(KA/m)	790	597	235	63
$(BH)_{max}$ KJ/m^3	210	142	30	43
Relative permeability	1.05	1.05	1.1	4.1
Curie temp. ^0C	320	720	450	860
Max. operat. temp. ^0C	140	250	350	550
Density x10 Kg/m^3	7.4	8.3	4.75	7.5
Reversible Temp. coef. % ^0C	-0.12	-0.04	-0.2	-0.022

Table 2.1: Magnetic and physical properties of different classes of permanent magnets.

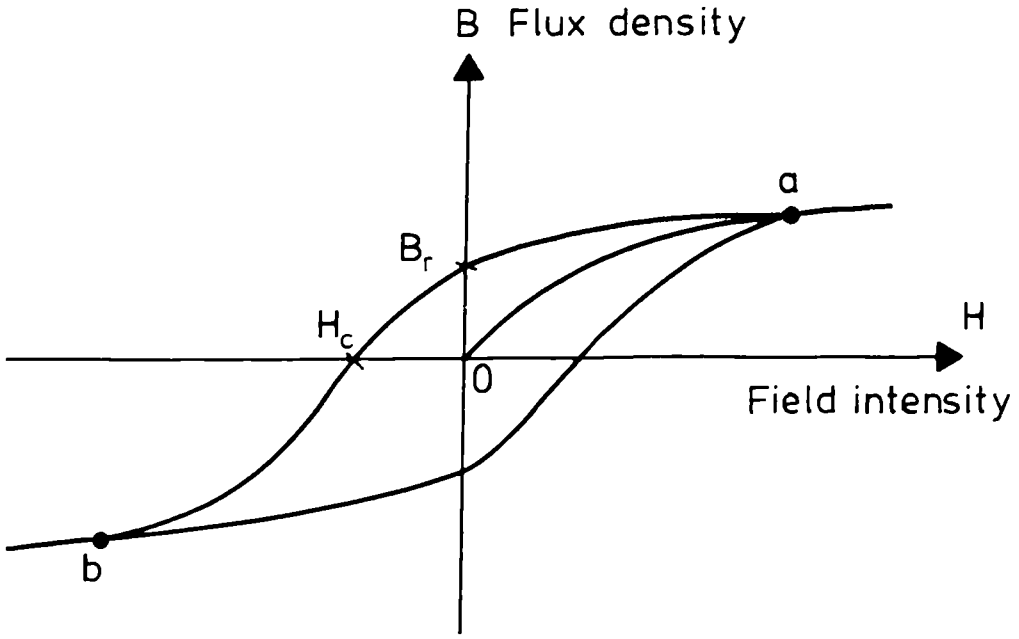

Fig. 2.1 Major hysteresis loop obtained by varying the magnetising force between limits which will saturate the material in each direction.

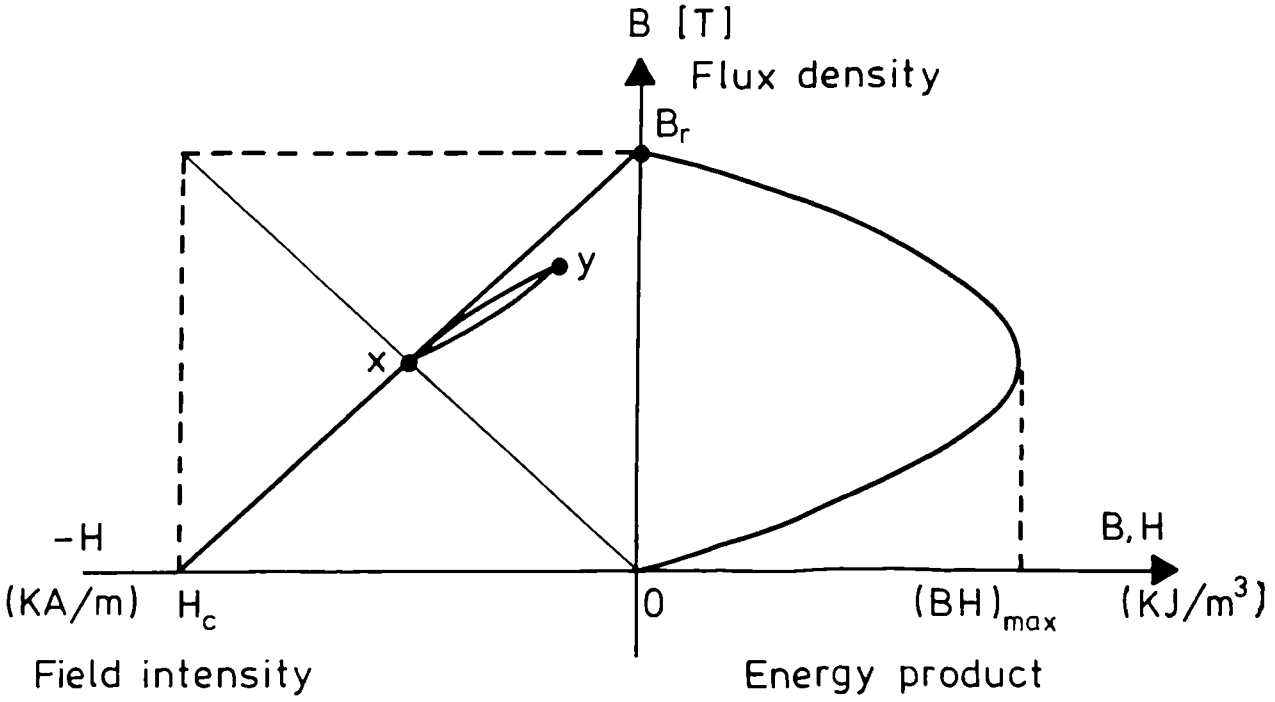

Fig. 2.2 BH product curve and the approximation of the (BH)max point at the intersection of the constructed diafonal.

a... high remanence alnico 5
b... high coercivity alnico 8
c... high coercivity ferrite (ceramic 8)
d... polymer- bonded rare- earth cobalt
e... sintered rare- earth cobalt (H-90A)
f... sintered rare- earth cobalt (H-90B)
g... sintered rare- earth cobalt (H-99A)
h... MnAlc
i... sintered neodymium iron boron (27H)
k... sintered neodymium iron boron (30H)

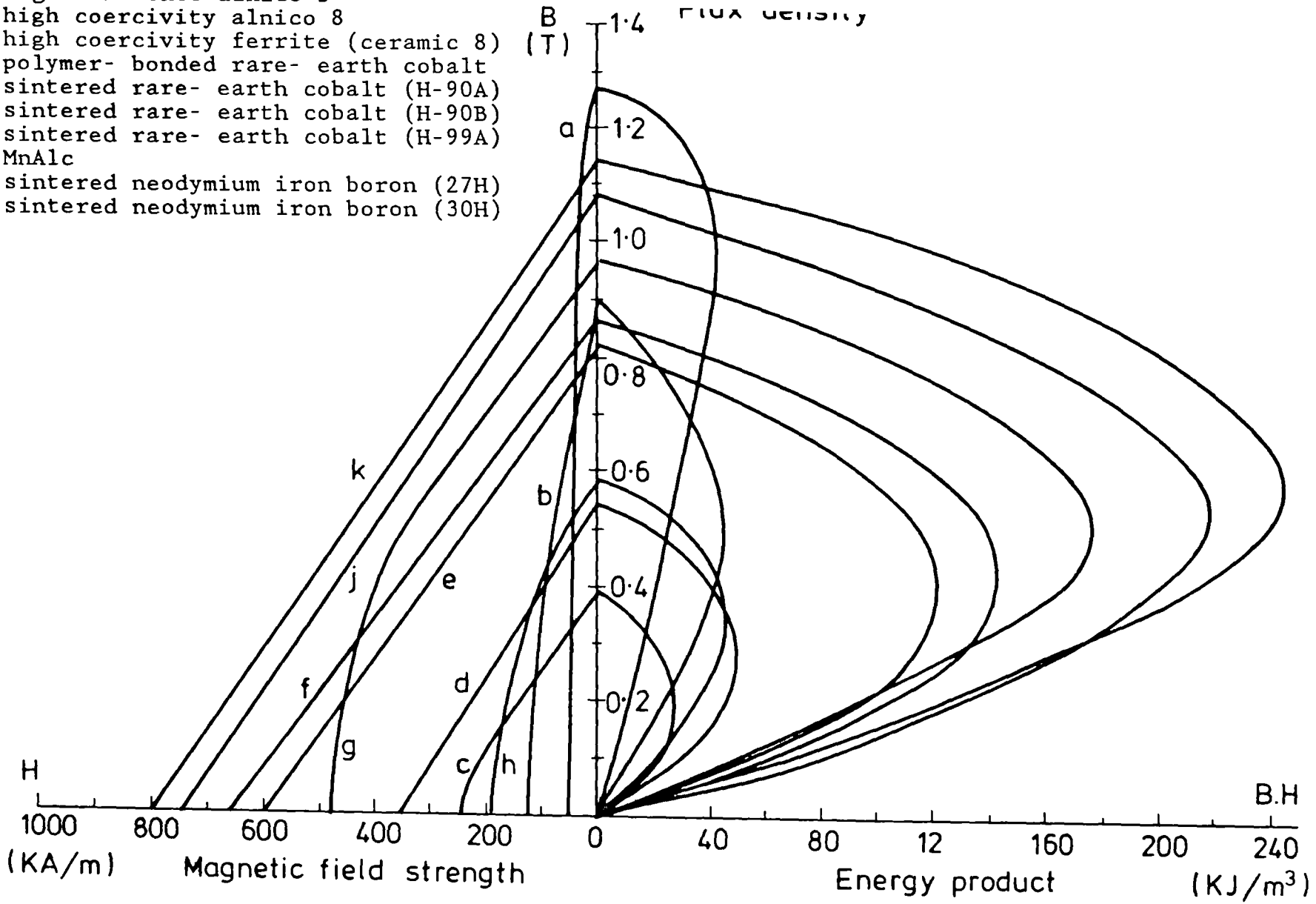

Fig. 2.3 Demagnetisation characteristics and energy product curves of the commercially available permanent magnets.

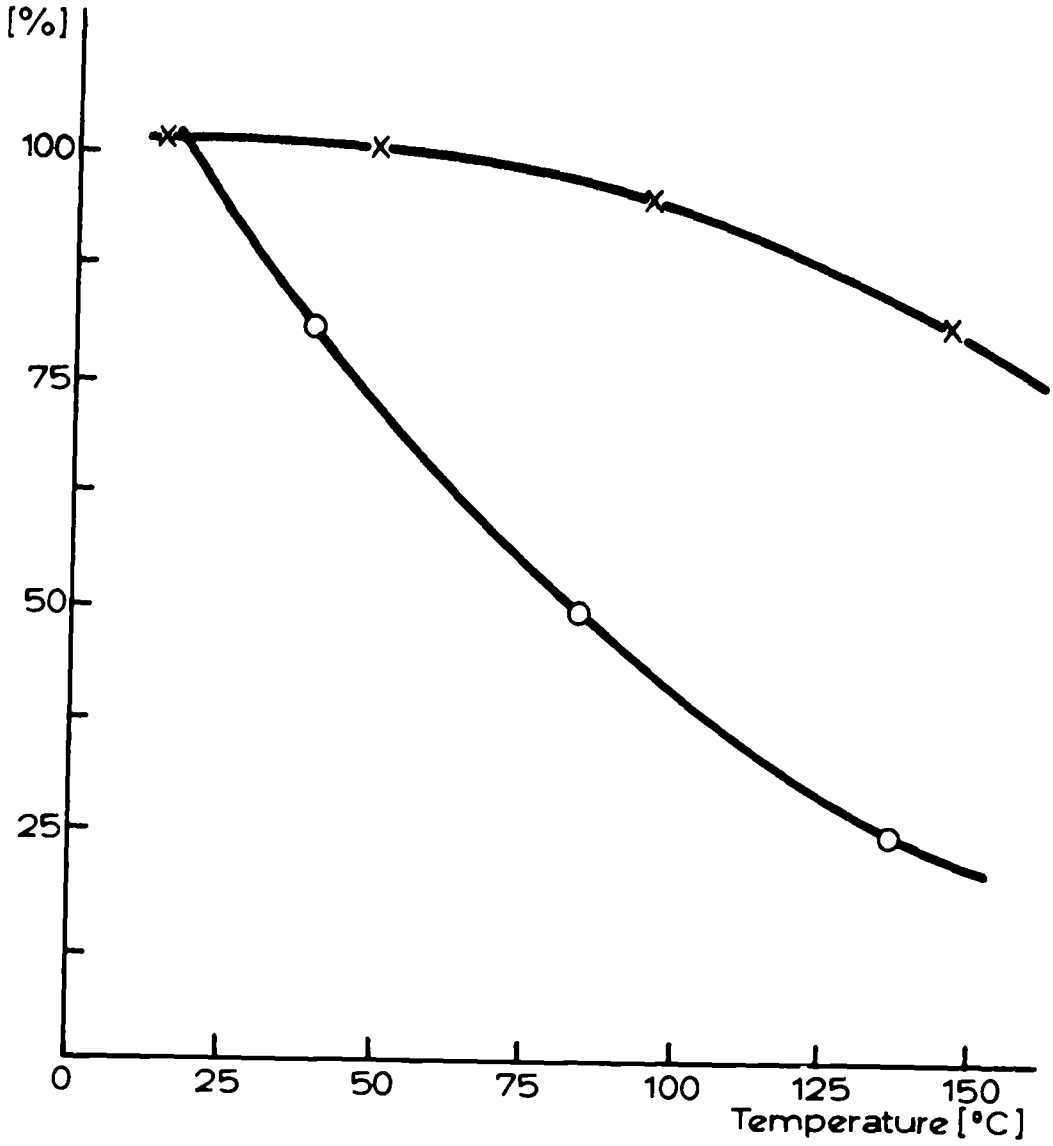

o... change in coercivity
x... change in remanence

Fig.2.4 Coercivity and remanence dependence on temperature for the NdFeB magnets.

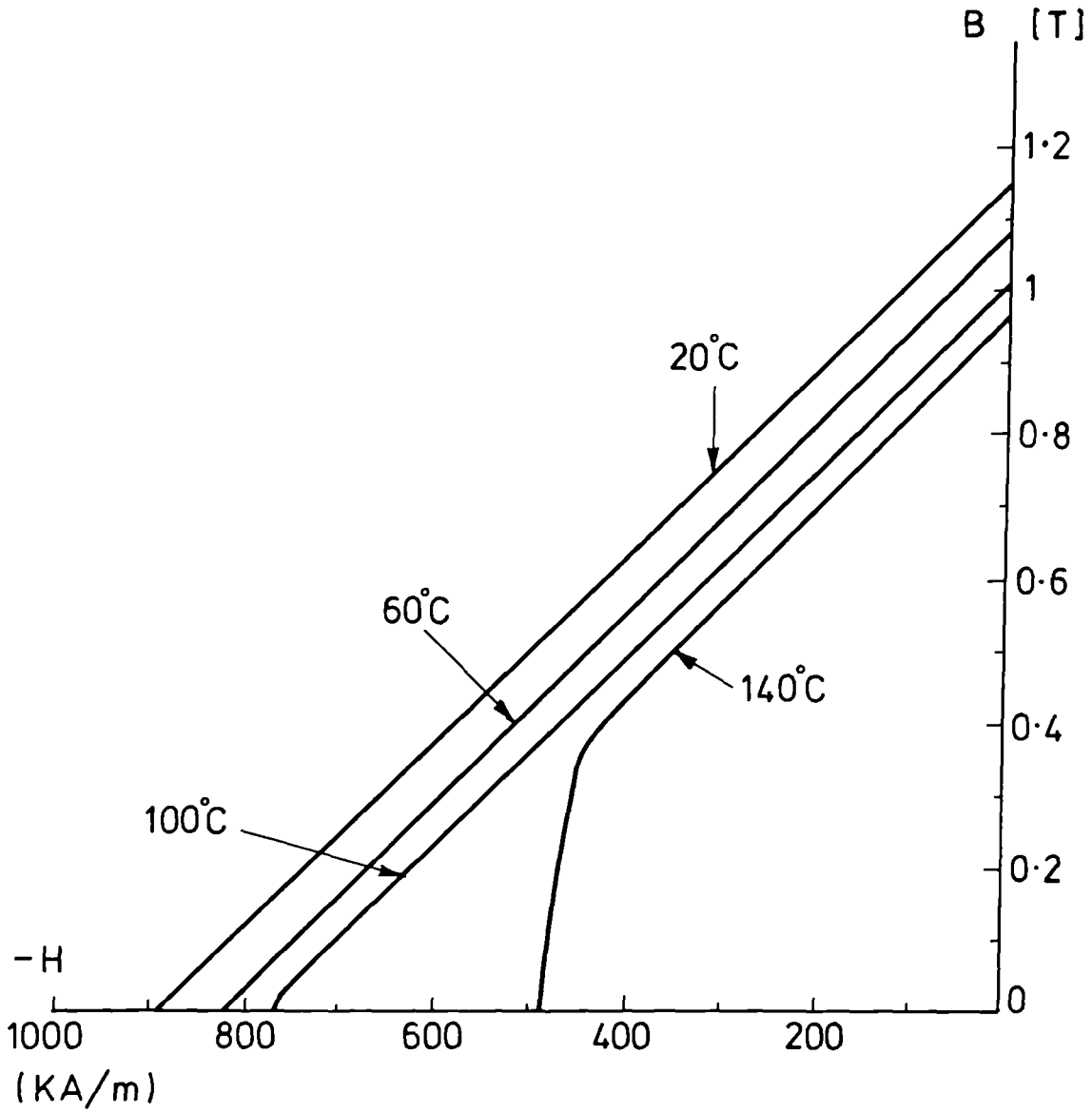

Fig. 2.5 Temperature dependence of the demagnetisation curve for R- Fe- B based magnets.

CHAPTER THREE

FIELD ANALYSIS BY A TWO DIMENSIONAL FINITE ELEMENT MODEL

CHAPTER THREE

FIELD ANALYSIS BY A TWO DIMENSIONAL FINITE ELEMENT MODEL

3.1 Introduction

Recent trends in the design of electrical machines and devices have required the development of accurate methods for predicting the electromagnetic fields produced in the machine under various operating conditions. Classical and analytical solutions to this problem are possible only for idealised cases with a lot of simplifying assumptions concerning geometries, material properties and boundary conditions. Complex geometries, material non- linearities and the effects of magnetic materials, if any, require the use of numerical methods. During the last decade finite element method has become an established tool for magnetic field analysis of electrical machines. It was first used to solve problems of stress and strain in complicated mechanical structures and in the analysis of saturation effects in accelerator magnets, (35,36). According to (46) the the finite element method was first used in electromagnetics to solve a standard problem involving homogeneous waveguides. Several finite element computer programs using first or higher order elements have since then been developed for solving electromagnetic fields in two or three dimensions, (34,37,38,39). The computing time required for the solution of the resulting set of simul-

taneous equations has been minimised by using proper solving routines. The availability of interactive graphical pre- and post- processing programs to assist in the preparation of data and examination of the results, in particular flux density and torque, have made finite element method even more attractive and more user friendly. Two finite element programs and two computer graphics packages are discussed in this chapter.

3.2 PE2D Program Theory

PE2D (Poisson Equation in Two Dimensions) is a general-purpose 2D- finite element program that can be used to solve Poisson's equation. It was originally developed in the Rutherford Appleton Laboratories (RAL) by Trowbridge et al.(40,41). This package uses first or second order triangular mesh elements with a wide range of soluble problems like static fields, linear eddy currents and transient non- linear eddy currents. Triangular mesh elements of this type are currently most widely used in electrical machines modelling because they are convenient to fit the complicated geometries of machines especially when magnet segments and cage windings are included in the rotor.

The program solves general equations of the form:

$$\nabla \times \frac{1}{K} \nabla \times A = G \qquad (3.1)$$

in Cartesian or polar coordinates systems where:

∇ ... del operator

A... one component vector potential

K... volume constant e.g. permeability

G... current or volume charges.

For two dimensions A is in the direction normal to the plane of analysis. This partial differential equation can be solved by a Galerkin weighted residual method, (39,42). For the magnetic fields in rotating electrical machines the magnetic vector potential satisfies Poisson's non- linear equation in the form:

$$\frac{\partial}{\partial x}(\lambda \frac{\partial A}{\partial x}) + \frac{\partial}{\partial y}(\lambda \frac{\partial A}{\partial y}) = -J \qquad (3.2)$$

where J...current density

λ...magnetic reluctivity

A particular interpolation technique is used for the nodal magnetic vector potential. This technique involves the minimisation of the non- linear energy function F such that:

$$F = \int_R (\int_0^B H.dB - \int_0^A J.dA)\, dR \qquad (3.3)$$

where H...magnetic field intensity

B...magnetic flux density

R...region of integration

The value of B in each region is obtained from the relation:

$$B = \nabla \times A \tag{3.4}$$

Because of symmetry the region of the machine over which the field needs to be solved can be reduced to a single pole. This is applied to compromise between the accurate mesh representation of the machine geometry and the increase in computer core memory and computing time required. Symmetry and periodicity conditions are applied to the boundaries of this pole so that:

$$A(\phi) = -A(\phi + \pi/p) \tag{3.5}$$

ϕ... angle of nodes on the pole symmetrical boundaries

p... pole pairs

3.3 Pre- and post- processor and the analysis program

The program consists of two separate parts, the pre- and post- processor and the analysis programs. The pre- and post- processor is used to define problem geometry and to interrogate and display the solution. In the pre-processor the field model of a PM synchronous machine could be obtained considering the following assumptions:

a- The electromagnetic field quantities are independent of the z- coordinates measured along the axial direction of the machine.

b- The magnetic field outside the machine is neglected to save the computing time. The boundary contour of the stator is considered as a line of zero vector potential.

c- The iron regions are isotropic and the magnetisation characteristics are single valued and independent of the past magnetic condition of the material.

d- Eddy currents are neglected, also the insulations between the iron and the copper are ignored.

e- The magnets remain at a constant temperature so that no irreversible demagnetisation occurs.

Six commands are provided for setting up the data. Once the model is built the mesh is generated from the previously determined regions data including the material types as shown in Fig.3.1. The Mesh command forms the data necessary to analyse the problem or to interrogate the results i.e. node tables, element definition table, element properties etc... In the mesh generation procedure, small triangles are used where the electromagnetic field changes rapidly and large triangles can be used in other areas.

For the output retrieval or the post- processor ten commands are provided to give the resulting vector potential solutions. Values of fluxes through different magnetic paths could be obtained in addition to the graphical displays of the field distribution. Many useful properties of the machine such as torque, generated voltage and different flux leakages could be calculated by integrating field values along contours or over areas. Fig.3.2 shows the characteristics of the normal flux density of PM machine at no- load and full- load conditions. These calculations have been provided throughout this thesis and they are found to agree well with the measurements.

The analysis program uses a double precision computation to evaluate the element matrices and to solve the set of equations. After the computation the analysis program returns the regions data with the solution potential at each node. This can be used as data for the post processor for interrogating the results. The information needed to launch the computation include the choice of a linear or a non- linear run and the number of iterations in case of non- linear run. The package was run either on the RAL PRIME computer through a direct link or on the local VAX system in the university. Batch as well as on- line facilities are available on both systems. Quality control of the results of the program calculations has depended on the judgement of the designer, assessment of the errors has been partly experience and partly trial. Error estimation methods have been expensive but a new inexpensive technique has been reported lately, (44,45).

3.4 MOTORCAD program

Another finite element program that is used extensively in this work is the MOTORCAD package. This program has been developed by Hameed and Binns (39,81) and is specially prepared to analyse permanent magnet machines. Basically the statics analysis program is similar to that of the PE2D. However, being focused only on machine analysis, the post- processor of MOTORCAD gives more details concerning the machine performance. Besides the flux plotting, the calculation of the synchronous torque using lorentz force is included. Fourier analysis to find out

the fundamental component as well as higher harmonics is carried out automatically. Another feature is the determination of:

- the direct and quadrature components of the synchronous reactance
- the terminal voltage and the power factor
- the internal and the external load angles.

In the pre- processor the rotor and the stator are kept in separate files. This allows the computation of different rotor and stator designs with lower computing time consumption. Samples of the MOTORCAD output are shown in Fig.3.3 and 3.4.

3.5 Electromagnetic Torque Evaluation

3.5.1 Maxwell field stresses

A general method to evaluate the forces and hence the electromagnetic torques in machines involves the use of Maxwell field stresses, (1,43). The tangential component of the electromagnetic stress is given by:

$$F_t = \int_S \frac{B_t B_n}{2\mu} \, dS \qquad (3.6)$$

The surface of integration (S) throughout the air gap encloses the rotor pole completely. The optimum choice of this surface is midway between the rotor and the stator particularly when the air gap is divided into three layers. Computation results have shown that the choice of the surface of integration has a significant effect on the

values obtained. Figures 3.5 and 3.6 show the variation of the value of the computed torque with the surface of integration. The effect of the reluctance torque is clear at low currents with the surface of integration being close to the rotor boundaries. The shape of the triangular elements inside the air gap has to be as regular as possible. The error limit is being minimised to avoid any variation in the results if the curvature of the surface (S) is slightly changed. The torque is then expressed by the following equation:

$$T = 2.p.r.l.F_t$$

that is:

$$T = \frac{p.r.l}{\mu} \int_e B_t B_n \, ds \qquad (3.7)$$

p... number of pole pairs

r... radius of the surface of integration

l... axial length of the machine.

The torque values obtained from the Maxwell stresses for a high- field PM machine may be of low accuracy. This is because along the surface of integration the tangential component 'B_t' swings rapidly from high positive to negative values about a small average due to the effect of the stator teeth whereas B_n varies smoothly. Hence the numerical integration of these two components as provided in equation (3.7) is unlikely to give accurate results unless

an extremely fine mesh is used. However in PE2D this method does not require a considerable amount of computing time and therefore could be used for comparing the performance of different rotor configurations or to study the effects of the variation of some of the rotor parameters.

3.5.2 Lorentz (Azimuthal) Force

The torque can also be determined by calculating the Lorentz force over a slot pitch using a surface of integration with the same conditions as applied for Maxwell stresses. It is based on the direct application of the force law under each slot which can be given by:

$$F = B_n \, .I.l$$

from which the total torque is determined by:

$$T = l.r.p.2\sum_{i=1}^{m} B_{ni} I_i \qquad (3.8)$$

m is the number of tooth pitches per pole

The finite element analysis of the Lorentz force involves the computation of the normal flux density over each slot pitch throughout the air gap. This has been provided by means of two methods:

1- B_n is obtained by applying Simpson's rule of integration over each slot pitch. Generally the corresponding post- processing command used (for example INTL in PE2D) integrates field values like flux density along lines to calculate quantities such as force.

2- The second method is to apply the post- processing command (LINE in PE2D) to get solutions and field values along the surface of integration. A set of 'α' points, where α could be the number of degrees in one pole pitch, is obtained. If m is the number of tooth pitches then the average value of Bn along the tooth pitch is:

$$B_{av} = \frac{\Sigma B_n}{\beta} \qquad (3.9)$$

where $\beta = \frac{\alpha}{m}$

Calculation of the torque by lorentz force gives more accurate results than the Maxwell stresses method, however it is more time consuming. It has been assessed throughout this thesis wherever a comparison of the computed results with those obtained from the tests is needed.

3.6 Interactive Computer graphics systems

CADAM (Computer- Aided Design And Manufacture) is a 2D interactive computer graphics system which utilises a high function graphics display and a responsive environment that can be used for:

- engineering design and analysis particularly machine and other devices design.
- all types of draughting such as layout and detailed draughting
- Numerical control programming direct from the detail drawings.

CADAM provides analysis functions which help in establishing some important properties related to the current models such as component properties like moment of inertia, weight and volume. This has proved to be very helpful in predicting the parameters, for example in the machine design process. CADAM also has the facility to build a mesh- model, however this function is not applied in this work due to the availability of the finite element packages described earlier.

CATIA, another graphics system, stands for Computer-Aided Three- dimensional Interactive Application. It provides three- dimensional modelling and two- dimensional draughting facilities together with a number of design analysis tools. CATIA consists of of several basic modules (5,12) some of which are:

- The Solid Geometry module which has the capability to define and operate on solid models which has been built using cylinders, spheres, prisms and other simple volumes. One of the features of the solid module generation is the hidden line removal and local transformation (translation, rotation...) as shown in Fig.3.7 and 3.8. Starting with a 2D model the z- axis is defined for each element of the machine (rotor, shaft) and using the PRISM option of the SOLID function a 3D model as shown in Fig.3.7 is obtained. This switch to 3D model is possible only after limiting these elements in the form of closed volumes.

- The Advanced Surface Module which creates surfaces passing through planar surfaces which can be divided into segments,circles, or conics.
- Another important module, though it has not been assessed in this work, is the Robotics Module which provides facilities to define and operate models of robots in their working environment and generate data to be used to program the robot.

CATIA and CADAM systems at Liverpool University use IBM 5080 graphics and workstations as the interactive device. Direct interfacing between these two systems can be provided so that a 3D model produced by CATIA is viewed in CADAM or drawing data in CADAM can be used to build a 3D models using the PRISM function as discussed earlier.

3.7 Conclusion

Updated versions of the PE2D and the MOTORCAD finite element packages are briefly discussed. The flux distribution in the model is presented as well as variation of the flux density along the air gap. Computation has shown that optimum results could be obtained by integrating the field values along a line passing midway throughout the air gap. Special emphasis has been given for the effect of the variation of the integrating surface along the air gap.

Torque computation has been carried out by means of two methods and the experience (1,67) indicated that the

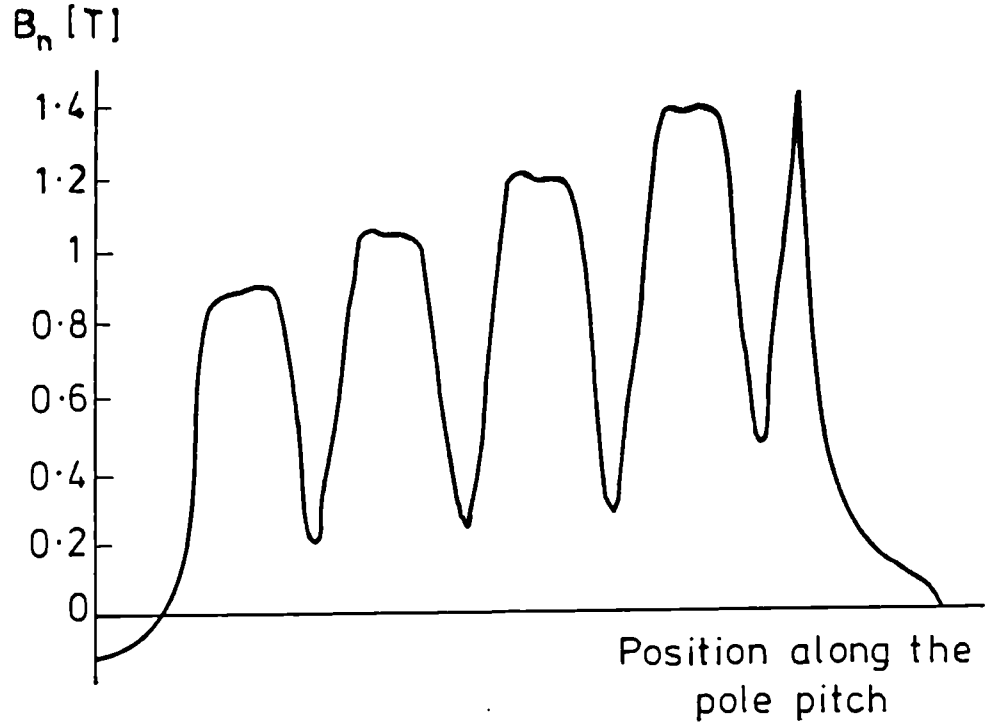

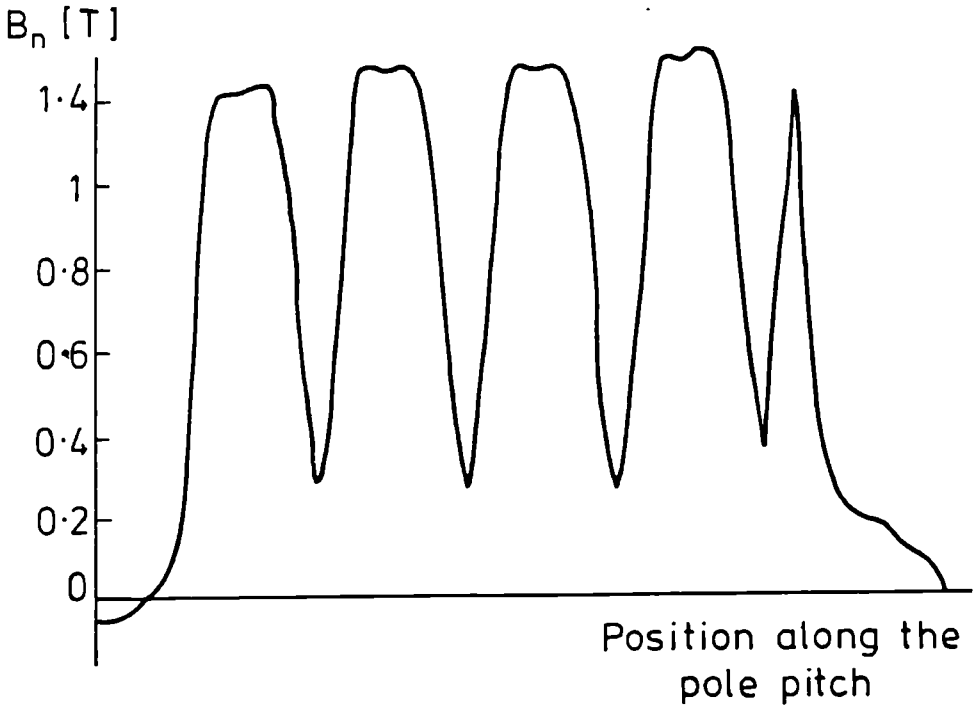

a... full- load condition
b... no- load condition

Fig.3.2 Variation of the flux density along the air gap at different load conditions.

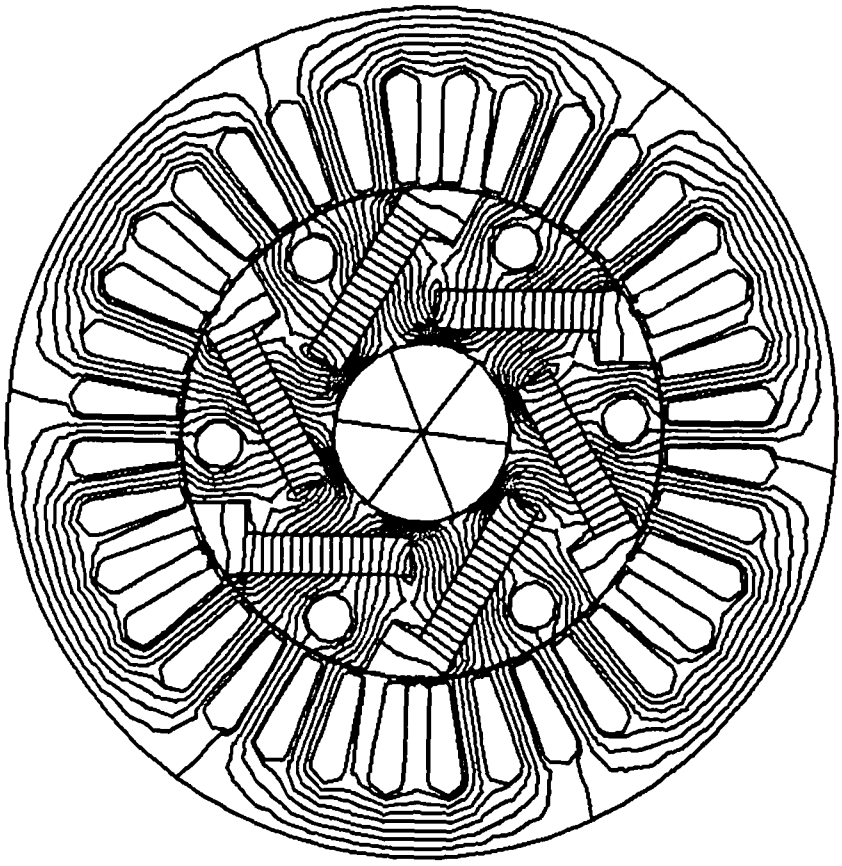

Fig.3.3 Full- load flux distribution inside a PM machine with buried magnets.

Fig.3.4 MOTORCAD layout: Flux distribution and air gap flux density of one pole at full load.

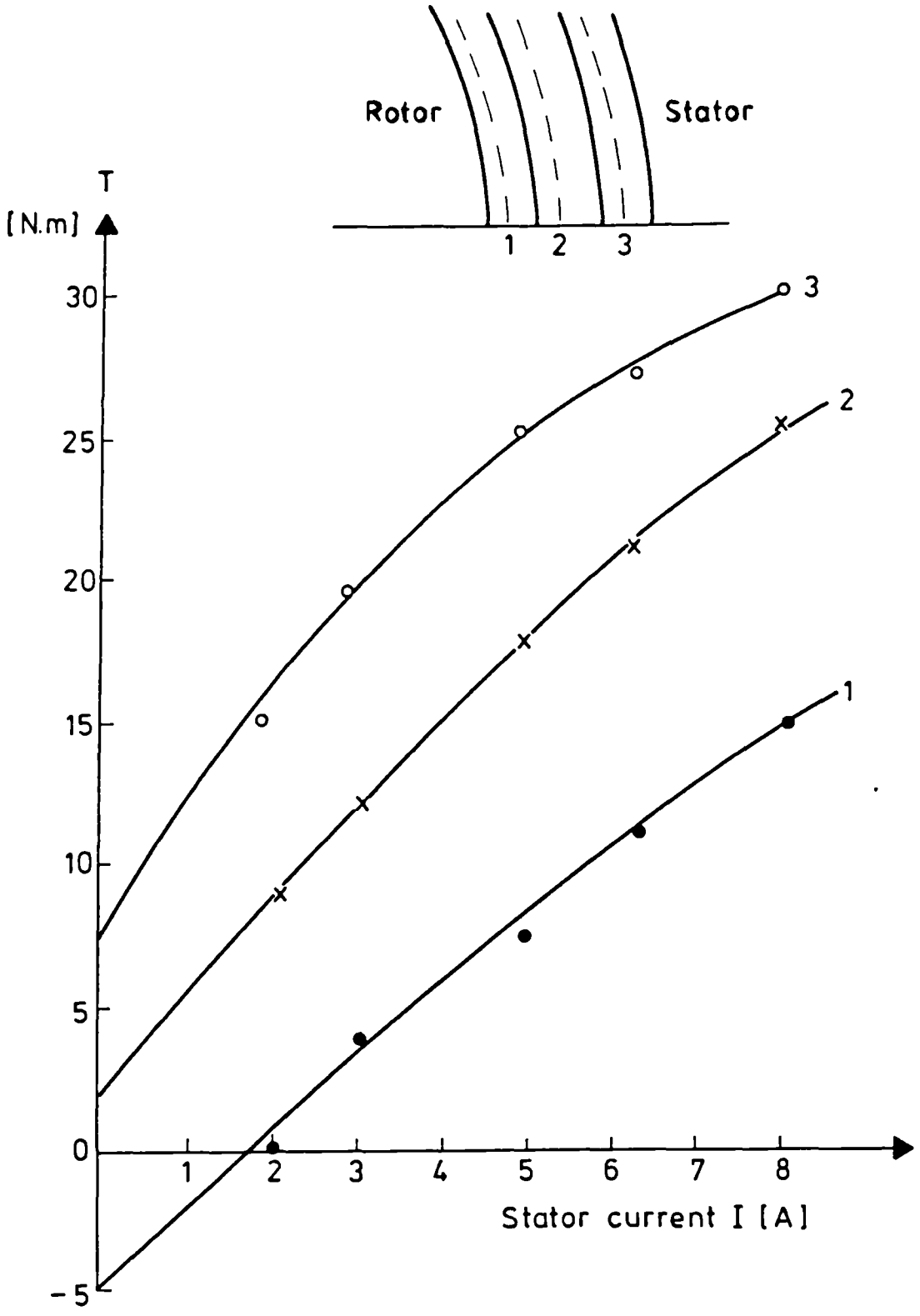

Fig.3.5 Torque characteristic versus stator current as computed along different surfaces in the air gap.

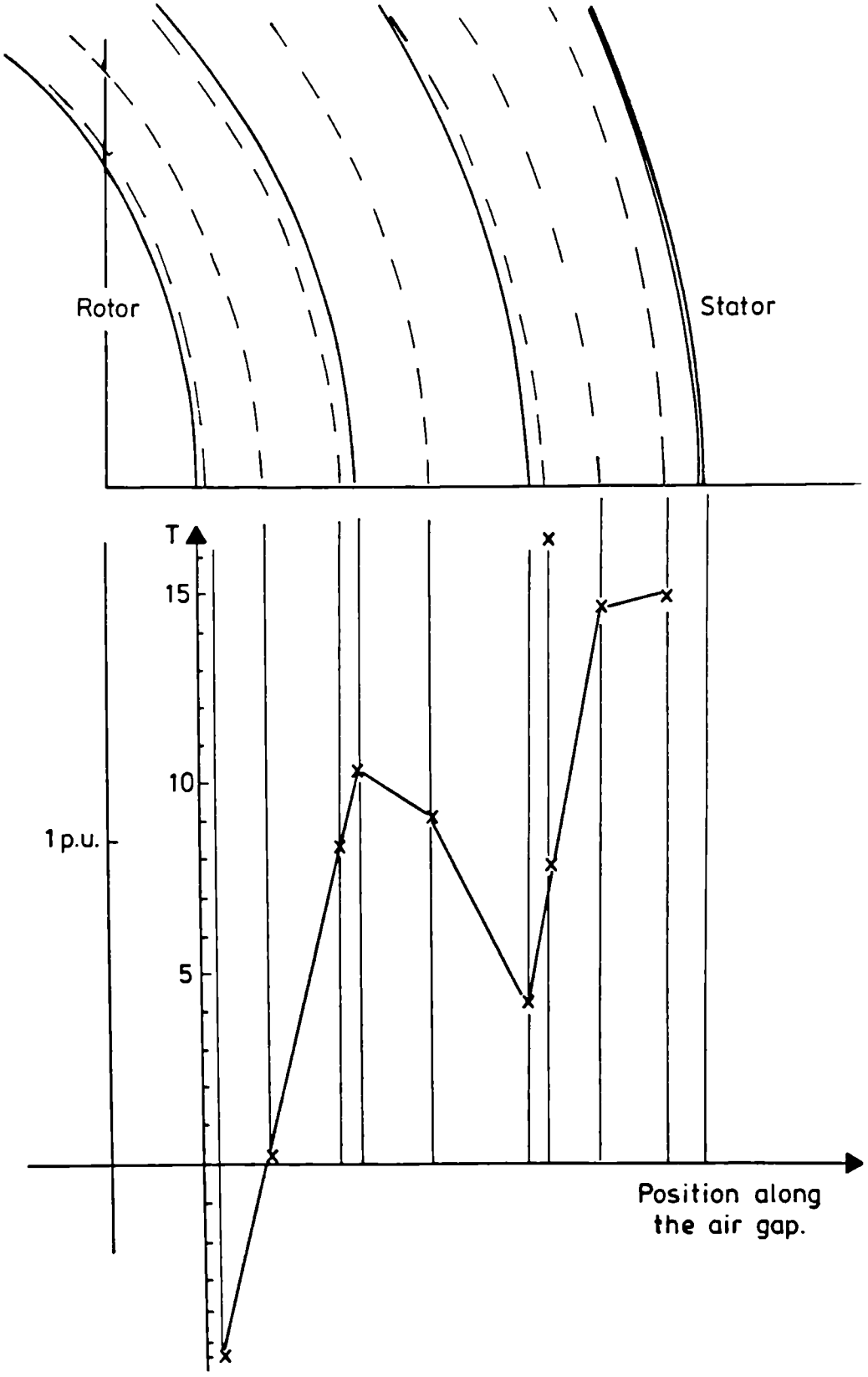

Fig.3.6 Effect of the choice of the surface of integration on the torque values at full load, (I = 8 A).

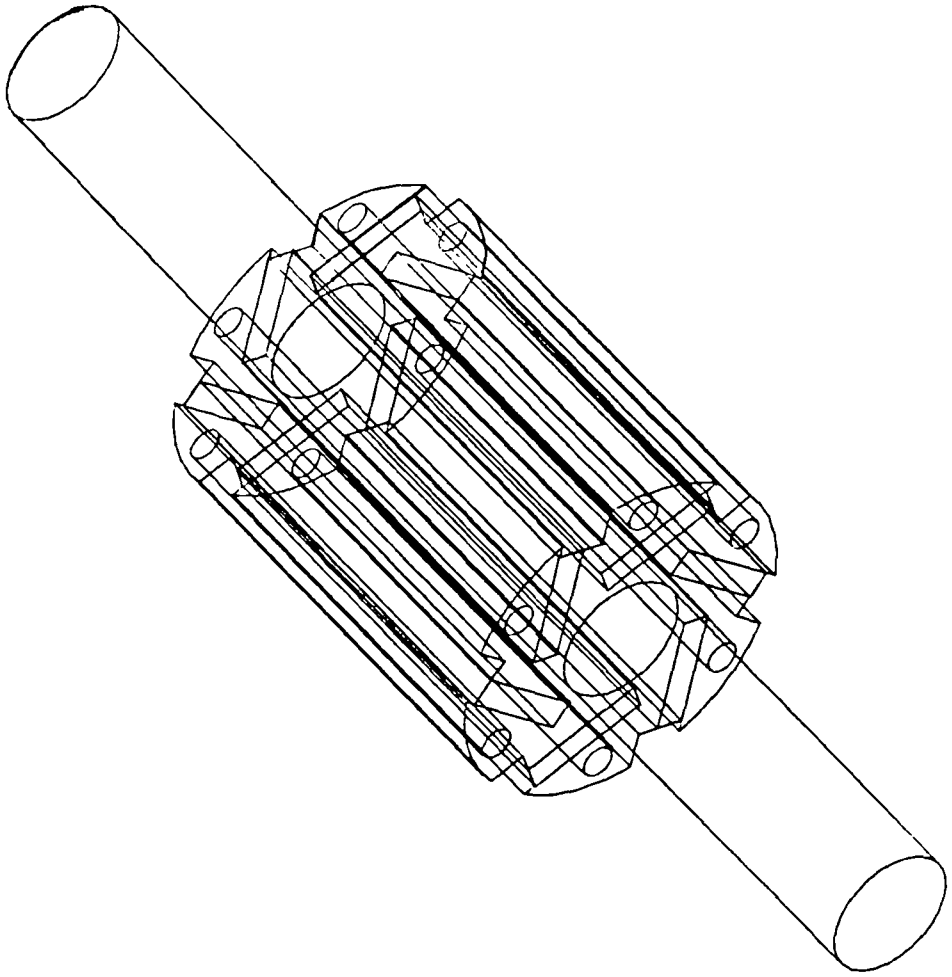

Fig.3.7 CATIA layout: 3D- configuration of 6- pole rotor without removing the hidden lines

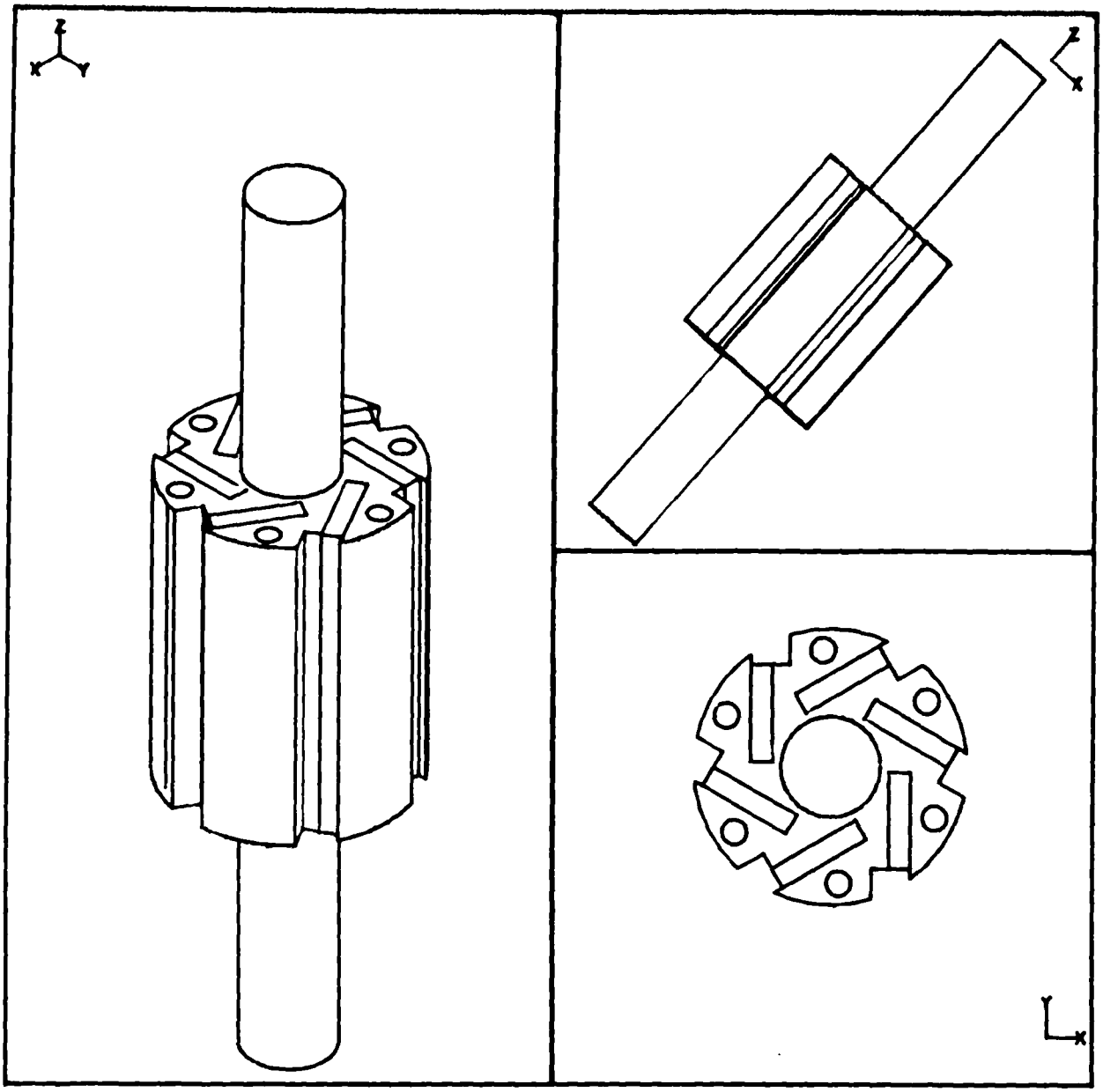

Fig.3.8 Solid 3D- module as regarded along different planes

CHAPTER FOUR

COMPARISON OF THE PERFORMANCE OF HIGH- FIELD PERMANENT MAGNET MACHINES FOR DIFFERENT MAGNET MATERIALS

CHAPTER FOUR

COMPARISON OF THE PERFORMANCE OF HIGH- FIELD PERMANENT MAGNET MACHINES FOR DIFFERENT MAGNET MATERIALS

4.1 Introduction

In the light of the characteristics of three magnetic materials, ferrite, samarium cobalt ($SmCo_5$) and neodymium iron boron (NdFeB), a comparison of achievable performance of permanent magnet machines with these magnets has been carried out. In this comparison it is essential to realise that optimal dimensions are material- dependent so the simple exchange of magnet materials in the same geometry is not sufficient in assessing relative performance capability. The difference in magnetic properties leads to different optimal magnet dimensions and thus different volumetric ratios between iron and magnet in the rotor as shown in Appendix B. The criterium in the parameters optimisation is to achieve the maximum torque.

The analysis involves the finite element representation of the machine and the computation of its performance using the ferrite, the samarium cobalt and the neodymium iron boron magnets. Since the characteristics of the neodymium magnets are temperature dependent, the BH curve is chosen for an operating temperature of 100°C. The slightly idealised demagnetising curve at this temperature

is presented in Fig.4.1 together with those of the ferrite and the samarium magnets.

4.2 Rotor Configuration

The machine used has four poles and is of the high-field self- starting class of permanent magnet machines. The rotor geometry is shown in Fig.4.2 and it has been discussed in detail in several publications (37,55,58,62). Only a summary of the main characteristics of this design will therefore be provided:

1- The magnets in the rotor poles are perpendicular to each other and they have a simple rectangular section. The width of the iron bridge between the non- magnetic shaft and the magnet is accurately determined.

2- Some flux can pass under the magnets giving an additional path for induction motor operation at starting. Also some of the useful flux passes through two magnets which results in a higher flux leaving the rotor pole than that in the magnet itself. The magnets can work at a higher density since each of them needs to provide only a part of the field strength required by a single magnet driving flux through an identical path.

3- In order for the machine to be a self starting, a cage bar winding is incorporated in the rotor. This winding has also the effect of damping any hunting tendency. For good asynchronous torque during starting the cage bars are positioned at an appropriate depth below the surface of the pole.

4- The rotor configuration is non- symmetrical in the

direction of rotation. This results in a small but interesting difference in the performance for the two directions of rotation (55,56). The tests for the comparison purposes are all performed in the so called preferred direction of rotation, in this case the anti-clockwise direction in which the displacement of flux axis is strongly resisted by the adjacent magnet pushing the flux in the opposite direction.

4.3 Experimental Results

For testing purposes the permanent magnet machine, using a standard induction motor stator, is coupled to a d.c. dynamometer. The three- phase variable frequency supply is connected to the machine through a three- phase variable auto- transformer to make it possible to vary the voltage. The experimental equipment for the measurement is illustrated in the blocks diagram in Fig.4.3.

Machines using magnets in the rotor with non- linear demagnetising curves, like ferrites, can always be subjected to partial demagnetisation during operation. The ferrite machine, before being tested for purposes of comparison, was remagnetised in situ using the stator coil. A high direct current, which is a function of the supply voltage, is passed through the stator with the rotor being locked. Although this method is not very efficient because part of the current flux passes only through the air gap and returns without affecting the magnets, the open-circuit generated voltage after remagnetisation increased

by 80%. The high demagnetising current during the starting the machine has been also avoided by driving the machine up to synchronous speed using the d.c. dynamometer before being synchronised.

The performance of each of the three machines is tested over a range of frequencies. Tables 4.2- 4.4 represent some of the results obtained from these tests for both directions of rotation. The choice of the supply voltage level (or stator winding turns) is an important factor for any particular application mainly because it is not possible to control the excitation level of the permanent magnets. The rated supply voltage for each frequency level is considered to be that induced in the winding when the machine is run as an open- circuited generator. The characteristics in Fig.4.4 represent the induced voltage for the tested rotors. The effect of the remagnetisation of the ferrite magnets is also evident. The measured torque for three voltage levels for the samarium cobalt machine is shown in Fig.4.5 as a function of the load current for a 50 Hz mains supply. With this type of high field machine there is little to be gained in torque by using a voltage higher than the rated value. Neodymium iron boron magnets on the other hand have a higher flux carrying capacity. Higher torque is obtained for a given current; hence operation at higher voltage gives a benefit, see Fig.4.6. The ferrite magnet rotor has a totally different characteristic and has to be operated well beyond the generated value in a regime where reluctance action is significant.

The torque characteristics of the three magnetic materials at the defined rated voltage give a clear comparison of output as shown in Fig.4.7. The NdFeB machine has a significantly higher output. This is due to the higher coercivity and flux density and partially because more magnet is used to avoid any rise in temperature. The higher flux density increases the torque without increasing the ohmic losses. Efficiency and power factor are significant parameters for motors, but these parameters become particularly important in variable- frequency applications where the motor is supplied from an inverter. The efficiency is an important parameter and its variation for all three machines is plotted in Fig.4.8. The ferrite machine has a relatively low value but it improves with load. The two rare earth- magnet machines are comparable in efficiency. At low currents the samarium cobalt machine is overexcited and is operating at leading power factor. As the load increases it becomes underexcited and operates at lagging power factor. The high power factor permits more motors to be supplied through the same inverter. For the ferrite it improves with load but still, as illustrated in Fig.4.9, is much lower in comparison.

4.4 Computational Analysis

The machine is modelled using the two- dimensional PE2D finite element package. Each magnet is described through the pre- processor in terms of the the demagnetising BH curve. The field computation under steady- state condi-

tion is provided by discretising only a pole pitch of the machine as shown in Fig.4.10. Load conditions are simulated by applying symmetry and periodicity conditions on the boundaries as explained earlier. It is clear that the flux density in the air gap is higher than in the magnet itself, a feature of this configuration. The torque is computed for the three machines using Maxwell stresses and the results are presented by the graphs of Fig.4.11.

From the field solution of the finite element analysis it is possible to determine the internal load angle of the machine at any load. This angle may be defined as the phase shift of the magnet axis (field axis) at any load from its original no- load position. At no- load the magnet axis passes through a point in the air gap where the vector potential field changes its sign as illustrated in Fig.4.12. The magnet axis at no load is shifted from the x- axis by an angle δ_i such that:

$$\delta_i = \text{Atan}\ \frac{y}{x} \quad \text{in mechanical degrees}$$

The same angle is calculated under load condition and the internal load angle will be the difference of the two angles.

Material	NdFeB	$SmCo_5$	Ferrite
δ_i	14	22	42

Table 4.4: Variation of the internal load angle with different magnetic materials.

Table 4.4 presents the values for the internal load angle at full load for the computed models. The large value obtained for the ferrite machine indicates that the magnet axis is highly lagging behind the rotating mmf and thus the reluctance of the torque has some significant value. Small values of the internal load angle lead to smaller values of power- factor angle allowing the machine to operate at a power factor close to unity. Also the range of operation of the machine is extended before the pull- out torque occurs. The plots in Fig.4.13, representing the magnitude of the potential field, show as well the significant change in the ferrite machine under full load conditions. This is because the ratio of the current density in the stator to the magnet flux is very large relative to the ratios for the two rare earth magnets.

4.5 Four- Pole Rotor With Peripheral Magnets

In permanent magnet machines the magnets can be placed inside the rotor lamination and the rotor is referred to as an interior- type rotor or as a rotor with buried magnets. An alternative to this is the design in which the magnets are fitted to the periphery of the rotor thus giving the peripheral- type rotor. The different characteristics of these types could be briefed as follows:

1- With round- rotor core there is no reluctance torque due to the low, nearly unity permeability of the magnet which, therefore, appears to the stator mmf as an equivalent air gap. Fig.4.14 represents the torque- load angle characteristics for round peripheral type rotor as well

as that of salient pole rotor. For the peripheral type the maximum torque is achieved at load angle of 90° whereas the salient- pole characteristic is shifted due to the additional effect of the reluctance torque.

2- The flux in the air gap can not exceed that of the magnet itself. Using the same amount of magnet the buried design produces higher flux by the flux concentration at the pole face.

3- Unlike the interior type where the magnets are protected, the peripheral rotors are not suitable for high-speed applications because of the effects of the centrifugal forces acting on the magnets. However this could be avoided by fitting a can around the rotor. This technique is discussed in details later in this work.

4- The position of the magnets at the rotor edges eliminates most of the leakage flux thus giving more freedom in extending the pole arc of the machine. Fig.4.15 shows the variation of the torque with the pole arc for a constant magnet volume.

4.6 Effects of Transient Demagnetising Forces

Machine parameters are normally chosen to give the optimum performance under steady state conditions. With the assessment of magnetic materials in the rotor design it becomes very critical to take into consideration the effects of transient conditions during which these magnets could be subjected into severe demagnetising force. Under these conditions, a short circuit for example, a high

current several times the rated value passes in the stator winding.

Salient- pole machines with interior magnets are virtually protected against such phenomena because the salient poles act as a barier against any overloading conditions. The presence of high currents in the stator can result in a high degree of saturation in the rotor-pole thus limiting the demagnetising field. The peripheral magnets, on the other hand, lack such pole- core protection and therefore could undergo an irreversible demagnetisation.

To illustrate these effects a computation is carried out in which a current 5 times the rated value is passed through the stator windings of the two different machines. These machines, as shown in Fig.4.16 and 4.17, are modelled using the same stator, the same air gap, and the same NdFeB magnet. Graphs in Fig.4.18 represent the variation of the operating point of the magnetic material under these overloading conditions. For the interior salient- pole machine the operating point, represented by the flux density B, drops to the lowest value of 0.38 T then rises again as the saliency of the pole approaches. Such decline is recoverable when the machine is back into normal operating conditions. In the case of the peripheral rotor the negative value of B (-0.2 T) indicates that the operating point has moved into the third quadrant of the BH curve in which the magnets are partially and

irreversibly demagnetised. This damaging effect is illustrated in Fig.4.17 where the flux lines enter and leave the magnet through the same pole. It applies for all types of rotors with peripheral magnets regardless whether the magnetic material is projected on the pole surface as shown in Fig.4.18, or is inset with the salient poles, Fig.4.19. The inset magnets appear as a large air gap in the direct axis while the interpolar iron acts as a small air gap in the quadrature axis.

4.7 Discussion

The comparison of the power capability and performance characteristics of each type of the three magnets is discussed. The use of rare earth magnets can lead to a drive system with higher output- to- weight ratio than any other practical alternative. The high efficiency and near unity power factor are essential for the ideal inverter fed system. The cost of the inverter is governed by the maximum KVA demand. A high efficiency power factor product results in a minimal KVA demand for a given load so reducing the inverter cost. The remagnetisation process confirms that the ferrite magnets can be magnetised easily without a special rig, simply by making use of the stator winding. This test may be extended to cover the rare earth magnets. It is clear from the results obtained that the rare earth magnets have a very significant potential for use in high performance drive systems (55,56), however one must bear in mind the cost comparison of the different types of magnet. In a total drive system the cost of

ferrite magnets is less than 1% . The rare earth magnets cost about 50% or more of the total cost, however it is expected that the cost of the new neodymium magnets will drop by a factor of about four. The finite element analysis results are used here as a supplement to those obtained from the tests for the provided comparison.

Unlike the peripheral- magnet types, rotors with buried magnets are mechanically robust and capable of operating at high speeds since the magnets are physically protected inside the core. The effects of the demagnetising forces during transient conditions on interior and peripheral-types of rotors have been illustrated.

Table 4.1.a: NdFeB machine.

Torque N.m	Output W	Efficiency %	Power factor	Efficiency x power factor
3.75	471	65.45	0.845 lead	0.5588
6.45	810	72	0.904 lead	0.6512
9.1	1131	76.4	0.949 lead	0.7255
11.85	1489	79.21	0.962 lead	0.7618
14.4	1810	79.37	0.974 lead	0.7731
17.1	2149	80.78	0.976 lead	0.7885
19.35	2431	80	0.978 lead	0.7824

Table 4.1.b: $SmCo_5$ machine.

Torque N.m	Output W	Efficiency %	Power factor	Efficiency x power factor
4.1	515	72.56	0.923 lead	0.6699
5.7	716	79.6	0.936 lead	0.745
8	1005	81.33	0.964 lead	0.7843
10.1	1269	82.1	0.965 lead	0.7923
12	1508	81.7	0.966 lag	0.7891
13.5	1696	78.68	0.96 lag	0.7553
14.9	1872	78	0.936 lag	0.7304

Table 4.1: Measured synchronous performance of the two rare earth machines at nominal rated voltage at f= 40 Hz.

Table 4.2.a: V = 1 p.u.

Current A	Output W	Efficiency %	Power factor	Efficiency x power factor
3	1103	76.58	0.827 lead	0.6335
4	1696	80.78	0.905 lead	0.7309
5	2228	81.54	0.958 lead	0.7813
6	2800	82.82	0.978 lead	0.81
7	3308	84.12	0.991 lag	0.838
8	3789	83.45	0.988 lag	0.8244

Table 4.2.b: V = 1.05 p.u.

Current A	Output W	Efficiency %	Power factor	Efficiency x power factor
3	877	71.84	0.779 lag	0.5595
4	1696	78.54	0.891 lag	0.765
5	2318	82.22	0.930 lag	0.765
6	2884	82.87	0.947 lag	0.7846
7	3365	82.77	0.957 lag	0.7929
8	3817	82.62	0.975 lag	0.8057

Table 4.2.c: V = 0.95 p.u.

Current A	Output W	Efficiency %	Power factor	Efficiency x power factor
3	594	60.59	0.589 lead	0.3571
4	1244	74.05	0.758 lead	0.5612
5	1922	78.16	0.888 lead	0.6938
6	2516	80.14	0.944 lead	0.7567
7	3054	80.78	0.964 lead	0.7799
8	3506	81.54	0.98 lead	0.7989

Table 4.2: Synchronous performance of the NdFeB machine at different voltage levels at f = 60 Hz.

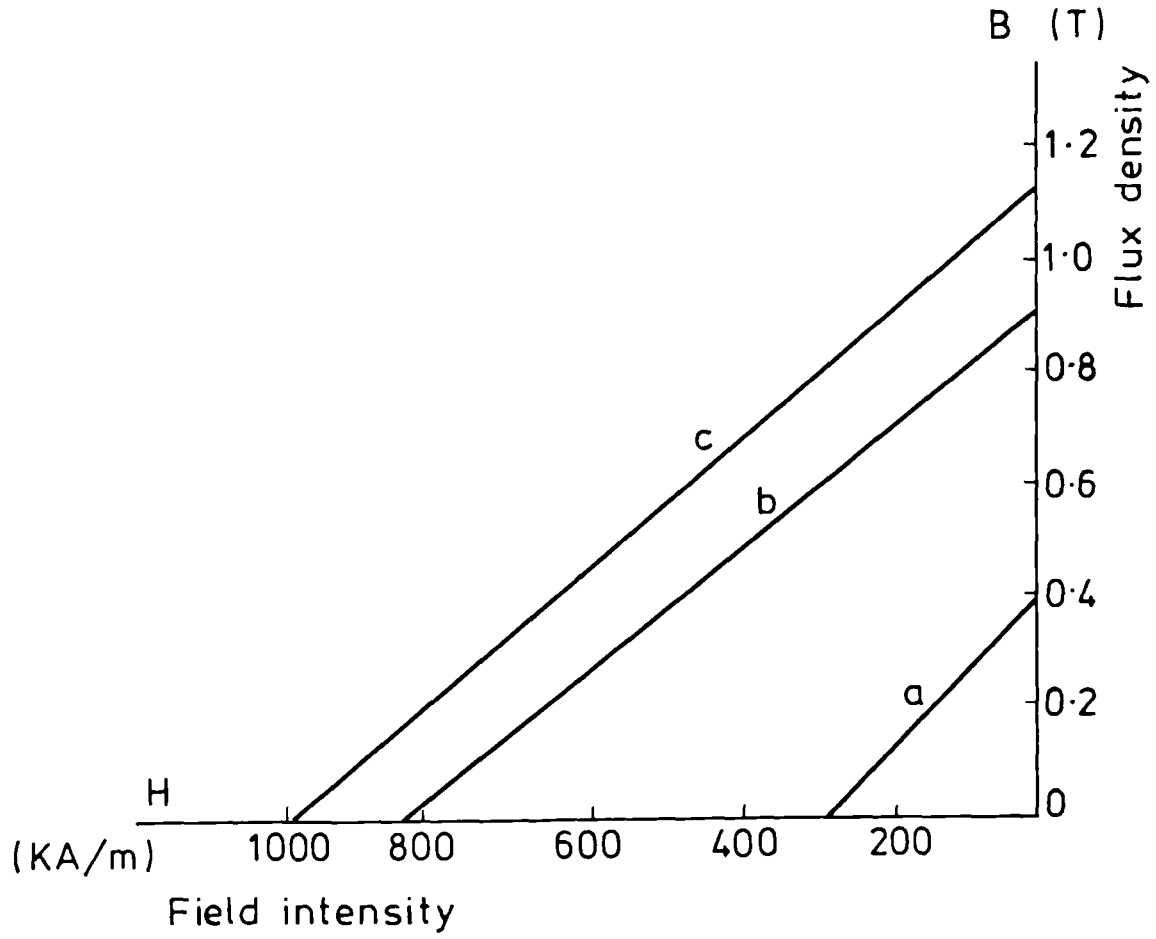

a... Ferrite magnet
b... $SmCo_5$ magnet
c... NdFeB magnet

Fig.4.1 Demagnetisation curves of the three magnetic materials used for machine excitation.

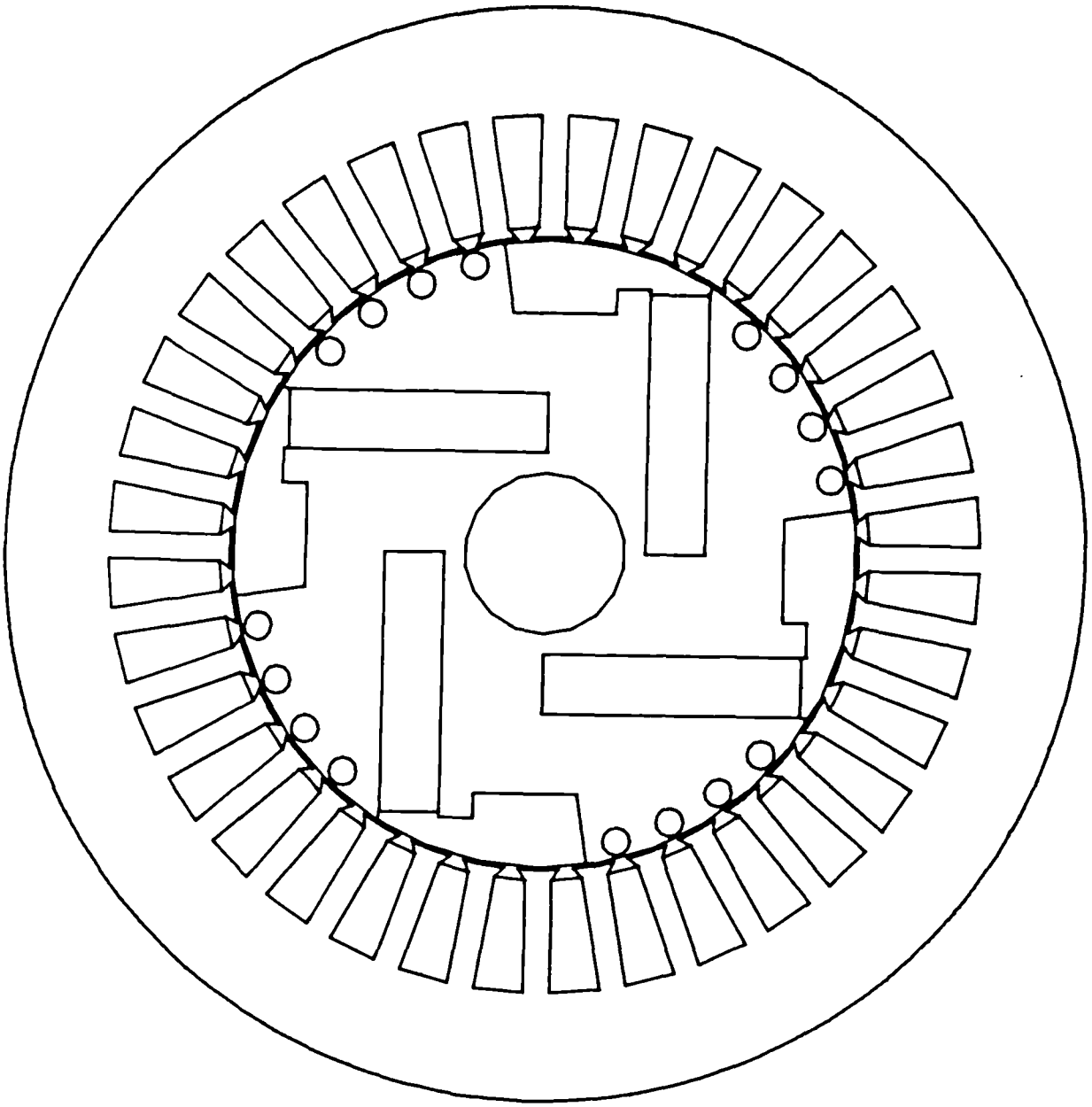

Fig.4.2 Configuration of the high- field self- starting synchronous machine with NdFeB magnets.

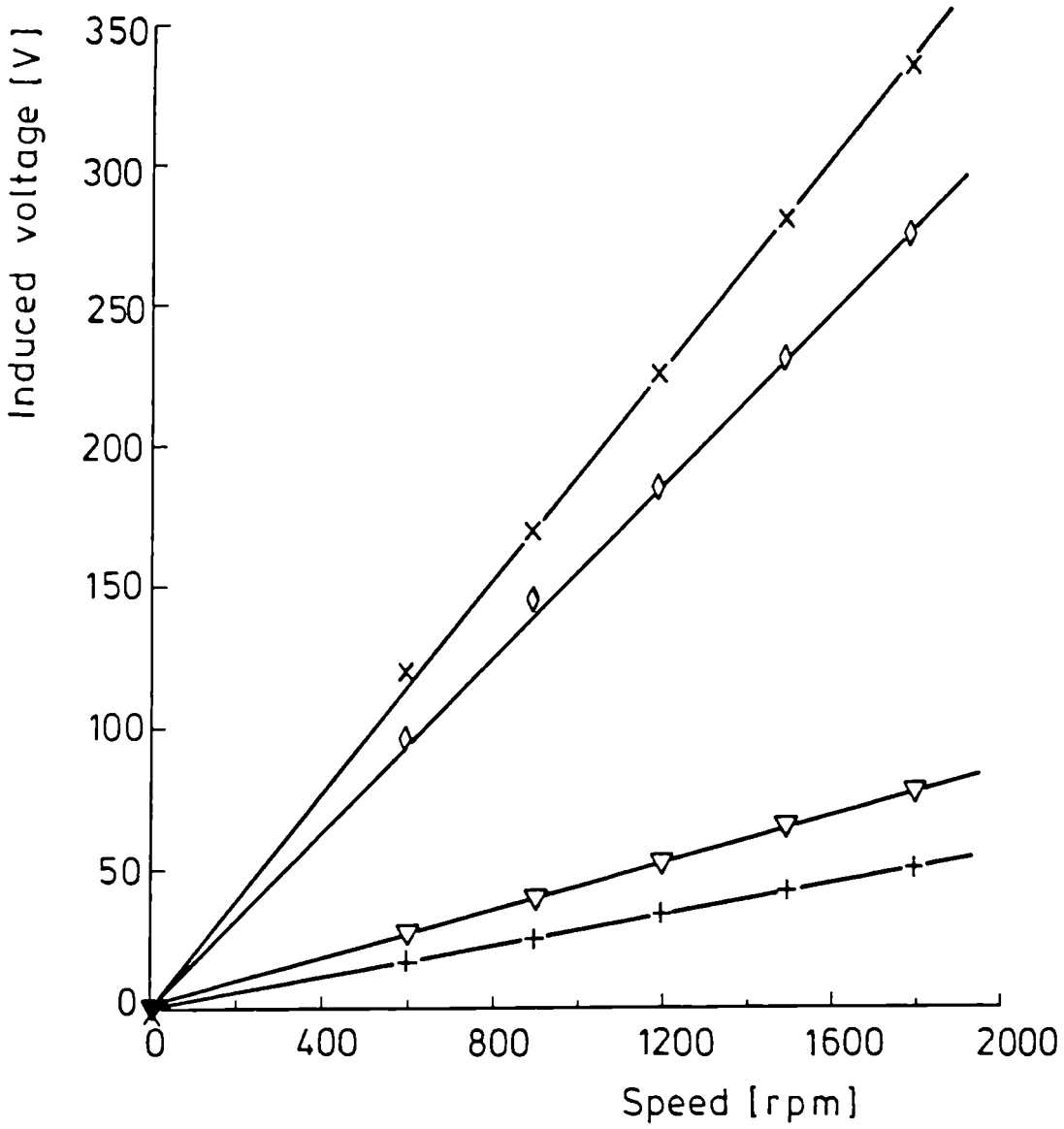

+...Ferrite machine
▽...Ferrite machine after remagnetisation
◇...$SmCo_5$ machine
x...NdFeB machine

Fig.4.4 Open- circuited generated voltage obtained from PM machines with different magnets.

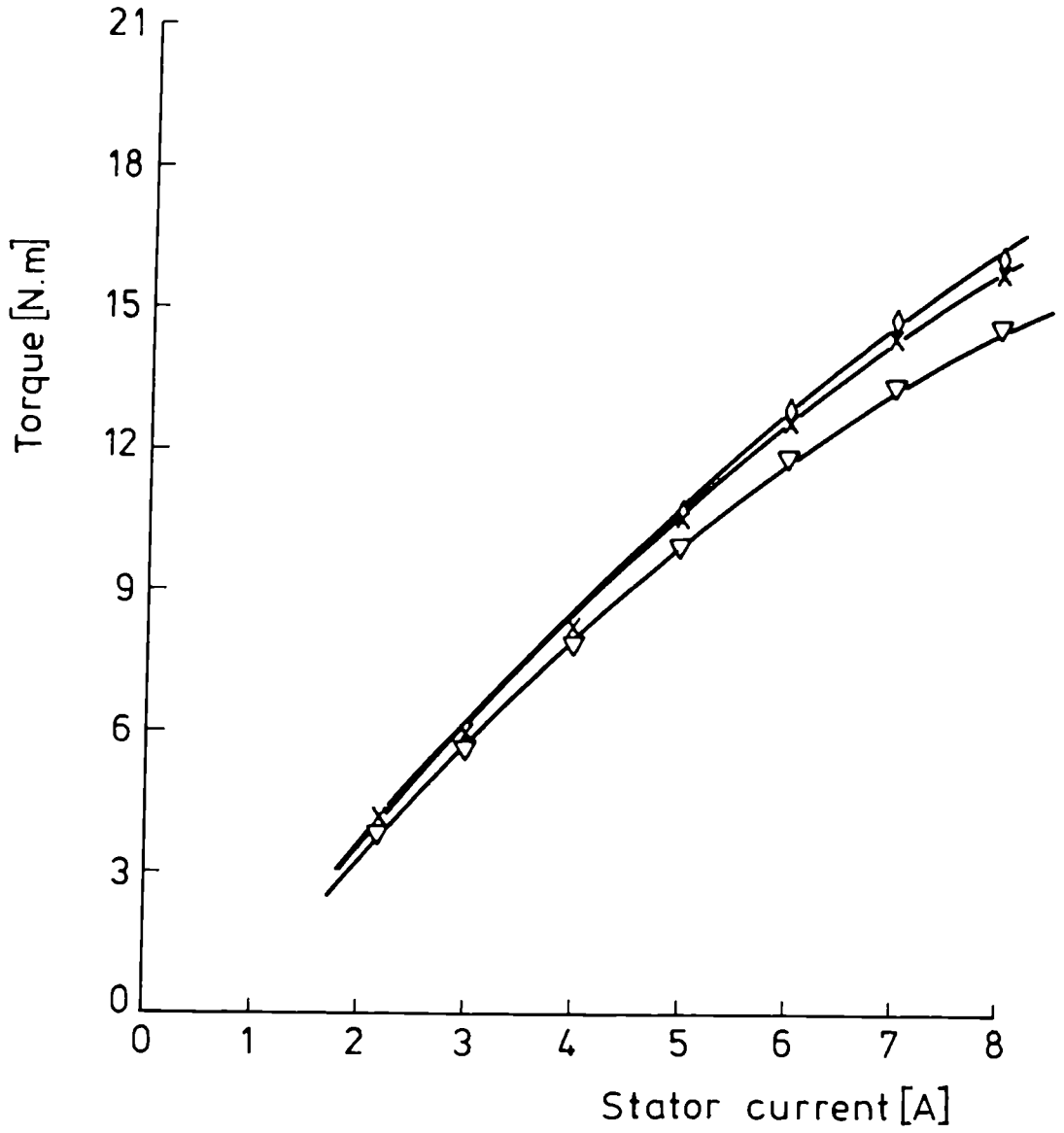

x...V = 0.95 p.u.
◇...V = 1 p.u.
▽...V = 1.05 p.u.

Fig. 4.5 Variation of the torque as a function of the stator current at different voltage levels.

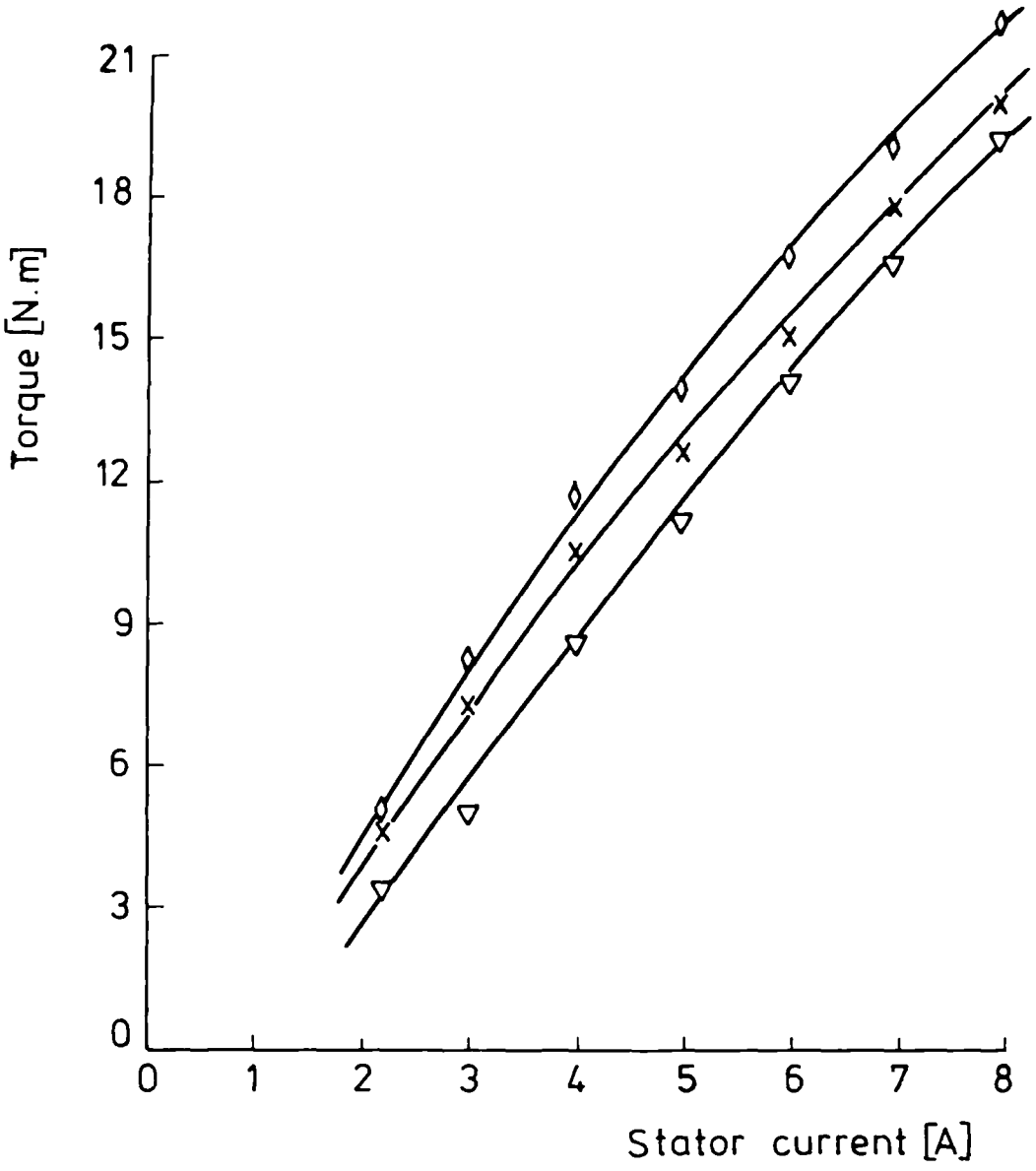

▽...V = 0.95 p.u.
x...V = 1 p.u.
◇...V = 1.05 p.u.

Fig. 4.6 Variation of the torque as a function of the stator current at different voltage levels. (NdFeB machine)

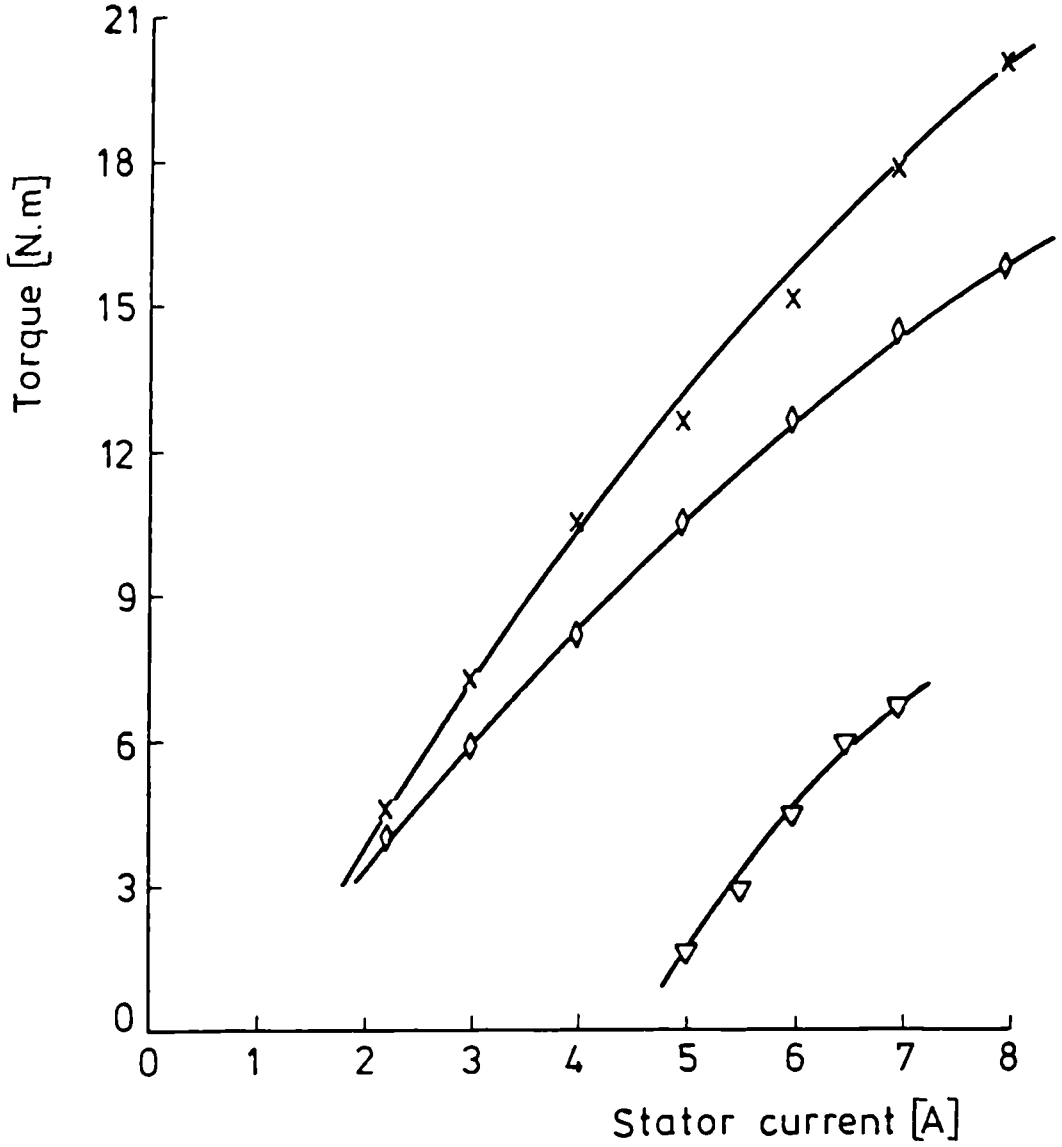

▽...Ferrite machine (V = 210 V)
◇...$SmCo_5$ machine (V = 1 p.u.)
x...NdFeB machine (V = 1 p.u.)

Fig.4.7 Comparison of the torque characteristic

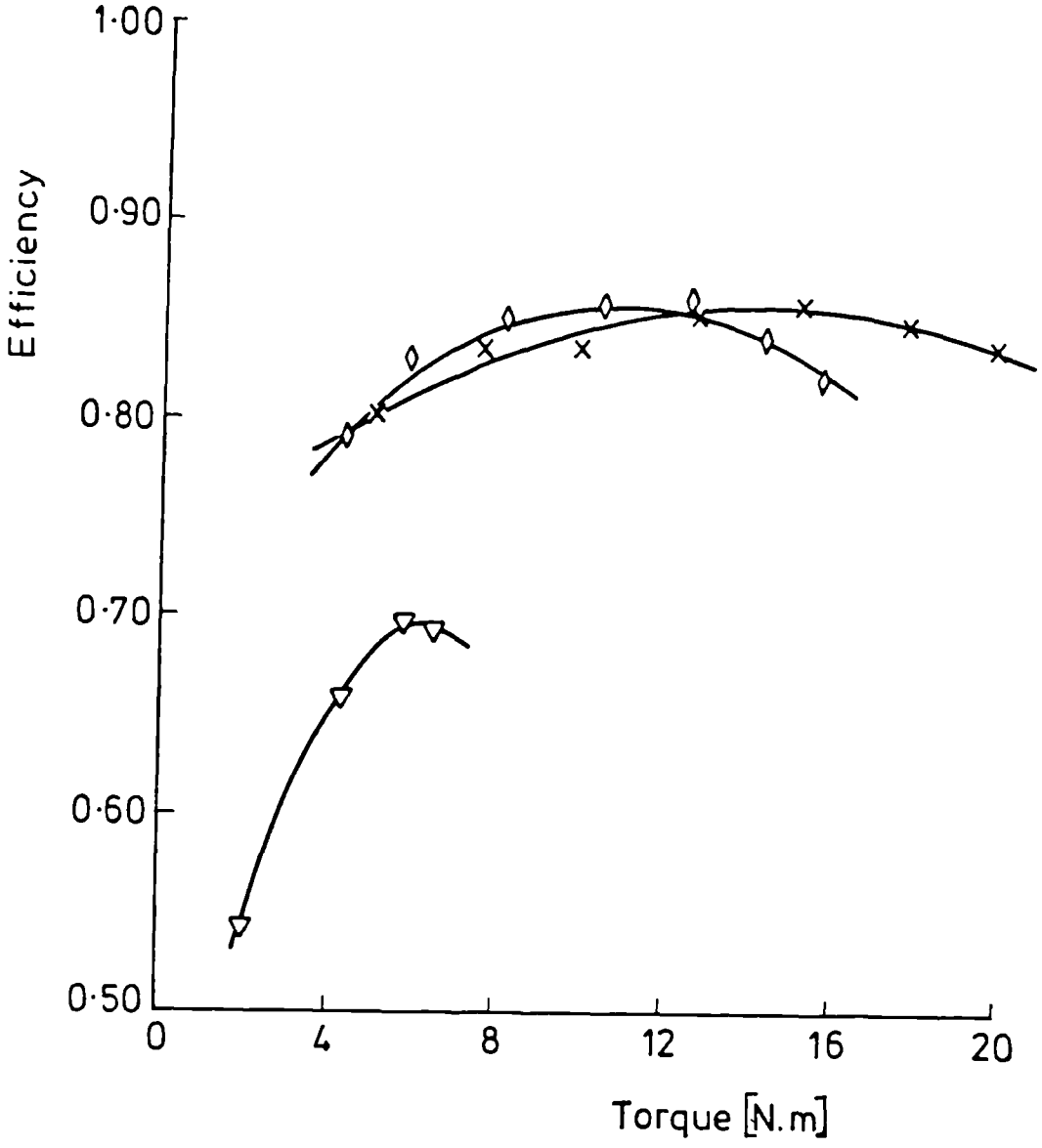

▽...Ferrite machine (V = 210 V)
◇...$SmCo_5$ machine (V = 1 p.u.)
x...NdFeB machine (V = 1 p.u.)

Fig.4.8 Efficiency variation with the torque for the three machines.

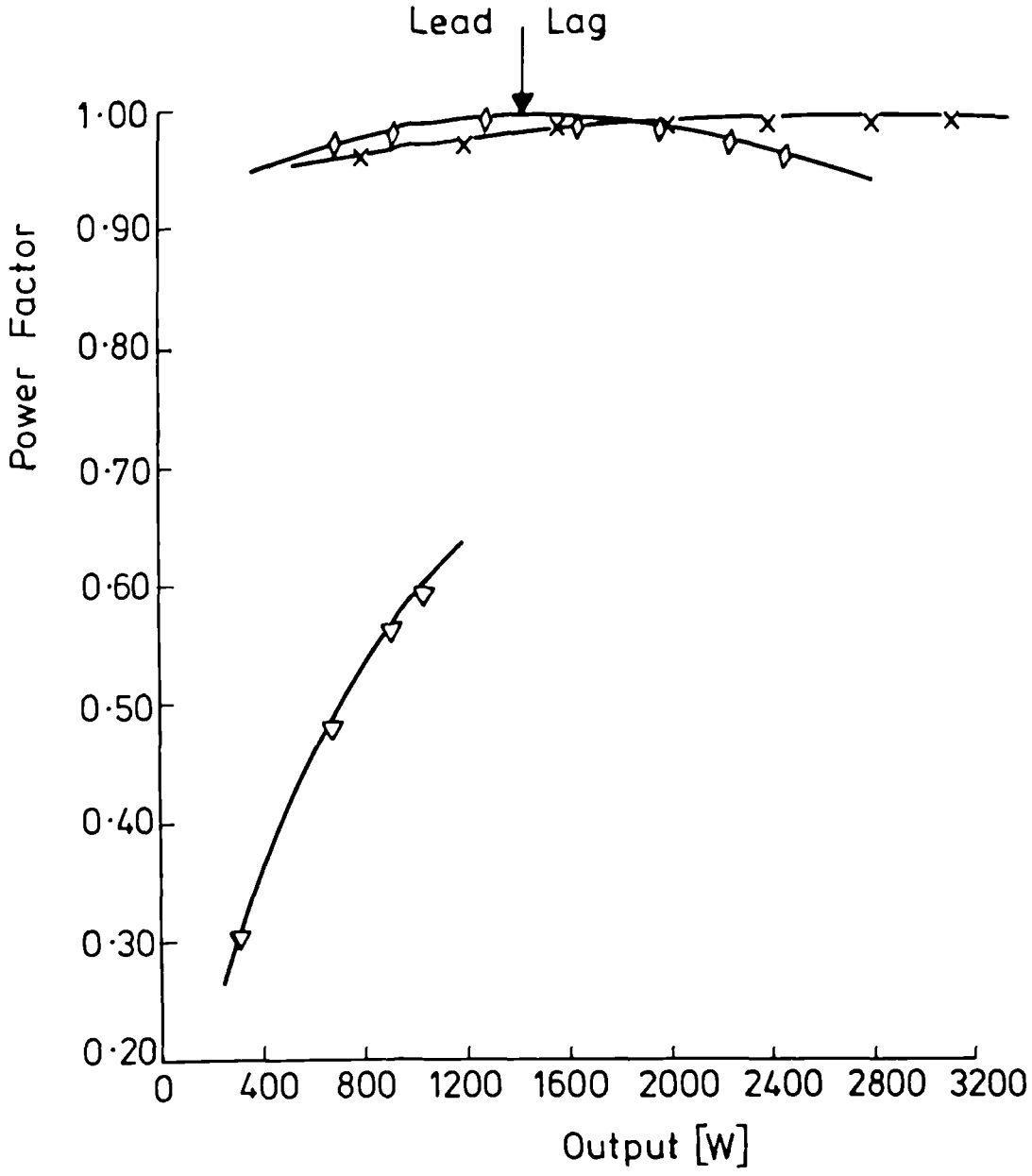

▽...Ferrite machine (V = 210 V)
◇...$SmCo_5$ machine (V = 1 p.u.)
x...NdFeB machine (V = 1 p.u.)

Fig.4.9 Power factor - output characteristics for each of the tested machines.

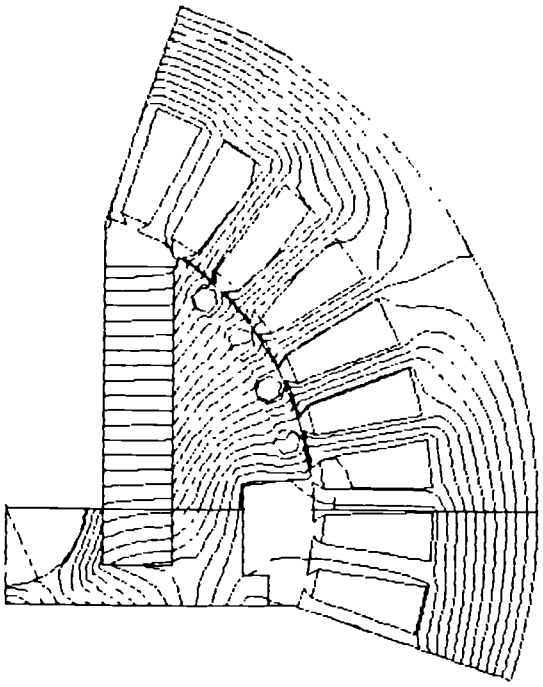

Fig.4.10 Flux distribution along one pole of the NdFeB machine at full load.

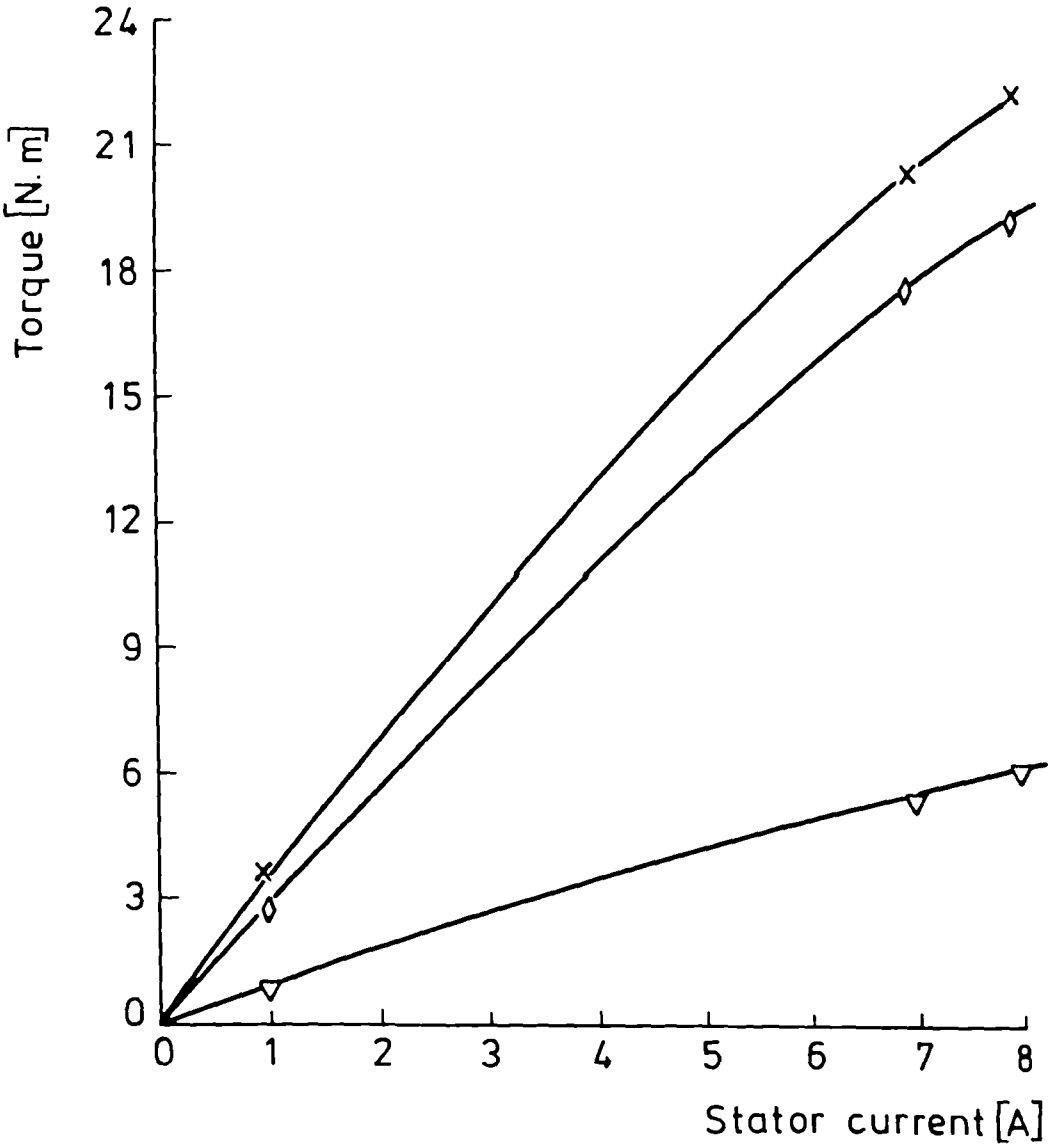

▽...Ferrite machine
◇...$SmCo_5$ machine
x...NdFeB machine

Fig.4.11 Computed results of the torque as a function of the stator current.

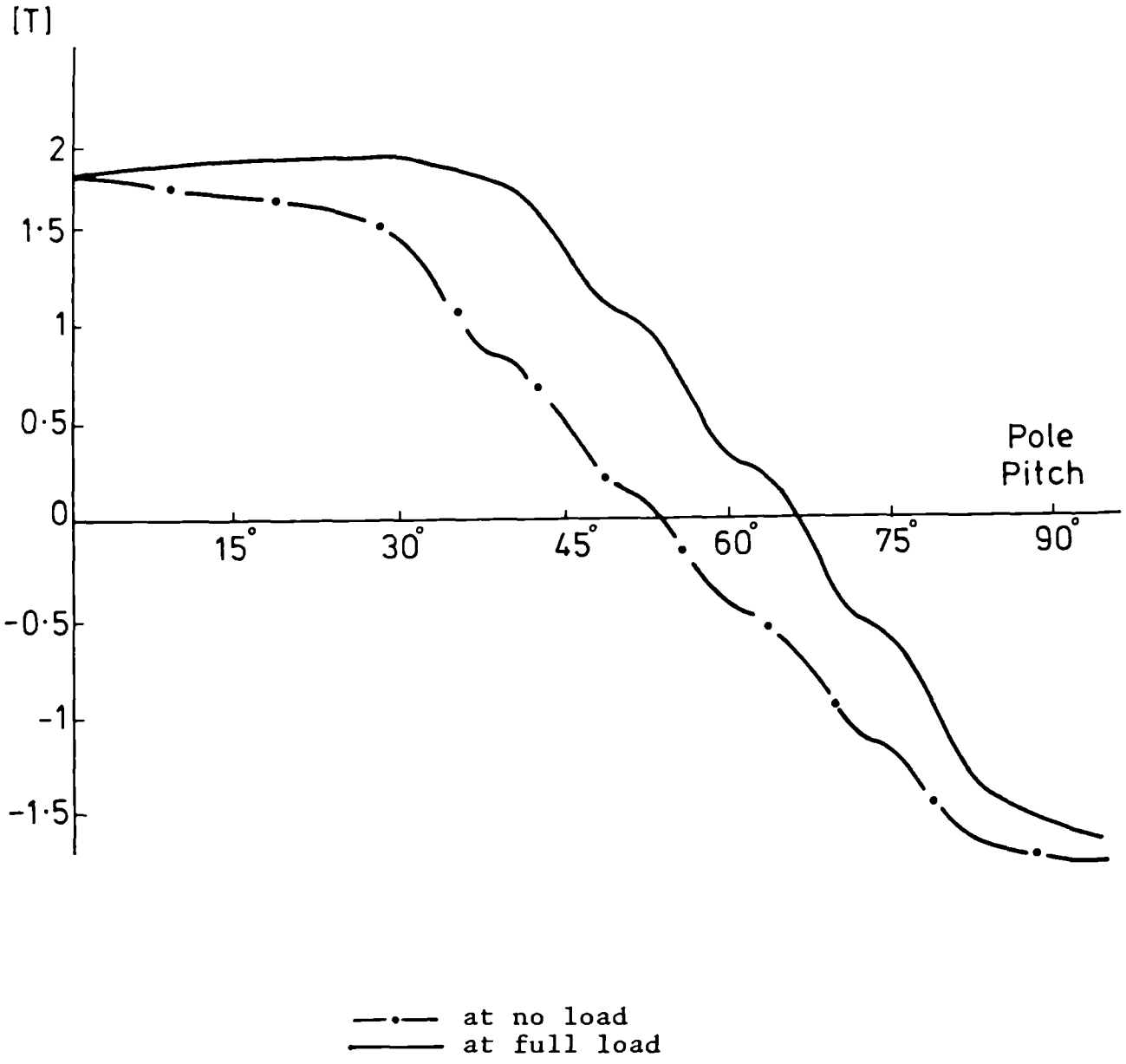

Fig.4.12 Variation of the vector potential throughout the air gap of the rotor with rare- earth magnets

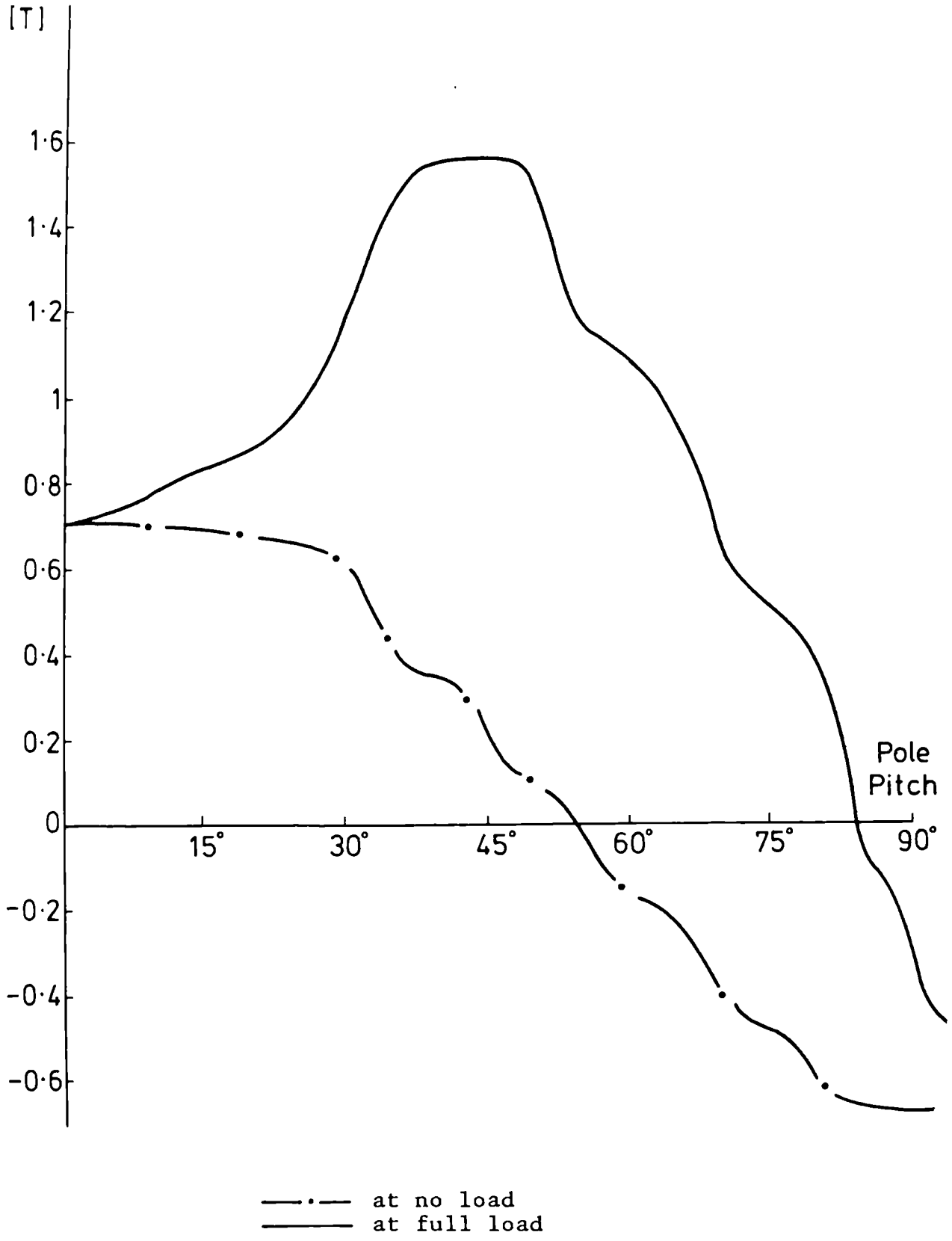

Fig.4.13 Variation of the vector potential throughout the air gap of the rotor with Ferrite magnets.

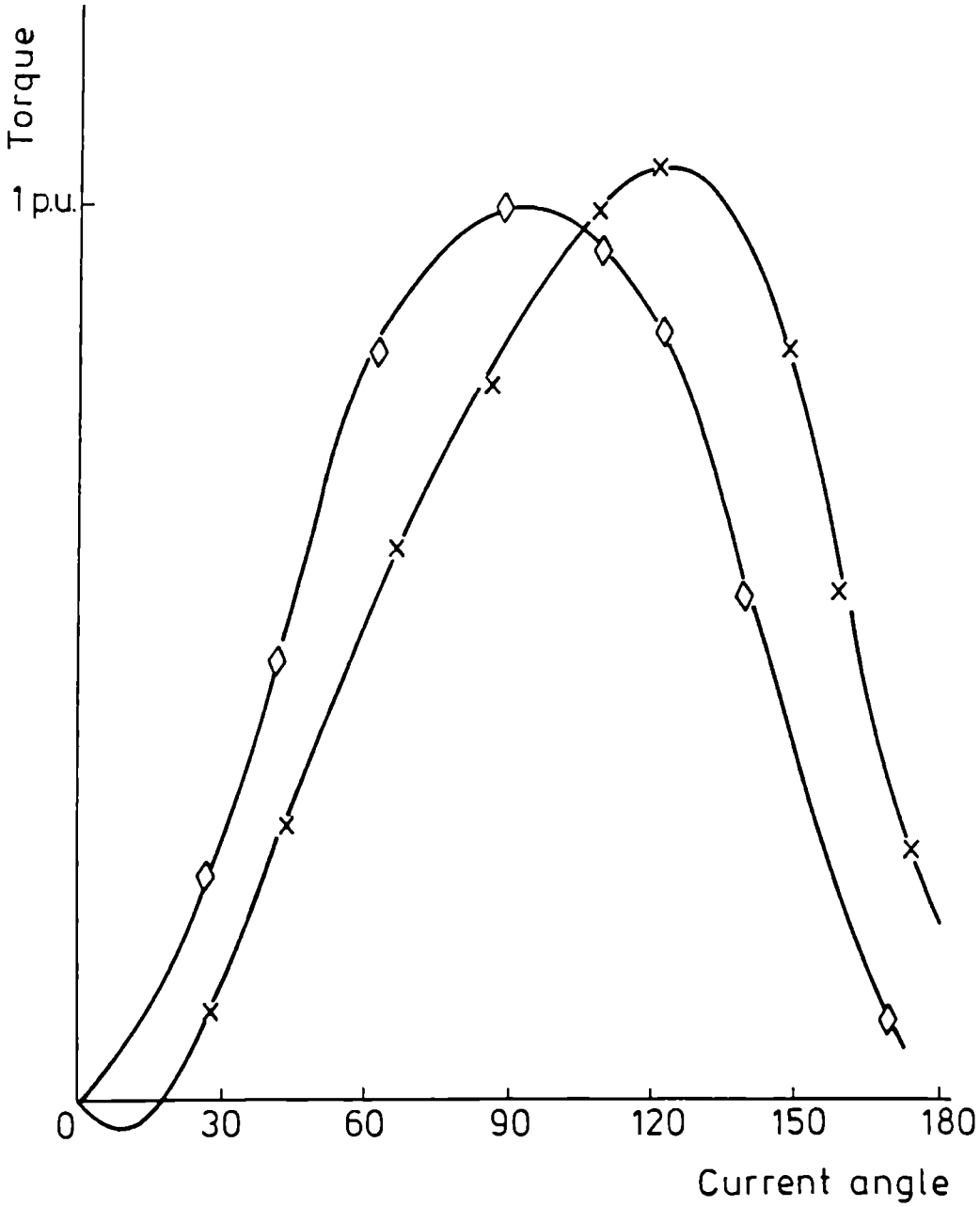

◇... round rotor
x... salient pole rotor

Fig.4.14 Torque versus current angle characteristics

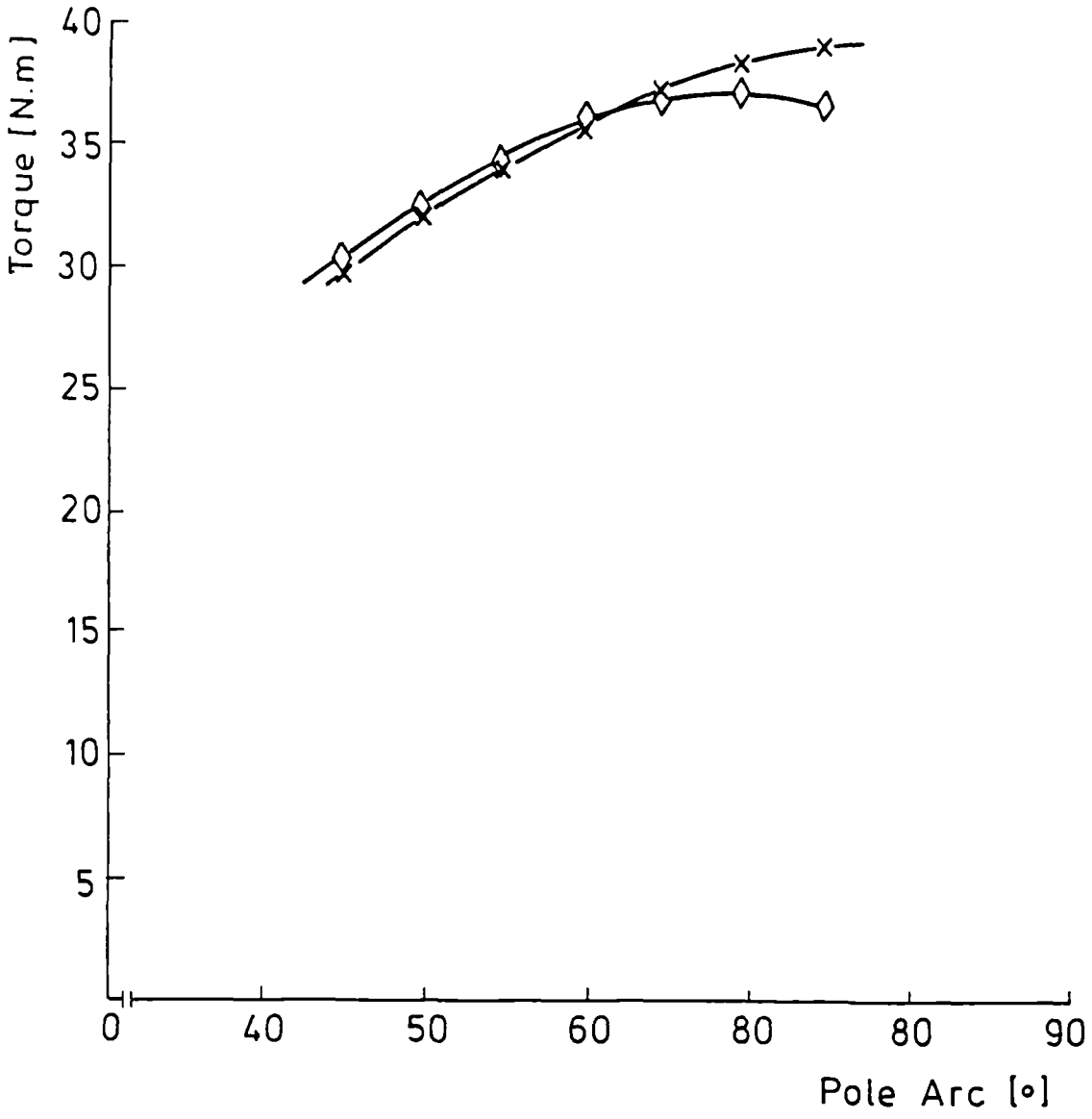

◇... rotor with peripheral magnets
x... rotor with buried magnets

Fig.4.15 Computed synchronous torque for different values of the pole arc.

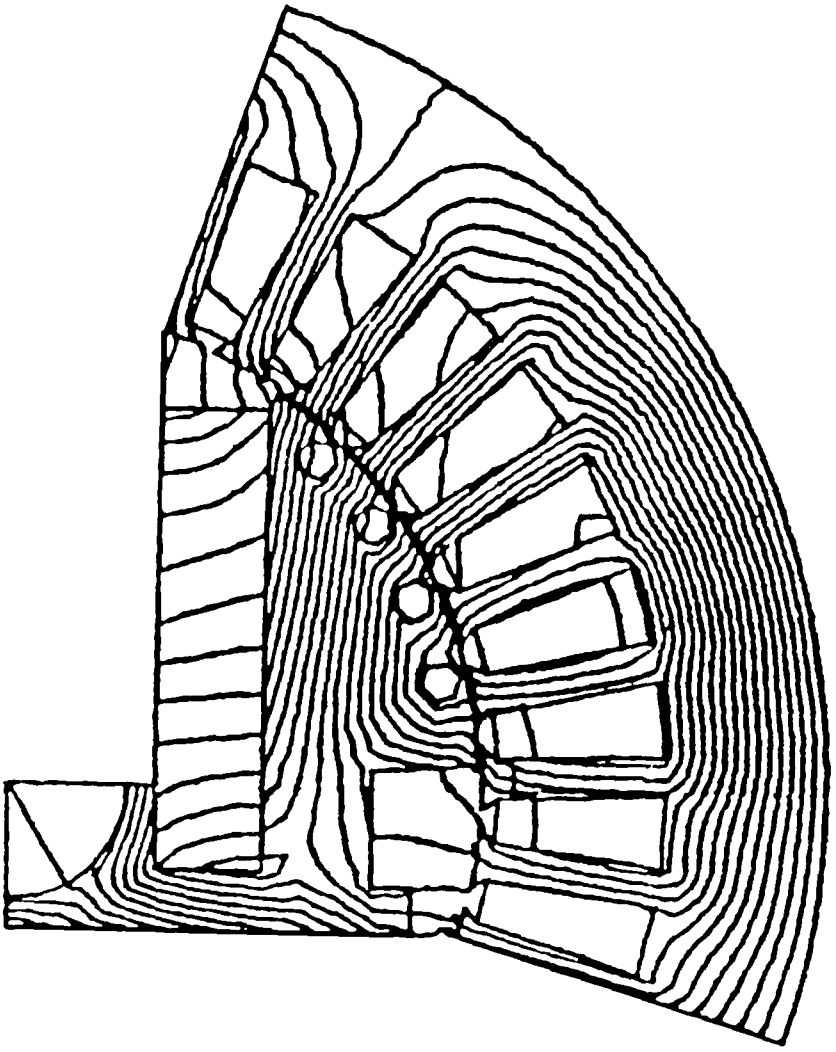

Fig.4.16 Flux distribution of PM machine with buried at transient demagnetising condition.
(I = 50 A) Rated current = 8 A

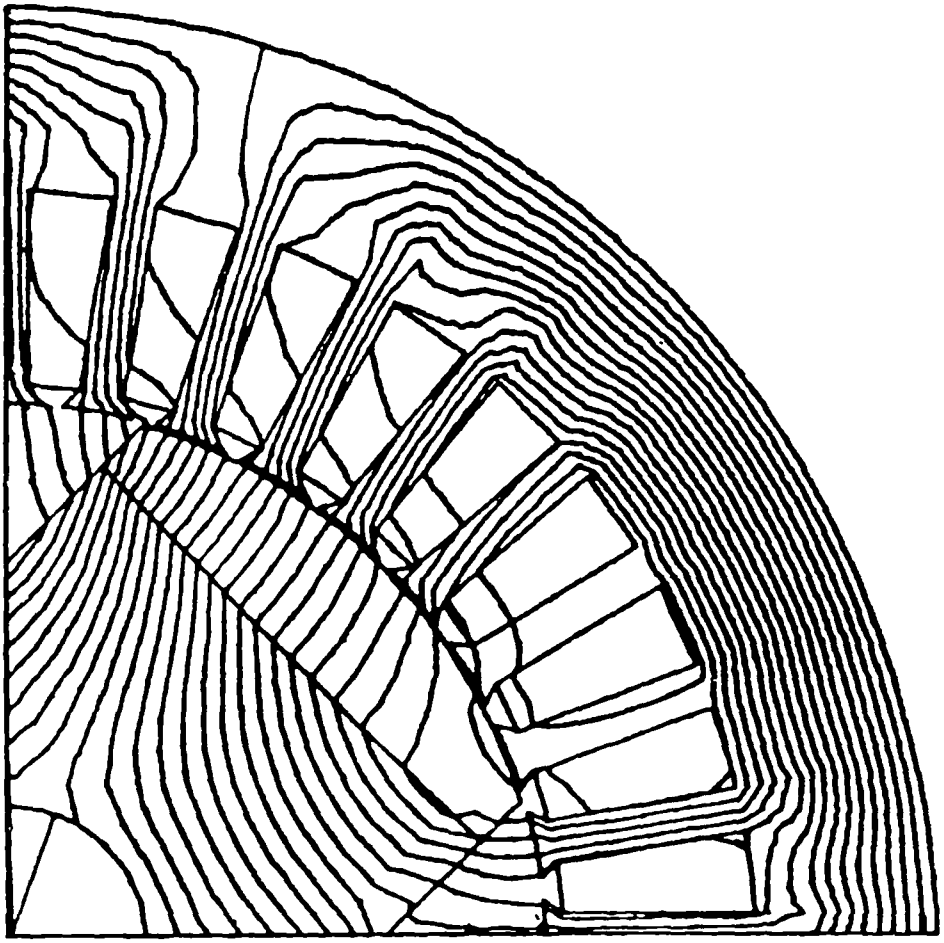

Fig.4.17 Demagnetising effect of transient current on the peripheral magnets.
(I = 50 A) Rated current = 8 A

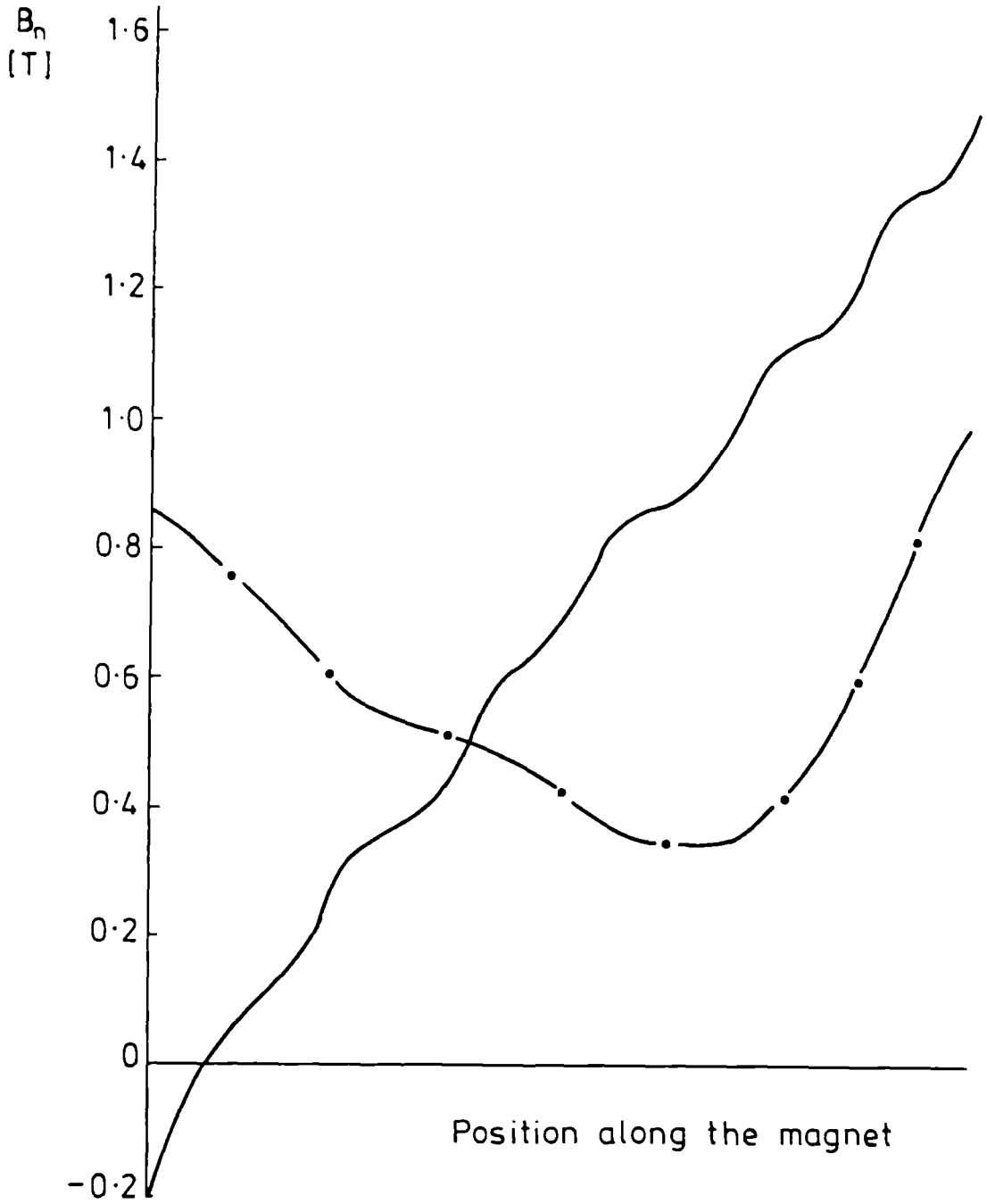

Fig.4.18 Variation of the magnet's operating point during high- current transient condition.

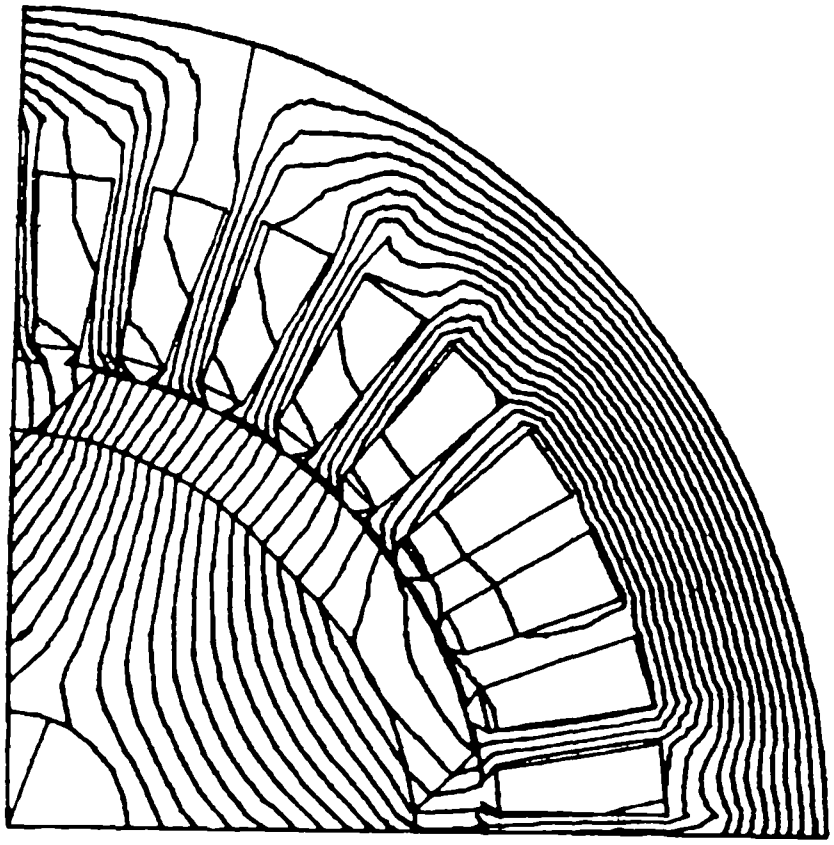

Fig.4.19 Flux distribution over one pole of machine with 'projected' magnets at overloading condition.

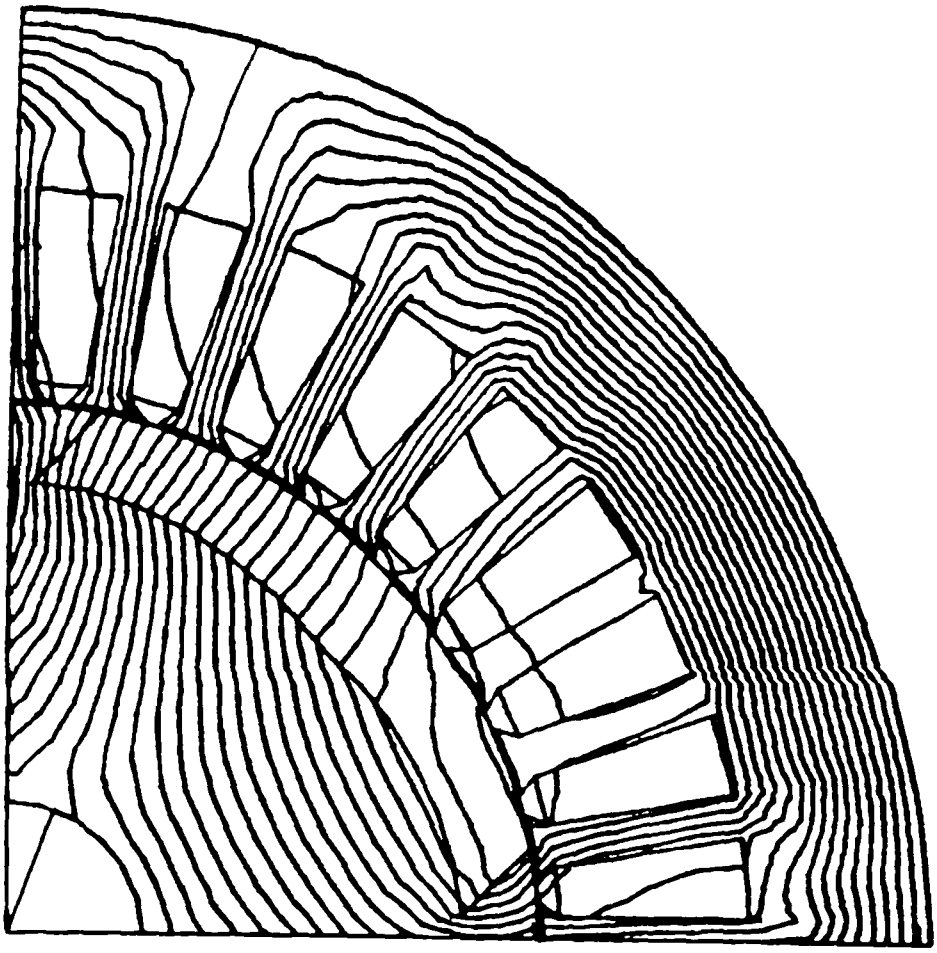

Fig.4.20 Flux distribution over one pole of machine with 'inset' magnets at overloading condition.

CHAPTER FIVE

INFLUENCE OF DESIGN PARAMETERS OF A SOLID CANNED SIX- POLE ROTOR WITH SKEWED MAGNETS

CHAPTER FIVE

INFLUENCE OF DESIGN PARAMETERS OF A SOLID CANNED SIX- POLE ROTOR WITH SKEWED MAGNETS

5.1 Introduction

The permanent magnet material in the rotor provides the machine with permanent field excitation. Therefore the characteristics of the machine will depend mainly on the rotor design parameters. There are several parameters in the rotor design which affect the general performance of the machine and these are worth optimising. A prototype six- pole machine with a solid- steel rotor has been constructed. The NdFeB magnets are radially positioned in the rotor core and are skewed with respect to the stator slots. A 3D- model of this prototype is shown in Fig.5.1. Another feature of this prototype is that the rotor is surrounded by a can. This can is made of inconel, a non-magnetic conducting material physically capable of withstanding the pressure of centrifugal forces at high speeds. The main design aspects of PM machine are:

1- characteristics of the magnetic material
2- configuration of the magnets (radial or parallel) and their positioning in the rotor.
3- pole- arc to pole- pitch ratio
4- width of the air gap
5- dimensions of the magnetic material

6- skew angle of the magnets

7- width of the iron bridge

8- nature of the canning material

Design variables 1 and 2 are discussed in chapter four while detailed analysis of variables 3, 4 and 5 is reported in (14,60,67). The variation of the pole arc is limited in this design because the saliency of the rotor depends on the magnet width. The effect of different types of magnets and their dimensions has been computed and the optimum values are chosen. Fig.5.2 shows the variation of the flux density in the air gap per unit volume with the magnet width for different magnetic materials. Influence of the design parameters 6 to 8 are discussed in this chapter. Although these parameters could result in a change in excess of 30% in the machine output for the same applied voltage and current, they are not independent variables. To achieve the required optimum design, a certain compromise amongst these parameters has been considered.

5.2 Effects of skewing the magnets

During its rotation the rotor poles are moving with respect to the stator teeth thus causing periodical variations and ripples in the waveform of the flux density accompanied by magnetic noise. Higher harmonics are also travelling relative to the stator at different speeds and therefore induce emf's of different frequencies in the stator winding. In machine design in general the commonly

used technique to minimise such phenomena is by skewing either rotor or stator slots or both, (47,68,90). In the design of permanent magnet machines similar results could be achieved by skewing the magnets inside the rotor. The magnets field is then distributed more uniformly over a distance equivalent to a fundamental electrical degree angle (α)

5.2.a Analytical determination of the skew factor

Skewing the magnets results in a phase shift and hence a reduction in the induced emf. This reduction is represented in the calculations by the skew factor which is proportional to the angle of inclination of the magnets. The analytical derivation as provided in (69,90) represents the fundamental skew factor by the following expression:

$$k_{sk} = \frac{\sin \frac{\alpha}{2}}{\frac{\alpha}{2}} \tag{5.1}$$

and the factor for the n^{th} harmonic as:

$$k_{skn} = \frac{\sin n(\frac{\alpha}{2})}{n\frac{\alpha}{2}} \tag{5.2}$$

5.2.b Numerical derivation of the skew factor

Skew factor could as well be derived numerically by considering the phase shift of α° of the terminal voltage as seen in Fig.5.3 where V_i is the original induced volt-

age and V_s is the voltage induced by the skewed magnets such that:

$$V_{s1} = V_{i1} \cos(\frac{\Delta\alpha}{2})$$

$$V_{s2} = V_{i2} \cos 2(\frac{\Delta\alpha}{2})$$

. . .
. . .

$$V_{sm} = V_{im} \cos m(\frac{\Delta\alpha}{2})$$

giving a total of:

$$V_s = \sum_{x=1}^{m} (V_{ix} \cos x(\frac{\Delta\alpha}{2}))$$

$$\text{where } V_{i1} = V_{i2} = \ldots = V_{im} = \frac{V_i}{m} \qquad (5.3)$$

and $\Delta\alpha = \frac{\alpha}{m}$, m being the number of subdivisions. Substituting from equation 5.3 the per- unit skewed voltage is:

$$V_s = \frac{V_i}{m} \sum_{x=1}^{m} (\cos x(\frac{\Delta\alpha}{2})) \qquad (5.4)$$

The skew factor is then expressed as:

$$K_{sk} = \frac{V_s}{V_i} \qquad (5.5)$$

The values of the skew factor obtained by both methods are listed in Tables 5.1 and 5.2. Table 5.1 also shows

the variation of the skew factor as the angle of inclination (skewing angle) of the magnets varies.

Skewing the magnets by one slot pitch eliminates the periodic variations in the total flux per pole and prevents the generation of slot harmonics of the 11^{th} and 13^{th} order, (75,80). Figure 5.4 shows the effect of skewing in eliminating all the tooth ripples in the waveform of the open- circuit generated voltage. It has been observed that the machine is quieter. This might be related to the reduction of the harmonics causing this noise. Skewed magnets are also advantageous in reducing the pulsation of the starting current and torque because the rotor, even with powerful rare- earth magnets, is not locked at any pole position before starting.

In the 2D- finite element analysis the effect of skewing can only be accounted for by the introduction of the skewing factor to the results obtained.

5.3 Effect of the non- magnetic rotor shaft

It is well known that the iron bridge affects the mechanical strength of the machine, (13,52). Since the six pole rotor, whose parameters are under investigation, is designed for high- speed applications, the mechanical strength becomes a critical factor in determining the maximum speed at which the machine can be operated. The variation of the iron- bridge width, or in another words the variation of the non- magnetic shaft diameter, has the following consequences:

a- With a smaller iron bridge the flux leakage around the magnets edges is reduced because less flux is now required to saturate the path. As a result more flux is driven across the air gap. To give an idea of the changes in the flux levels inside the machine Figures 5.5 and 5.6 show the flux plots at full load. Fig.5.5 represents the machine with maximum iron- bridge i.e. without any non-magnetic shaft while Fig.5.6 shows the design where the magnets are attached to the non- magnetic shaft hence eliminating the leakage entirely. A comparison of these two figures indicates that though the operating point of the magnets has not changed ($0.4 < B < 0.8$), the flux density inside the machine with the non- magnetic shaft has risen significantly. The fundamental air gap flux density has increased by 22%. The graph in Fig.5.7 represents the variation in the computed synchronous torque with the gradual reduction of the iron bridge. With maximum iron bridge width the saturated paths under the magnets have already formed a certain zone at the rotor centre where no flux is passing. The reduction in the iron- bridge, therefore, does not affect the torque values as long as the non- magnetic shaft diameter does not exceed this zone. Beyond this point any increase in the shaft diameter results in greater synchronous torque. The total increase of the torque is found to be around 23%.

b- With constant voltage and current in the stator winding the increase in the field excitation decreases the internal load angle and hence the power factor is closer to unity or changes from leading to lagging operation.

c- The absence of the iron bridge, or its minimisation, might have an undesirable influence on the machine mechanical strength since it holds all the rotor parts together. Canning the rotor is very useful in overcoming the centrifugal forces, its effects are discussed in the following section.

5.4 Experimental measurements and tests results

The prototype rotor is fitted into a standard six pole stator with three phase single- layer winding. The same experimental equipment described in section 4.2 is used. The rotor is initially made oversize and subsequently turned down and finally shrunk into the non- magnetic can. To summarise the air gaps are as follows:

stage 1 ... g = 0.2 mm

stage 2 ... g = 0.8 mm

stage 3 ... g = 0.8 *mm (including can thickness)*

For each of these stages the machine performance has been tested at different load conditions for various applied voltages and frequency levels. These voltages are chosen such that the machine operates around unity power factor, that is at both leading and lagging operations as shown in Fig.5.8. At terminal voltages below the rated value the machine is overexcited and is operating at leading power factor. For voltages above the rated value the machine becomes underexcited and operates at lagging power factor. The level of the applied voltage also determines the pull- out torque and plays an important role

in the control since the magnet excitation is constant. The constant- current tests are carried out to determine the maximum output torque of the machine for each load. This value of the torque is used to compare the experimental results with those of the computation. The characteristics in Fig.5.9 show that the terminal voltage corresponding to the maximum torque increases with the load. The peak values of the torque characteristics shown in Fig.5.10 are used for comparing the test results with those obtained from the numerical analysis since they correspond to a zero current angle. The synchronous performance of this prototype has been tested with different loading conditions at frequencies 30, 50, and 75 Hz. Variation of the output with the stator current at each of these frequencies is shown in Fig.5.12. The torque characteristics for different air gaps have already been illustrated in Fig.5.10.

A comparison of the performance of the skewed- magnet rotor with that of a previous design has been carried out. Both rotors are tested using the same induction- motor stator, the same air gap width of 0.2 mm, and the same amount of magnetic material. Figure 5.13 illustrates the variation of the output torque with the stator current. The lower values of the machine with skewed magnets are due to the significant flux leakage at the rotor centre which consumes up to 30% of the field flux. Skewing the magnets results in another 5% reduction as shown earlier.

Otherwise, both machines show the same trend in operating at a power factor close to unity and with high efficiency.

5.5 Influence of the rotor can

For high- speed applications the design of the permanent magnet machine should take into account the effects of the centrifugal forces which could cause the rotor to disintegrate. Consideration is given to the use of both a non-magnetic and ferromagnetic (solid steel) can around the rotor.

5.5.a Assessment of a non- magnetic can

The fitted rotor can is made of inconel, a non- magnetic conducting material. The aspects of the canning are as follows:

1- In the initial design an air gap width of 0.2 mm has been chosen. The introduction of the inconel non- magnetic can virtually increases the air gap width to 0.8 mm so reluctance of the magnetic circuit increases with a corresponding reduction in the gap density and therefore core saturation. This has been compromised in the design stage by a slight increase in the magnet volume. As a result of this precaution the value of the air gap flux density has dropped by only 20% for a 400% increase in the air gap.

2- Smaller iron loss is another obvious result of the reduced saturation. These losses are slightly higher for the canned rotor, as shown in Fig.5.14, because of the eddy currents that are flowing in the closed conducting

surface of the can. This is slightly overcome by the lower windage loss along the smooth surface of the can.

3- The canned rotor is mechanically capable of operating at high speeds. The results in this work, however relate to a maximum operating speeds of 5000 rpm.

5.5.b Ferromagnetic can

Computation has been carried to examine the influence of a ferromagnetic can on the machine performance. The model used for this purpose differs from the original one (with air gap g = 0.2 mm) by the thin path between the magnet and the air gap at the rotor saliency. The computed results are shown in Table 5.3. From these results it is evident that the change from the inconel to the ferromagnetic can would increase the rotor field due to the drop in the total reluctance in the magnetic circuit. The fundamental air gap density would increase by 11% while the torque would rise by 13%. The internal load angle would drop by 36%. With ferromagnetic can the machine performance is almost the same as that obtained with the narrow air gap (g = 0.2 mm). The thin path becomes inevitably saturated and hence does not affect the overall performance of the machine. The flux leakage across the saturated path as shown in Fig.5.15 is less than 5% of the total magnet flux.

5.6 Conclusion

This chapter describes the effects of new design parameters on the performance of the machine. A prototype

rotor has been built and tested. It has been shown that skewing the magnets, though reduces the induced voltage by few percentage (up to 5%), could be very effective in reducing the harmonics and ridding the flux waveform of all the slots ripples. The skew factor expresses the reduction in the induced voltage and other machine characteristics. This factor is determined analytically and numerically. The numerical derivation as provided in this chapter could be used for slots skewing as well.

The influence of the non- magnetic shaft is also discussed. The computational results show that the reduction in the bridge width increases the field in the rotor. Air gap flux density as well as the synchronous torque have also increased. It has also been shown that enclosing the rotor in a can would provide the machine with enough mechanical strength that enables it to operate at high speeds. Moreover, the choice of the material of the can has a significant influence on the overall performance of the machine. Computation has shown that the machine with a ferromagnetic, solid steel, can being fitted could have higher gap flux density and thus higher torque because only a low percentage of the field flux is used to saturate the thin path above the magnets. Experimental tests have been carried out and a comparison among the obtained results is provided. The solid- steel canned rotor is found to be very stable and is easy to manufacture.

m \ α°	15	30	45	60	75	90
1	0.991	0.966	0.9238	0.866	0.7934	0.7071
10	0.9967	0.9868	0.9705	0.948	0.9194	0.8852
50	0.9971	0.9883	0.9737	0.9535	0.928	0.8974
100	0.9971	0.9884	0.9741	0.9542	0.9291	0.8988
1000	0.9971	0.9885	0.9744	0.9548	0.93	0.9
10000	0.9971	0.9886	0.9745	0.9549	0.93	0.9

Table 5.1: Results of the numerical determination of the skew factor for different skewing angles (α) in electrical degrees.

α°	15	30	45	60	75	90
k_{sk}	0.9971	0.9886	0.9745	0.9549	0.9301	0.9

Table 5.2: Results of the analytical determination of fundamental skew factor. (n=1)

	g=0.2 mm	g=0.8 mm inconel can	g=0.8 mm ferromag. can
fundamental gap flux density B_f (T)	1.27	1.09	1.24
internal load angle δ_i	7.9	13.4	8.2
synch. torque T_s (N.m)	10.2	8.55	9.9

Table 5.3: *Influence of the canning material on the* machine performance

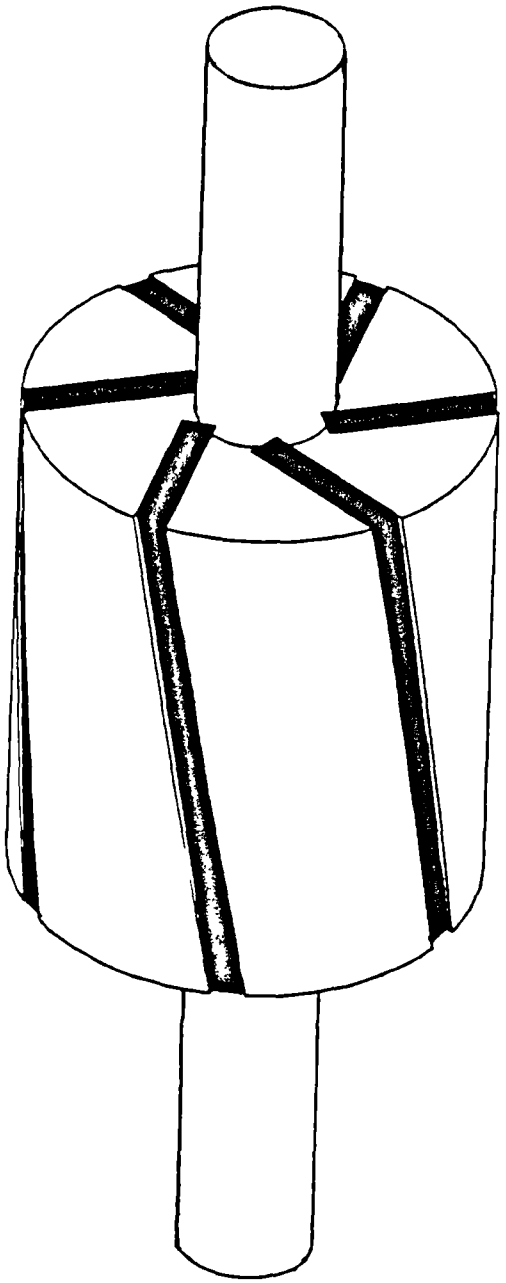

Fig.5.1 3D- configuration of solid- steel rotor with skewed neodymium magnets.

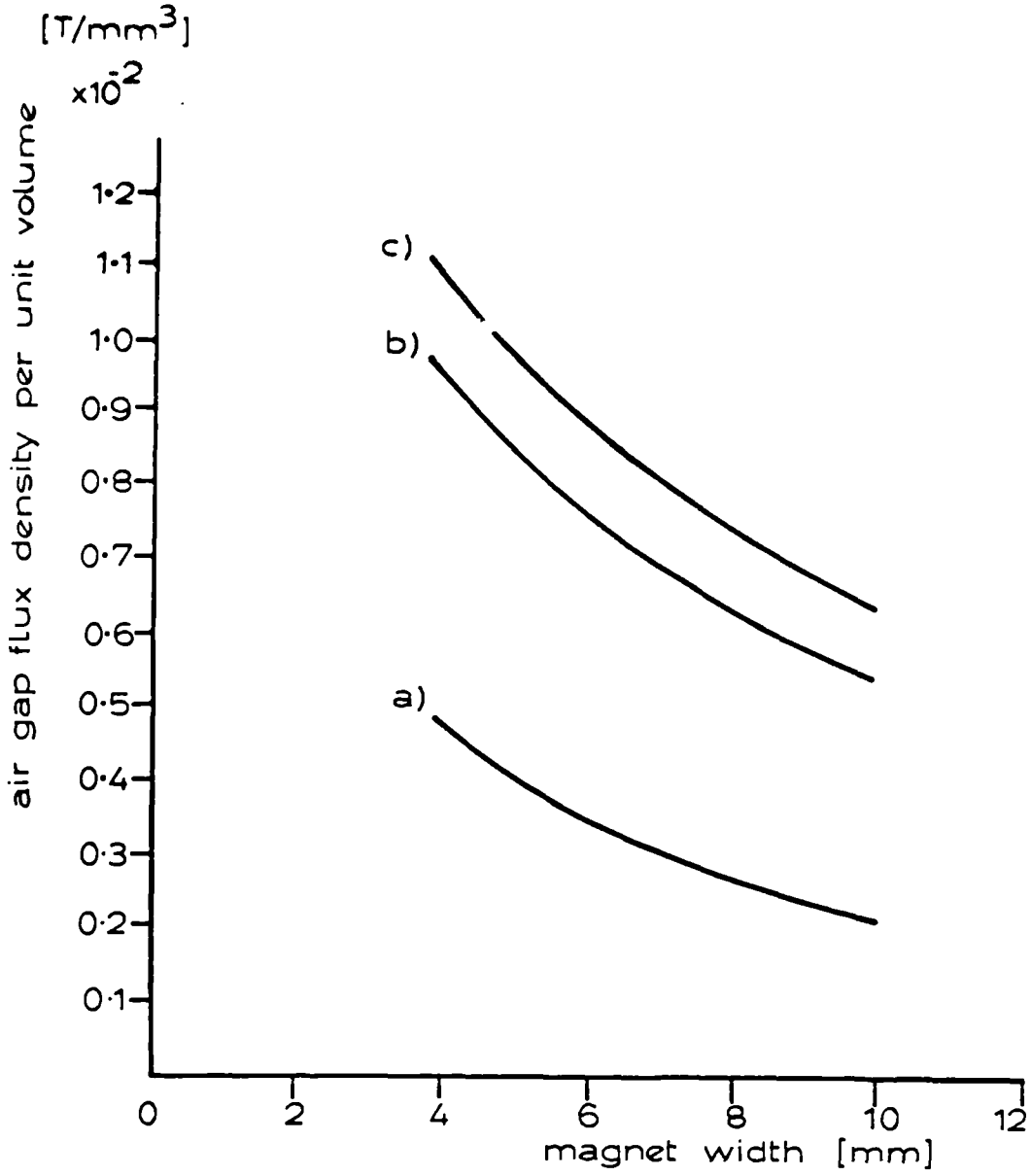

a... Ferrite magnet
b...$SmCo_5$...magnet
c... NdFeB magnet

Fig.5.2 Variation of the air gap flux density per unit volume with the magnet width for different magnet materials

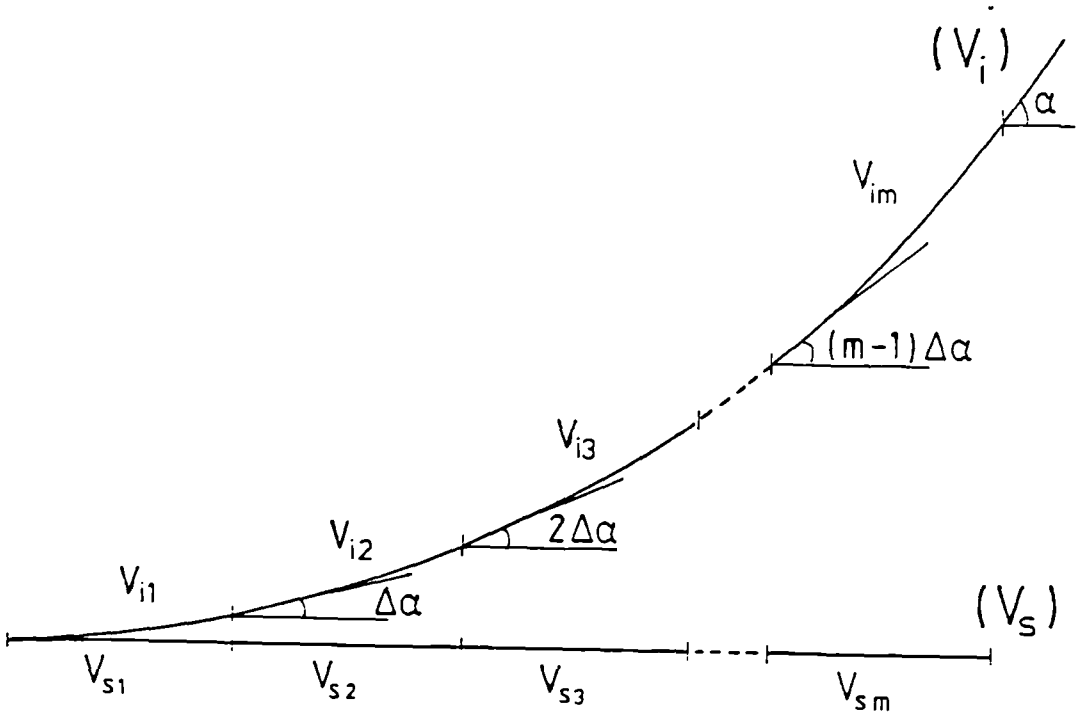

Fig.5.3 Magnet skewing: Numerical derivation of the phase shift of the induced voltage.

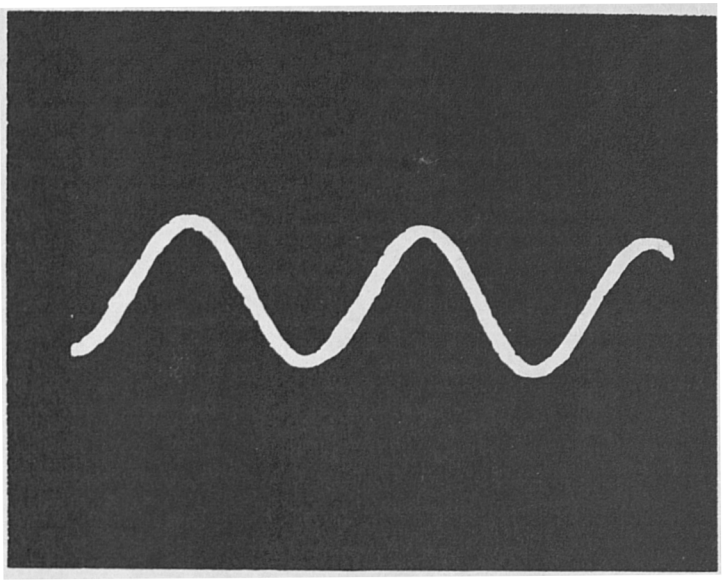

(a)

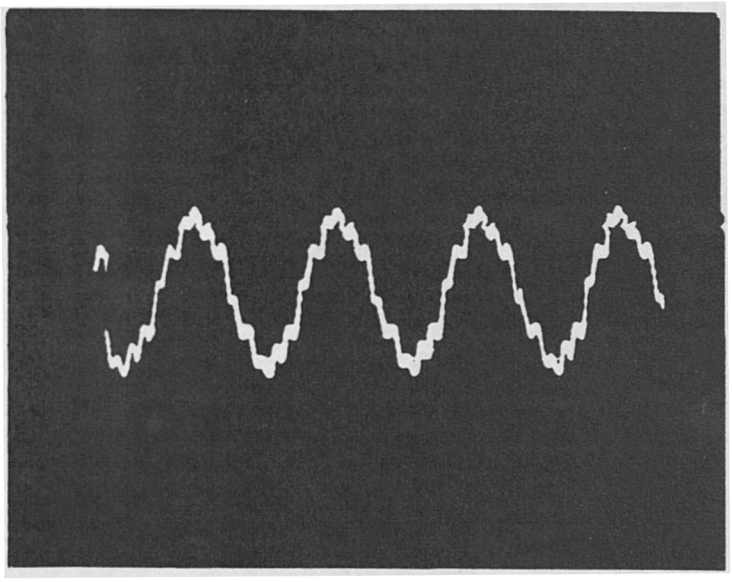

(b)

a... rotor with skewed magnets
b... conventional PM rotor

Fig.5.4 Open- circuit generated voltage waveforms at f = 50 Hz.

---- B>1.2 T
---- 0.8< B <1.2 T
---- 0.4< B <0.8 T
---- B <0.4 T

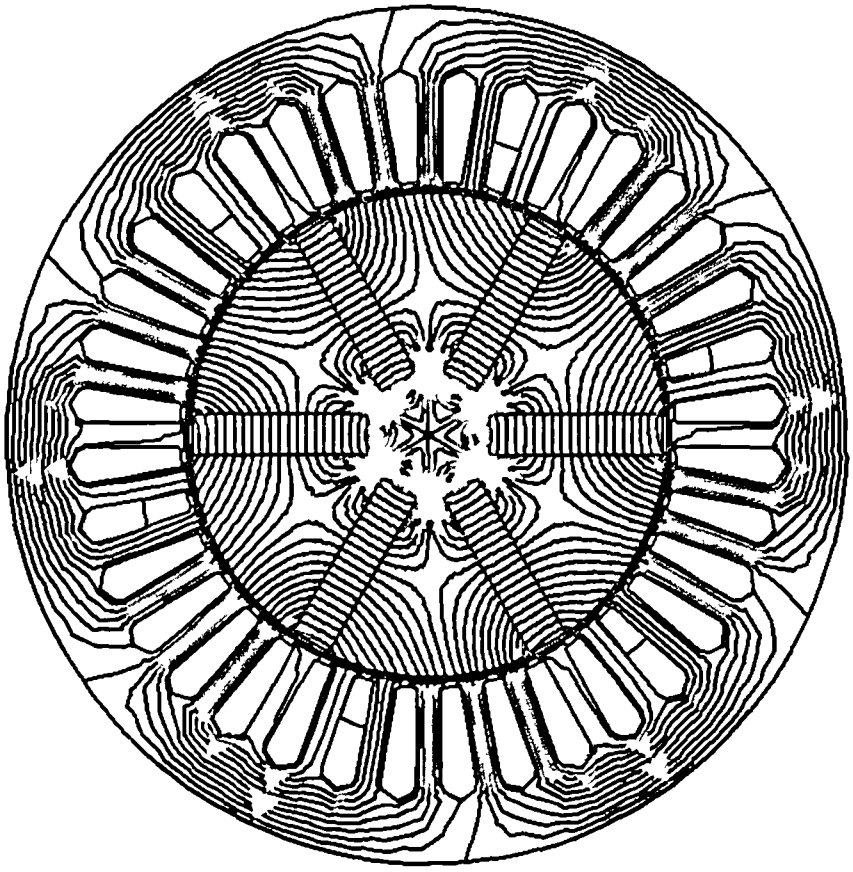

Fig (5.5):Flux lines
S K 8 G 8 T 9 0
IA= 8.0 CANG= 90.0 NCOND= 15 LTH= 82.3 BR=1.08
BF= 0.99 ILANG=-16.38 TORQ= -7.34 ITER.=25
DIFFERENCE IN VP BETWEEN LINES= 0.001 AMP

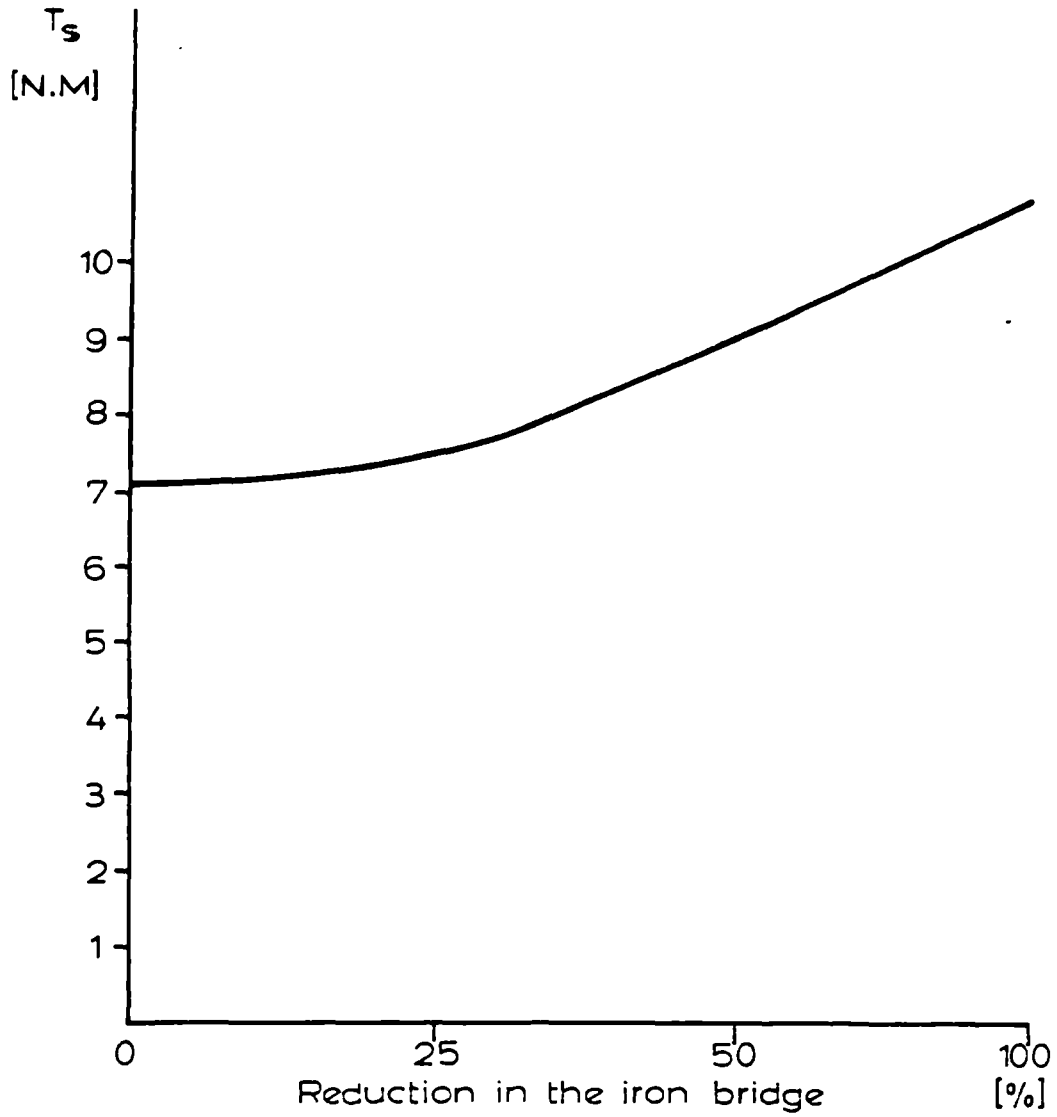

Fig.5.7 Effects of the bridge of magnetic material on the synchronous torque.

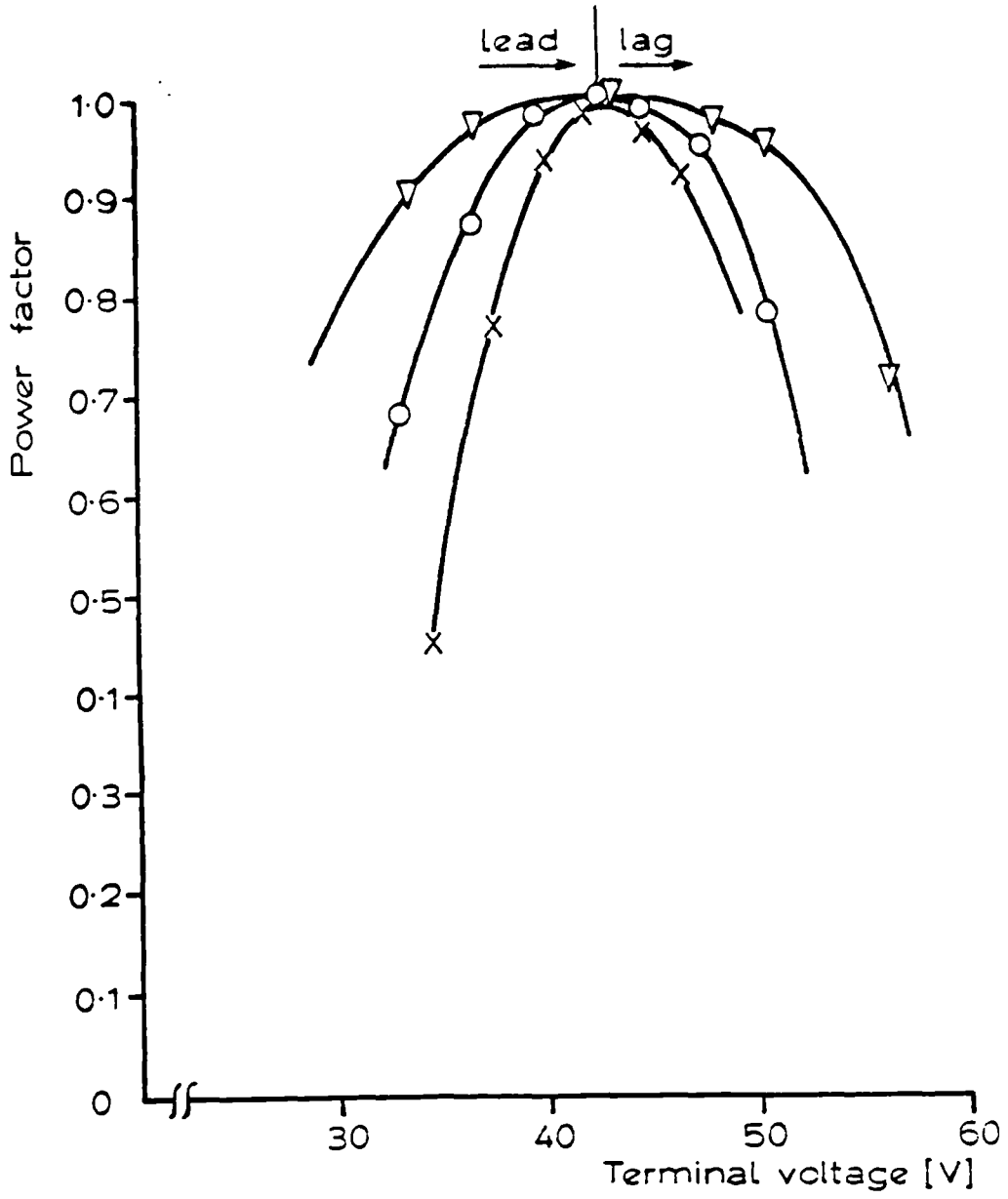

x... I = 3 A
o... I = 5 A
∇... I = 8 A

Fig.5.8 Measured characteristic of the power factor for different voltage levels at different loads.

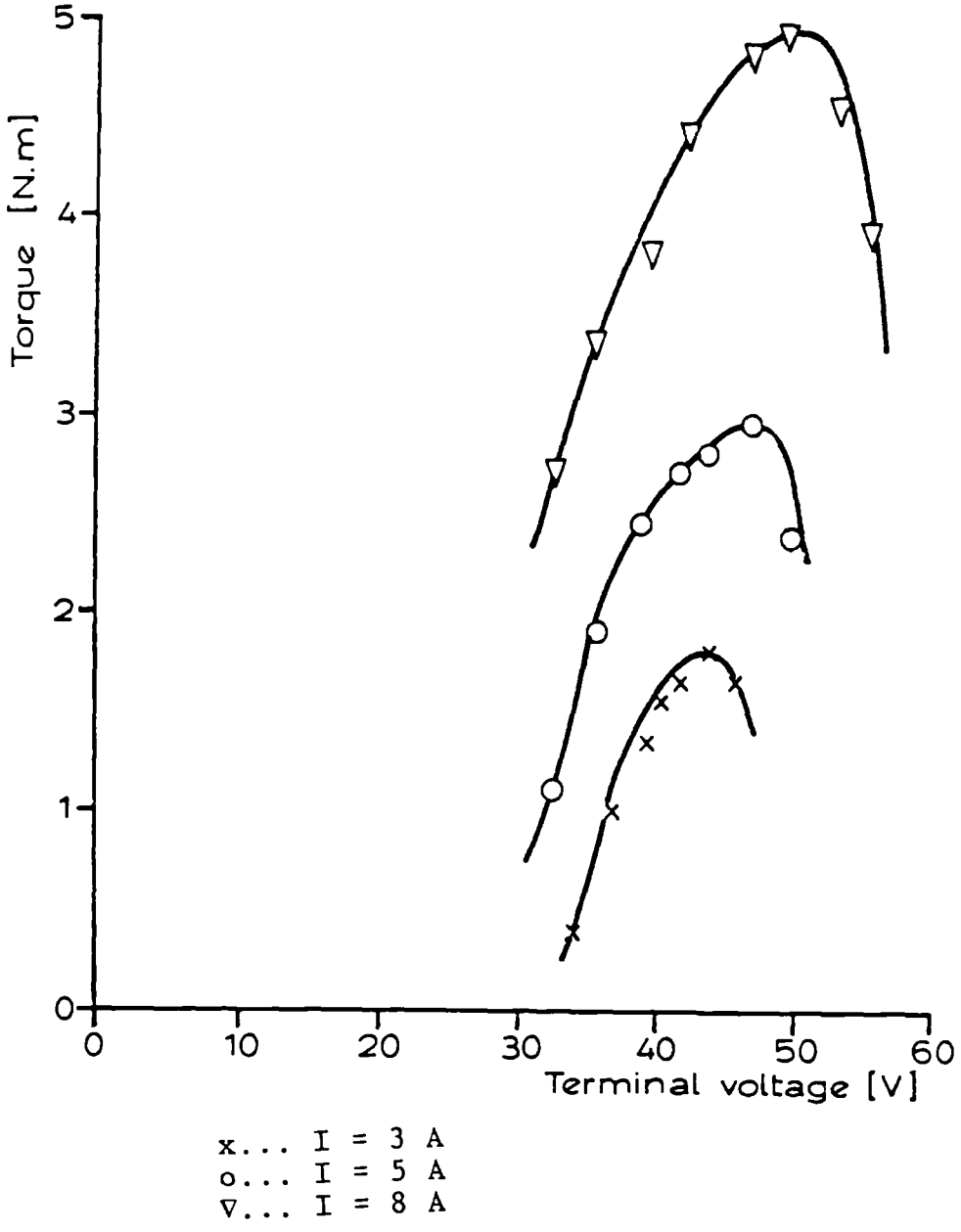

Fig.5.9 Torque versus terminal voltage at different loads for f = 50 Hz.

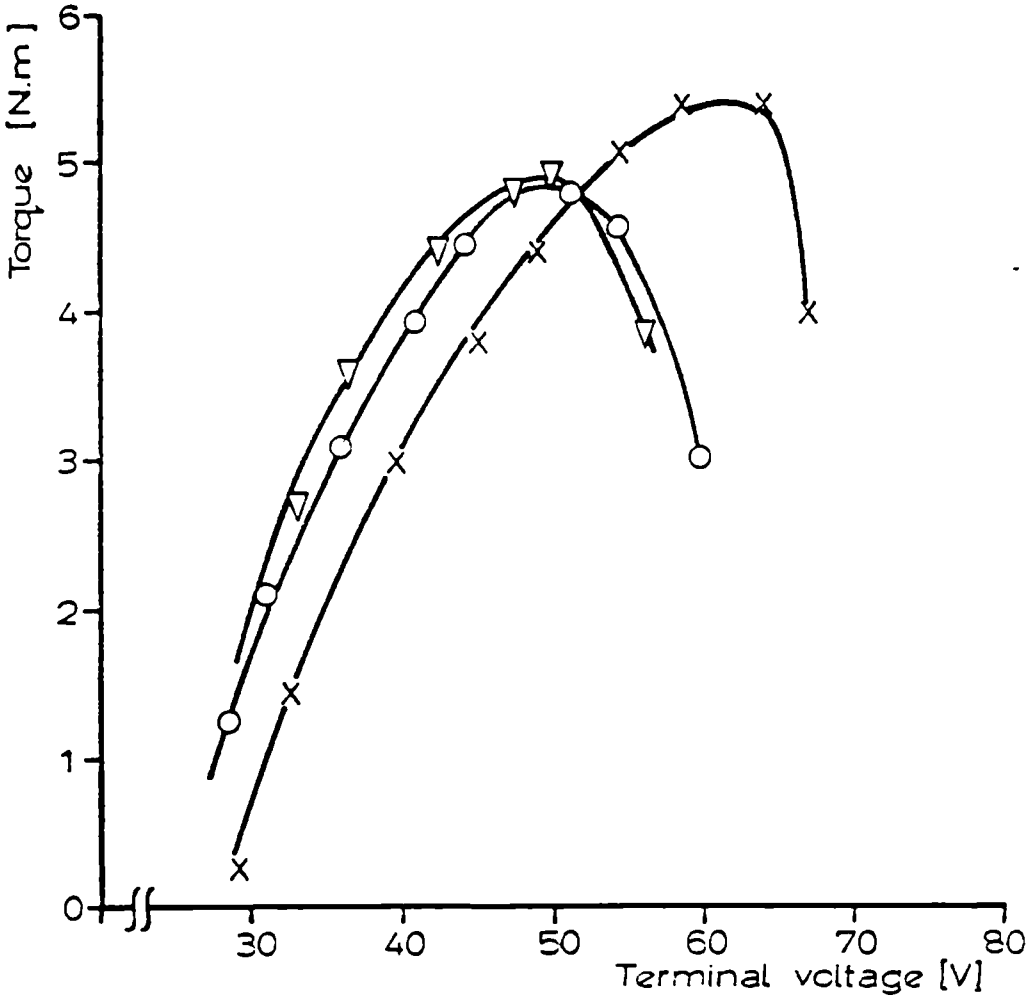

x... g = 0.2 mm
o... g = 0.8 mm
∇... g = 0.8 mm (canned rotor)

Fig.5.10 Variation of the torque with the terminal voltage at full load, f = 50 Hz.

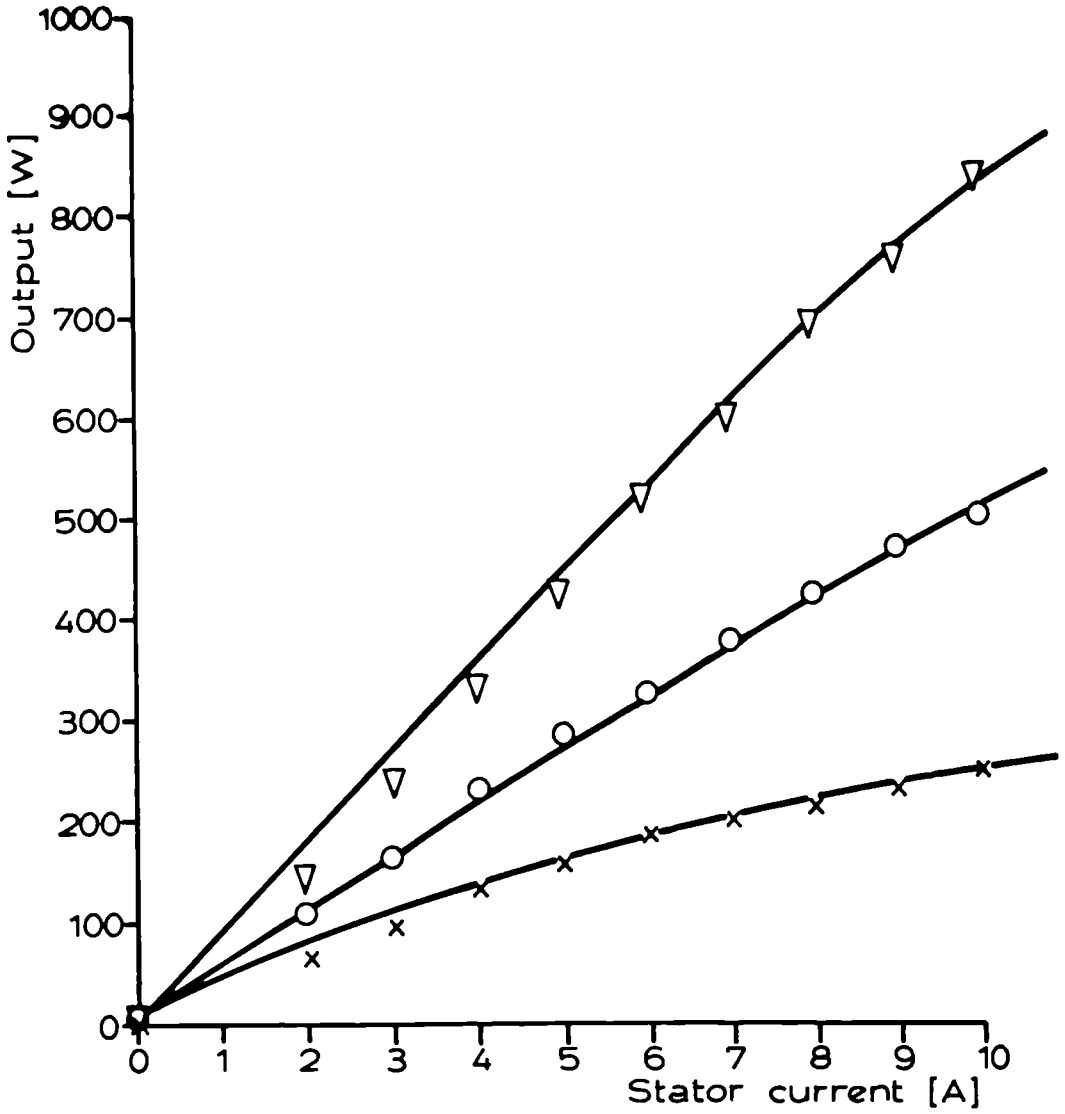

x... f = 30 Hz
o... f = 50 Hz
∇... f = 75 Hz

Fig.5.11 Output characteristic of the machine at different frequency levels.

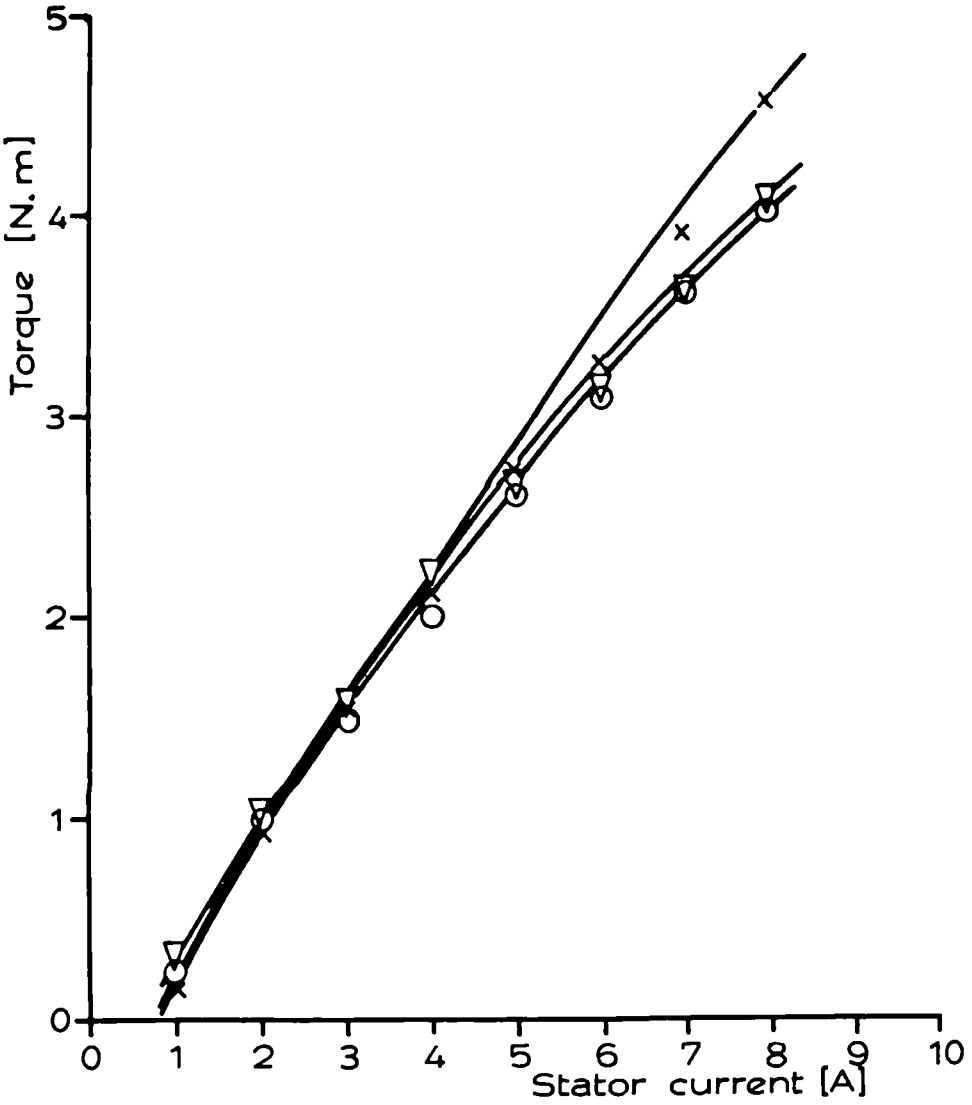

x... g = 0.2 mm
o... g = 0.8 mm
∇... g = 0.8 mm (canned rotor)

Fig.5.12 Torque characteristic for different air gaps.

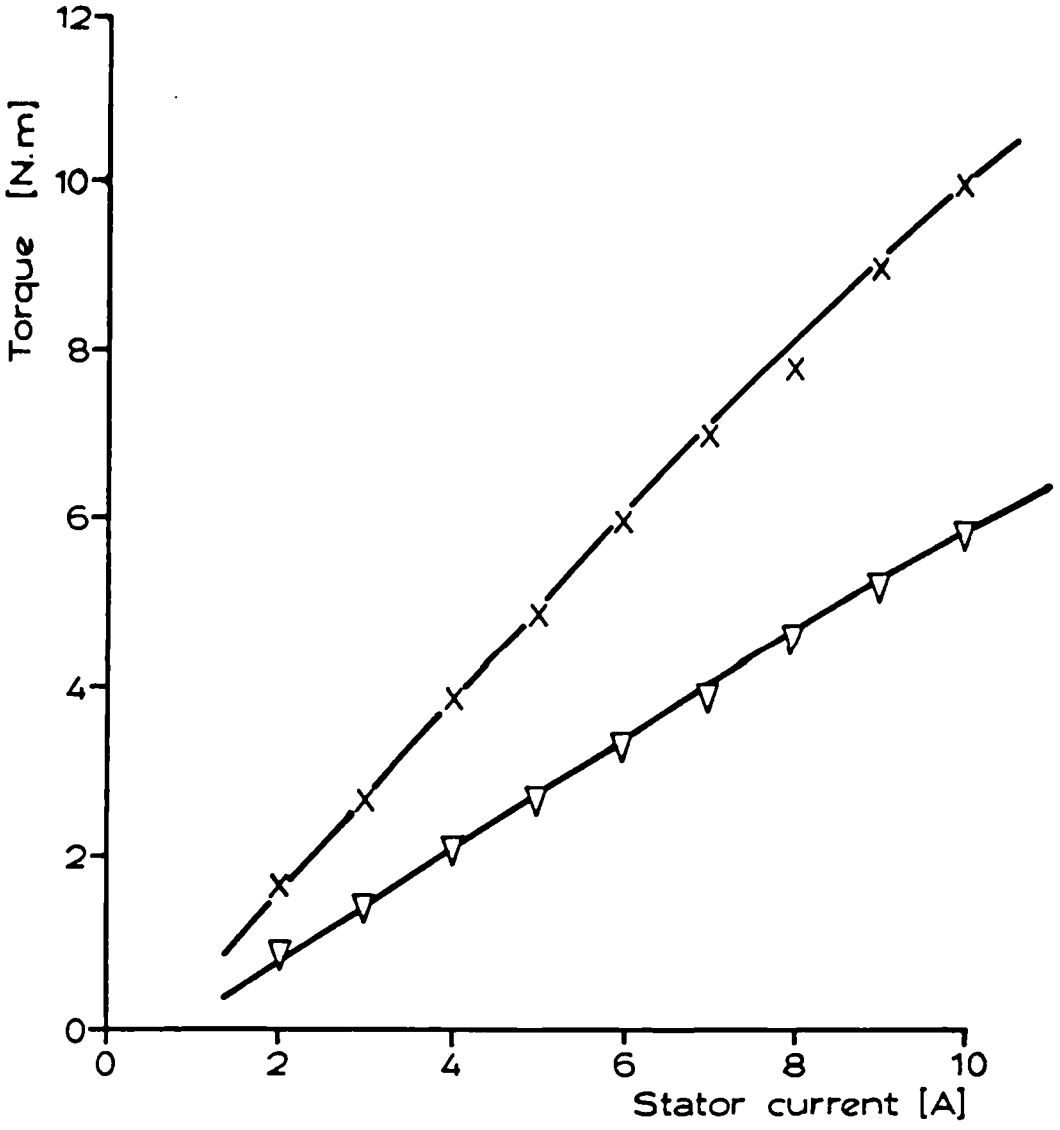

x... conventional PM rotor
V... rotor with skewed magnets

Fig.5.13 Comparison of the output torque of the two tested PM machines. f = 50 Hz, V = 1 p.u.

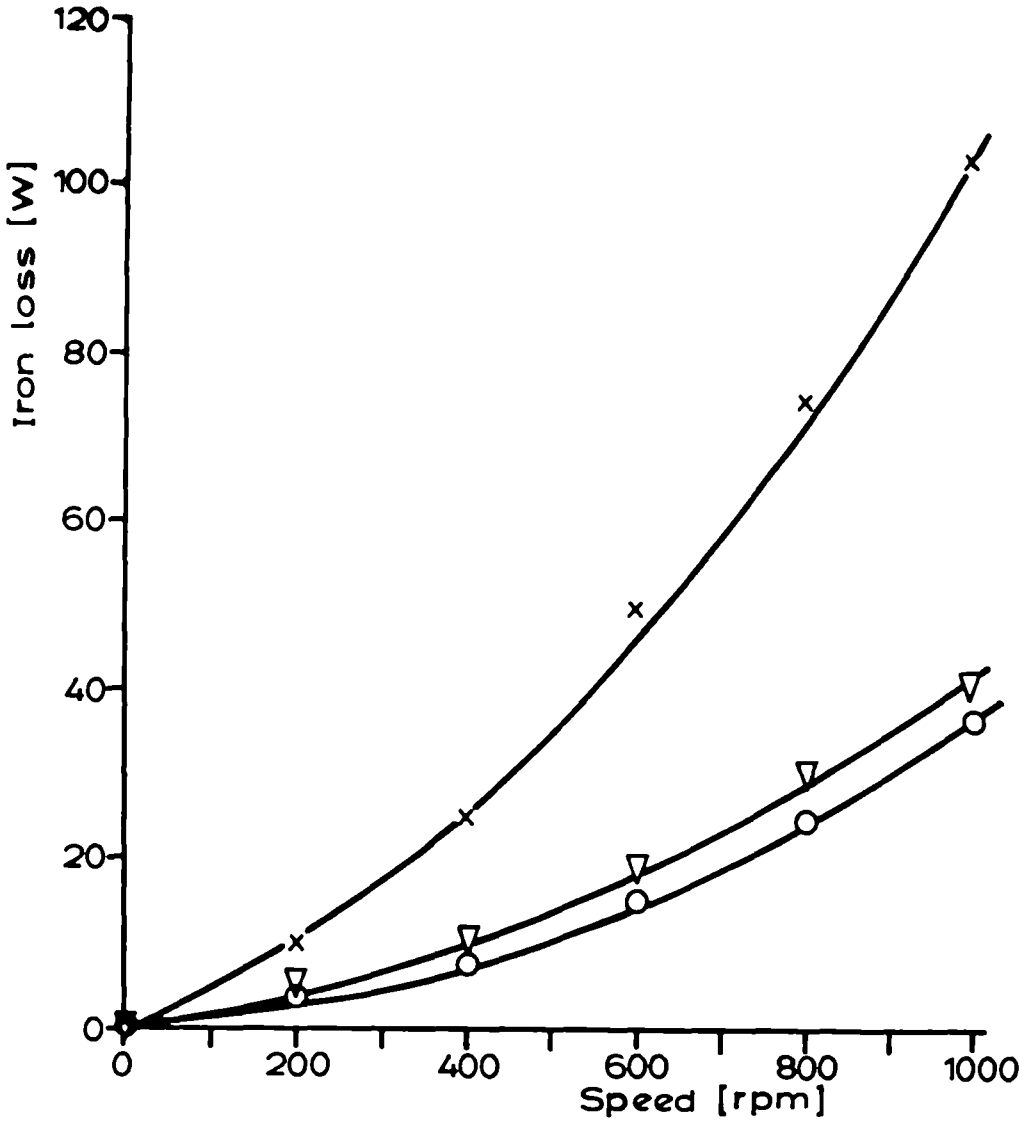

x... g = 0.2 mm
o... g = 0.8 mm
∇... g = 0.8 mm (canned rotor)

Fig.5.14 Open- circuit generator test: Iron loss as a function of speed.

---- B>1.2 T
---- 0.8< B <1.2 T
---- 0.4< B <0.8 T
---- B <0.4 T

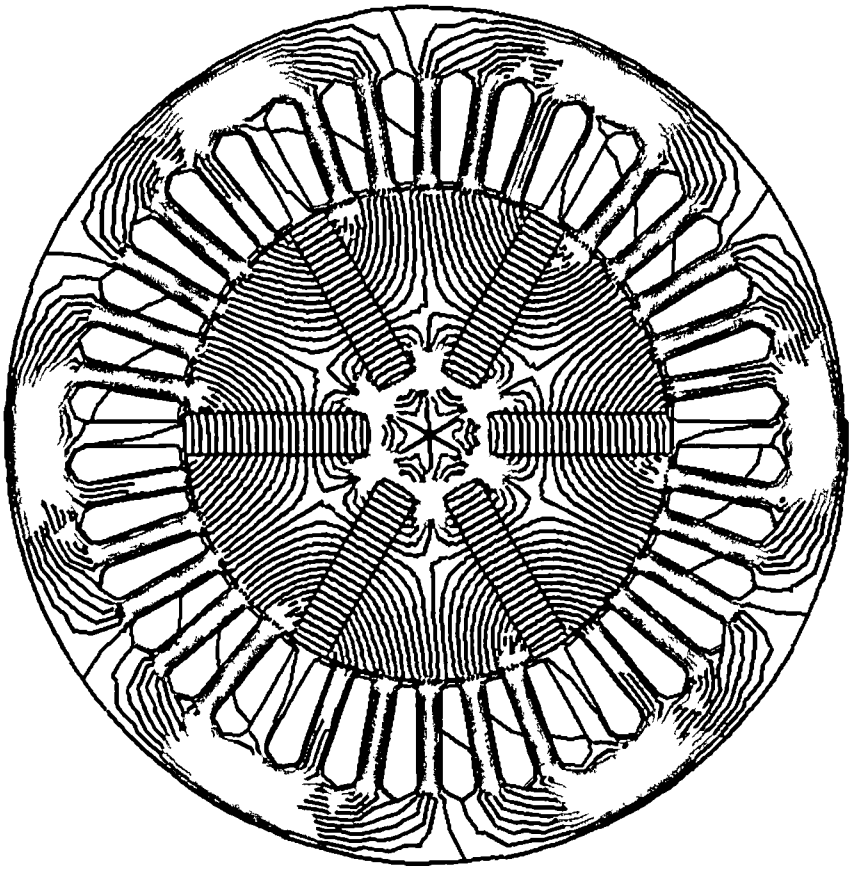

Fig (5.15):Flux lines
S K 2 G 8 T 9 0
IA= 8.0 CANG= 90.0 NCOND= 15 LTH= 82.3 BR=1.08
BF= 1.19 ILANG= -9.62 TORQ= -9.54 ITER.=25
DIFFERENCE IN VP BETWEEN LINES= 0.001 AMP

CHAPTER SIX

EXPERIMENTAL AND NUMERICAL DETERMINATION OF THE MACHINE EQUIVALENT CIRCUIT PARAMETERS

CHAPTER SIX

EXPERIMENTAL AND NUMERICAL DETERMINATION OF THE MACHINE EQUIVALENT CIRCUIT PARAMETERS

6.1 Introduction

The testing and characterisation of PM machines is basically similar to the procedure applied to conventional synchronous motors. However, due to the constant field excitation provided by the magnets, modified (non- classical) methods have to be followed to determine the significant parameters. In this chapter new and modified methods to determine the machine equivalent circuit parameters experimentally and numerically are proposed. The machine used for this analysis consists of a 6- pole rotor with interior neodymium magnets, Fig.6.1. The stator is a standard induction motor type having a three- phase single- layer winding. The coils are connected in series and placed in semi- closed slots.

In high- field machines like the one under investigation the effect of saturation has to be considered. In this analysis appropriate modifications to the classic two-reaction theory, as suggested by Honsinger (78), are considered to achieve accurate and realistic prediction of the machine performance.

6.2 Equivalent circuit and phasor diagram without the core loss

The equivalent circuit of PM machine may be derived from that of a field- excited synchronous motor. From the air gap outwards both types have the same parameters including the winding resistance 'R_a', the leakage reactance 'X_l', and the magnetising reactance 'X_m' that reflects the reluctance of the air gap and the stator magnetic path, (73,80,87). There exist several methods of representing the magnetic material (76,80) by converting the magnetic circuit into an equivalent electric circuit. Figure 6.2 shows the equivalent circuit in which the magnet is represented by a voltage source 'E_m' in series with equivalent linearised reactance 'X_0' representing the rotor path.

Applying Thevenin's theorem gives a rather simplified equivalent circuit as shown in Fig.6.3 where:

$$E_0 = \frac{X_m}{X_m + X_0} E_m \tag{6.1}$$

$$X_s = X_m \frac{X_0}{X_m + X_0} \tag{6.2}$$

E_0 is the induced voltage

X_s is the synchronous reactance which can be defined as the reactance offered by a synchronous machine to a balanced three- phase voltage of rated frequency applied to

its armature winding when the rotor is unexcited and rotates at synchronous speed. For the PM machine considered here high- energy magnets have permeability close to unity. The equivalence of switching off the field excitation in a conventional machine is therefore the removal of the magnets. Due to the rotor saliency the synchronous reactance is resolved into two components along the machine direct and quadrature axes giving a direct-axis reactance X_d and a quadrature- axis reactance X_q. The field waveforms along these two axes is discussed in section 6.6.1.

In conventional synchronous machines with field windings 'X_q' is less than 'X_d' because of the greater reluctance of the air gap in the quadrature axis. Generally the quadrature- axis reactance is 60 to 70% of the direct- axis reactance. In addition the effect of saturation on X_q is small and usually neglected whereas on X_d saturation effect is quite large, (91).

However in PM machines, where the direct axis coincides with the direction of magnetisation of the magnet, this inequality is reversed due to the following factors:

a- The permanent magnet with low effective permeability (nearly unity) lies in the path of the direct- axis flux giving a low value of X_d.

b- The high pole arc/pole pitch ratio due to the small saliency of some machine designs results in a high value of X_q.

Hence for PM machines:

$$X_q > X_d$$

and the quadrature axis is far more susceptible to saturation than the direct axis.

6.3 Losses in permanent magnet machines

In the equivalent circuit representation losses are divided into two main groups, load- dependent ,and load-independent losses.

6.3.1 Load- dependent loss

The major part of load- dependent loss is the copper loss. This can be determined by knowledge of the material, length, and diameter of wire used in the stator winding. Alternatively it can be found by direct measurement. Besides copper loss other load dependent loss mechanisms exist in the machine for example the leakage core loss.

The winding resistance measurement is carried out by passing an a.c current 'I_a' into the stator winding after the machine rotor has been removed and measuring the input power 'W'. This measurement will thus take the skin effect phenomena into consideration and to a certain extent will include the stator leakage load loss. Table 6.1 shows values of the resistance calculated as:

$$R_a = \frac{W}{I_a^2} \qquad (6.3)$$

The values of the stator current and the input power are varied by changing the supply voltage. The effect of temperature on the resistance is also examined by conducting the same test at different operating temperatures and the results are illustrated in Table 6.2. The constant value of resistance (24.5 Ω) used in the equivalent circuit is taken at the rated current and winding temperature.

6.3.2 Load- independent loss

Load- independent loss includes friction and windage of all mechanically connected apparatus and the core loss corresponding to the field flux and therefore related to the induced winding voltage and frequency. Core loss is regarded as the result of combined effects of hysteresis and eddy current loss.

The following section describes a sequence of tests that were performed to measure the friction and windage loss and the distribution of the core loss in the machine when excited at 1000 rpm, 50 Hz.

6.3.2.a Friction and windage loss

The friction and windage loss is determined by replacing the PM rotor with an unexcited induction motor rotor, having exactly the same dimensions as the original PM rotor. The motor is operated at no load such that:

$$\underset{\text{power}}{\text{input}} = \underset{\text{loss}}{\text{copper}} + \underset{\text{loss}}{\text{core}} + \underset{\text{loss}}{\text{friction \& windage}} \qquad (6.4)$$

The aim is to determine the friction and windage loss and hence to segregate it from the core loss. The input power is measured as the motor runs for a range of voltage levels between 15% and 125% of the rated value. The results, excluding the total copper loss, are plotted in a graph as shown in Fig.6.4 which is then extrapolated to intercept the zero- voltage axis. The obtained value of 9W represents the loss due to friction and windage for the six pole machine. Copper loss in the rotor cage bar has been measured by applying the locked rotor test and its value is added to that of the stator winding.

6.3.2.b Core loss

Core loss is determined by running the PM machine as an open- circuited generator being driven by the d.c. dynamometer. Its value is then deduced from the mechanical torque recorded for each speed after making allowance for the friction and windage loss. The loss characteristics as shown in Fig.6.5 are plotted against the square of the frequency and as expected the core loss has a good linear relation with the square of the frequency. Core loss depends on the flux linkage of the machine, which could be changed by varying the supply voltage, and therefore is related to the state of saturation of the machine. This has been illustrated by measuring the core loss in the same machine but with two different air gaps. The results obtained from these measurements clearly indicate that increasing the air gap will reduce flux link-

age and saturation resulting in a lower core loss at each speed.

Accurate numerical determination of core loss is a very complex and hence beyond the aim of this work. In what follows a simplified approximation is used to estimate the core loss. This calculation is provided by computing the two major factors contributing to its formation. These are:

a- The fundamental component of flux density in the stator core. The corresponding core loss is deduced from the "specific total core loss" curve as supplied by the manufacturer, (Appendix C) and the peak field distribution in the machine. Stator weight is calculated from the model geometry and hence core loss due to this fundamental flux density is determined. It should be noted that for more accurate calculation the peak value of the flux density should be considered separately in the stator teeth as well as in the stator core back. The corresponding values of core loss are then calculated for each of these two regions seperately.

b- Core loss is also a result of the rotor harmonics due to the stator slots. The amplitude of these harmonics is determined by computing the flux density in the area right under the rotor pole face to the depth of harmonic penetration.

Compared to tests results, core loss computation as described gives only an approximation as figures in Table

6.3 indicate. In a steady state analysis it is hard to determine precisely the exact depth of harmonic penetration in the rotor core and the weight of core affected by this penetration.

6.4 Equivalent circuit and phasor diagram with the core being considered

From the loss analysis as provided in section 6.3 it is evident that for accurate modelling of high- field machines the core loss has to be considered mainly for efficiency calculations. As the no- load core loss is dependent upon the air gap flux then it is well represented in the equivalent circuit by a shunt resistor 'R_c' connected across the induced voltage 'E_i'. This leads to a modified equivalent circuit and the corresponding phasor diagram as shown in Fig.6.6.

The value of the resistor 'R_c' is deduced from the equation:

$$W_c = \frac{E_i^2}{R_c} \tag{6.5}$$

where 'W_c' is the core loss calculated as described in the previous section. The loss current is calculated according to the following equation:

$$I_c = \frac{E_i}{R_c} \tag{6.6}$$

Equation 6.4 can now be rewritten as:

$$W = \frac{E_i^2}{R_c} + I_a^2 R_a^2 \qquad (6.7)$$

From the adjusted phasor diagram of Fig.6.6 it is clear that only the current 'I', which is the vector difference between the armature current and the loss current, participates in the energy conversion process. Neglecting the loss current 'I_c' will result clearly in an overestimation of the output torque obtained from the model. The magnitude of 'I' is:

$$I = \sqrt{I_a^2 + I_c^2 - 2I_a I_c \cos(\theta + \alpha)} \qquad (6.8)$$

and the modified power factor angle is:

$$\theta' = \mathrm{Atan}\left(\frac{I_a \sin\theta + I_c \sin\alpha}{I_a \cos\theta - I_c \cos\alpha}\right) \qquad (6.9)$$

It should be noted that the representation of the core loss by a constant value illustrates accurately the dependence of the eddy current loss on the flux and frequency, however it gives only an approximation for the hysteresis loss.

6.5 Measurement of direct- and quadrature- axis reactances

Testing the performance of PM machines is in principle similar to that of conventional types of synchronous machines. However, due to the special method of excitation by permanent magnets some difficulties arise one of which is the measurement of the synchronous reactance since all

tests provided for conventional types required the reduction of the field excitation to zero, (68,90,91). For this purpose even some PM machines with weak magnets used to be demagnetised by passing an appropriate direct current through the armature winding (77). With the assessment of the new family of strong rare earth magnets this unpopular technique became totally inapplicable. Two modified methods have been applied to carry out these measurements. These are the static induction test and the zero power factor test.

6.5.1 Static inductance test.

Measurement of the synchronous reactance has been provided in this case statically with the rotor being kept stationary. This has been achievable because the 6- pole rotor used for this purpose has no cage bar winding hence the effect of any induced voltage has been avoided. In the test a single phase supply voltage is connected to the armature winding while the other two phases of the winding are kept open- circuited. A constant current is kept flowing in the armature while the load angle is varied from 0 - 90^0 by changing the rotor position. For each value of the load angle the input power is measured as well as the three voltages across the armature winding.

According to the definition of the impedance 'Z':

$$Z = \sqrt{X^2 + R^2}$$

$$X = \sqrt{Z^2 - R^2}$$

Substituting for $Z = V/I$ and $R = W/I^2$ gives:

$$X = \frac{1}{I}\sqrt{V^2 - \frac{W^2}{I^2}} \qquad (6.10)$$

From the test a set of values is obtained according to the rotor position, the largest value being related to X_q and the smallest corresponding to X_d.

The single phase results however need to be adjusted for a three phase winding by including the effect of the mutual inductance. For PM machines it has been shown (91,94) that the mutual inductance is added to the values of X_q and X_d in different ratios as explained in (100). The mutual inductance between the stator coils can be measured by various methods, (90,91,92). The simple way of measuring the mutual inductance as a self inductance has been used for the purpose of this work. In this method the stator winding is considered to be a set of two coils connected in series such that the two open- circuited phases are considered as one coil.
The inductance in these two coils is:

$$L = L_a + L_b + 2L_{ab}$$

The terminals of the second coil are reversed and the measurement is repeated to give:

$$L' = L_a + L_b - 2L_{ab}$$

From these two equations the mutual inductance is:

$$L_{ab} = \frac{L - L'}{4} \qquad (6.11)$$

It should be noted that the mutual inductance could already be accounted for if all the three phases are connected to the supply. This, however, is found to be reliable only at low values of the stator current (I<0.5A). It must be ensured that the rotor is kept at its standstill position, since any vibration of the rotor will result in higher values of the reactance because part of the input power is dissipated in the mechanical vibration.

6.5.2 Zero- power factor test

Zero- power factor test is generally used for conventional synchronous machines because closer approximations to the saturated synchronous reactance can be obtained for cylindrical rotors as well as salient- pole rotors. The machine is tested under saturation conditions due to the presence of the armature current. In testing PM machines, however, some modifications have to be made. Fig.6.7.a shows a PM machine running as a generator with a purely inductive load connected to its terminals. When the switch (S) is closed, the terminal voltage will drop significantly from its original open- circuit value 'E_0'. The armature current is changed by the variation of the load inductance keeping the speed of the machine constant. This measurement gives the direct- axis value of the synchronous reactance as shown in Fig.6.7.b. where:

$$X_d = \frac{E_0 - V_t}{I} \qquad (6.12)$$

The phasor diagram of Fig.6.7.b represents an ideal condition where the armature resistance is neglected. The dotted lines show the diagram when the resistance is taken into account, which demonstrates that the effect of the winding resistance is normally negligible. The leakage reactance is however included as part of the measurement.

A load measurement of X_q has been suggested in (78,95) by locating the operating point on the torque- vs- load angle characteristic the no- load operation is at point $\delta = \delta_0$ instead of the origin (δ = 0). For this condition values of V_t and I could be measured and X_q is determined as:

$$X_q = \frac{V_t}{I} \qquad (6.13)$$

Experimentally this test is complex as it requires the provision of an accurately mounted shaft encoder. Hence it is not carried out because it is costly and difficult to perform.

Another method, the maximum- lagging current test, when applied to conventional machines, takes into account saturation and its effects. For permanent magnet machines this test is inapplicable because the technique of reducing the effect of the field excitation by increasing the

terminal voltage results in a no- load current much higher than the rated value. This may damage the stator winding and may also have severe demagnetising effects on the magnets as their temperatures may rise above the Curie point.

6.6 Computation of X_d and X_q

6.6.1 Stator winding representation

To compute X_d and X_q the stator current system of the winding has to be represented by inserting the current phase- by- phase into the appropriate slots. The instantaneous current values of the three phases are given as:

$$I_a = \hat{I} \cos(\omega t) \tag{6.14}$$

$$I_b = \hat{I} \cos(\omega t - 120°) \tag{6.15}$$

$$I_c = \hat{I} \cos(\omega t + 120°) \tag{6.16}$$

For the finite element analysis the steady state condition, where the field is computed by a snap shot of the current at a particular instant, is considered. The phase of the current is normally referenced to an axes passing radially through the middle of the pole pitch. The currents in each slot winding is represented by a single conductor which has the shape of the slot. Figures 6.8 and 6.9 illustrate the current distribution in the direct and quadrature axis respectively. In each case the current density 'J' shifts in steps related to the tooth pitch in electrical degrees. The armature mmf being given as $\oint J.dx$

also changes in similar manner. This mmf produces an armature reaction flux Φ_a whose fundamental flux density in the air gap is denoted by B_a .

In the direct- axis distribution (where $\omega t = 0$) the maximum value of the mmf is lying along the reference axis. The rotor produces a flux density B_f whose waveform is shown in Fig. 6.8.c. The resultant flux density in the air gap is denoted by B_r and has its maximum value along the reference axis. In the quadrature axis distribution as shown in Fig. 6.9.b ($\omega t = 90°$) , the mmf is shifted by 90 electrical degrees. Its minimum value is now lying along the reference axis. As a result the resultant flux density of the air gap is shifted as seen in Fig.6.9.c. The investigated machine has a non- symmetrical rotor pole with respect to the reference axes. Therefore the pole (magnet) axis is shifted from the reference axes by an angle whose value is usually relevant to the degree of non- symmetry of the design. For the given design the instant current distribution corresponding to the direct axis and quadrature axis is shown in Fig.6.10 and 6.11 respectively. The shift angle for this design is found to be 15 electrical degrees.

6.6.2 Computation results

The synchronous reactance can be calculated from the additional energy stored in the motor field that results from the winding current. The PE2D post- processor inte-

2- To remove the field excitation the magnet is replaced by a air which has a unity relative permeability equal to that of the magnet. The effect of saturation is considered by considering the values of the permeability obtained in (1) as input data. The program is then run linearly to avoid any change in the saturation conditions.

3- The relative positions of the rotor and the stator axis are determined by the current distribution in the stator winding. X_d is computed when the two axis are in alignment, and X_q when they are mutually perpendicular, as previously illustrated in Fig.6.10 and 6.11.

6.6.3 Effect of saturation

In high- field synchronous machines where iron as well as the magnetic material form an essential part of the construction it is essential to examine the effect of saturation on the performance of these machines. The magnetisation curve, representing the induction 'B' as a function of the magnetising force 'H', is characteristic of the material that is a function of its composition as indicated in Fig.6.12. The variation of the relative permeability corresponds to the variation of the induction. Starting from the initial value of the permeability the curve then rises to its peak value before dropping under the effect of saturation.

As the reluctance paths in the direct axis are through the magnetic material with permeability close to unity, the variation of X_d associated with saturation is found

to be very small, as seen in Fig.6.13 whereas the variation of X_q is shown to be significant. The measurements of these parameters as described in the previous section have been made under actual operating conditions with the armature current varying from zero up to full- load conditions.

The results of the experimental tests as well as the computation are being presented in Table 6.4. The computed figures show lower values of X_d and X_q than those obtained from the tests. This is mainly because the computation only includes the stator leakage whereas the test would include all leakage effects. Of the two tests provided, the results of the zero- power factor test appear to be slightly higher. This could be attributed to the additional leakage (hysteresis) when the machine is rotating.

6.7 Induced emf

As discussed earlier, in PM machines the voltage induced in the stator winding is that generated when the machine is running as an open- circuited generator driven by the d.c dynamometer at different speeds.

The computation of the flux density in the air gap with no current density in the stator winding (open- circuit test) leads to the approximate evaluation of the induced emf. Using a Fourier analysis program the fundamental component 'B_1' as well as the higher harmonics are deter-

mined and the corresponding values of the emf are calculated according to the following standard equations (47,90):

$$E_1 = 2\sqrt{(2)}\,\tau_1.l.N.B_1.f_1.K_{p1}.K_{d1}.K_{st}$$

$$E_5 = 2\sqrt{(2)}\,\tau_5.l.N.B_5.f_5.K_{p5}.K_{d5}.K_{st}$$

. . .

$$E_n = 2\sqrt{(2).}\,\tau_n.l.N.B_n.f_n.K_{pn}.K_{dn}.K_{st} \qquad (6.21)$$

τ .....pole pitch

N .....No. of conductors per slot

B_n ....n^{th} component of the flux density

f .....frequency

K_{pn} ...pitch factor

K_{dn} ...distribution factor

K_{st} ...stacking factor

The fundamental value of the pitch factor K_p is determined as:

$$K_p = \sin(\frac{s}{2})$$

For a six- pole stator with 6 slots per pole span s=6. In electrical degrees that gives 180, hence:

$$K_p = \sin(\frac{180}{2}) = 1$$

The distribution factor, applied as the total emf is less than the arithmetic sum of the emf's in each coil, is calculated according to the following equation:

$$K_d = \frac{\sin(\frac{q\alpha}{2})}{q \sin(\frac{\alpha}{2})}$$

and for the n^{th} harmonic:

$$K_{dn} = \frac{\sin(\frac{nq\alpha}{2})}{q \sin(\frac{n\alpha}{2})}$$

α represents here the slot angle = $\frac{360}{36} = 30°$, hence:

$$K_d = \frac{\sin(30)}{2 \sin(15)} = 0.966$$

The effective value of the induced emf taking into account the odd higher harmonics up to the n^{th} is:

$$E = E_1 \sqrt{1 + (\frac{E_5}{E_1})^2 + \ldots + (\frac{E_n}{E_1})^2} \qquad (6.22)$$

The results up to the 13^{th} harmonic of the voltage induced in the single layer 3- phase winding as well as the corresponding distribution factor are presented in Table 6.5. The 3^{rd} harmonic and its multiples are neglected because of the three- phase winding used.

The stacking factor ' K_{st} ' is the ratio of the actual thickness of the ferromagnetic material in the laminations to the gross thickness, as measured when the laminations

are stacked with the insulating material. Data of the BH curve, as supplied from the manufacturer often takes the stacking factor into consideration and therefore it is not included in the above voltage equation.
The computed value of the induced voltage (311 V) is in very close to the measured value of 310 V, see Table 6.6.

6.8 Slot Leakage

The determination of the leakage reactance is important for the analysis of the machine characteristics and performance. The leakage fluxes can be classified into (50,57):

a- slot leakage, 70% of the total leakage

b- end- winding leakage, 10%

c- the harmonic leakage.

The detailed analysis of these components are beyond the scope of this thesis. Attention will be focused only on the slot leakage which is determined by two methods:

1- using the recognised design formulae

2- by finite element analysis.

6.8.1 Design formulae assessment

The mathematical design formulae (as derived in appendix A) are applied with two assumptions. First the flux lines crossing the slot are parallel to each other. Secondly the permeability of the iron is infinite. Previous work (49,50) has shown that these calculations, besides using long complex equations and formulae, usually give overes-

timated value of the slot leakage due to the two assumptions under which they are provided.

6.8.2 Computational results

The finite element computation starts from the definition of the inductance as:

$$L = \frac{\Phi}{I} = \frac{BS}{I} \tag{6.23}$$

The computation is carried out by the determination of the normal component of the flux density 'B_n' along middle of a slot. The field excitation is ignored by removing the magnets from the rotor. Figure 6.14 represents the variation of the flux density along the slot. At the semi-circular- shaped bottom the field is weak and the flux density is almost zero. The field increases along the slot until it reaches the maximum value at the bridge of the semi- closed end, then it drops as it approaches the rotor surface across the air gap.

The slot leakage is also determined by computing the energy stored in the slot at any load current. This method requires the computation to be provided in each slot of the pole individually. The results of this computation show that flux leakage depends significantly on the position of the slot with respect to the rotor pole. The high reluctance due to the pole saliency results in higher leakage flux across the slot. The slot leakage at each loading condition is the average value of all slots

leakage The results, as shown in Fig.6.15, are very close to those obtained by computing the normal flux density along the slot.

The finite element analysis gives more accurate results for the slot leakage because it considers a complete improved flux map shown in Fig.6.16. while the design formulae assume the lines to be parallel. Another advantage is the computation under the effect of saturation which gives more practical results. These results show that at lower currents the inductance of the iron path of the slot pitch will increase up to the state of saturation. Beyond this point the inductance and hence the slot leakage will drop due to increased saturation.

6.9 Conclusion

Suitable techniques to determine the PM machine equivalent circuit parameters both experimentally and by finite element analysis are described. In all cases comparison of the results show good agreement between the computed and measured values. Analysis of the machine losses in relation to the load is provided. Results have also shown that for high- field machines it is very important to represent core loss by a shunt resistor across the induced voltage. The corresponding equivalent circuit and phasor diagram are presented. It has also been illustrated that the saturation effect on X_q is significant and hence it should be accounted for in the subsequent analysis. Two methods to determine the slot leakage have been discussed.

These methods have more practical consideration than the corresponding "design formulae".

terminal voltage V_t	stator current I_a	input power W	winding resistance R_a
10	0.34	7	19.2
30	0.95	57	21
50	1.5	152	22.7
70	2	298	24.3
80	2.3	400	25
100	2.9	640	25.6

Table 6.1: Values of winding resistance for different voltage levels at 50 Hz.

stator current I_a	temperature T°c	input power W	winding resistance R_a
1.5	20	153	22.6
1.47	40	154	23.6
1.42	60	155	24.5
1.4	80	155	25.8

Table 6.2: Effect of temperature on the winding resistance for v = 50 V at 50 Hz.

test	FEM
94	86

Table 6.3: Core loss obtained from tests and finite element analysis.
f = 50 Hz

current I	computation X_d	computation X_q	static ind. X_d	static ind. X_q	zero p.f. X_d
0.5	22	35	24	40	25
1.0	21	28	22	30	23.5
1.5	20	23	22	25	23
2.0	19	21	20	19	22

Table 6.4: Values of X_d and X_q obtained experimentally and numerically.

Harmonic Order n	Distrib. Factor K_d	K_{bn}	Ke_n	Flux Density B_n
1	0.966	1	1	1.0757
5	0.259	0.129	0.0345	0.1388
7	-0.259	0.1639	0.0439	0.1764
11	-0.966	0.2594	0.2594	0.2791
13	-0.966	0.2627	0.2627	0.2826

Table 6.5: Results of the determination of the fundamental and the higher harmonics with the corresponding factors.

test	FEM
310	311

Table 6.6: Induced voltage values obtained form tests and finite element analysis at f = 50 Hz

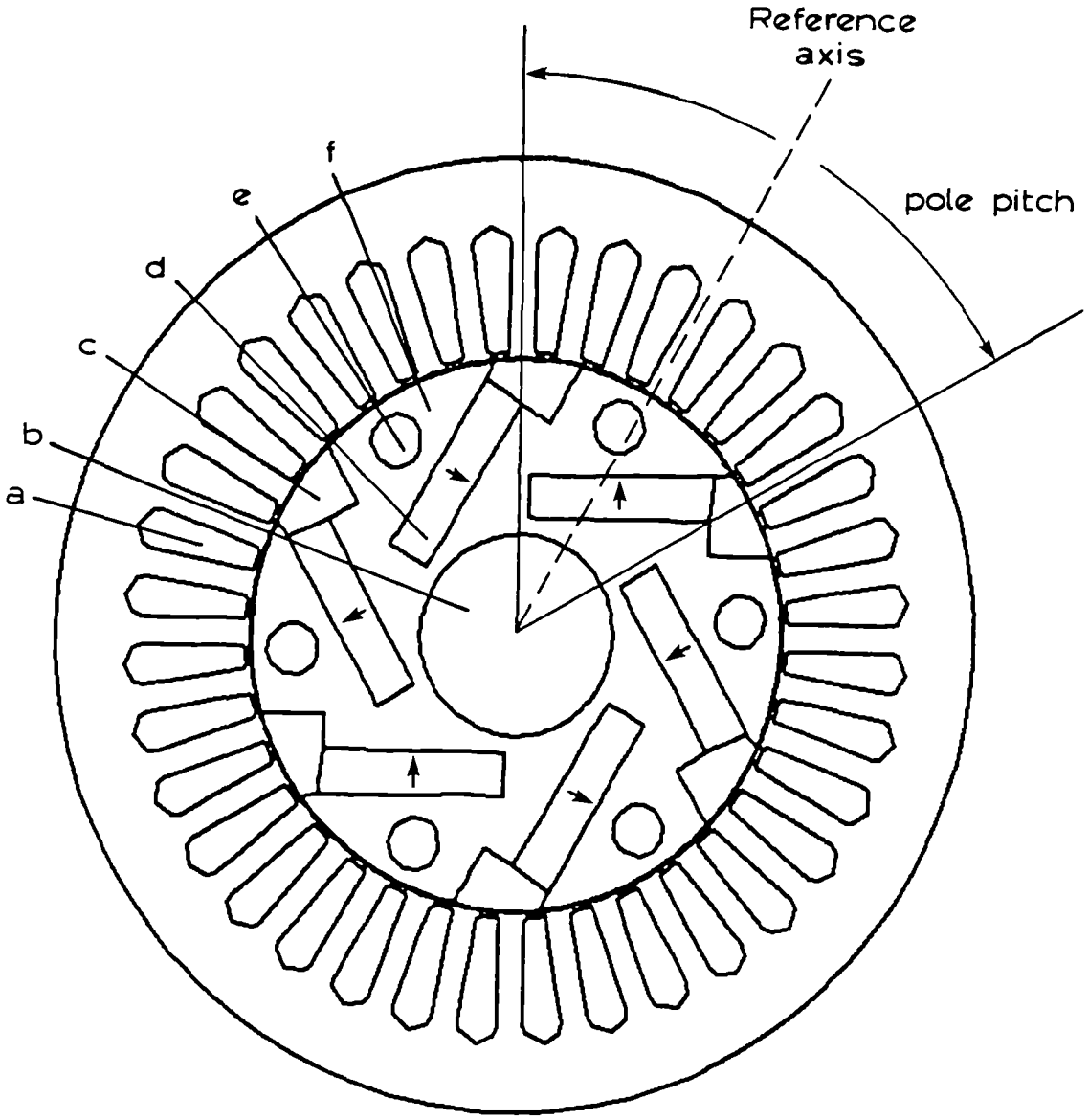

►... direction of magnetisation
a... semi- closed slot
b... non- magnetic shaft
c... non- magnetic material
d... magnet
e... ventilation hole
f... rotor iron lamination

Fig.6.1 Cross- sectional configuration of high- field 6- pole PM machine with NdFeB magnets.

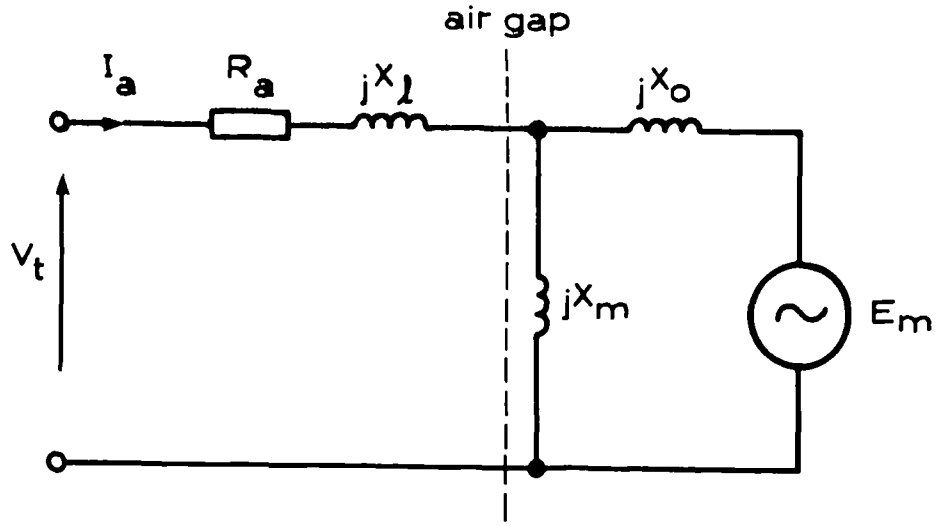

Fig.6.2 Equivalent circuit of PM synchronous machine.

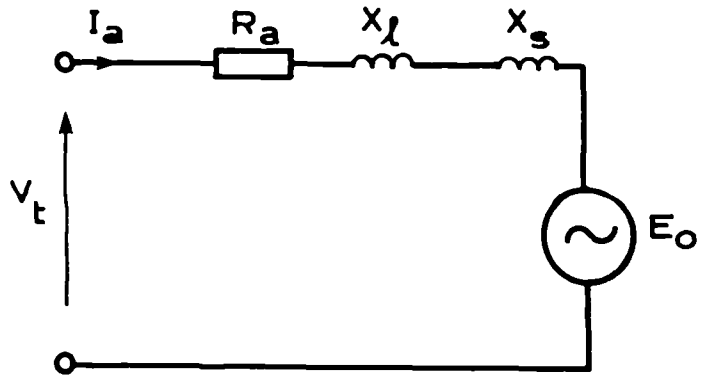

Fig.6.3 Thevenin theorem: Simplified equivalent circuit of PM machine.

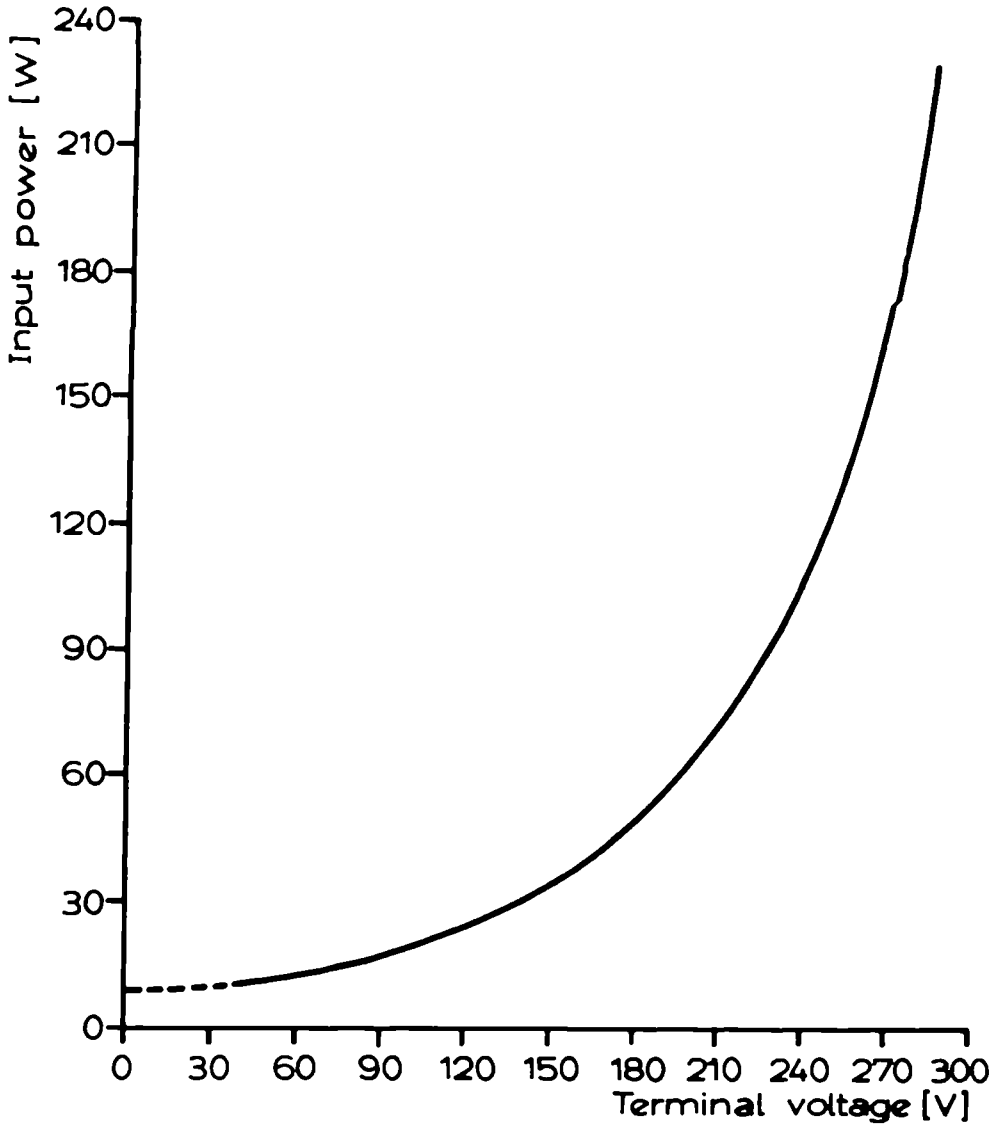

Fig.6.4 Extrapolation of the input power- voltage curve to determine friction and windage loss.

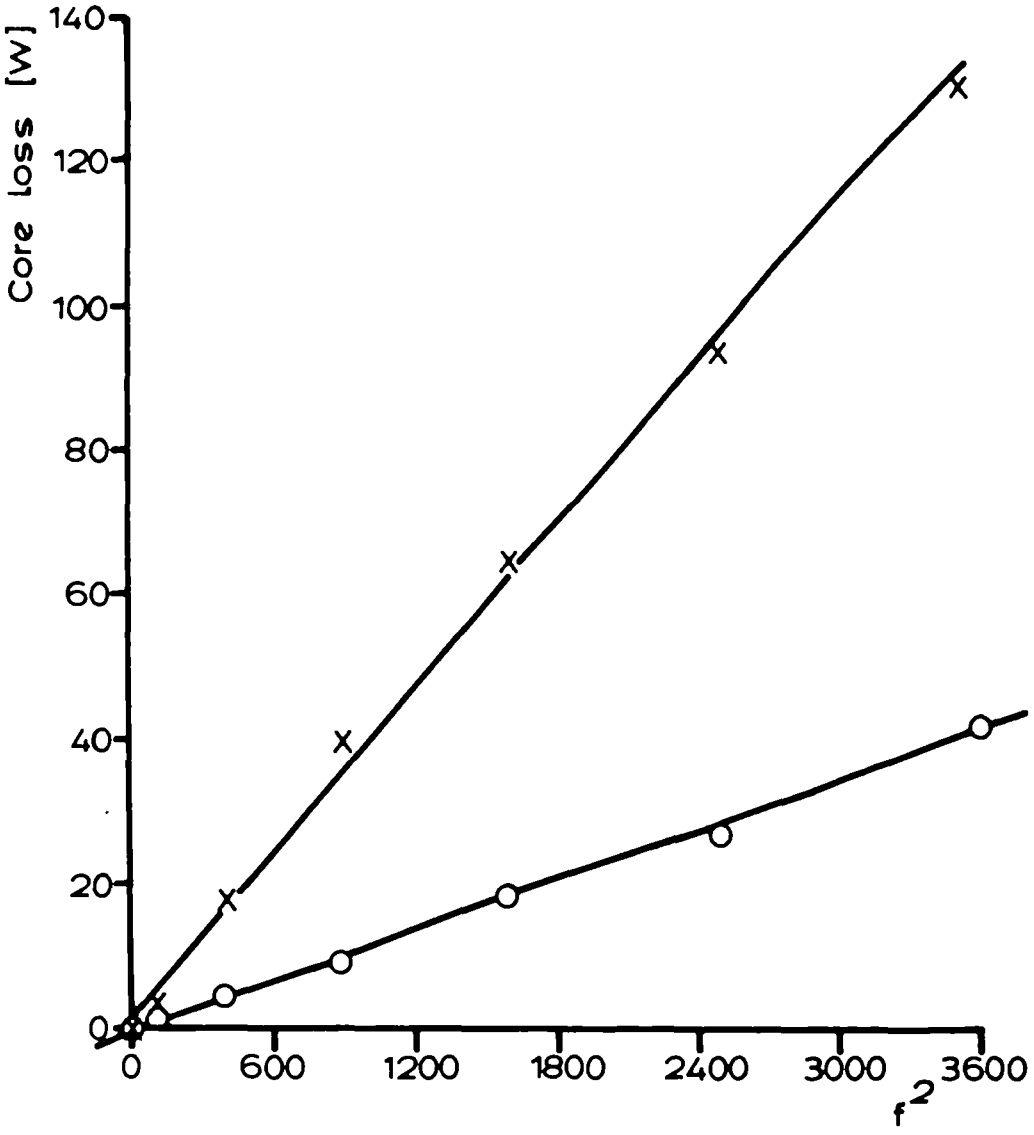

x... g = 0.2 mm
o... g = 0.8 mm

Fig.6.5 Variation of core loss with square value of frequency for different air gaps.

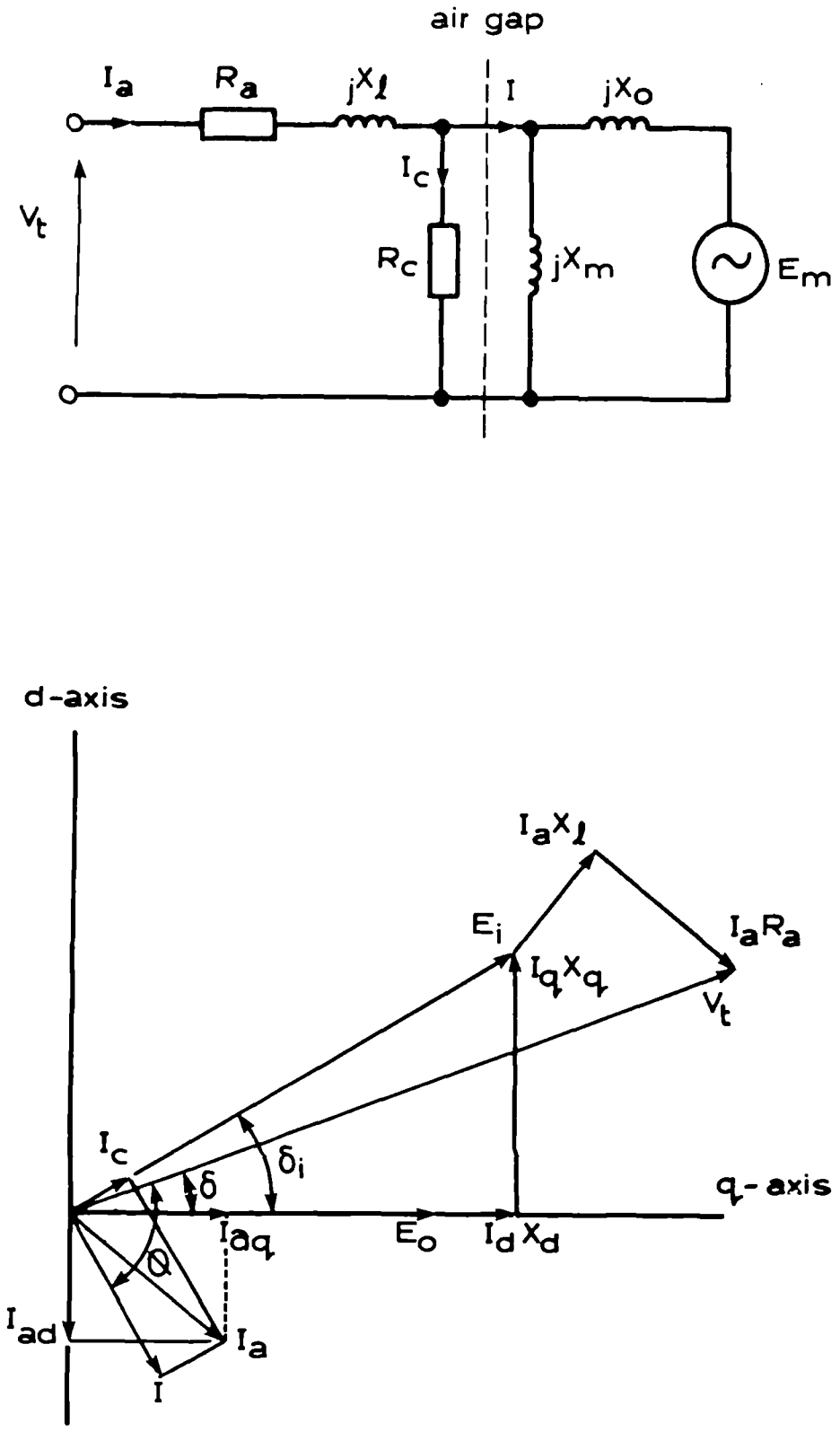

Fig.6.6 Modified equivalent circuit and phasor diagram with core loss being included.

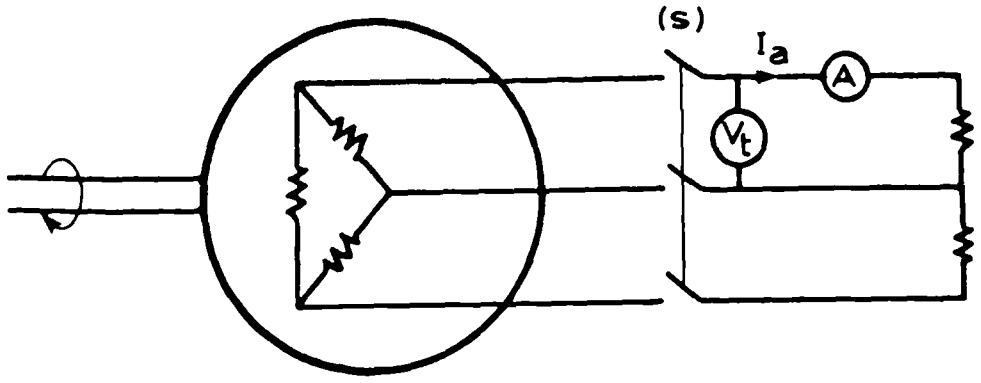

(a)

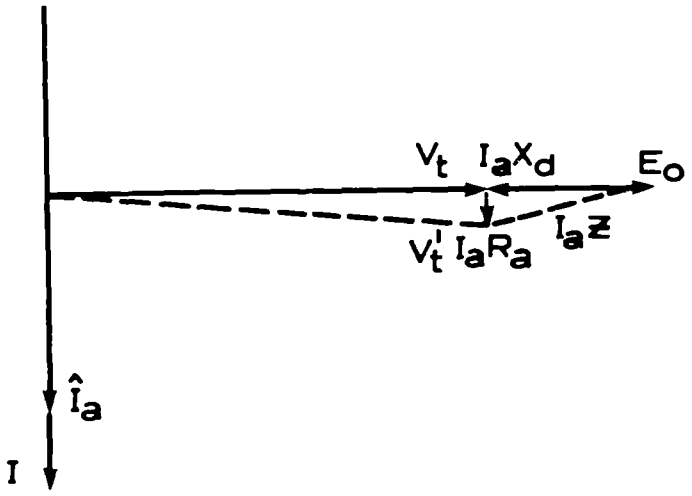

(b)

a... connection
b... phasor diagram

Fig.6.7 Zero- power factor test.

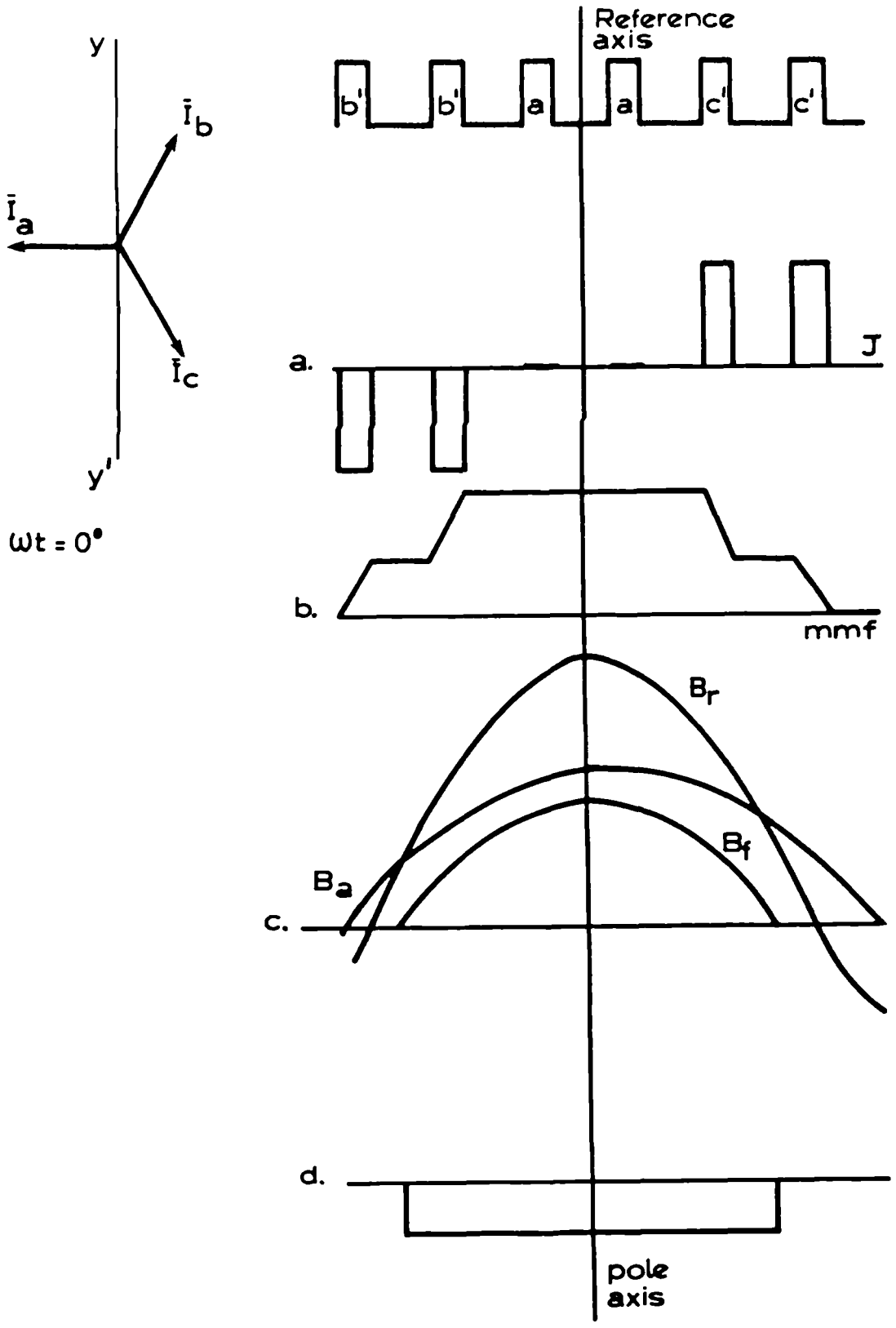

Fig.6.8 Representation of stator winding and air gap fluxes in the direct axis.

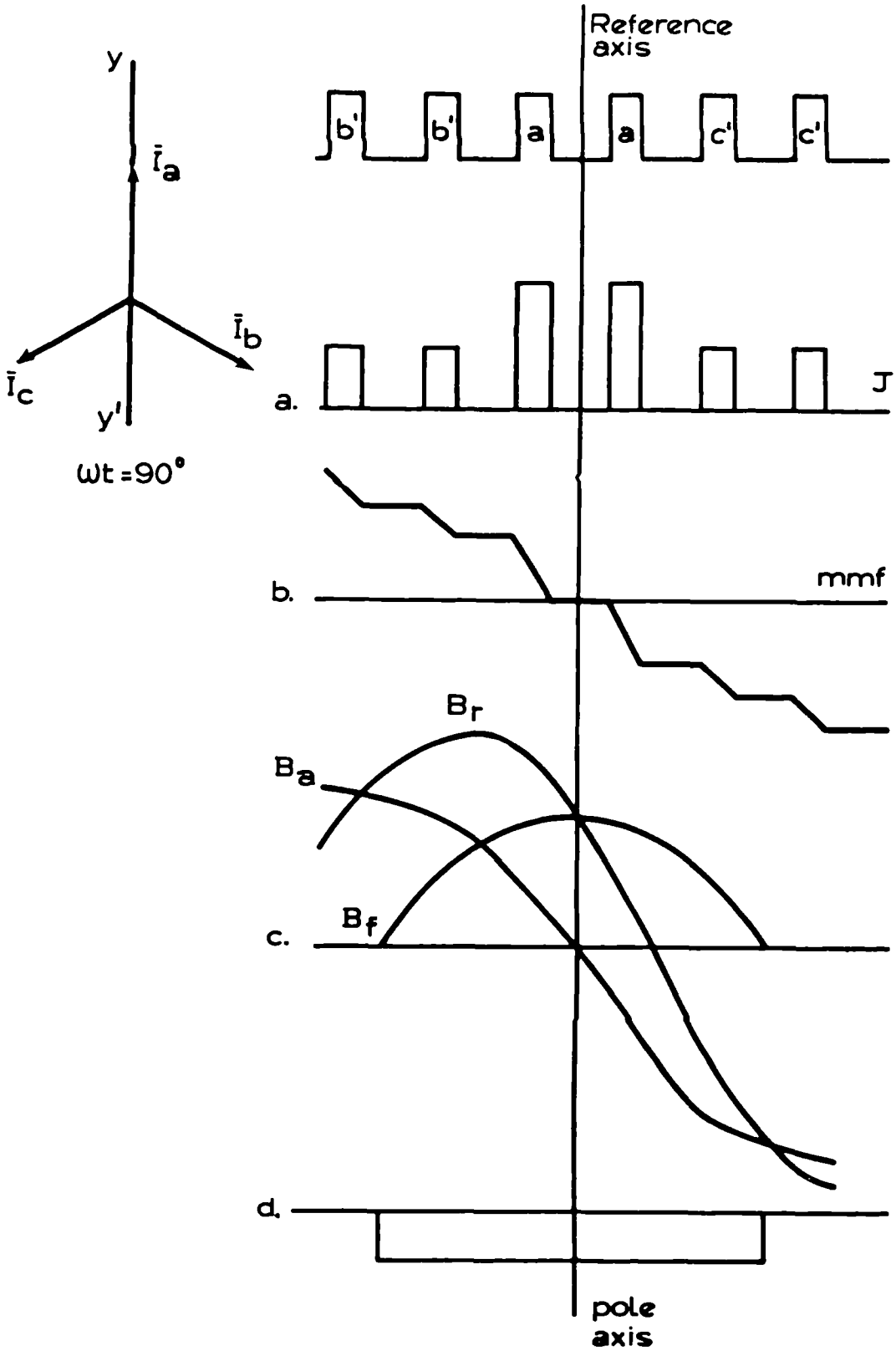

Fig.6.9 Representation of stator winding and air gap fluxes in the quadrature axis.

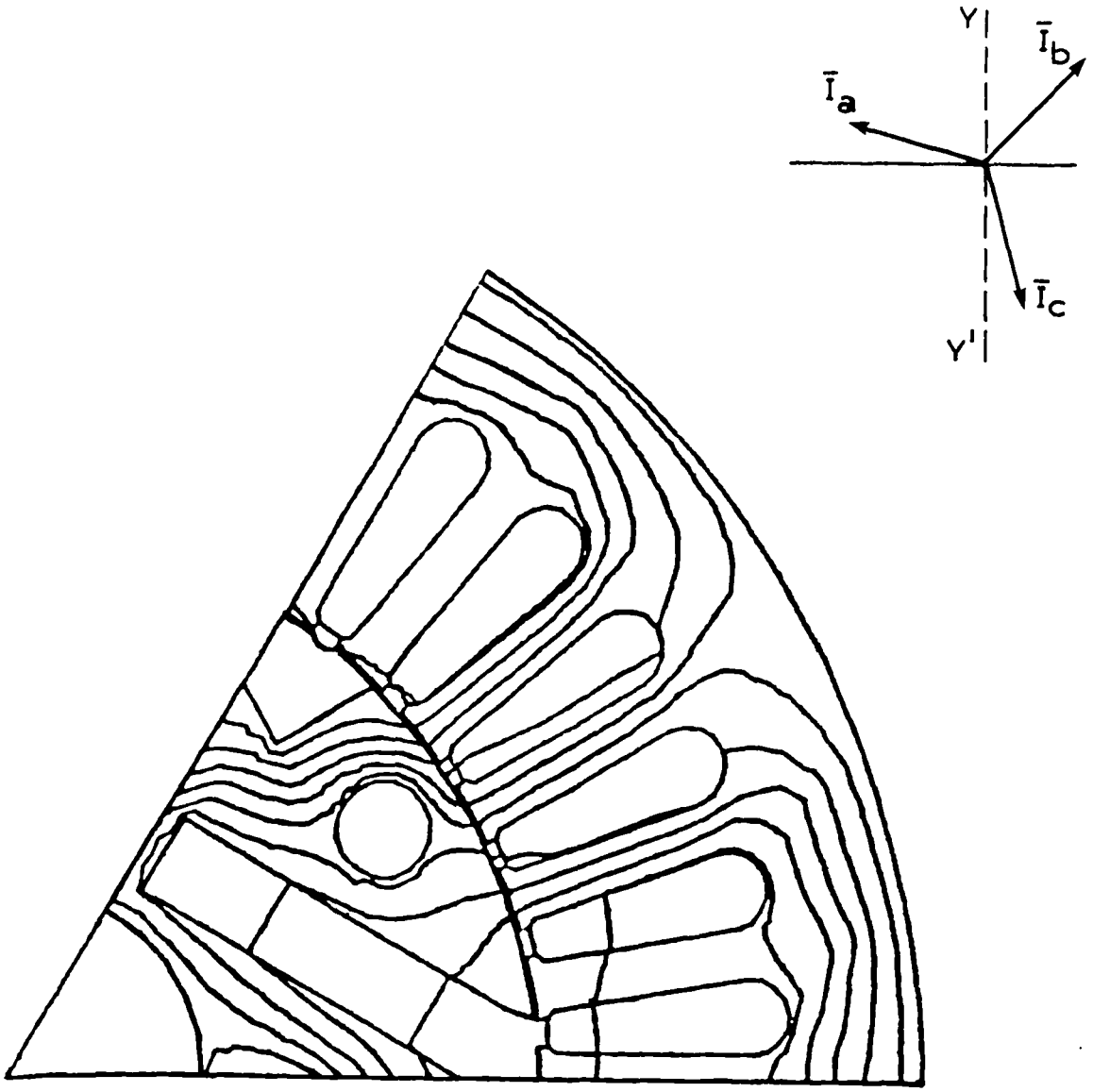

Fig.6.10 Flux distribution in the direct axis of non-symmetrical rotor pole.
$\omega t = 15°$

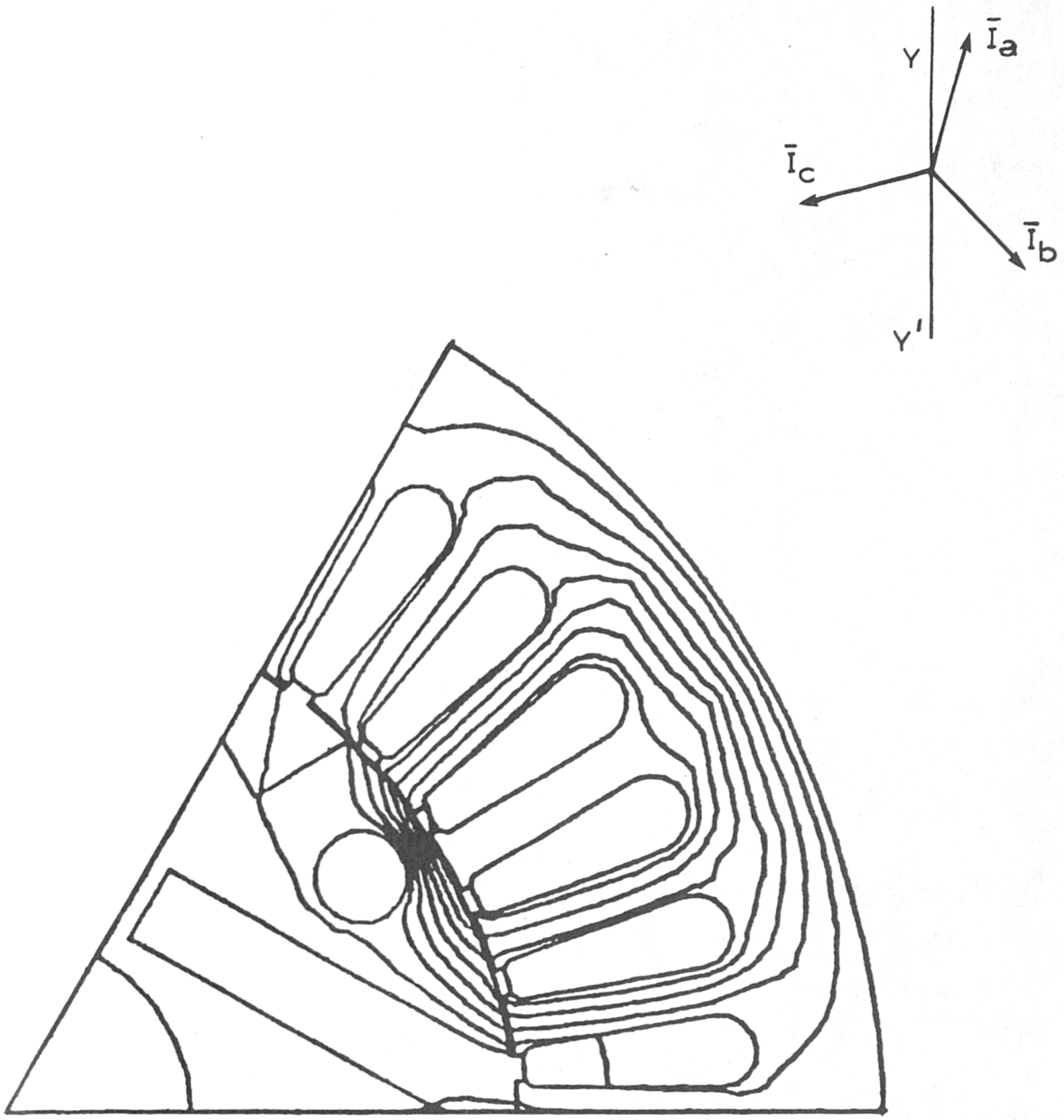

Fig.6.11 Flux distribution in the quadrature axis of non- symmetrical rotor pole.
ωt = 105°

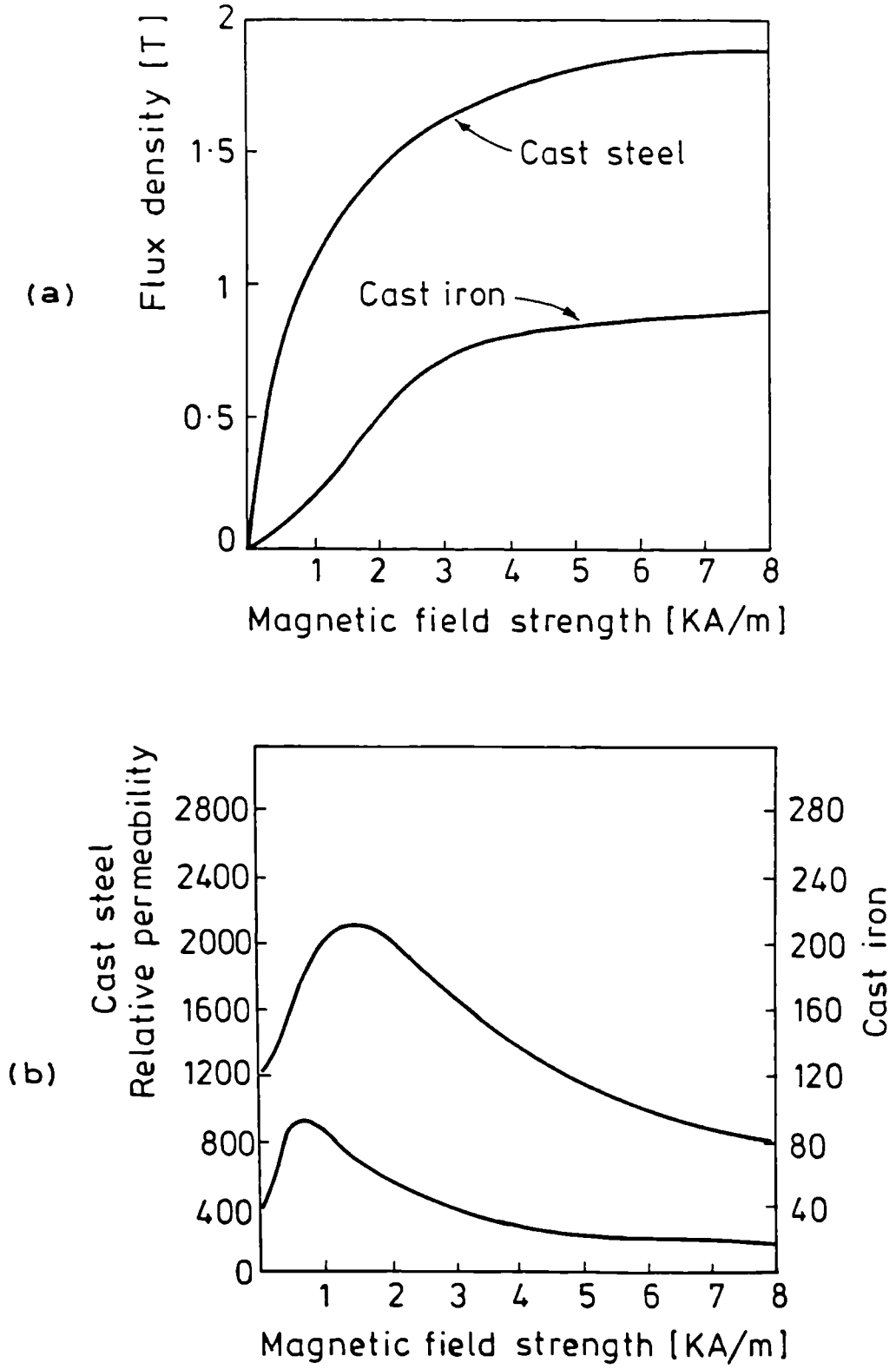

a... magnetisation curves of cast steel and iron.
b... variation of relative permeability with magnetic field strength.

Fig.6.12 Effect of saturation.

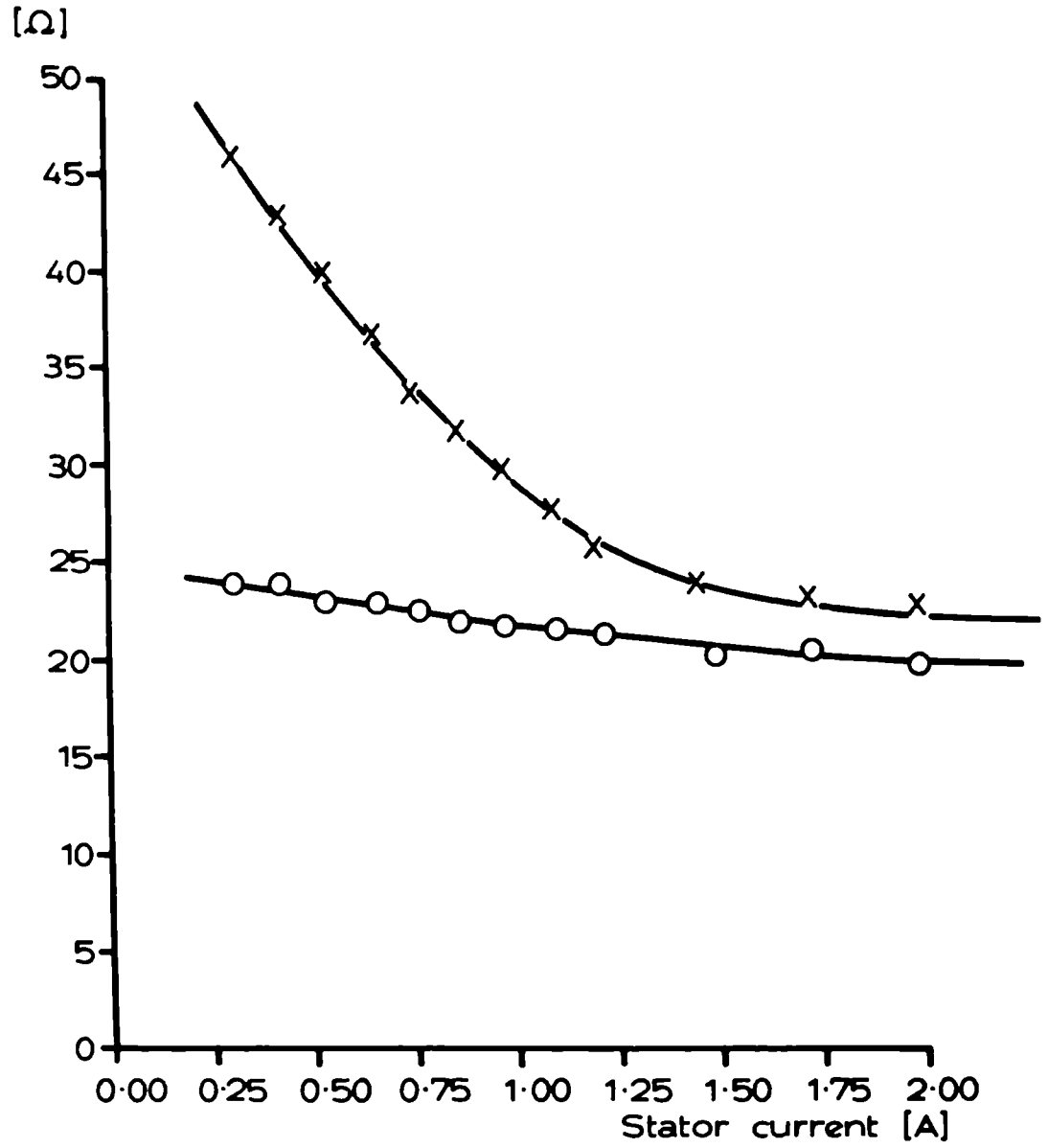

o... X_d
x... X_q

Fig.6.13 Computed direct and quadrature reactances at f = 50 Hz.

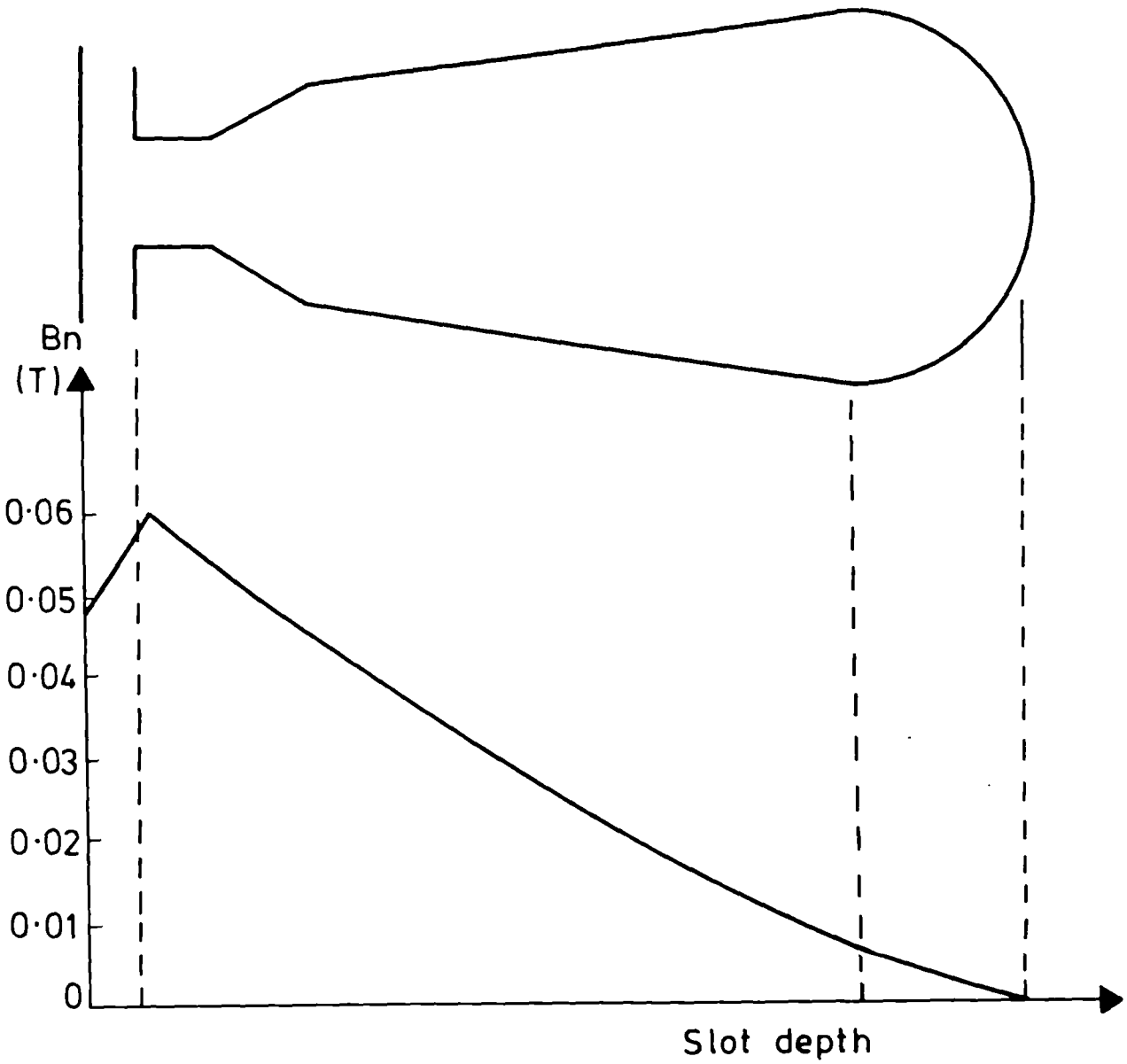

Fig.6.14 Slot leakage determination: Variation of normal flux density along the stator slot.

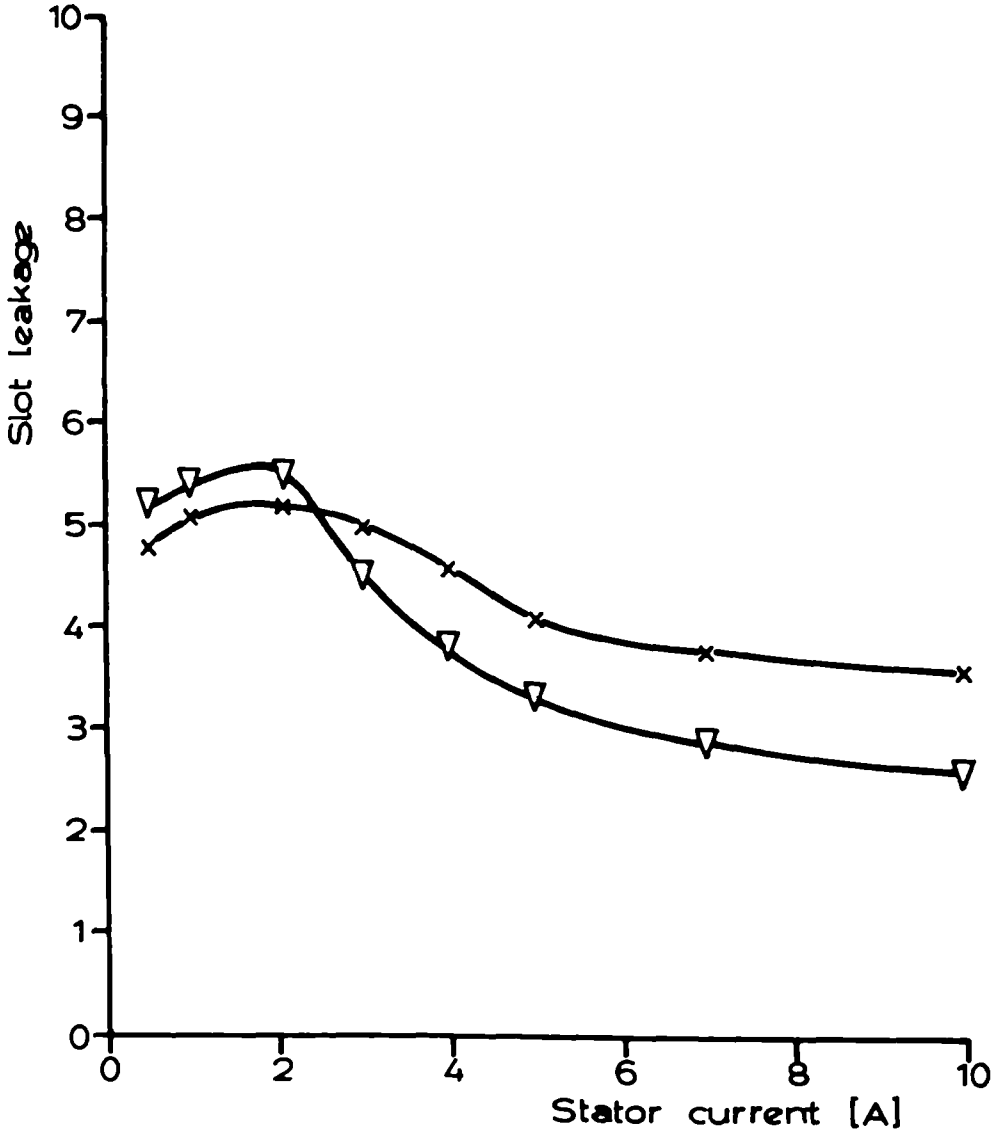

x... computation of B_n along the slot
V... computation of stored energy in each slot

Fig.6.15 Comparison of the slot leakage results obtained using different computing methods.

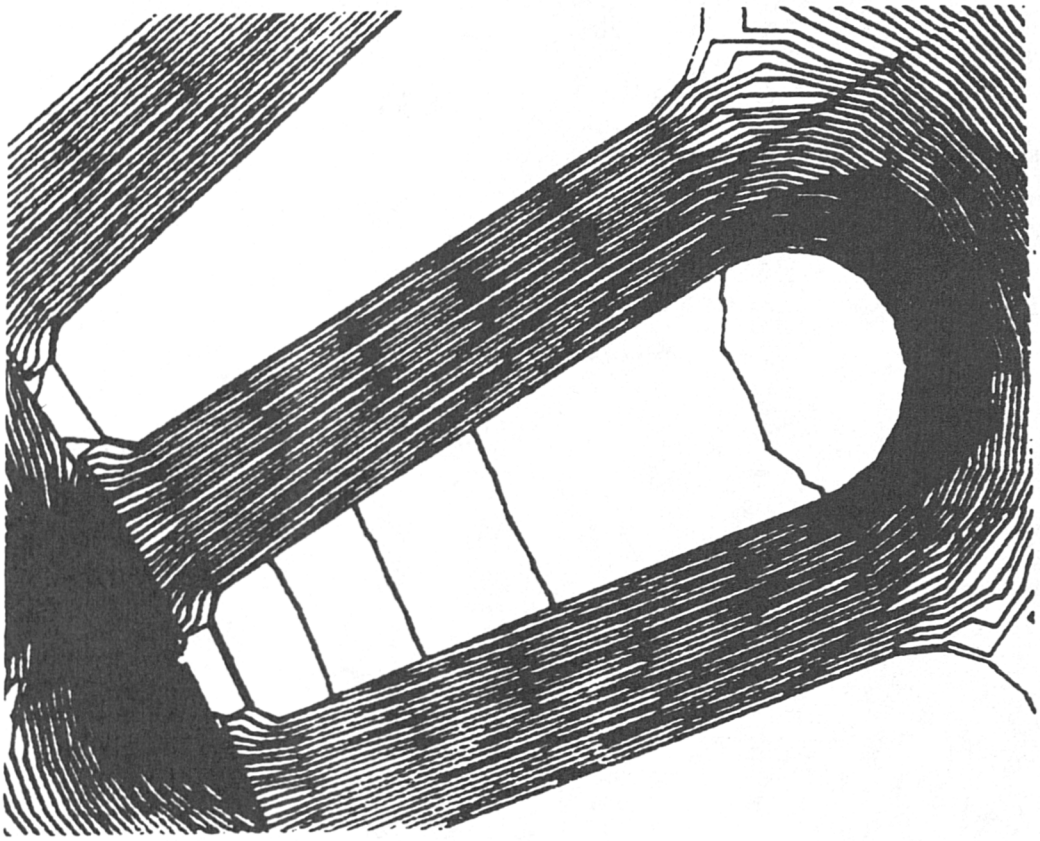

Fig.6.16 Flux map of the slot leakage.

CHAPTER SEVEN

MATHEMATICAL MODELLING OF HIGH- FIELD PERMANENT MAGNET MACHINES.

CHAPTER SEVEN

MATHEMATICAL MODELLING OF HIGH- FIELD PERMANENT MAGNET MACHINES.

7.1 Introduction

The finite element analysis used earlier in this thesis requires an input of stator current and current angle (angle between E_0 and I) from which the terminal voltage and torque can be computed. However in practice a motor is operated at fixed terminal voltage and loaded with a specific torque. To simulate this condition a model is required in which the torque and terminal voltage form the input. The output from this practical model would be the stator current, power factor, efficiency, and load angle. To achieve this using finite element analysis alone is difficult and the practical model is better accomplished by using a per- phase equivalent circuit in which the parameters have been determined using the finite element method.

In this chapter the analysis of per- phase equivalent circuit model is discussed and its performance is tested. The six- pole machine equivalent circuit parameters needed in the model have been determined in the previous chapter. It will be shown however that to solve the equivalent circuit with inputs of torque and voltage requires complex

mathematical iteration. Therefore for convenience in the initial testing a model which has a direct mathematical solution is applied in which the current, terminal voltage and the load angle form the input data and torque predictions from the output are compared with test results. The three separate approaches of the finite element analysis, the practical model, and the direct convenient model are summarised in block diagram form in Fig.7.1.

7.2 Simplified torque equation

The steady state performance of the machine is described using a set of equations derived from the phasor diagram, (51,72). These equations are set by appropriate projections of various quantities of the circuit on the direct and quadrature axes. The phasor diagram of a salient pole machine operating at lagging power factor is shown in Fig.7.2.a.

It has been shown in the previous chapter that for PM machines the quadrature synchronous reactance X_q is greater than the direct value X_d. To discuss the consequences of this relation we refer to the phasor diagram of Fig.7.2 from which the equation for the developed power is given by:

$$P = I_q V_t \cos\delta - I_d V_t \sin\delta \qquad (7.1)$$

Neglecting the armature resistance and lumping leakage reactance into X_d and X_q, as shown in Fig.7.2.b, gives the following expressions:

$$\sin \delta = \frac{I_q X_q}{V_t}$$

from which

$$I_q = \frac{V_t}{X_q} \sin \delta$$

$$\cos \delta = \frac{E_0 + I_d X_d}{V_t}$$

so that

$$I_d = \frac{V_t \cos \delta - E_0}{X_d} \qquad (7.2)$$

Substituting into eq.(7.1) gives:

$$P = \frac{E_0 V_t \sin \delta}{X_d} + \frac{V_t^2}{2} \left(\frac{1}{X_q} - \frac{1}{X_d} \right) \sin 2\delta \qquad (7.3)$$

from which the approximate torque per 3 phases would be:

$$T = \frac{3}{\omega} \left(\frac{E_0 V_t \sin \delta}{X_d} + \frac{V_t^2}{2} \left(\frac{1}{X_q} - \frac{1}{X_d} \right) \sin 2\delta \right) \qquad (7.4)$$

(a) (b)

This torque equation is the basis for design and modelling because it describes the dependence of the output torque on both the machine and the supply parameters.

The first term in the torque expression (a) represents the normal synchronous torque whereas the second term (b) represents a component of the torque due to the saliency of the rotor known as the reluctance torque, (89,96). The consequences of the relation $X_q > X_d$ on the torque equation are:

1- The value of the synchronous torque in term (a) is increased due to the smaller value of X_d . The value of $\sin\delta$ is on the other hand, decreasing but not at the same rate.

2- The reluctance torque of term (b) is reversed in sign leading to a torque- vs- load angle characteristic as shown in Fig.7.3. The no- load operating point of the machine is at $\sin\delta = \sin\delta_0$ instead of at $\sin\delta = 0$. This means that at the no- load condition neither axis is in alignment with the axis of the maximum armature current. That is because the reluctance torque tends to align the rotor quadrature axis, being the axis of minimum reluctance, whereas the magnet flux tends to align the direct axis with the armature current.

3- The addition of these two torques will result in maximum torque occurring at load angle greater than 90^o giving the machine better working capability.

7.3 Mathematical modelling of permanent magnet machine

The two- axis theory (77,88) is often used in building models that describe the machine synchronous performance. In most of these the load angle is required as an input

to the model thus involving the use of shaft sensing equipment. In the approach described in this section the model avoids any such equipment since the measured parameters are sufficient to solve the equations of the model. The key factor for this approach to be possible is the segregation of the leakage reactance from the total value of the synchronous reactance. This model also takes into account the effect of the core loss on the machine performance.

Initially it was found convenient in order to test the model to use a direct analysis model which is supplied with test values of terminal voltage, stator current and power factor to estimate the corresponding torque delivered by the machine. This is described in sections 7.3.1 and 7.3.2. In section 7.3.3 the practical application of the model, where the reverse of the above is required, is discussed. That is given a torque value and supply voltage it is required to find at what stator current, power factor, efficiency and load angle will the machine operate.

7.3.1 Determination of the induced voltage

The first step in building a complete model is to calculate the voltage 'E_i' induced in the winding under different load conditions for operations with both leading and lagging power factor. This voltage is calculated by the vector subtraction of the leakage and resistive voltage drop from the terminal voltage as shown in the phasor diagrams of Fig.7.4 where:

$$E_i = \sqrt{(V_t^2 - 2I_a V_t(R_a \cos\theta + X_l \sin\theta) + I_a^2 X_l^2 + I_a^2 R_a^2)} \qquad (7.5)$$

and the angle between the terminal voltage and the induced voltage is:

$$\alpha = \text{Atan}\left(\frac{I_a R_a \sin\theta - I_a X_l \cos\theta}{V_t - I_a R_a \cos\theta - I_a X_l \sin\theta}\right) \qquad (7.6)$$

Power factor angle ' θ ' and I_d are positive for lagging operation and negative for leading. Unity power factor operation is a special case that could be derived from either of the above cases by substituting $\theta = 0$.

7.3.2 Direct model equations considering core loss

With E_i being calculated the next step is to derive from the phasor diagram a set of equations which would directly determine the unknown currents and load angles within the machine with core loss being presented by shunt resistor R_c across the induced voltage such that:

$$W_c = I_c^2 R_c = \frac{E_i^2}{R_c} \qquad (7.7)$$

The armature current is the vector sum of the core current and the current that crosses the air gap, hence:

$$\vec{I}_a = \vec{I} + \vec{I}_c \qquad (7.8)$$

The model equations to calculate machine values are:

$$I_d = E_0 \frac{X_d}{X_q^2 - X_d^2} - \sqrt{\frac{E_0^2 + X_q^2 I^2 - E_i^2}{X_q^2 - X_d^2} + \frac{E_0^2 X_d^2}{(X_q^2 - X_d^2)^2}} \qquad (7.9)$$

$$I_q = \sqrt{I^2 - I_d^2} \tag{7.10}$$

$$\delta_i = \text{Asin}\left(\frac{I_q X_q}{E_i}\right) \tag{7.11}$$

$$\delta = \text{Asin}\left(\frac{I_q X_q + I_{aq} X_l - I_{ad} R_a}{V_t}\right) \tag{7.12}$$

and the torque is found from:

$$T = \frac{3}{\omega}\left(\frac{E_0 E_i \sin\delta_i}{X_d} + \frac{E_i^2}{2}\left(\frac{1}{X_q} - \frac{1}{X_d}\right)\sin 2\delta_i\right) \tag{7.13}$$

It should be noted that in the modified equivalent circuit stator current 'I_a' flows through the armature winding and the leakage reactance while only current 'I' passes through synchronous reactance components. Since I_c is in phase with E_i as shown in Fig.7.4 then the power factor angle of the current I differs to that of I_a.
Over the range of currents drawn by the machine up to a value of 1.1 A it can be seen with reference to Fig.7.5 that X_d remains relatively constant whereas X_q has a linear characteristic of the form:

$$X_q = X_{qo} - kI_q \tag{7.14}$$

7.3.3 Practical approach

The analysis, to be discussed in this section, meets the practical requirements in the normal motor operation where for a specific load torque, frequency, and voltage

it is required to predict the current that will flow in the stator winding, its power factor, the load angle, and the machine efficiency. In this case there is no direct solution to the equivalent circuit equations and instead an iterative procedure needs to be adopted.

From the torque equation the following expression is implied:

$$\frac{\omega T}{3} = \frac{E_0 E_i \sin \delta_i}{X_d} + \frac{E_i^2}{2}\left(\frac{1}{X_q} - \frac{1}{X_d}\right) \sin 2\delta_i \qquad (7.15)$$

and from the phasor diagram:

$$\sin \delta_i = \frac{I_q X_q}{E_i} \qquad (7.16)$$

$$\cos \delta_i = \frac{E_o + I_d X_d}{E_i} \qquad (7.17)$$

substituting equations 7.16 and 7.17 back into 7.15 gives:

$$\frac{\omega T}{3} = I_q X_q\left(\frac{E_o}{X_d} + \left(\frac{1}{X_q} - \frac{1}{X_d}\right)(E_o + I_d X_d)\right) \qquad (7.18)$$

Rearranging and solving for I_q gives:

$$I_q = \frac{\omega T}{3} \frac{1}{E_o + I_d(X_d - X_q)} \qquad (7.19)$$

The iteration procedure is started with Equation (7.19) by setting an initial value for I_d chosen here to be zero, (I_d = 0). The following calculations are then performed

in order. These equations have been derived by resolving the voltages and currents of the equivalent circuit as shown in Fig.7.2 along the d- and q- axis respectively.

$$X_q = X_{qo} - kI_q \tag{7.20}$$

$$I_{cq} = \frac{E_0 + I_d X_d}{R_c} \tag{7.21}$$

$$I_{cd} = \frac{I_q X_q}{R_c} \tag{7.22}$$

$$I_c = \sqrt{I_{cq}^2 + I_{cd}^2} \tag{7.23}$$

$$I_{aq} = I_q + I_{cq} \tag{7.24}$$

$$I_{ad} = I_d - I_{cd} \tag{7.25}$$

$$V_{td} = I_q X_q + I_{aq} X_l - I_d R_a \tag{7.26}$$

$$V_{tq} = \sqrt{V_t^2 - V_{td}^2} \tag{7.27}$$

$$I_d = \frac{V_{tq} - E_0 - I_{ad} X_l - I_{aq} R_a}{X_d} \tag{7.28}$$

The value of I_d determined by Equation (7.28) is substituted back to Equation (7.19) and the calculation is repeated until I_d converges to within a specific accuracy. In general convergence occurs well within 10 iterations.

7.4 Model performance

Initially the model is tested using the direct analysis previously described in section 7.3.2 by comparing its

torque predictions with test results of the six- pole machine at different frequencies and excitations. The results of this comparison are shown in Fig.7.6 to 7.8. In particular in Fig.7.6 the model has been solved with and without the core loss term (R_c). From this figure it is evident that inclusion of core loss in the model leads to more accurate estimation of the machine performance. Again in Fig.7.7 and 7.8 with the core loss being included the estimated values of the torque are very close to the test results.

The results for the practical analysis where the terminal voltage and torque are the only input to the model are shown in Fig.7.9 to 7.11. The characteristics of the machine frequency and power factor are plotted against the torque for different voltage levels as shown in Fig.7.9 and 7.10 respectively. In these two figures the values obtained by the model are slightly underestimated at leading power factor. This is contributed to the fact that the direct- axis reactance has been considered constant whereas actually it has a relatively higher value when the machine is overexcited and operating at leading power factor. The estimated values of both, the load angle and the internal load angle, with the current as calculated by the model are presented in Fig.7.11. The low values of the load angle is due to the high field produced by the rare earth magnets as explained in Chapter 4.

7.5 Sensitivity analysis of the model

To analyse the sensitivity of the developed model, the variation of the output torque with the change of each of the equivalent circuit parameters is investigated.

7.5.1 Influence of machine parameters on the output

The sensitivity of the torque predictions of the model to changes in the equivalent circuit parameters is analysed with the machine operating at rated current and each of three conditions of excitation corresponding to leading, lagging and unity power factors. The PM machine used operates normally at power factor close to unity. For the purpose of this analysis a lower power factor ($\cos\theta$) has been chosen in order to make the difference between leading and operation more significant. In the following, the effects of changing X_l, R_a, X_d, X_q and E_0 by a percentage up to ± 10 % are discussed and the results are presented in Tables 7.1 - 7.5.

a- Increasing X_l has the effect of slightly increasing the estimated torque at both leading and lagging power factors. As expected at unity power factor changing X_l has no effect. As Fig.7.4.a indicates, at leading power factor any increase in X_l at a fixed terminal voltage leads to an increase in E_i. The machine is then operating closer to the unity power factor point and the torque therefore increases. For lagging power factor operation when the machine is underexcited an increase in X_l will tend to reduce E_i and consequently again the torque will improve

as shown in Fig.7.4.b. In both cases torque changes are small as shown in Table 7.1 thus confirming that leakage reactance has little influence on the output. Moreover, due to the signs of X_l in equation (7.5), torque variation is more significant for leading because both terms of the leakage are added to the total value whereas in lagging operation the two terms of X_l have different signs.

b- Sensitivity analysis of the variation of the winding resistance is similar to that of X_l. However there is a difference at at leading power factor where the machine is overexcited since increasing R_a would add to this overexcitation and hence the power factor and output would drop as shown in Table 7.2. At lagging operation where terminal voltage is greater than E_0, increasing R_a would reduce the difference between the two voltages, as a result power factor would be closer to unity and torque would increase.

c- As X_d increases, synchronous torque presented by term (a) of equation (7.4) decreases while reluctance torque of term (b) is on the other hand increasing in higher rate. As a result total torque increases slightly with larger X_d for both leading and lagging operations.

d- Variation of X_q depends to a great extent on the machine saturation and therefore X_q has an important influence on the machine performance. However, in this analysis the variation of parameters is limited to only 10% of the rated value which is somewhat lower than the change in X_q from zero to full saturation. For an increase in X_q the reluctance torque drops slightly but the synchronous

torque increases at greater rate leading to a small overall increase in torque as shown in Table 7.4.

e- Of all the machine parameters the variation of E_0 has the most significant effect. As indicated in table 7.5 a variation in E_0 of only a few percent can lead to considerable changes in the estimated torque. Care therefore must be taken in ensuring a correct value of E_0 is used in the model.

7.5.2 Influence of I_d on the magnets

Demagnetisation of the magnetic material is one of the problems associated with PM machines. The direct- axis component of the stator current can have either a magnetising or a demagnetising effect. It has been presented in the model by Equation (7.9). However, it could be expressed as:

$$I_d = I \sin \beta \tag{7.29}$$

where β is the difference between the power factor angle and the load angle, that is:

$$\beta = \theta - \delta$$

I_d has a magnetising effect when the above equation is positive. This corresponds to the condition where the current is lagging behind the magnet's E_0 as shown in Fig.7.12.a.

The demagnetisation occurs when I_d is negative and the current is leading E_0 as illustrated in Fig.7.12.b. The demagnetisation current under these conditions is maximum

at the instant of the pull- out torque where the admissible value I_d equal to I and:

$$E_i = E_0 - I_d X_d - I_a X_l \qquad (7.30)$$

There is a range where I_d is difficult to determine. This is the range when β is changing from positive to negative and with it I_d is changing from magnetising to demagnetising. Although it has been assumed that the value of X_d is unaffected by saturation, from Fig.7.5 it can be observed that X_d changes in both magnetising and demagnetising conditions.

7.6 Conclusion

A modified equivalent circuit, in which the core loss is represented by a shunt resistor across the induced voltage, is described. A mathematical model derived from this modified circuit has two main features. First, it avoids the need for shaft sensing equipment to determine some of the necessary parameters. Secondly, it takes into account the non- linearity of the machine analysis mainly by considering the effect of saturation on the values of X_d and X_q and by representing the core loss in the equivalent circuit by a shunt resistor across the induced voltage. This model permits the simulation of the machine at steady state condition.

The results obtained from this new model are found to be very close to those obtained form the experimental measurements and finite element computation. Sensitivity

analysis has shown that leakage reactance, winding resistance, and the direct- axis reactance have little influence on the results obtained from the proposed model. On the other hand quadrature- axis reactance could be very influential if the rate of change is higher. The effect of the induced voltage is proved to be the most significant.

X_l		calculated torque					
		lead		lag		unity	
%	value	%	value	%	value	%	value
-10	5.4	-0.8	8.69	-0.2	9.69	0	9.727
-5	5.7	-0.4	8.73	-0.07	9.70	0	9.727
0	6	0	8.77	0	9.71	0	9.727
5	6.3	0.4	8.80	0.1	9.72	0	9.727
10	6.6	0.8	8.84	0.17	9.73	0	9.727

Table 7.1 Influence of the leakage reactance on the output torque.

R_a		calculated torque					
		lead		lag		unity	
%	value	%	value	%	value	%	value
-10	22	4.4	9.17	-1.7	9.55	-2	9.54
-5	23.3	2.3	8.97	-0.7	9.65	-0.7	9.66
0	24.5	0	8.77	0	9.71	0	9.727
5	25.7	-2.7	8.53	0.4	9.75	0.3	9.76
10	26.9	-5.7	8.27	0.6	9.77	0.4	9.77

Table 7.2 Influence of the winding resistance on the output torque.

X_d		calculated torque					
		lead		lag		unity	
%	value	%	value	%	value	%	value
-10	19	-2.3	8.56	-0.2	9.69	0.15	9.71
-5	20	-1	8.67	-0.1	9.7	0.06	9.721
0	21	0	8.77	0	9.71	0	9.727
5	22	0.9	8.85	0.1	9.72	0.05	9.732
10	23	1.7	8.92	0.2	9.73	0.1	9.737

Table 7.3 Influence of the direct- axis reactance on the output torque.

X_q		calculated torque					
		lead		lag		unity	
%	value	%	value	%	value	%	value
-10	24.3	0.06	8.774	-0.04	9.71	-0.04	9.723
-5	25.6	0.04	8.772	-0.02	9.71	-0.02	9.725
0	27	0	8.77	0	9.71	0	9.727
5	28.3	0.05	8.76	0.03	9.71	0.02	9.73
10	29.7	-0.1	8.757	0.06	9.72	0.04	9.32

Table 7.4 Influence of the quadrature- axis reactance on the output torque.

E_0		calculated torque					
		lead		lag		unity	
%	value	%	value	%	value	%	value
-2	304	6.7	9.4	-8.5	8.88	-8	8.94
-1	307	4.5	9.18	-3.3	9.39	-3	9.42
0	310	0	8.77	0	9.71	0	9.72
1	313	-7.2	8.13	1.5	9.86	1.4	9.86
2	316	-18	7.2	1.4	9.85	-0.1	9.71

Table 7.5 Influence of the induced voltage on the output torque.

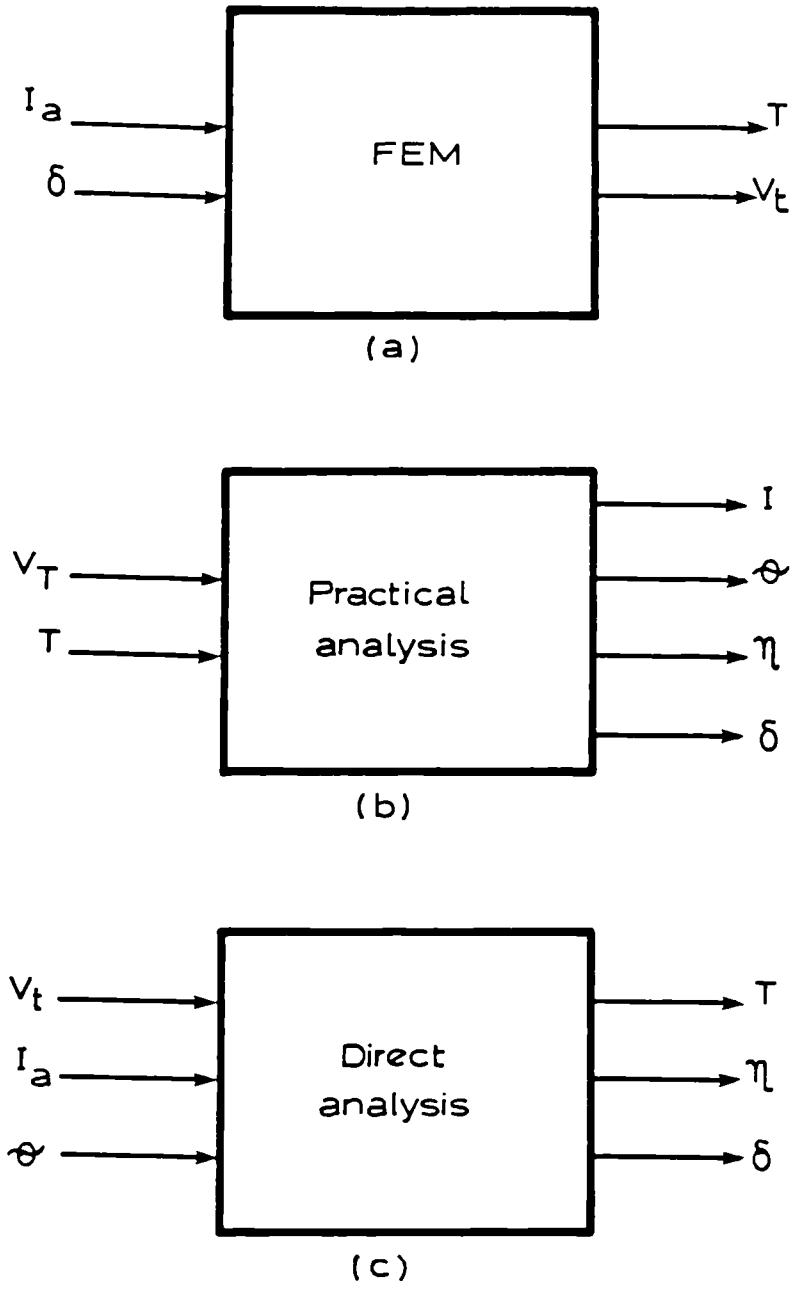

Fig.7.1 Classification of modelling analysis according to the input data.

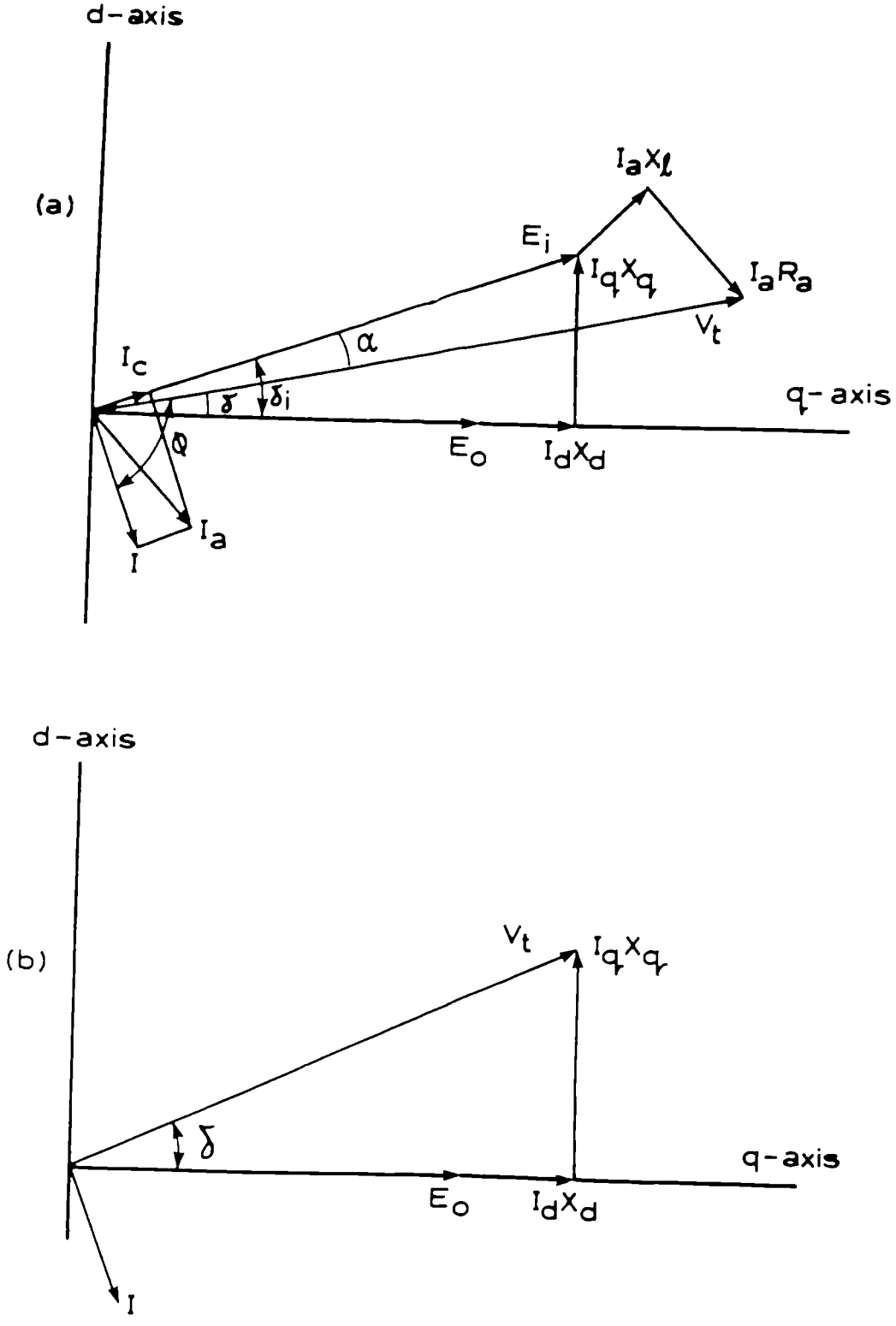

Fig.7.2 Modified phasor diagram of PM motor at lagging power factor.

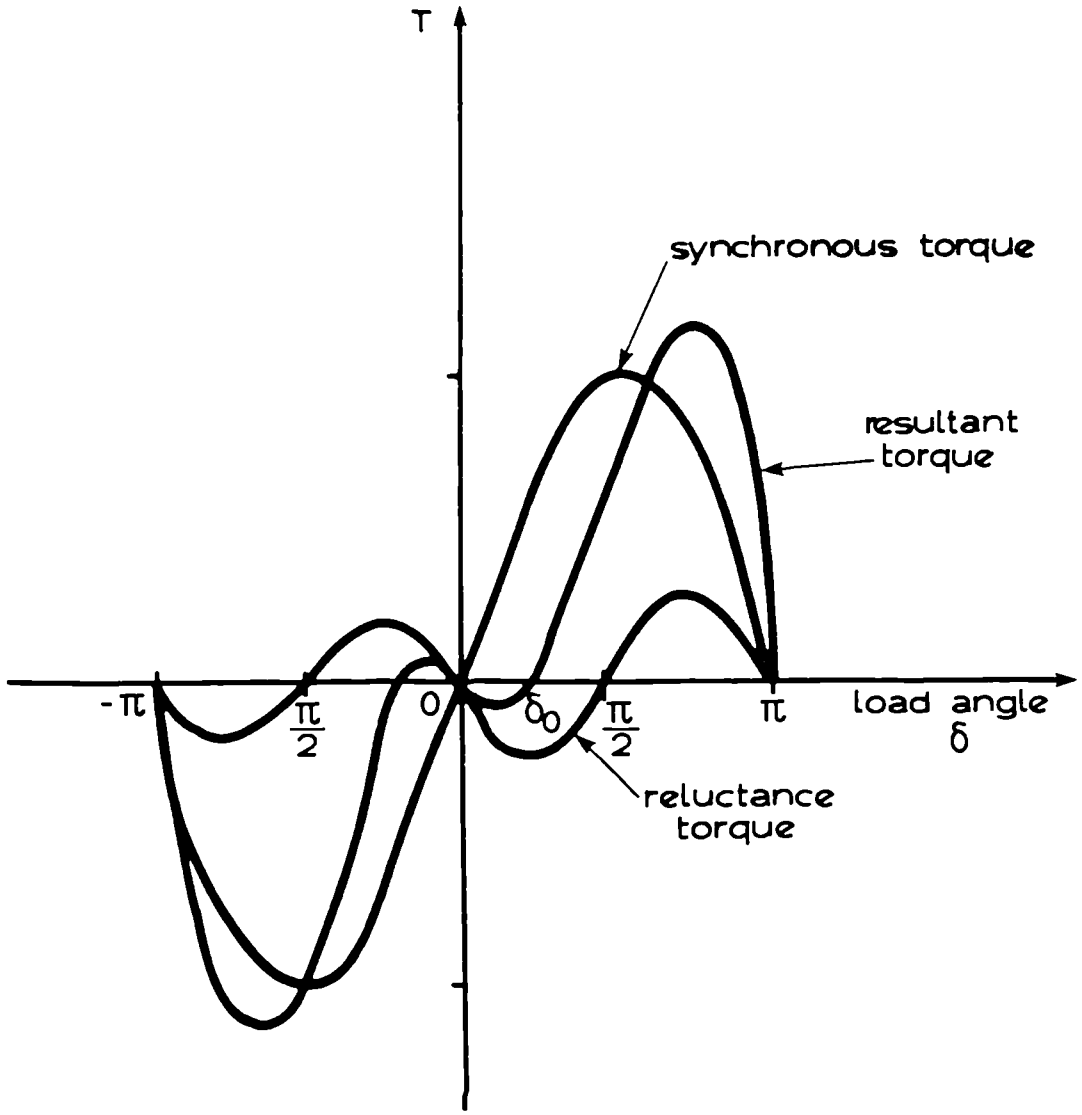

Fig.7.3 Torque versus load angle curves for salient pole PM motor with $X_q > X_d$.

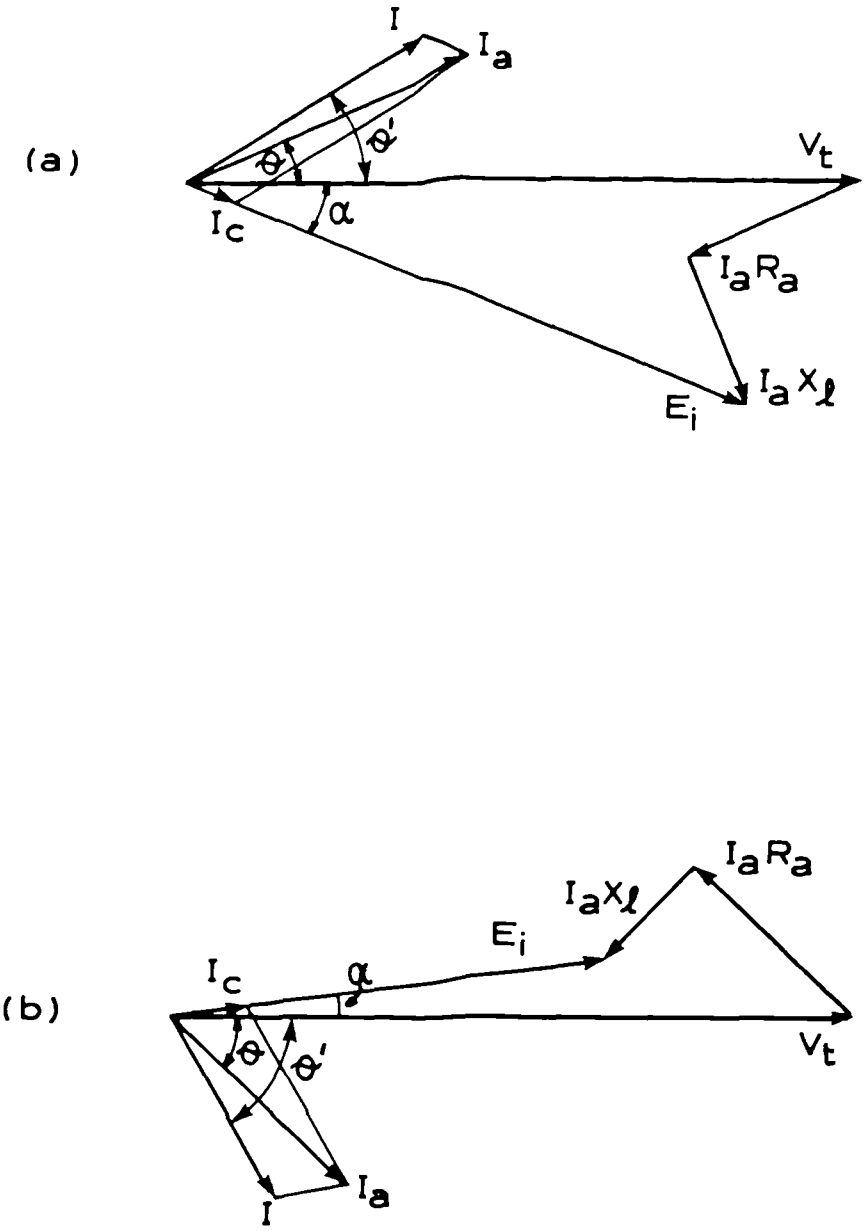

a... leading power factor
b... lagging power factor

Fig.7.4 Calculation of the voltage induced in the air gap.

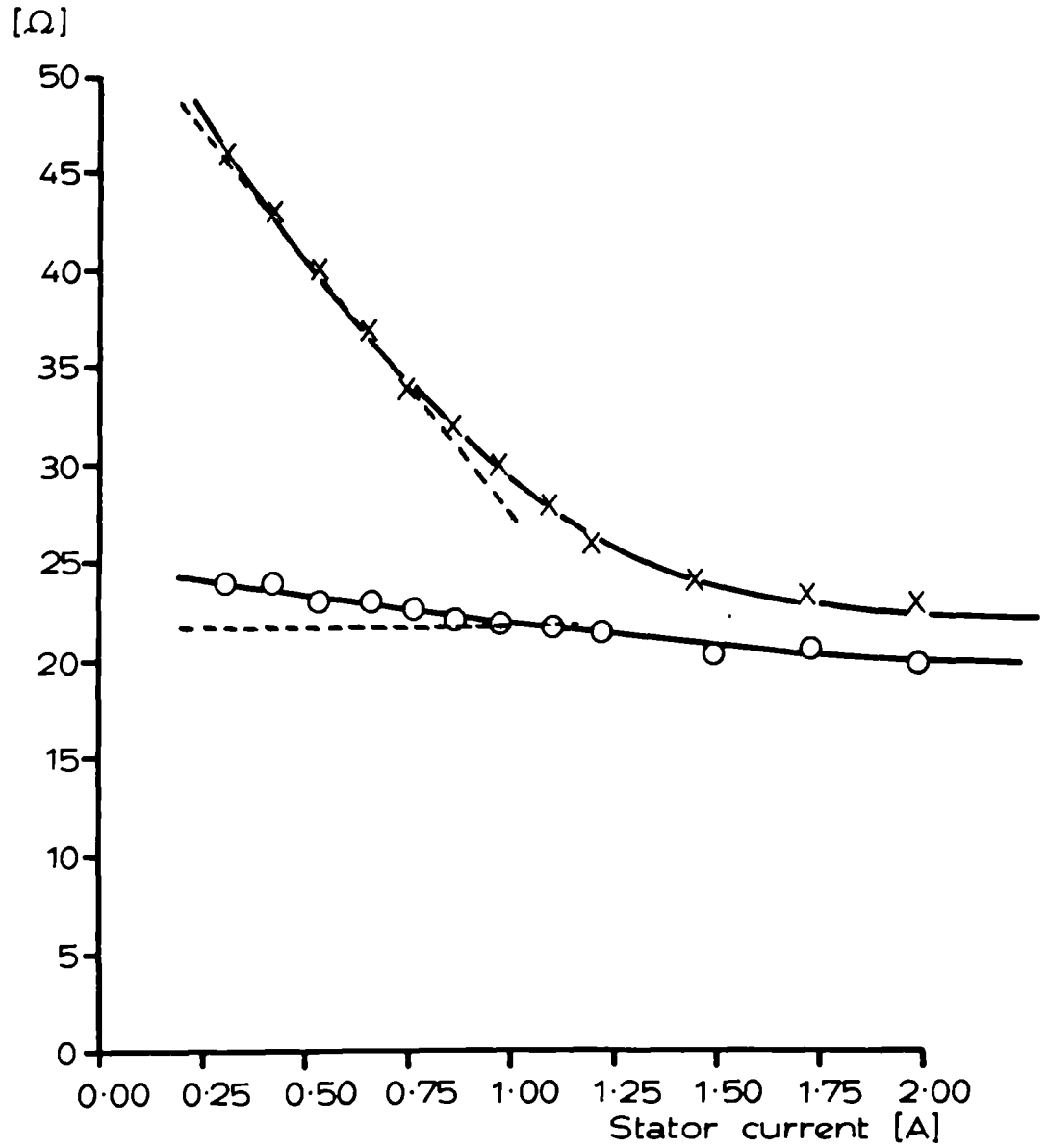

o... X_d
x... X_q

Fig.7.5 Linearised characteristics (dotted) of direct- and quadrature- axis reactances.

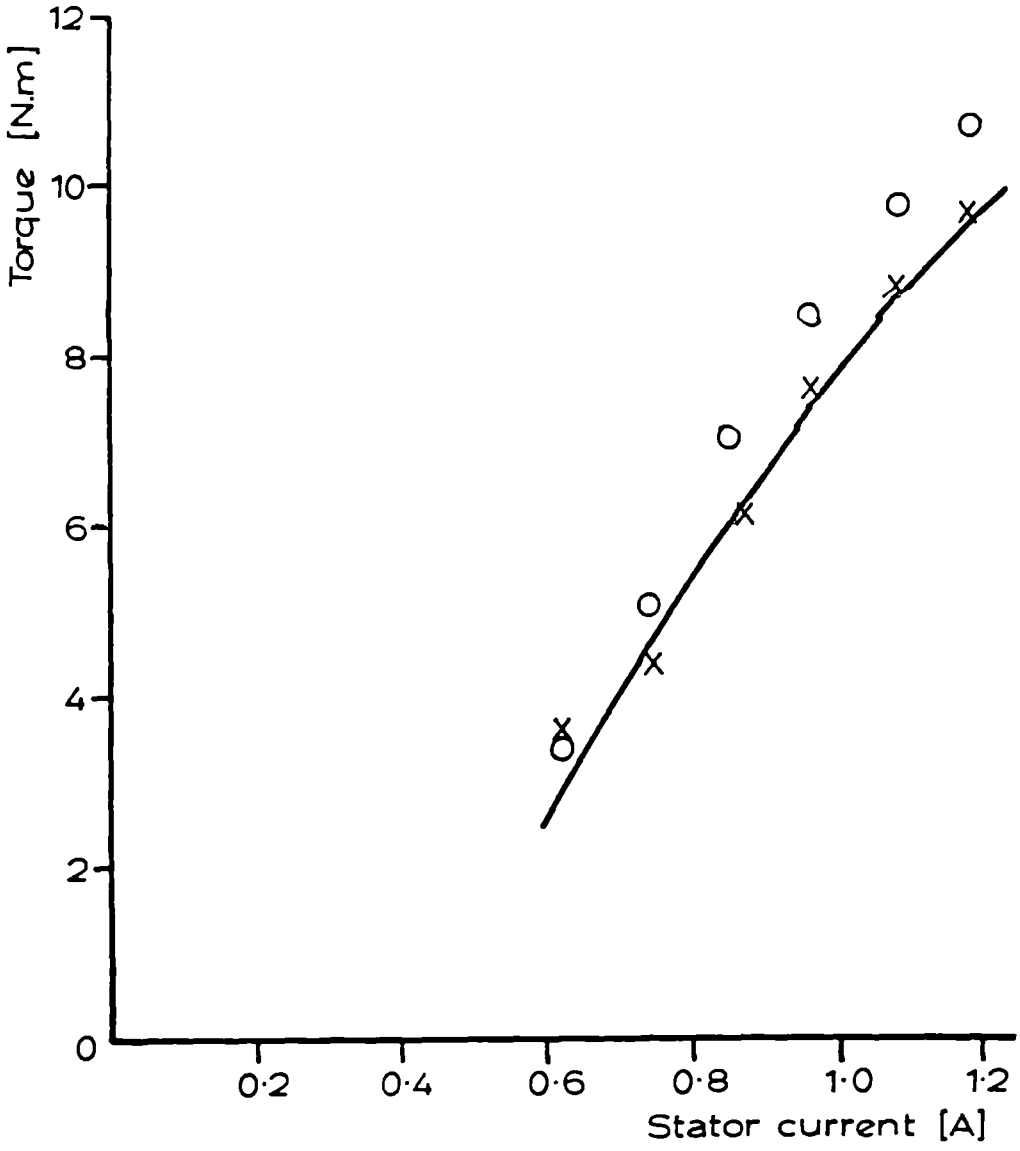

—... test results
o... results of modelling without core
x... results of modelling with core loss

Fig.7.6 Measured torque characteristic in comparison to model results.

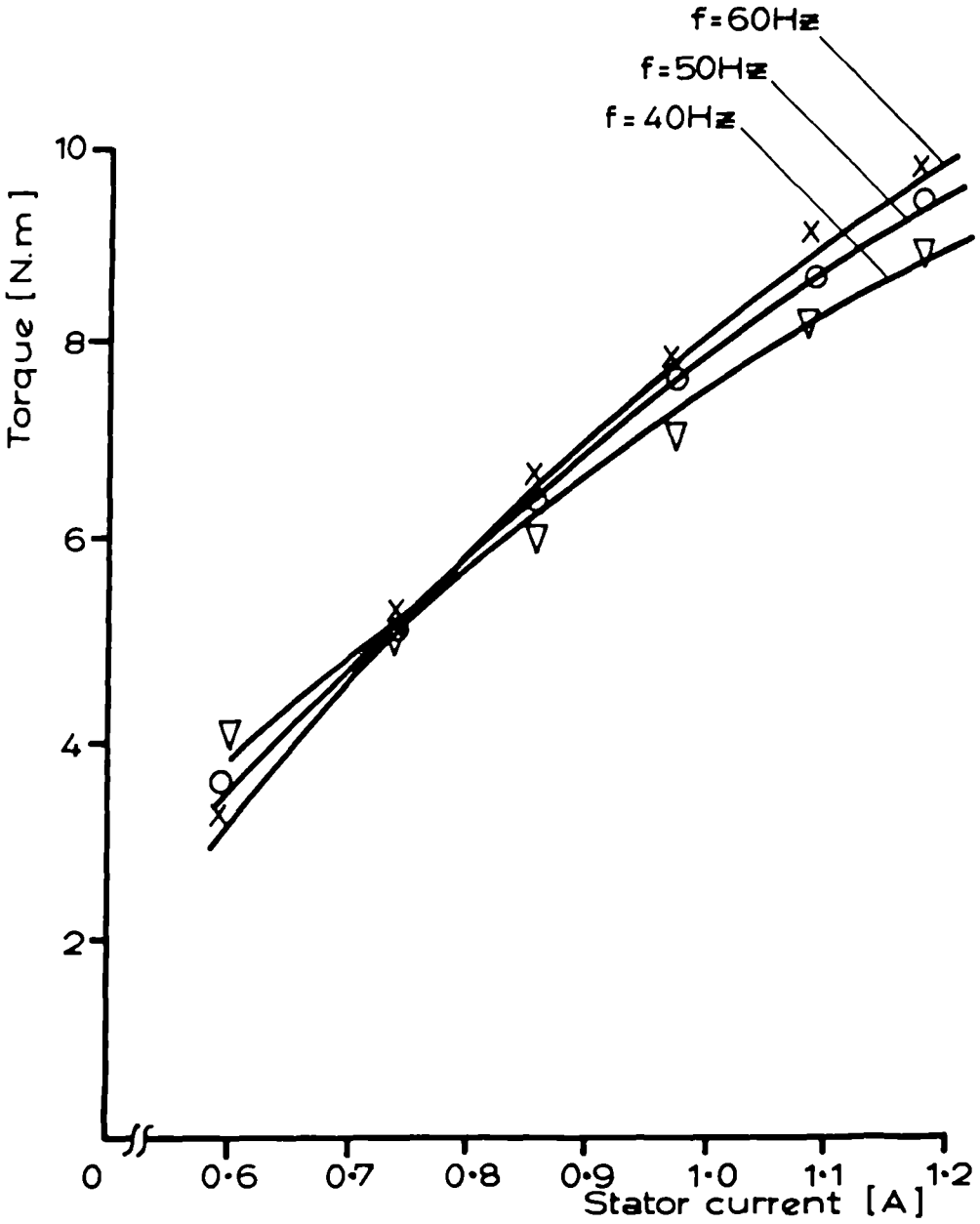

∇... model results at f = 40 Hz
o... model results at f = 50 Hz
x... model results at f = 60 Hz

Fig.7.7 Torque characteristics at different frequencies as obtained experimentally and from the model.

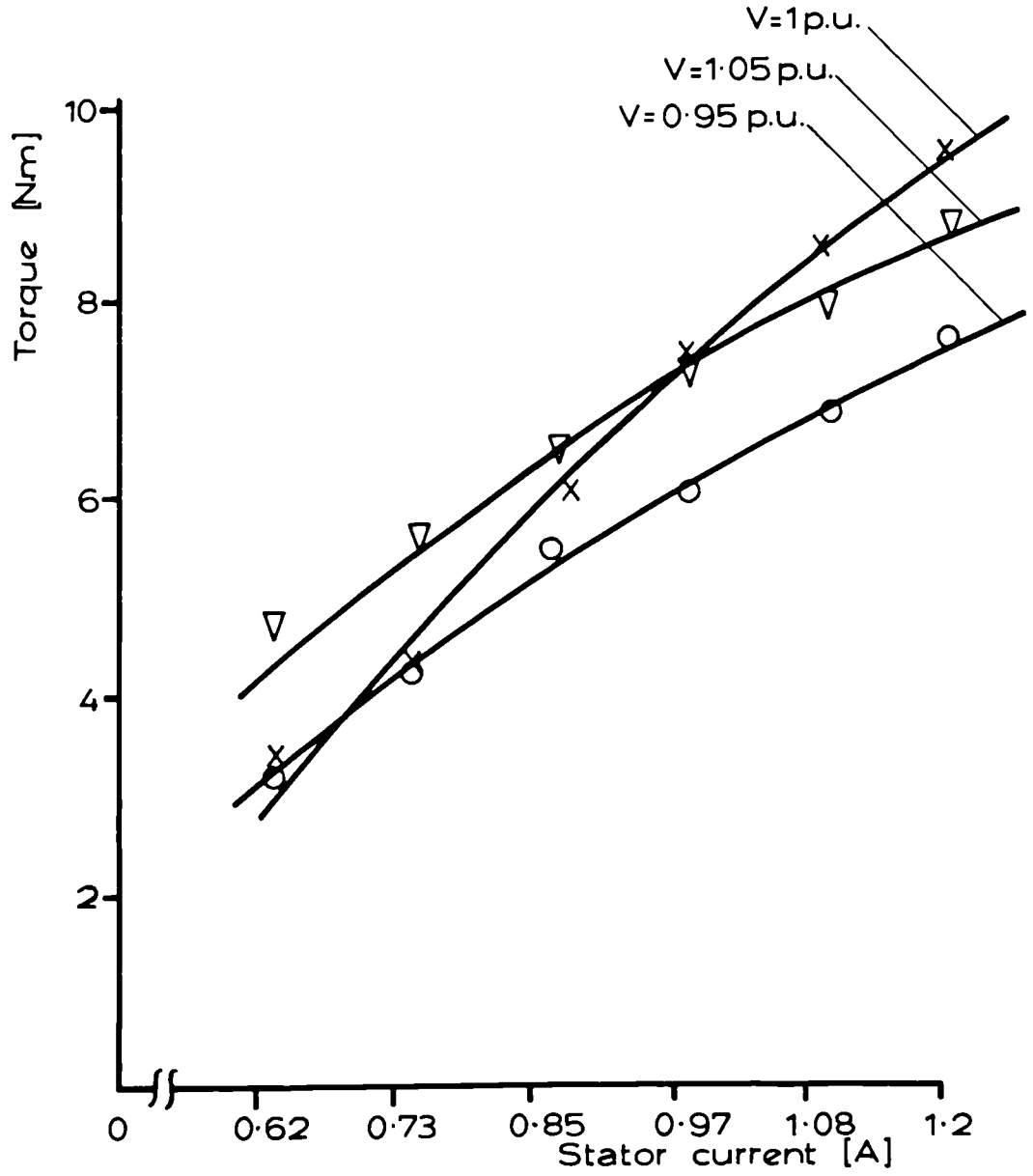

o... model results for V = 0.95 p.u.
x... model results for V = 1 p.u.
∇... model results for V = 1.05 p.u.

Fig.7.8 Torque characteristics at different voltage levels as obtained experimentally and from the model.

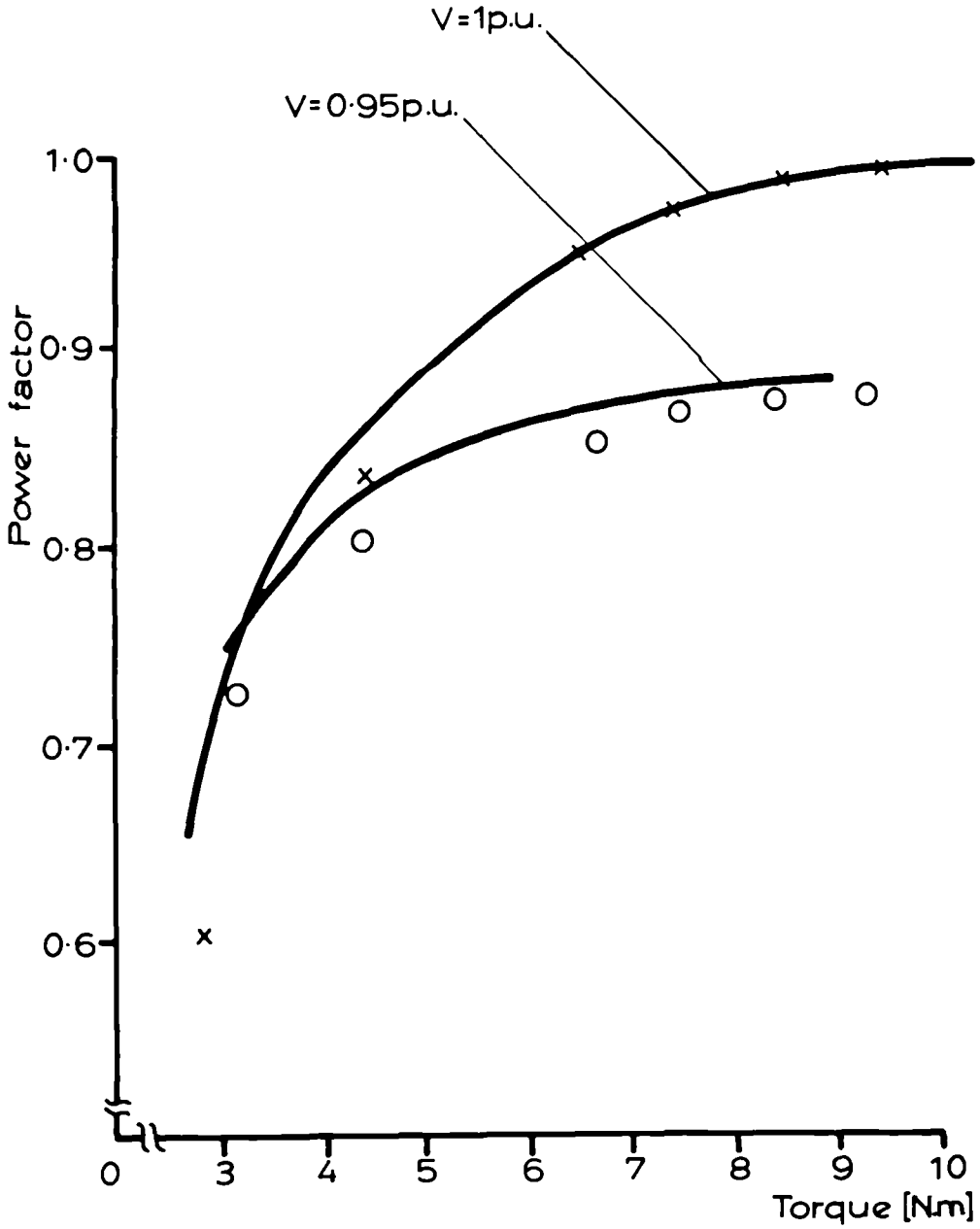

o... model results for V = 0.95 p.u.
x... model results for V = 1 p.u.

Fig.7.9 Power factor - torque characteristics for different voltage levels.

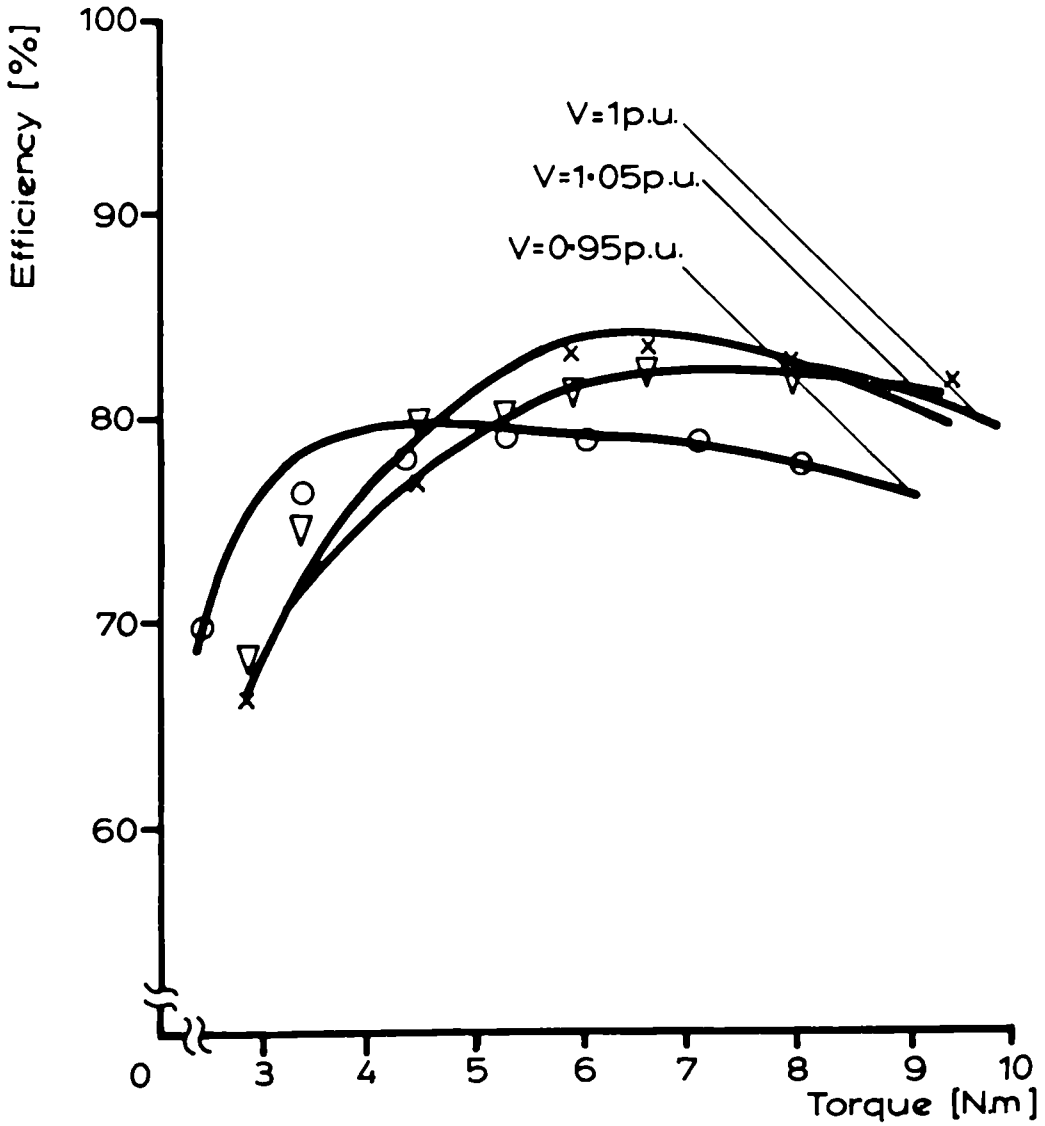

o... model results for V = 0.95 p.u.
∇... model results for V = 1 p.u.
x... model results for V = 1.05 p.u.

Fig.7.10 Characteristic of the machine efficiency as obtained experimentally and from the model.

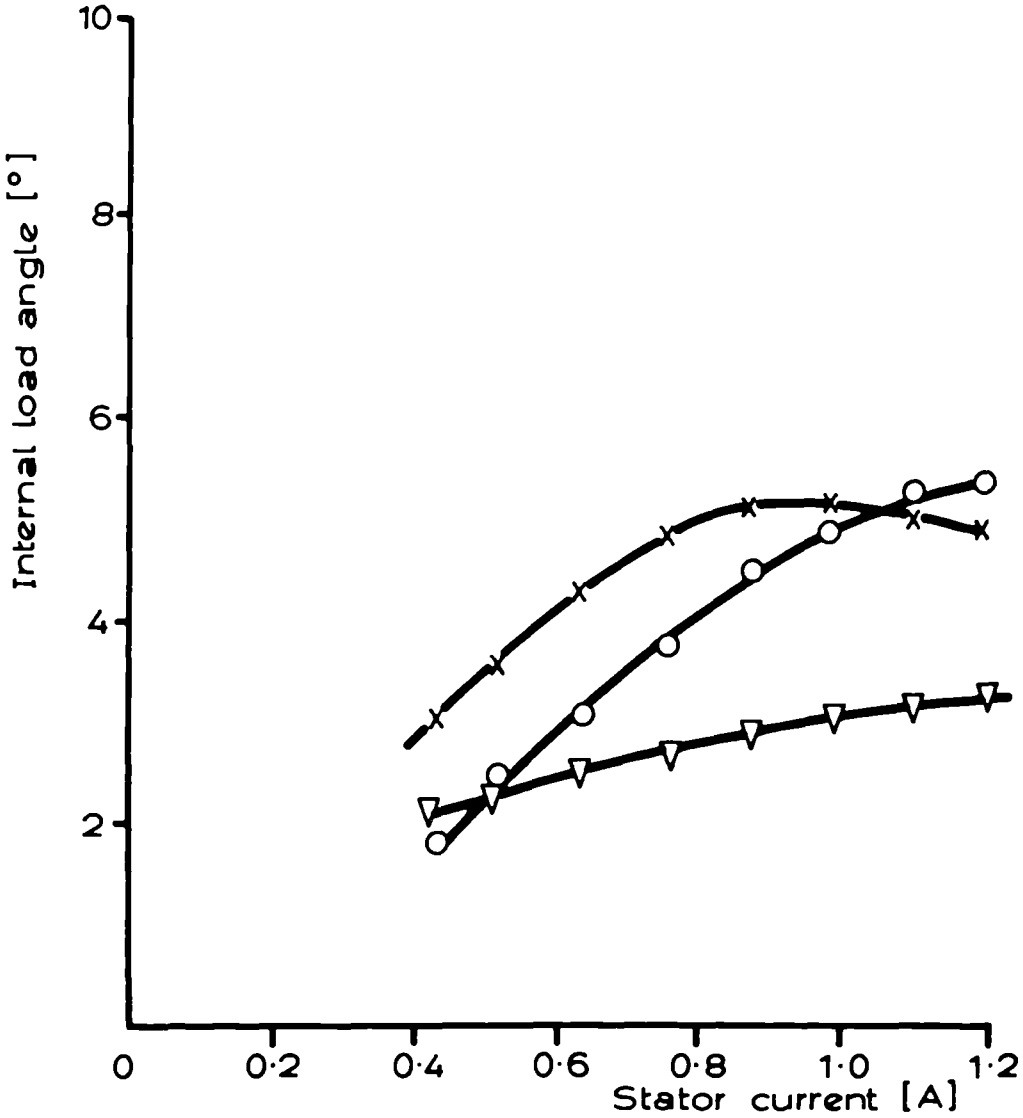

∇... V = 0.95 p.u.
x... V = 1 p.u.
o... V = 1.05 p.u.

Fig.7.11 Calculated internal load angle characteristic.

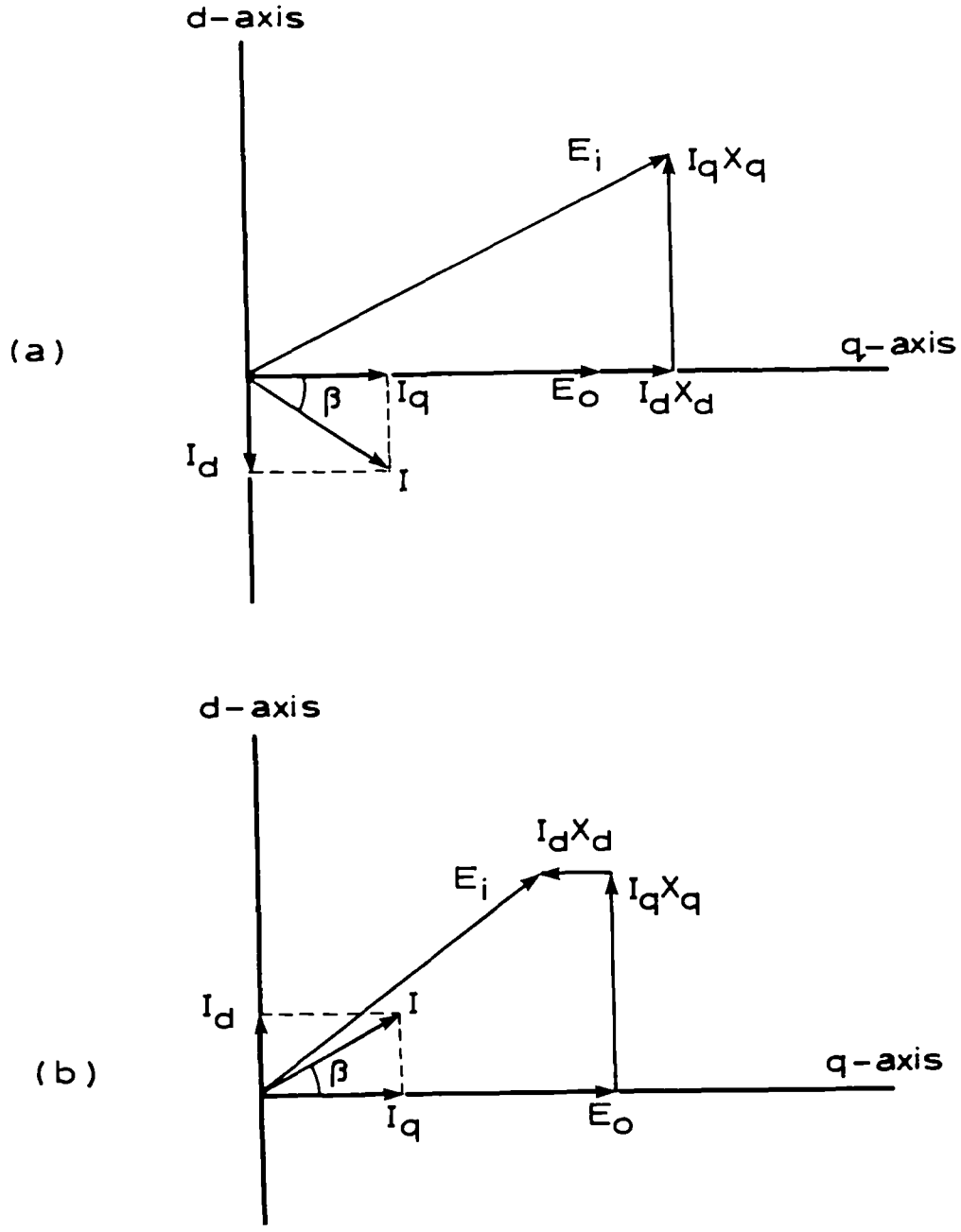

a... lagging operation
b... leading operation

Fig.7.12 Influence of I_d on the magnets.

CHAPTER EIGHT

CONCLUSION

8.1 Applications of PM machines with high- energy magnets

8.2 Conclusions

8.3 Suggestions for further work

CHAPTER EIGHT

CONCLUSIONS

8.1 Applications of PM machines with high- energy magnets

The development in high- energy magnetic materials and power electronics as well as in CAD packages will lead to major improvements in PM machine drives. The new materials offer the opportunity for best designs in areas where light weight, quick response, and large continuous torque are required. Some of the major fields for such applications are:

a- Aerospace: PM machines with maximum power- to- weight ratio can be very attractive for the aerospace industry where high speed and low weight are required. Conventional synchronous machines with rotor fields supplied by d.c windings might not be practical for high- speed operations due to the brush wear. This problem is avoided when brushless PM machines are employed. Reports (59,64) have indicated that in such application the performance of the optimised rotor is not limited by the magnet capability but rather by losses in the stator winding.

b- Robotics: The optimised performance of general purpose robots requires light weight slim arms to achieve good accessibility in limited spaces with higher acceleration and speed, (104). The application of PM machines in robotics promises good results provided that suitable

control strategies and suitable design parameters such as magnet skewing are used to limit torque pulsation.

c- Traction drives: In traction drives, such as ground transportation, and other industrial applications it is required to operate in a power limited region, (34,89) where the torque can be inversely proportional to the speed of the drive. This aim is traditionally achieved by reducing the field current of a d.c drive as the speed is increased. In PM machines where field excitation is constant the same result can be obtained by varying the current angle which is the spatial angle between the armature mmf and the magnet flux. This field weakening strategy controls the net flux of the air gap thus providing torque reduction at increased speed.

d- Machines using high- energy magnets can be appropriate for large electrical applications in industrial drives with fixed or adjustable speeds such as pumps, compressors, mills, fans, etc... In building these machines the potential problems of assembling large magnets in adjacent poles can be serious but sometimes minimised by 'in situ' magnetising procedures, (101,105,107).

8.2 Conclusions

Interest in PM machines for particular industrial applications is rapidly increasing due to the superior advantages that these machines posses over commercial alternatives in the same range. PM machines are gaining increasing popularity due to the introduction of new high energy low cost NdFeB magnets. This new rare earth mag-

netic material has in many aspects better properties than other already existing magnets. The achievable value of energy product for NdFeB is of the order of 210 KJ/m^3. This is 7 times the value achieved by ferrite magnets and 5 times that of alnico. The cost of the new material is still much higher than that of ferrites and comparable to that of cobalt magnets, (2 - 3 times lower), but this is expected to drop with the increasing demand. Characteristics of NdFeB fill the the gap between the powerful, but expensive, samarium cobalt and the low remanence cheap ferrites. Their wide applications, however, in electric machines is still limited because of the low Curie temperature, and the coercivity of the magnet falls progressively with increasing temperature. An updating of the techniques to improve the magnetic properties of neodymium has been discussed. The addition of non- magnetic metals such as Al could result in higher Curie temperature with larger coercivity.

The rapid development of CAD/CAA, particularly the finite element solution technique also has a significant effect on the popularity of PM machines. These packages are used to improve the performance prediction at the design stage with the aim of achieving economical and energy efficient devices. A new generation of computer software, which contains specific conditions under which the parameters become unacceptable, can assist the designer in the design phase with the choice of these parameters. The involvement of computers in machine design as well as in

other fields has lead to a change in the cost effectiveness curve. The peak of the cost is now concentrated in the design phase which includes the cost of CAD facilities and computing time.

There exists already a great number of computer programs that solve the electromagnetic field of electric machines using the finite element method. Two programs have been used in this work and their characteristics are discussed. Basically both programs have the same analysis program that solves the electromagnetic field. Whilst the PE2D package offers a more general solution for different analysis problems, MOTORCAD is focused mainly on solving the steady- state equations of electric machines. Its facilities, particularly the post- processor, have been updated to meet the requirements of this research.

The finite element analysis is not used only to explain the electromagnetic field during the machine operation but also to determine those parameters that significantly affect the whole performance of the machine. Methods have been applied to compute the slot leakage, the internal load angle, and the direct- and quadrature- axis reactances of salient pole PM machine. In each of the these cases saturation, which is very significant in high-field machines, has been included in the analysis. Computation of the open- circuit generated voltage and synchronous torque is useful in predicting the machine performance and characteristics. Accurate methods for

calculating these values are discussed with emphasis on the importance of the regular and uniform mesh generation. In general the computed results give a slightly overestimated value for the torque of the machine. This is expected since the 2D- analysis of the non- linear magnetostatic field does not take into account all loss mechanisms such as eddy current loss, end- winding loss, and bearing and friction loss; though the later is expected to be very small compared to the output power of the machine.

A comparison of the power capability and performance characteristics of NdFeB magnets related to $SmCo_5$ and ferrite magnets are discussed. A typical high- field 4- pole machine with buried magnets has been tested using each of the three magnets. The use of rare earth magnet material leads to a drive system with higher output- to- weight ratio than any other practical alternative. Many important synchronous characteristic curves are calculated and presented. From these results it is evident that the NdFeB magnets give the best performance but the working temperature is limited. The preferred geometry of PM machines uses buried magnets, (54,56) because this type, compared to rotors with peripheral magnets, provides a robust machine mechanically capable of operating at high speeds. Also saturation of the pole above the magnets protects them from any demagnetising forces during transient or short- circuit conditions.

New design aspects and their influence on the machine performance and output are discussed. A prototype rotor has been built with some parameters, such as magnet dimensions, being optimised using the finite element analysis. The aim is to produce a very cheap rotor. It has been shown that skewing the magnets along the axial length of the rotor rids the generated voltage waveform of most of the tooth ripples and reduces harmonics. The skew factor, which expresses the reduction in the field values such as induced voltage, has been calculated both analytically and numerically. The analytical expression is derived from that generally used for stator slots skewing. The numerical derivation is carried out and as the number of subdivisions is increased the value of skew factor converges towards the analytically calculated one.

Another important design parameter is the width of the iron bridge which has a direct effect on the machine field. Another feature of the prototype is enclosing the rotor in a non- magnetic can thus allowing the machine to operate at high speeds without risking the disintegration of the rotor parts. The influence of this can has been examined by testing the machine before and after introducing the can. Test results of the prototype have shown that a PM machine with skewed magnets and canned rotor is capable of operating at high speed and with high efficiency. Further computation has been conducted to examine the consequences of using a ferromagnetic ,solid steel, can. The results have indicated that the ferromagnetic can

provides the machine virtually with a smaller air gap thus giving higher field and higher torque in the air gap. The thin path above the magnets is inevitably saturated hence the field drop due to this flux leakage is almost negligible.

Due to the unique methods of excitation by permanent magnets, traditional methods to determine their important characteristics such as synchronous reactance are not always applicable. Modified experimental methods to measure the direct- and quadrature- axis reactances are being proposed. Results have shown that the direct- axis reactance remains relatively constant with load variation because of the high reluctance in the direct axis due to the low, nearly unity, permeability of the neodymium magnets. A significant variation of the quadrature- axis reactance with load has been revealed as a result of the magnetic saturation on the quadrature axis core. The ratio of X_d to X_q depends to a great extent on the rotor saliency, thickness of the magnets, and on state of saturation. For PM machines X_q is greater than X_d; the effects of this relation on the resultant torque characteristic has been discussed. In high- field machines the effect of saturation is significant and therefore must be taken into consideration in predicting the machine performance and estimating the equivalent circuit parameters. Measurement of the machine losses has been conducted. Measurement of other parameters, namely the induced voltage and winding resistance, have also been carried out.

The machine parameters, as determined both numerically and experimentally, are used to develop an equivalent circuit model which has two advantages over traditional linear models. First it avoids the need for shaft sensing equipment because in this model the load angle is calculated from the measured parameters. Secondly, it takes into account the effects of saturation in the quadrature axis. Core loss is also included in the equivalent circuit. A comparison of the results obtained from the models with test indicates clearly that the inclusion of core loss in the equivalent circuit enhances the accuracy of the model. A sensitivity analysis has been carried out to show the influence of each of the equivalent circuit parameters on the machine performance. Results have shown that the induced voltage plays the most significant role in determining the machine behaviour.

8.3 Suggestions for further work

Interest in PM machines development is still gaining more momentum. More research to accompany this development can be done in computer software related to machine design and in experimental analysis of the machine itself.

1- Computer software (numerically)

a- The performance of NdFeB machines depends to a great extent on its operating temperature. In finite element analysis this effect has been considered by introducing a suitable BH curve for each temperature. A more realistic approach is to include thermal analysis in the modelling.

Computation of the machine losses, as described in this work, and air flow dynamics could lead to determination of the actual operating temperature and hence define the operating point of the magnets at any loading condition.

b- The addition of the mathematical model, used to predict the machine performance with core loss being included, to the finite element post- processor could enable the designer to predict, besides the usual field values, the core loss, loss current, and direct and quadrature components of the current and the synchronous reactance.

c- Further analysis could be conducted to evaluate the cogging torque, produced by the interaction between the stator teeth and the rotor poles, which is usually responsible for producing noise and vibration during the running of the machine.

2- Experimentally

Various design aspects of the canned rotor with skewed magnets are already discussed. However more research can be carried out mainly the following:

a- Fitting a ferromagnetic, solid steel, can around the rotor would virtually provide the machine with a smaller air gap. This may give rise to the field flux hence leading to a reduction of the magnet volume required.

b- In order to exploit the full potential of this rotor to operate at high speeds, an investigation of its synchronous performance could be conducted with special emphasis on the efficiency and eddy current values at such high speeds.

c- In the process of fully understanding the behaviour of PM machines it is important to study and analyse their transient performance.

****

REFERENCES

1 BINNS K. J., RILEY C. P. and WONG M.
"The efficient evaluation of torque and field gradient in permanent- magnet machines with small air gap". IEEE Trans. on Magnetics, Vol. MAG- 21, No.6, Nov. 1985.

2 LOWTHER D. A. and SALDANHA C. M.
"A frame- based system for the design of electromagnetic devices". IEEE Trans. on Magnetics, Vol. MAG-22, No.5, Sept. 1986.

3 WEIMANN D., NICOUD G. and GALLO F.
"Advantages of permanent magnet motors". IEE Conf. on Drives/ Motors/ Control, Brighton, Oct. 1984.

4 PAULY D., PFAFF G. and WESCHTA A.
"Brushless servo drives with permanent magnet motors or squirrel cage induction motors - a comparison". IEEE Trans. on Industry Applications, Vol.IA, No.20 1984.

5 MORGAN J. S. and THORP M.
"Introduction to CADAM on the IBM 4341- UG 30/3". Liverpool University Computer Lab., Sept. 1986.

6 CHUNG J.
"Predicting maximum enclosure temperatures". Machine Design Journal, Sept. 1987.

7 STEADMAN P. and ROONEY J.
"Principles of computer- aided- design". Pitman, 1987.

8 LOWTHER D. A., FREEMAN E. M., EMSON C. R. I. and SALDANHA C. M.
"Knowledge based systems applied to the design of electrical devices". IEEE Trans. on Magnetics Vol. MAG- 24, No.6, Nov. 1988.

9 FREEMAN E. M. and MUKOLERA J. R.
"Knowledge based systems for the dc machines". IEE Conf. on EMD, London, Nov. 1987.

10 ROUSE E. N.
"Building composites with computers". Machine Design Journal, Nov. 1987.

11 THORP M.
"Introduction to CATIA on IBM 3081- UG 31/6". Liverpool University Computer Laboratory, Jan. 1989

12 NEWTON P.
"Course notes for CADAM 'Teach the Teacher Course' EA91". Graphic Marketing Support Group, Warwick,

Feb. 1985.

13 BINNS K. J. and JABBAR M. A.
"High- field self- starting permanent- magnet synchronous motor".IEE Proc., Vol.128, No.3, May, 1981.

14 BINNS K. J. and WONG T. M.
"Analysis and performance of a high- field permanent magnet synchronous machine". IEE Proc., Vol.131, No.6, Nov. 1984.

15 NEUMANN T. W. and TOMPKINS R. E.
"Line start motors designed with NdFeB permanent magnets". Proc.8^{th} Inter. Workshop on Rare Earth Magnets, May, 1985.

16 HADJIPANAYIS G. C.
"The history of the discovery of cobalt- free Fe-R-B based permanent magnets: a personal view". Newsletter of The Concerted European Action on magnets, No.2, 1986.

17 JUBB G. A. and McCURRIE R. A.
"Hysteresis and magnetic viscosity in a Nd- Fe- B permanent magnet". IEEE Trans. on Magnetics, Vol. MAG- 23, No.2, March, 1987.

18 SAGAWA M., FUJIMURA S., TOGAWA N., YAMAMOTO H. and MATSUURA Y.
"New material for permanent magnets on a base of Nd and Fe". J. Appl. Physics, No.55, March, 1984.

19 GROSSINGER R., HASLINGER F., SHOUGONG Z., EIBLER R. SCHNEIDER L., SCHNEIDER J., HANDSTEIN A. and KIRCHMAYR H.
"The effect of substitution of Al on the magnetic properties of$Nd_{18}Fe_{78}B_8$ permanent magnets". IEEE Trans. on Magnetics Vol.24, No.2, March, 1988.

20 CARLISLE B. H.
"Neodymium challenges ferrite magnets". Machine Design Journal, Jan. 1986.

21 POLLARD R. J., GRUNDY P. J., PARKER S. F. H. and LORD D. G.
"The effect of Zr additions on the microstructural and magnetic properties of NdFeB based magnets". IEEE Trans. on Magnetics, Vol.24, No.2, March 1988.

22 BAO- MIN Ma and NARASIMHAN S. V. L.
"NdFeB magnets with higher Curie temperature". IEEE Trans. on Magnetics, Vol.MAG- 22, No.5, Sept. 1986.

23 RICHTER E. and NEUMANN T. W.
"Line start permanent magnet motors with different materials". IEEE Trans. on Magnetics, Vol.MAG- 20,

No.5, Sept. 1984.

24 GROSSINGER R., HARADA H., KERESZTES A., Kirchmayr H. A. and Tokunaya M. "Anisotropy and hysteresis studies of highly substituted Nd- Fe- B based magnets". IEEE Trans. on Magnetics, Vol. MAG- 23, No.5, Sept. 1987.

25 Philips Technical Specifications of NdFeB magnets.

26 HADJIPANAYIS G. C., LAWLESS K. R. and DICKERSON R.C. "Magnetic hardening in iron- neodymium- boron permanent magnets". J. Appl. Physics, Vol.57, No.3, April, 1985.

27 MIZOGUCHI T., SAKAI I., NIU H. and INOMATA K. "Nd- Fe- B- Co- Al based permanent magnets with improved magnetic properties and temperature characteristics". IEEE Trans. on Magnetics, Vol. MAG- 22, No.5, Sept. 1986.

28 SEMONES B. C. "Volumetric improvements in high energy magnet motors". IEEE Trans. on Magnetics, Vol. MAG- 21, No.5, Sept. 1985.

29 CHIN T. S., HARA Y., LAVERINA E. J., O'HANDLEY R. C. and GRANT N. J. "(FeCo)- Nd- B permanent magnets by liquid dynamic compaction". J. Appl. Physics, Vol.59, No.15, Feb. 1986.

30 RAHMAN M. A., and SLEMON G. R. "Promising applications of neodymium boron iron magnets in electrical machines". IEEE Trans. on Magnetics, Vol. MAG- 21, No.5, Sept. 1985.

31 PARKER R. J. and STUDDERS R. J. "Permanent magnets and their application". John Wiley and Sons, Inc. 1962.

32 TAYLOR J. S. and WARD M. "The magnetic and physical properties of NdFeB magnets and their implications; an end users point of view". IEEE Meeting on Current Research In Applied Magnetics, Preston, Nov. 1988.

33 WILLEY R. J. "Classification of airborne asbestos using magnetic field orientation techniques". IEEE Meeting on Current Research In Applied Magnetics, Preston, Nov. 1988.

34 CSENDES Z. J., FREEMAN E. M., LOWTHER D. A. and SILVESTER P. P. "Interactive computer graphics in magnetic field analysis and electric machine design". IEEE Trans.

on Power Apparatus and Systems, Vol. PAS- 100, No.6, June, 1981.

35 WILSON A. M.
"Magnetic field calculation in an irregular triangular mesh". Lawrence Radiation Lab., California, UCRL- 7784, Rev. 1, 1965.

36 ZIENKIEWICS O. C. and CHEUNG Y. K.
"The finite element method in structural and continuum mechanics". McGraw- Hill, London, 1968.

37 BINNS K. J., JABBAR M. A. and BARNARD W. R.
"Computation of the magnetic field of permanent magnets in iron cores". IEE Proc. 1975.

38 SILVESTER P. and CHARI M. V. K.
"Analysis of the turbo- alternator magnetic field by finite element". IEEE Trans. Vol. PAS- 90, No.2, 1971.

39 ABDUL HAMEED A. A.
"The finite element modelling and design optimisation of a multipole permanent magnet synchronous machine". Ph.D. Thesis, Leuven University, Dec. 1984.

40 TROWBRIDGE C. W. and SIMKIN J.
"Three- dimensional non- linear electromagnetic field computations using scalar potentials". IEEE Proc., Vol.127, No.6, 1980.

41 BIDDLECOMBE C. S., DISERENS N. T., RILEY C. P. and SIMKIN J.
"PE2D user guide". RAL, 1986.

42 SILVESTER P. P. and FERRARI R. L.
"Finite elements for electrical engineers". Cambridge University Press, 1983.

43 KAMBERBEEK E. M.
"On the theoretical and experimental determination of the electromagnetic torque in electrical machines". Philips Report, No.4, 1970.

44 TORTSCHANOFF T.
"Survey of the numerical methods in field calculations". IEEE Trans. on Magnetics, Vol. MAG- 20, No.5, Sept. 1985.

45 BIDDLECOMBE C. S., SIMKIN J. and TROWBRIDGE C. W.
"Error analysis in finite element models of electromagnetic fields". IEEE Trans. on Magnetics, Vol. MAG- 22 No.5, Sept. 1986.

46 CENDES Z. J.
"Unlocking the magic of Maxwell's equations". IEEE

Spectrum, April, 1989.

47 KOSTENKO M. and PETROVSKY L.
"Electrical machines- vol.2". Mir Publishers, 1969.

48 PUCHSTEIN A. F.
"Calculations of slot constants". AIEE Trans. Vol. 66, 1947.

49 COTTON H.
"Advanced electrical technology". Pitman, London, 1967.

50 LIWSCHITZ - GARIK M. and WHIPPLE C.
"Alternating current machines".
Van Nostrand, Princeton, N. J., 1961.

51 ENGELMANN R. H.
"Static and rotating electromagnetic devices."
Marcel Dekker Inc. 1982.

52 BINNS K. J.
"Handbook of electric machines (edited by S. A. Nasar) permanent magnet machines, chapter 9".
McGraw- Hill, March, 1987.

53 RICHTER E., MILLER T. J., NEUMANN T. W. and HUDSON T. L.
"The ferrite permanent magnet AC motor- a technical and economical assessment". IEEE Trans. on Industry Applications, Vol.IA- 21, No.4, May, 1985.

54 SNEYERS B., NOVOTNY D. W. and LIPO T. A.
"Field weakening in buried permanent magnet AC motor drives". IEEE Trans. on Industry Applications, Vol. IA- 21, No.2, April, 1985.

55 BINNS K. J. and WONG T. M.
"Analysis and performance of a high field permanent magnet synchronous machine". IEE Proc., Vol 131, No. 6, 1984.

56 BINNS K. J.
"Permanent magnet motors for inverter fed drives".
Conf. on Drives/motores/controls. Brighton, 1984.

57 BINNS K. J. and RILEY C. P.
"The scope for development of permanent magnet machines in the light of new materials". Proc. ICEM, Part 3, Munich, 1986.

58 BINNS K. J. , WONG T. M. and JABBAR M.A.
"Some design aspects of self starting permanent magnet machines". EMDA Conference, London, July, 1983.

59 AMARATUNGA G. and MCLAREN P.
"Permanent magnet generators for aerospace applications: optimisation of power to weight". Conf. on Electrical Machines and Drives, London, Nov. 1987.

60 BINNS K. J. , RILEY C. P. and WONG T. M.
"Some design aspects of high output permanent magnet synchronous machines with non radial magnets". IEE Conf. on E.M.D.A. London, Sept. 1985.

61 BINNS K. J. , CHAABAN F. B. , LISBOA P. J. and MELLOR P. H.
"The role of neodymium iron boron in relation to other materials for permanent magnet machines". Conf. on Electrical Machines and Drives, London, Nov. 1987.

62 WONG T. M.
"The finite element analysis of a high - field permanent - magnet synchronous machine". Ph.D. Thesis at University of Southampton, 1983.

63 HOWE D. and BIRCH T. S.
"Effective replacement of metallic magnets by rare-earth cobalt". Proc. 6^{th} Inter. Workshop on Rare-earth Cobalt Permanent Magnets, Sept. 1982.

64 SCHIFERL R. F., COLBY R. S., and NOVOTNY D. W.
"Efficiency considerations in permanent magnet synchronous motor drives". Electric Energy Conf. Adelaide, Oct. 1987.

65 SEBASTIAN T. and SLEMON G. R.
"Operating limits of inverter- driven permanent magnet motor drives".IEEE Trans. on Industry Applications, Vol.IA- 23, No.2, March/April, 1987.

66 JAHNS T. M., KLIMANN G. B. and NEUMANN T. W.
"Interior permanent- magnet synchronous motors for adjustable speed drives". IEEE Trans. on Industry Applications, Vol.IA- 22, No.4, July, 1986.

67 BINNS K. J. and CHAABAN F. B.
"The relative merits of rare- earth permanent magnet materials for use in the excitation of permanent magnet machines". Inter. Conf. on Electrical Machines, Pisa, Sept. 1988.

68 NASAR S.
"Handbook of el. machines". McGraw- Hill, 1987.

69 WOOD W. S.
"Theory of electrical machines". Butterworths Scientific Publications, 1958.

70 CHALMERS B. J., HAMED S. A. and BAINES G. D.
"Parameters and performance of a high- field permanent magnet synchronous motor for a variable frequency operation". IEE Proc. Vol. 132, Pt B, No.3, May, 1985

71 NIELSEN K. L.
"Methods in numerical analysis". Macmillan, 1956.

72 SEBASTIAN T., SLEMON G. R. and RAHMAN M. A.
"Modelling of permanent magnet synchronous motors". IEEE Trans. on Magnetics, Vol.MAG- 22, No.5, Sept. 1986.

73 SLEMON G. R. and STRAUGHEN A.
"Electric machines". Addison- Wesley Publ. 1980.

74 JACKSON K. J.
"Dictionary of electrical engineering". Butterworth & Co. Ltd. 1978.

75 NASAR S. A. and UNNEWEHR L. E.
"Electromechanics and electric machines". John Wiley & Sons, 1979.

76 SLEMON G. R.
"Analytical models for estimated synchronous machines". IEEE Trans. Vol. PAS- 90, No.2, March, 1971.

77 CAHILL D. P. and ADKINS B.
"The permanent magnet synchronous motor". IEE Proc. Vol.109, Part A, No.48, Dec. 1962.

78 HONSINGER V. B.
"Performance of polyphase permanent magnet machines". IEEE Trans. on Power Apparatus And Systems, Vol. PAS- 99, No.4, July, 1980.

79 BINNS K. J., BARNARD W. R. and JABBAR M. A.
"Hybrid permanent- magnet synchronous motors". IEE Proc. Vol.125, No.3, 1978.

80 DRAPER A.
"Electrical machines". Longman, 1976.

81 HAMEED A. and BINNS K. J.
"MOTORCAD finite element programme for designing 3- phase synchronous machines with or without magnets". User Guide, Liverpool University, Feb. 1989.

82 GOSDEN D. F.
"Permanent magnet motor performance". Inter. Conf. on Electric Machines (ICEM), Pisa, Sept. 1988.

83 VOLKRODT W.

"Machines of medium- high rating with ferrite-magnet field". Siemens Review, No.6, 1976.

84 JANSSENS N.
"Mathematical modelling of magnetic hysteresis". Conf. on The Computation of Magnetic Fields, (COMPUMAG), Oxford, 1976.

85 CONSOLI A. and ABELA A.
"Transient performance of permanent magnet AC motor drives". IEEE Trans. on Industry Applications, Vol. IA- 22, No.1, Jan. 1986.

86 BINNS K. J. and JABBAR M. A.
"A high- field permanent- magnet synchronous motor". Proc. ICEM, Athens, Sept. 1980.

87 WOLL R. F.
"Effect of unbalanced voltage on the operation of polyphase induction motors". IEEE Trans. on Industry Applications, Vol.IA- 11, No.1, Jan. 1975.

88 PARK R. H.
"Two- reaction theory of synchronous machines, generalised method of analysis- part I". AIEE Winter Convention, New York, 1929.

89 RICHARDSON K. M. and SPOONER E.
"Magnetisation procedures for Nd- Fe- B magnets in electrical machines". IEE Conf. on EMD, London, Nov. 1987.

90 FITZGERALD A. E.
"electric machinery". McGraw- Hill, 1971.

91 PEN- TUNG SAH A.
"Fundamentals of alternating current machines". McGraw- Hill, 1946.

92 GOLDING E. W.
"Electric measurements and measuring instruments". Fifth Edition, 1963.

93 STOUT M. B.
"Basic electrical measurements". Second Edition, 1960.

94 HUGHES E.
"Electrical technology". Fourth Edition, 1972.

95 MILLER T. J. E.
"Methods of testing permanent magnet polyphase alternating current machines". IEEE Trans. 1981.

96 CHALMERS B. J., HAMED S. A. and BAINES G. D.
"Parameters and performance of a high- field permanent magnet synchronous motor for a

variable frequency operation".
IEE Proc. Vol. 132, Pt B, No.3, May, 1985.

97 BINNS K. J. and WONG T. M.
"Development of a high- field permanent magnet machine". ICEM Conference, Lausanne, Sept. 1984.

98 BARTON R. K., KONARD A. and BERKERY J. F.
"Finite element post- processing for direct current machines". IEEE Trans. on Magnetics, Vol. MAG- 20, No. 5, Sept. 1984.

99 DEMERDASH N. A., FOUAD F. A. and NEHL T. W.
"Determination of winding inductances in ferrite type permanent magnet electric machinery by finite elements". IEEE Trans. on Magnetics, Vol. MAG- 18, No.6, Nov. 1982.

100 JONES C. V.
"The unified theory of electrical machines". Butterworths, London, 1967.

101 ZIMMERMANN P.
"Electrically commutated dc field drives for machine tools". Proc. Motorcon. Conference, 1982.

102 LOW T. S. and BINNS K. J.
"Multi- stacked imbricated rotors with permanent magnet excitation design for new magnet materials". IEE Proc. Part B, Vol.33, No.4, July, 1986.

103 JABBAR M. A.
"Design and operational aspects of high- speed appliances motors using ceramic magnets". IEE Conf. on EMD, London, Nov. 1987.

104 Presentation of the new industrial robot IRB 2000, ASEA Robotics, 1986.

105 SNEYERS B., MAGGETTO G. and VAN ECK J. L.
"Inverter fed permanent magnet synchronous motor for electric traction". ICEM Proc. Budapest, Sept. 1982.

106 EDWARDS J. D.
"Electrical machines". Int. Textbook Company Ltd, 1973.

107 MCDONALD D. C.
"Magnetizing and measuring B & H in high energy product rare earth permanent magnets". IEEE Trans. on Magnetics, Vol. MAG- 22, No.5, Sept. 1986.

108 NOBLE B.
"Numerical methods:1, Iteration programming and algebraic equations". Oliver & Boyd, Edinburgh, 1964.

109 BIRCH T. S., HOWE D., STATON D. A. and WILLIAMS I.
"The computer- aided design of permanent magnet D.C. motors". IEE Conf. on EMDA, London, Sept. 1985.

110 BINNS K. J., HAMEED A. A. and CHAABAN F. B.
"A canned solid rotor permanent magnet machine with skewed- radial neodymium- iron- boron magnets". 4^{th} Inter. Conf. on EMD, London, Sept. 1989, (in press).

111 BOLTON H. R. and ASHEN R. A.
"Influence of motor design and feed- current waveform on torque ripple in brushless DC drives". IEEE Proc. Vol. 131, pt. B, No.3, May, 1984.

112 SEBASTIAN T. and SLEMON G. R.
"Transient modelling and performance of variable-speed permanent- magnet motors". IEEE Trans. on Industry Applications, Vol. 25, No.1, Jan. 1989.

113 DENZ Z., BOLDEA I. and NASAR S. A.
"Fields in permanent magnet linear synchronous machines". IEEE Trans. on Magnetics, Vol. MAG- 22, No.2, March, 1986.

114 DE LA REE J. and BOULES N.
"Torque production in permanent- magnet synchronous motors". IEEE Trans. on Industry Applications, Vol. 25, No.1, Jan/Feb. 1989.

115 CHALMERS B. J. and DEVGAN S. K.
"Comparative performance of 7.5 KW permanent magnet synchronous motors with $SmCo_5$ and Nd- Fe- B magnets". Inter. Conf. on Electrical Machines (ICEM) Pisa, Sept. 1988.

116 ZIMAGLIA C., PESSINA G. and FAVA M.
"Unconventional AC drives for large speed ranges". Conf. on EMD, London, Nov. 1987.

117 HONSINGER V. B.
"The field and parameters of interior type AC permanent magnet machines". IEEE Trans. on Power Apparatus and Systems, Vol. PAS- 101, No.4, April, 1982.

118 SEMAIL B., PIRIOU F. and RAZEK A.
"Numerical method for PM synchronous motor drives to limit torque pulsation". IEE Conf. on EMD, London, Nov. 1987.

APPENDIX A

Slot Leakage Determination

The permeance oh the whole slot is the sum of of the permeance of the trapezoidal part (λ_1) and that of the semi- circular bottom of the slot (λ_2).

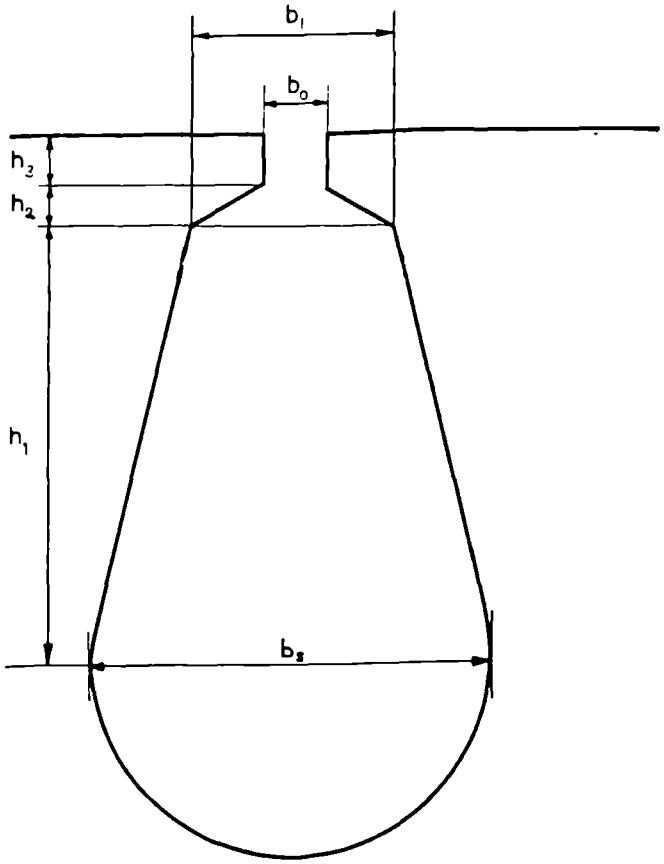

Fig.a.1

The semi- closed trapezoidal part as shown in Fig.a.1 is divided into three parts of heights h_1, h_2 and h_1. The permeance of this part, as derived in (48,50), is:

$$\lambda_1 = \mu_0\left(\frac{2h_1}{3(b_1 + b_s)} + \frac{2h_2}{3(b_1 + b_0)} + \frac{h_3}{b_0}\right)$$

The determination of the semi- circular bottom leakage starts from the geometry of Fig.a.2 where:

$$\sin\frac{\alpha}{2} = \frac{y}{2R}$$

giving $y = R \sin\frac{\alpha}{2}$

similarly $x = R \cos\frac{\alpha}{2}$

Area of triangle OAB $= \frac{xy}{2} = \frac{2R \sin\frac{\alpha}{2} R \cos\frac{\alpha}{2}}{2}$

Area of sector OACB $= \frac{\alpha R^2}{2}$

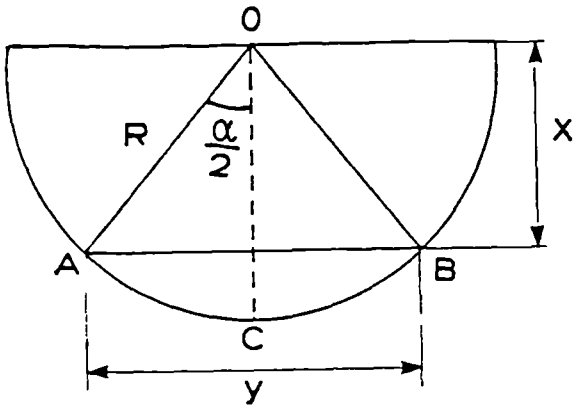

Fig.a.2

This implies that the area of the part of the circle related to height x is:

$$\frac{R^2}{2}(\alpha - \sin\alpha)$$

The ratio of this area to the area of the semi circle will be

$$\frac{\alpha - \sin\alpha}{\pi}$$

The permeance is found by integrating this ratio from $\alpha = 0$ to $\alpha = \pi$.

$$\lambda_2 = \mu_0 \int_0^{\pi} \left(\frac{(\alpha - \sin \alpha)}{\pi} \right)^2 \frac{d\alpha}{4}$$

which after rearranging and integrating yields:

$$\lambda_2 = \frac{\mu_0}{4\pi^2} \left(\frac{\pi^3}{3} - 2\pi + \frac{\pi}{2} \right) = 0.14\mu_0$$

The permeance of the whole slot will therefore be:

$$\lambda = \mu_0 \left(\frac{2h_1}{3(b_1 + b_s)} + \frac{2h_2}{3(b_1 + b_0)} + \frac{h_3}{b_0} + 0.14 \right)$$

The inductance is:

$$L = 4\pi \times 10^{-7} \lambda . N_x^2 . l . p$$

and the leakage reactance is: $X_l = \omega L$.

APPENDIX B

Electrical Parameters Of Various Types Of Machines Used Throughout This Thesis

1- Dimensions of the four- pole machines with different magnetic material as discussed in chapter four.

ROTOR PARAMETERS (mm)	A	B	C
shaft diameter	15.87	19.9	23.8
rotor diameter	93.14	93.02	92.94
rotor length excluding end- rings	82.75	82.75	82.75
pole arc (°)	39	50	51
cage bar diameter	4.7	3.968	4
magnet width	10	9	10.5
magnet length	36	37.76	45.5
machine single air gap	0.2575	0.318	0.3556

A...rotor with ferrite magnets

B...rotor with $SmCo_5$ magnets

C...rotor with NdFeB magnets

STATOR PARAMETERS

number of poles	4
number of phases	3
rated current (A)	8

rated voltage (V)	230
outside diameter (mm)	161.9
inside diameter (mm)	93.75
turns in series per phase	204
winding resistance per phase (Ω)	4
axial length (mm)	93.66
rated power (KW)	0.55

2- Electrical parameters of the six- pole machine used in chapters five, six, and seven.

STATOR PARAMETERS	IS2	IS3
number of poles	6	6
number of phases	3	3
rated current (A)	2.1	10.6
rated voltage (V)	320	65
outside diameter (mm)	120.5	120.5
inside diameter (mm)	69.9	69.9
number of slots	36	36
turns in series per phase	108	15
winding resistance per phase (Ω)	24.5	0.5
rated power (KW)	0.55	0.37
axial length (mm)	82.55	82.55
winding layers	1	1

IS2 is the stator used in the tests provided for modelling purposes, chapter six.

IS3 is used with both high- field rotors, the buried as well as the skewed one.

ROTOR PARAMETERS (mm)

shaft diameter	25.4
ventilation hole diameter	6.35
pole arc (°)	41
magnetic material	NdFeB
magnet width	5.5
magnet length	26
rotor diameter	69.5
rotor length excluding end- rings	91.44
iron bridge width	2.145
single air gap	0.2

APPENDIX C

Specific Total Loss Characteristic of The Stator Core as Supplied by The Manufacturer (GEC).

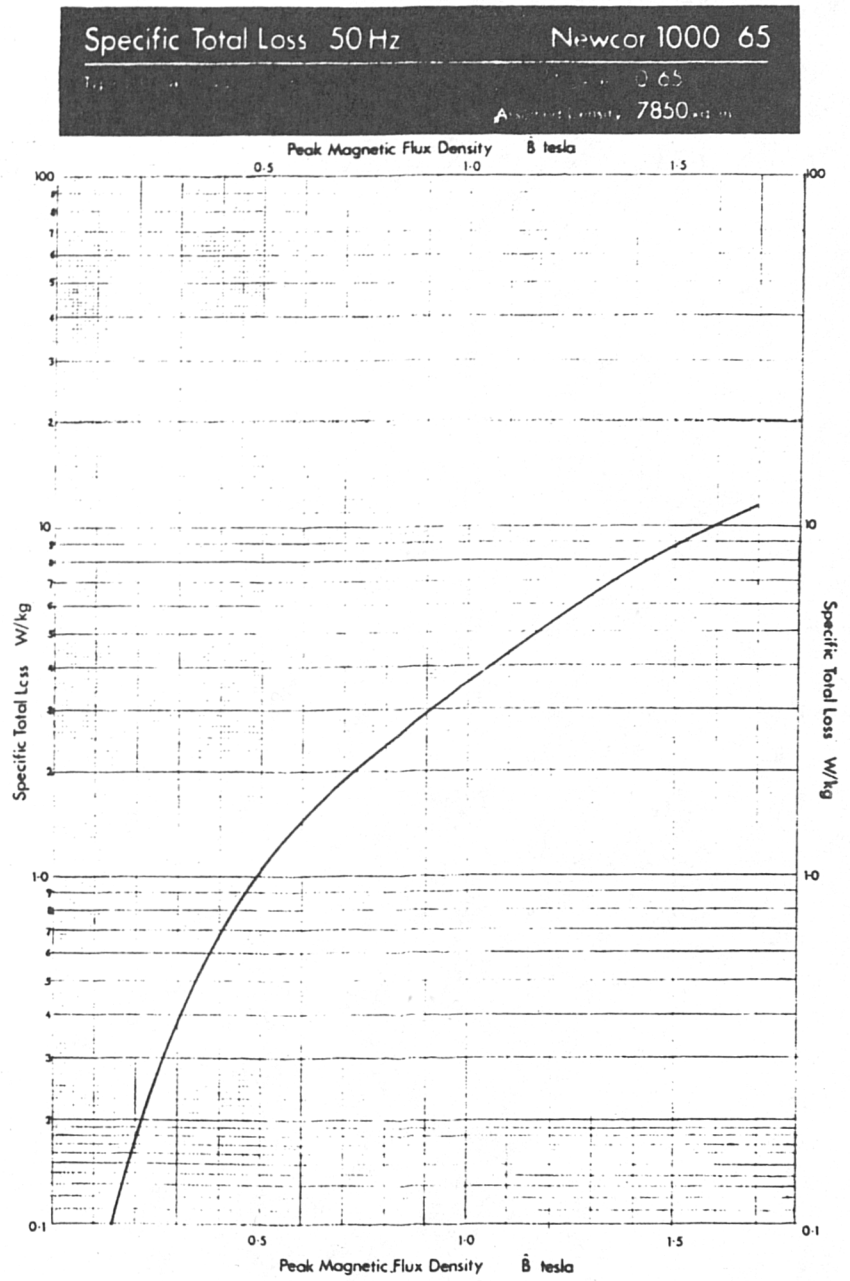

THE ROLE OF NEODYMIUM-IRON-BORON IN RELATION TO OTHER MATERIALS FOR PERMANENT MAGNET MACHINES

PROF. K. J. BINNS, MR. F.B.CHAABAN, DR. P. J. G. LISBOA AND DR. P. H. MELLOR (UNIVERSITY OF LIVERPOOL)

INTRODUCTION

Interest in permanent magnet machines for drive systems was almost non-existent fifteen to twenty years ago. Alnico magnets were used, for example in exciters, and still are. Ferrite magnets were found in automobile equipment like windscreen washer motors. Research was being carried out and patents applied for in the area of drive systems but only a small handful of people were involved (1) (2) (3).

It was only when samarium cobalt magnets with their high stored energy became available that industry recognised that permanent magnet machines were not simply low power special devices of minimal commercial importance.

Contracts were placed to develop prototype machines for a variety of applications. It was demonstrably clear that the magnet could be used to up-rate conventional systems, (4) including those using induction and reluctance motors, but the cost of the magnets was generally found to be too high for widespread use. Many designs were proposed in which the expensive material was under utilised.

In 1983 two firms, one in the USA and the other in Japan, announced the development of neodymium-iron-boron magnets and in the short interval since then many other magnet producers have developed and produced these magnets. The cost is currently comparable with samarium-cobalt but it is hoped that the cost will fall ultimately by a factor of about four. There are many claims about the growth in the use of Ne Fe B, but these are mainly made by non-experts who have been divorced from the task of designing machines for which the working temperature has to be kept low in the region containing the magnet.

In the light of the characteristics of three materials, ferrite, samarium-cobalt and neodymium-iron-boron, a comparison of achievable performance is made. A geometry with high performance potential (5) is used for the comparison since it makes possible a high air-gap field and hence a high torque to machine volume. Fig. 1 shows a cross section of the machine which can operate as line start synchronous motor or as a so-called 'brushed d.c. machine' if position sensing is incorporated. The performance capability of this machine has already (6) been discussed but in this paper the design has been optimised for each of the three materials. For a comparison to be worthwhile the dimensions have to be chosen to maximise performance for a given magnet.

Table 1 shows some of the important characteristics of the 3 materials chosen. Note the progressive increase in remanence and coercivity from the relative low values for the anisotropic ferrite to the much higher values for samarium cobalt and neodymium. However, the ferrites are, of course, relatively very cheap. The maximum operating temperature is most important for electrical machines and here neodymium magnets have a significant limitation. The temperature coefficient indicating a reversible loss of energy with temperature rise up to the maximum of operating point shows ferrite as the most temperature dependent.

Using finite element software (7) the rotor is designed for a given stator. The stator is that of a standard induction motor having a four-pole winding. The three rotors have been constructed and tested for synchronous performance in the same stator, the winding of which was rated at 8A.

EXPERIMENTAL RESULTS

The measured torque for three voltage levels is shown in Fig. 2 as a function of load current for a 50 Hz mains supply. The unit of voltage is that induced in the winding when the machine is run as a generator. With this type of high field machine and $SmCO_5$ magnets there is little to be gained in torque by using a voltage higher than the generated emf. NeFeB magnets on the other hand have a higher flux carrying capacity. The torque is higher for a given current and operation at higher voltage gives a benefit, see Fig. 3.

The ferrite magnet rotor has a totally different characteristic and has to be operated well beyond the generated voltage in a regime where reluctance action is significant. The test rig had quite a high minimal torque and pull out prescribed the upper limit, see Fig.4.

A torque comparison for the three materials using rated voltages as defined, gives a clear comparison of output, see Fig 5.

The efficiency is an important parameter and a comparison for the three materials at the rated voltages is presented in Fig. 6.

Table 1. Magnetic and Physical Properties of the Permanent Magnets Used.

Magnetic Material	Residual Induction Br, Tesla	Coercive Force - Hc, KA/m	Peak Energy Density BHmax, KJ/m^3	Max. Operating temperature ^oC	Reversible temp. coeff % per ^oC
Ferrite	0.4	247	29	350	-0.20
$SmCO_5$	0.82	597	122	250	-0.04
Nd Fe B	0.97	493	178	140	-0.12
	1.03	772	205	100	-0.12

The ferrite rotor is relatively low whilst the other two magnet materials are comparable in efficiency. The neodymium magnets have the advantage at higher outputs. The power factor is important particularly for inverter fed operation. Both rare earth rotors retain a power factor close to unity. The $SmCo_5$ rotor has a power factor which changes from leading to lagging as the output increases. For the ferrite rotor it improves with load but is much lower in comparison.

COMPUTATIONAL RESULTS

Fig. 8 shows a computed field distribution at 6A load showing the flux lines for a repeatable section of the machine. It is clear that the flux density in the air gap over the region of one pole is much higher than that in the magnet, a feature of this configuration. The flux emerging from each pole of the rotor is also greater than the flux from each magnet because some of the air gap flux from the rotor passes through two magnets. The magnet dimensions are chosen so as to produce a high air gap flux without undue saturation.

As explained earlier the different geometries for the 3 rotors were obtained by using computer software which gives torque, flux densities etc. as well as field maps, the latter serving mainly as an aid to understanding and presentation.

DISCUSSION

The comparison of power capability and performance characteristics such as efficiency and power factor is clearly brought out in the results. One must, however, bear in mind the cost comparison for the magnets. In a total drive system the cost of ferrite magnets is less than one percent. But for the rare earth magnets the cost is 50 per cent or more of the total motor cost.

On the other hand the use of rare earth magnets can lead to a drive system with a higher torque/weight ratio than any other practical alternative. The high efficiency and near unity power factor are exactly what is required for the ideal inverter fed system. There is no doubt that the neodymium magnets give the best performance but the working temperature is limited.

Tests have been carried out which confirm that the ferrite magnets can be magnetised easily without a special rig, simply making use of the stator winding. These tests will be extended to cover the magnetisation of rare earth magnets. This technique has enormous advantages in that the machine assembly is made much simpler by using unmagnetised material in the construction. The use of elevated temperatures to ease magnetisation of temperature dependent rare earths has an important role to play.

In conclusion, the characteristics of the motor for the three important types of magnet have been demonstrated. The cost effectiveness of the use of relatively expensive magnets can be assessed.

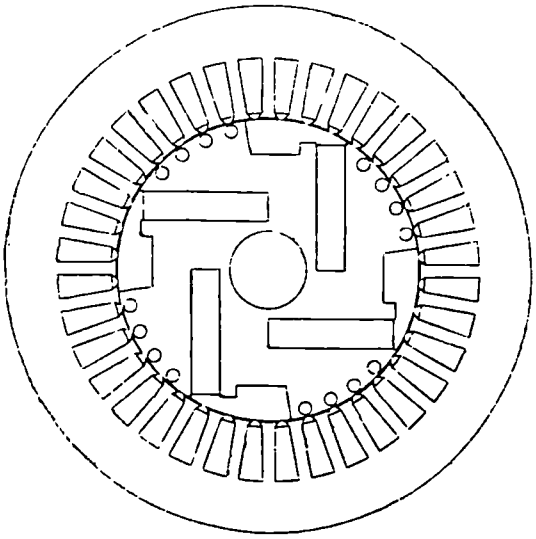

Fig. 1: Configuration of a high-field permanent magnet synchronous machine.

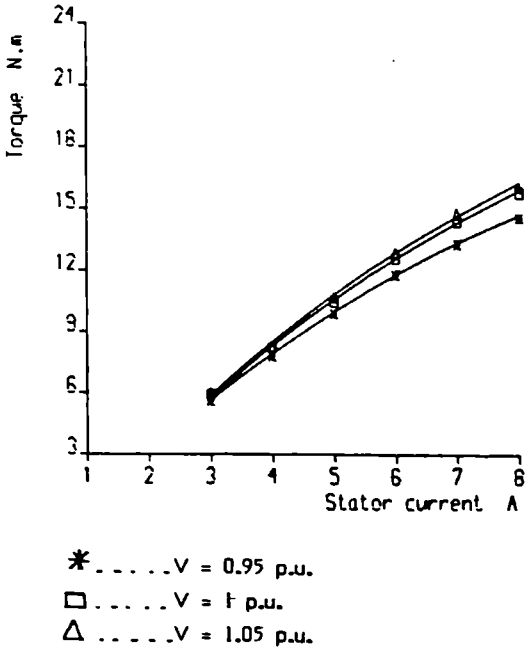

Fig. 2: Variation of torque as a function of the stator current for the Sm - Co_5 machine

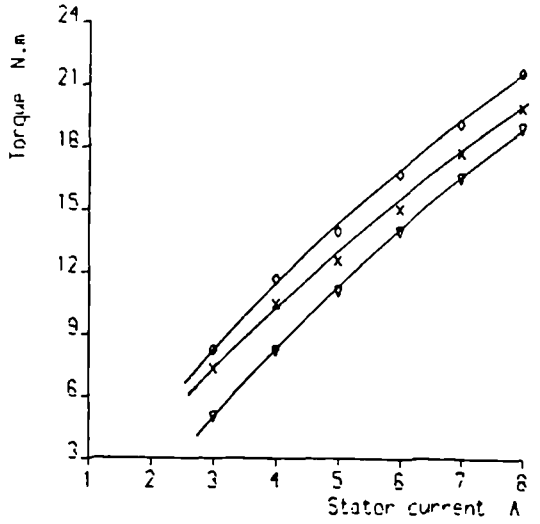

▽ ... V = 0.95 p.u.
× ... V = 1 P.u.
◇ ... V = 1.05 p.u.

Fig 3: Variation of torque as a function of the stator current for the Nd-Fe-B machine.

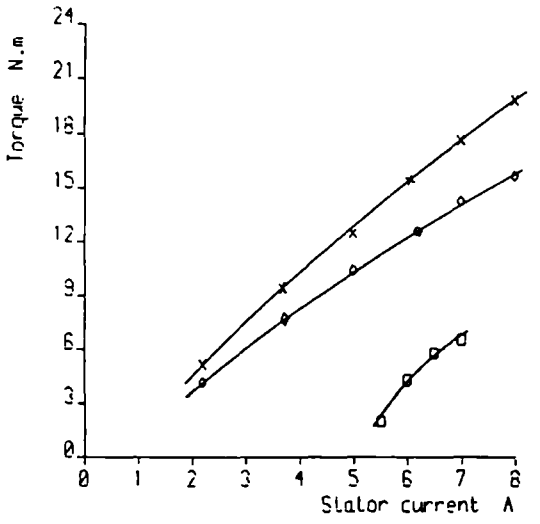

X... Nd Fe B machine V = 1 p.u.
◇... $SmCo_5$ machine V = 1 p.u.
□... ferrite machine V = 210V

Fig. 5: Comparison of the torque characteristics for the three machines used.

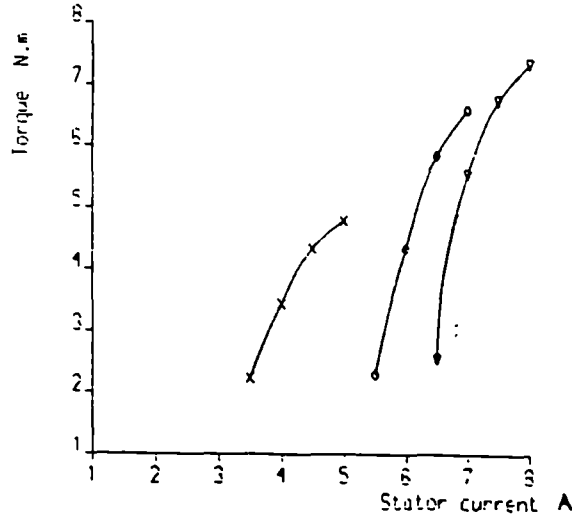

× ...V = 190V
◇ ...V = 210V
▽ ...V = 220V
generated voltage = 65V

Fig. 4: Variation of torque as a function of the stator current for the ferrite machine.

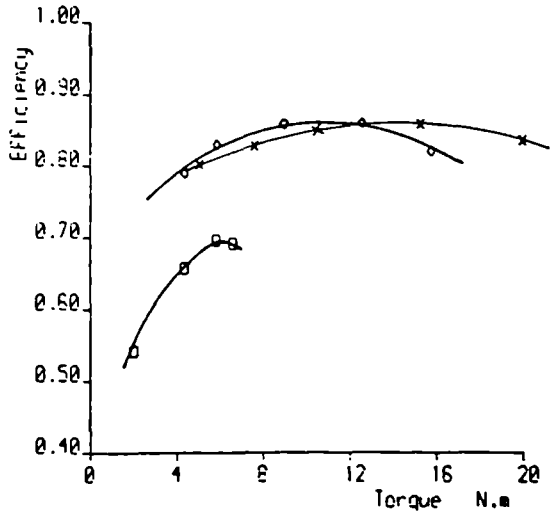

×... Nd Fe B machine V = 1 p.u.
◇... $SmCO_5$ machine V = 1 p.u.
□... ferrite machine V = 210V

Fig. 6: Efficiency torque characteristics for the three machines used.

REFERENCES

1. BINNS, K. J.:
'Alternating current generators or motors'
U.K. Patent 1437348, Nov. 1976.

2. BINNS, K. J. and JABBAR, M. A.:
'Some recent developments in permanent-magnet machines'
Proc. I.C.E.M., Brussels, Sept. 1978.

3. BINNS, K. J.:
'Alternating current rotating electrical machine'
U.K. Patent No. 1560971, U.S.A. Patent No. 4 188 554, Feb., 1980.

4. BINNS, K. J. and JABBAR, M. A.:
'Comparison of performance characteristics of a class of high-field permanent-magnet machines for different magnet materials'
I.E.E. Conference (S.S.E.M.), London, 1981.

5. BINNS, K. J. and JABBAR, M. A.:
'High-field self-starting permanent-magnet synchronous'
Proc. I.E.E., Vol. 128, Pt. B, No. 3, pp 157-160, May, 1981.

6. BINNS, K. J. and WONG, T. M.:
'Development of a high performance permanent magnet machine'
I.C.E.M. Conference, Lausanne, p.565, Sept. 1984.

7. BINNS, K. J. and WONG, T. M.:
'Analysis and performance of a high-field permanent-magnet synchronous machine'
Proc. I.E.E., Vol. 131, Pt. B, No. 6, pp. 252-258, Nov. 1984.

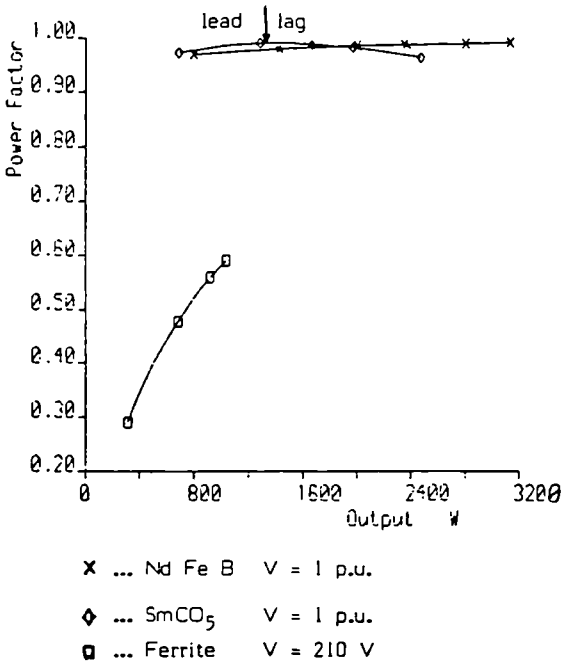

Fig. 7: Power factor - output characteristics for the three machines used.

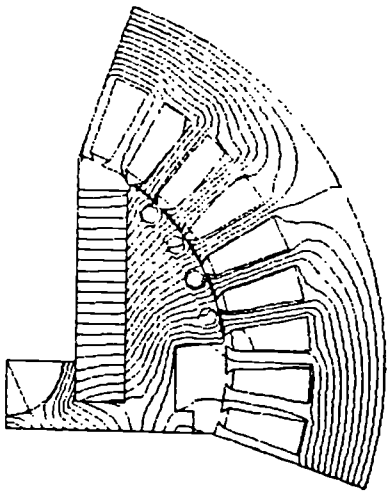

Fig. 8: Flux distribution for the Nd Fe B machine at full load.

PROFESSOR K. J. BINNS, B.Sc., D.Sc., C.Eng. F.I.E.E., AFIMA. MR. F. B. CHAABAN, M.Sc.,
UNIVERSITY OF LIVERPOOL,
'THE RELATIVE MERITS OF RARE EARTH PERMANENT MAGNET MATERIALS FOR USE IN THE EXCITATION OF PERMANENT MAGNET MACHINES.'

INTRODUCTION

Interest in permanent magnet machines for drive systems was almost non-existent fifteen to twenty ye rs ago. Alnico magnets were used, for example in exciters, and still are. Ferrite magnets were found in automobile equipment like windscreen washer motors. Research was being carried out and patents applied for in the area of drive systems but only a small handful of people were involved (1) (2) (3).

It was only when samarium cobalt magnets with their high stored energy became available that industry recognised that permanent magnet machines were not simply low power special devices of minimal commercial importance.

Contracts were placed to develop prototype machines for a variety of applications. It was demonstrably clear that the magnet could be used to up-rate conventional systems, (4) including those using induction and reluctance motors, but the cost of the magnets was generally found to be too high for widespread use. Many designs were proposed in which the expensive material was under utilised.

In 1983 two firms, one in the USA and one in Japan, announced the development of neodymium-iron-boron magnets and in the short interval since then many other magnet producers have developed and produced these magnets. The cost is currently comparable with samarium-cobalt but is is hoped that the cost will fall ultimately by a factor of about four.

Table 1: Magnetic and Physical Properties of the Two Permanent Magnets Used

Magnetic Material	$SmCo_5$	NdFeB	
Residual Induction Br, Tesla	0.82	0.97	1.03
Coercive Force -Hc, KA/m	597	493	772
Peak Energy Density (BH)max; KJ/m^3	122	178	205
Max. Operating Temperature, ^oC	250	140	100
Reversible Temp. Coefficient, % per ^oC	-0.04	-0.12	-0.12

There are many claims about the growth in the use of NdFeB, but these are mainly made by non-experts who have been divorced from the task of designing machines for which the working temperature has to be kept low in the region containing the magnet.

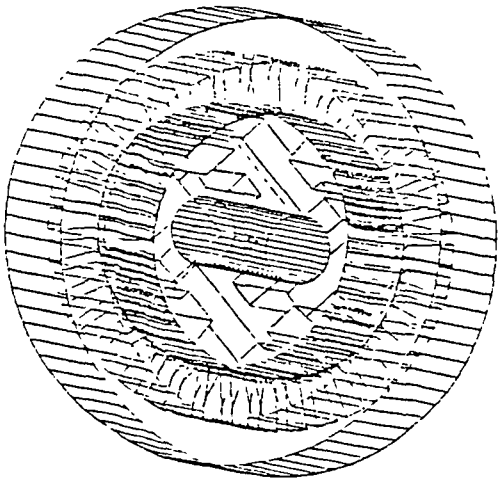

Fig. 1: 3-dimensional representation of a typical 4-pole machine

In the light of the characteristics of two materials, samarium-cobalt and neodymium-iron-boron, a comparison of achievable performance is made. A geometry with high performance potential (5) is used (see Fig. 1) for the comparison since it makes possible a high air-gap field and hence a high torque to machine volume. Fig. 2 shows the flux distribution in a cross section of the machine. The performance capability of this machine has already (6) been discussed but in this paper the design has been optimised for each of the two materials. For a comparison to be worthwhile the dimensions have to be chosen to maximise performance for a given magnet. The machine can operate as a line start or inverter-fed synchronous motor or as a so-called brushless d.c. machine if position sensing is incorporated.

Table 1 shows some of the important characteristics of the materials chosen. The max. operating temp. is most important for electrical machines and here neodymium magnets have a significant limitation.

Using finite element software (7) the rotor is designed for a given stator. The stator is that of a standard induction motor having a four-pole winding. The rotors have been constructed and tested for synchronous performance in the same stator, the winding of which was rated at 8A.

'THE RELATIVE MERITS OF RARE EARTH PERMANENT MAGNET MATERIALS FOR USE IN THE EXCITATION OF PERMANENT MAGNET MACHINES.'

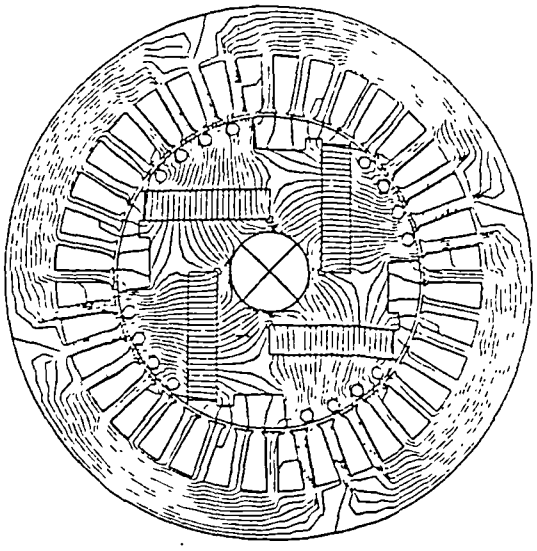

Fig. 2: Flux distribution in a 4-pole machine at full load

EXPERIMENTAL RESULTS

The measured torque for three voltage levels is shown in Fig. 3 as a function of load current for a 50 Hz mains supply. The unit of voltage is that of an open-circuited generator. With this type of high field machine and $SmCo_5$ magnets there is little to be gained in torque by using a voltage higher than the generated emf. NdFeB magnets on the other hand have a higher flux carrying capacity. The torque is higher for a given current and operation at a higher voltage gives a benefit, see Fig. 4.

A torque comparison for the two materials using rated voltages as defined, gives a clear comparison of output, see Fig. 5. The neodymium machine has a significantly higher torque. This is due to the higher Br and partially because more magnet is used to minimise temperature rise in the magnet.

The efficiency is an important parameter and a comparison at the rated voltage is presented in Fig. 6. The neodymium magnets have the advantage at higher outputs. The power factor is important particularly for inverter fed operation. Both rare earth rotors retain a power factor close to unity. The $SmCo_5$ rotor has a power factor which changes from leading to lagging as the output increases. Tables 2(a) and 2(b) show the measured performance at 40 Hz of the 4-pole samarium cobalt and neodymium-iron-boron rotors. Their operation close to unity power factoris clear and the higher torque of the neodymium rotor is evident. Similar characteristics are obtained at a frequency of 60 Hz.

RESULTS FOR THE 6-POLE MACHINE

Fig. 8 shows a computed field distribution on no-load for a 6 pole machine. It is clear that the flux density in the air gap over the region of one pole is higher than that in the the magnet, a feature of this configuration. The magnet dimensions are chosen so as to produce a high air gap flux without undue saturation. The holes in the rotor lamination are for ventilation purposes. Detailed analysis of this design will be discussed in future publications.

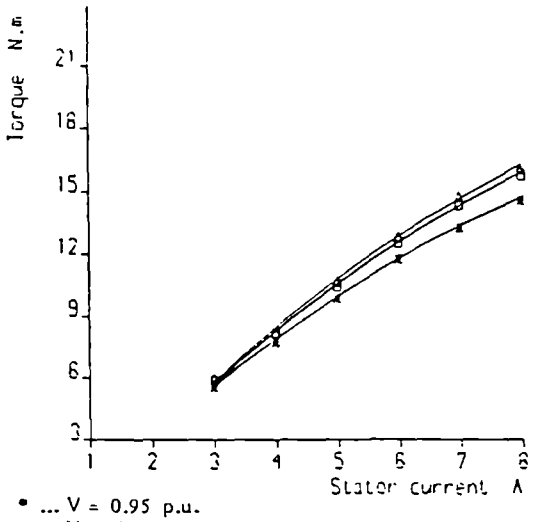

• ... V = 0.95 p.u.
□ ... V = 1 p.u.
Δ ... V = 1.05 p.u.

Fig. 3: Variation of torque as a function of the stator current for the $SmCo_5$ machine

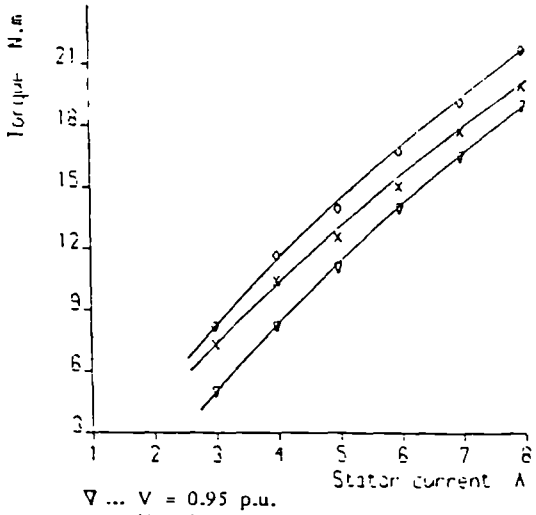

∇ ... V = 0.95 p.u.
x ... V = 1 p.u.
◇ ... V = 1,05 p.u.

Fig. 4: Variation of torque as a function of the stator current for the NdFeB machine

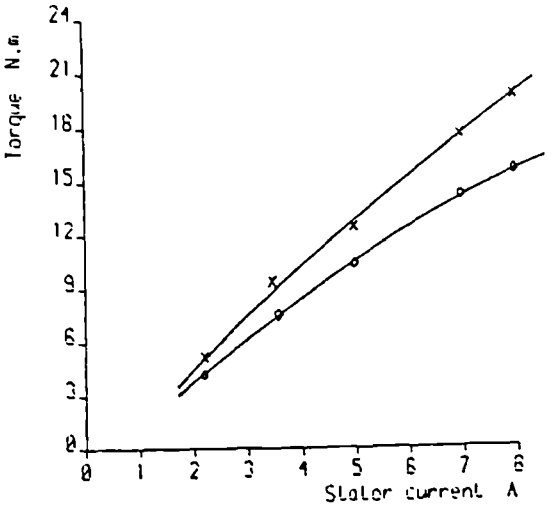

X ... NdFeB machine. ◇ ... $SmCo_5$ machine
V =1p.u.

Fig. 5: Comparison of the torque characteristics for the two 4-pole machines

As explained earlier the different geometries for the rotors were obtained by using computer software which gives torque, flux densities etc. as well as field maps, the latter serving mainly as an aid to understanding and presentation. The measured torque of a 6 pole machine making use of neodymium machines is shown in Fig. 9 for several frequencies. The voltage applied in each case is proportional to frequency. The torque increases with current in each case but is slightly less than proportional.

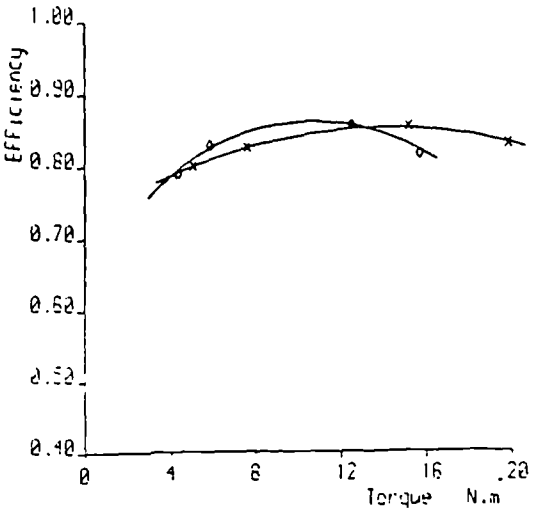

X ... NdFeB machine ◇... $SmCo_5$ machine
V = 1 p.u.

Fig. 6: Efficiency-torque characteristics for the two 4-pole machines

DISCUSSION

The comparison of power capability and performance characteristics such as efficiency and power factor is clearly brought out in the results. The use of rare earth magnets can lead to a drive system with a higher torque/weight ratio than any other practical alternative. The high efficiency and near unity power factor are exactly what is required for the ideal inverter fed system. There is no doubt that the neodymium magnets give the best performance but the working temperature is limited.

CONCLUSION

The characteristics of the motor in terms of the torque, efficiency and power factor for the two types of magnet have been demonstrated. The cost effectiveness of the use of relatively expensive magnets can be assessed.

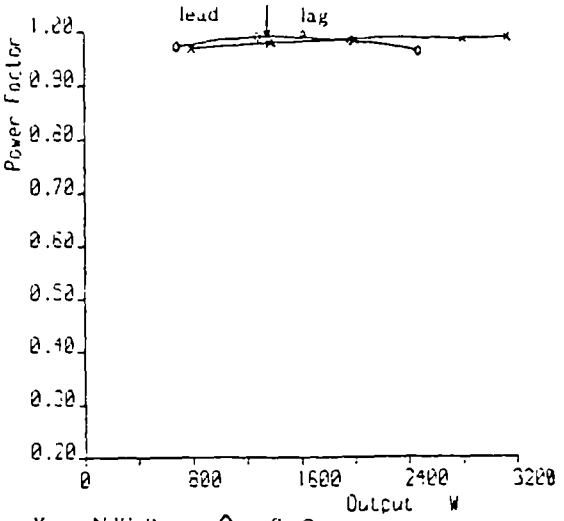

X ... NdFeB ◇... $SmCo_5$
V = 1 p.u.

Fig. 7: Power factor - output characteristics for the two machines used.

Table 2.a: Measured synchronous performance of the $SmCo_5$ machine at nominal rated voltage at 40 Hz

Torque N.m.	Output W	Efficiency %	Power Factor	Efficiency x Power Factor
4.1	515	72.56	0.923 lead	0.6699
5.7	716	79.58	0.936 lead	0.745
8	1005	81.33	0.964 lead	0.7843
10.1	1269	82.1	0.965 lead	0.7923
12	1508	81.7	0.966 lag	0.7891
13.5	1696	78.68	0.96 lag	0.7553
14.9	1872	78	0.936 lag	0.7304

Table 2.b: Measured synchronous performance of the NdFeB machine at nominal rated voltage at 40 Hz

Torque N.m.	Output W	Efficiency %	Power Factor	Efficiency x Power Factor
3.75	471	65.45	0.854 lead	0.5588
6.45	810	72	0.904 lead	0.6512
9.1	1131	76.4	0.949 lead	0.7255
11.85	1489	79.21	0.962 lead	0.7618
14.4	1810	79.37	0.974 lead	0.7731
17.1	2149	80.78	0.976 lead	0.7885
19.35	2431	80	0.978 lead	0.7824

REFERENCES

1. BINNS, K. J.:
'Alternating current generators or motors'
U.K. Patent 1437348, Nov. 1976.

2. BINNS, K. J. and JABBAR, M.A.:
'Some recent developments in permanent-magnet machines'
Proc. I.C.E.M., Brussels, Sept. 1978.

3. BINNS, K. J.:
'Alternating current rotating electrical machine'
U.K. Patent No. 1560971, U.S.A. Patent No. 4 188 554, Feb. 1980.

4. BINNS, K. J. and JABBAR, M. A.:
'Comparison of performance characteristics of a class of high-field permanent-magnet machines for different magnet materials'
I.E.E. Conference (S.S.E.M.) London, 1981.

5. BINNS, K. J. and JABBAR, M. A.:
'High-field self-starting permanent-magnet synchronous motor
Proc. I.E.E., Vol. 128, Pt. B, No. 3, pp 157-160, May, 1981.

6. BINNS, K. J. and WONG, T. M.:
'Development of a high performance permanent magnet machine'
I.C.E.M. Conference, Lausanne, p.565, Sept. 1984.

7. BINNS, K. J. and WONG, T. M.:
'Analysis and performance of a high-field permanent-magnet synchronous machine'
Proc. I.E.E., Vol. 131, Pt. B, No. 6, pp. 252-258, Nov. 1984.

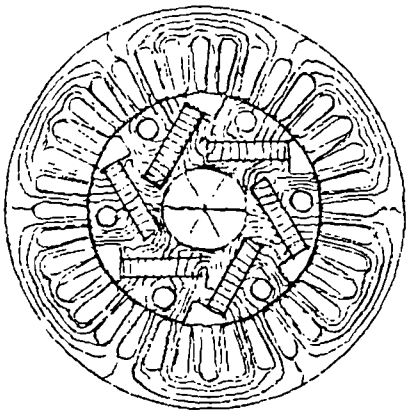

Fig. 8: Flux distribution in the cross-section of the 6-pole machine at no load.

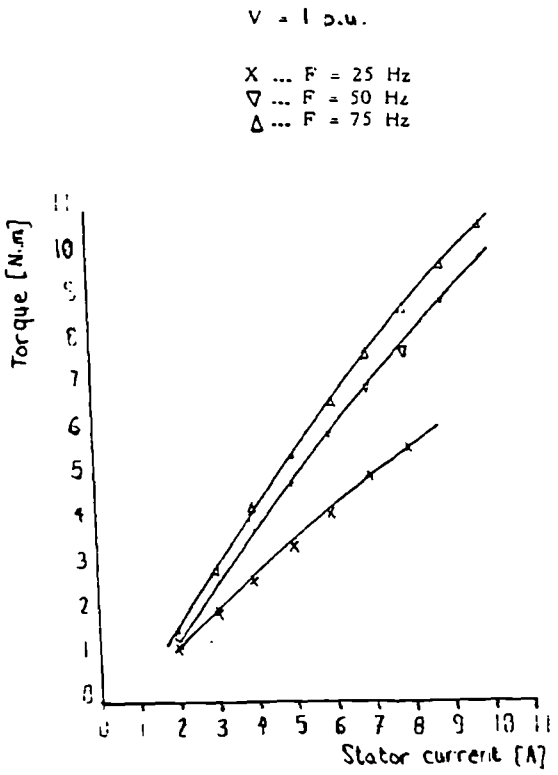

Fig. 9: 6-pole NdFeB machine measured torque - current characteristics at 3 different frequencies

A CANNED SOLID ROTOR PERMANENT MAGNET MACHINE WITH SKEWED-RADIAL NEODYMIUM-IRON-BORON MAGNETS

K. J. BINNS, A. A. K. HAMEED, AND F. B. CHAABAN

UNIVERSITY OF LIVERPOOL, U.K.

INTRODUCTION

Permanent magnet machines have found much greater acceptance in drive systems than was thought likely even 5 years ago. This is because of their performance advantages over the commercial alternatives. Many designs of permanent magnet field configurations are available, but only those involving excitation from an internal rotor [1 - 5] are relevant to this investigation.

A machine has been constructed which consist of a solid steel rotor with 6 magnets which are mounted radially but skewed, see Figure 1. This type of machine has been discussed in reference [6] except that the rotor magnets are skewed with respect to the stator slots. In addition, the rotor is surrounded by a non-magnetic conducting can made of inconel. This strengthens the rotor which otherwise has significant speed limitations due to centrifugal force. The machine rotor is designed to take 6 neodymium iron boron magnets having a characteristic shown in Figure 2.

EFFECTS OF SKEWING THE MAGNETS

It is unusual to skew a permanent magnet field system but it can result in a reduction of unwanted field harmonics. The rotor of this machine makes use of magnets embedded in slots which are skewed relative to the rotor axis. This has shown to have significant advantages in reduction of torque harmonics and noise produced by flux pulsation. The effect on the fundamental field is relatively small compared with the reduction of undesirable harmonic effects.

Skewing the magnets results in a phase shift along the axis of the machine and hence a reduction in the induced emf particularly that due to harmonic field components. This reduction is represented in the calculations by a skew factor which is related to the angle of inclination of the magnets. The analytical derivation is provided in Ref. 7 and gives a fundamental skewing factor expressed by:

$$k_{sk} = \frac{\sin \frac{\alpha}{2}}{\frac{\alpha}{2}}$$

and the factor for the n^{th} harmonic as :

$$k_{skn} = \frac{\sin n(\frac{\alpha}{2})}{n\frac{\alpha}{2}}$$

where α is the skew angle in electrical degrees.

The values of the skew factor for different skew angles are shown in Table 1.

Figure 3 shows the effect of skew in achieving a significant reduction in the tooth ripple effects in the waveform of the open-circuit generated voltage. It has also been observed that the machine is quiet. Skewed magnets are also advantageous in reducing the pulsation of the starting current and torque because the rotor, even with powerful rare-earth magnets, is not locked at any pole position before starting. In the 2D-finite element analysis the effect of skewing can only be accounted for by the introduction of the skewing factor to the results obtained.

Table 1: Results of the analytical determination of fundamental skewing factor.

α^o	15	30	45	60	75	90
k_{sk}	0.997	0.988	0.974	0.955	0.930	0.9

INFLUENCE OF THE ROTOR CAN

For high-speed applications the design of the permanent magnet machine has to take into account the effects of the centrifugal forces which could cause the rotor to disintegrate. The rotor can be strengthened by enclosing it in a non-magnetic can, but to allow for the can to be fitted around the rotor the air gap has to be increased. Consideration will be given to the use of both a non-magnetic can and magnetic can surrounding the rotor.

a) The use of a non-magnetic can:

The rotor can was fitted and is made of inconel. This material has the advantage of mechanical strength and is non-magnetic. Its conducting properties could be advantageous in this application. In the initial design an air gap width of 0.2 mm was chosen. The introduction of the inconel can requires an increase in the air gap width to 0.8 mm so the reluctance of the air gap increases with a corresponding reduction in the gap density and therefore core saturation. Smaller iron losses is an obvious result of the reduced saturation. These losses are slightly higher for the canned rotor due to excess harmonic losses of around 4% in the can as indicated in Figure 4. The canned rotor is mechanically capable of operating at high speeds. The results in this paper, however, relate to a maximum operating speed of 5000 rpm.

b) Ferromagnetic can:

Computation has been carried out to examine the influence of a ferromagnetic can on the machine performance. The model used for this purpose differs from the original one (with air gap g = 0.2 mm) by the thin path between the magnet and the air gap at the rotor saliency. Computation results are shown in Table 2. From these results it is evident that the change from the inconel to the ferromagnetic can would increase the rotor field due to the drop in the total reluctance of the magnetic circuit. The fundamental air gap density would increase by 11% while the torque would rise by 13%. The internal load angle would drop by 36%. With ferromagnetic can the machine performance is almost the same as that obtained with the narrow air gap (g = 0.2 mm). The thin path becomes inevitably saturated and hence does not affect the overall performance of the machine. In Figure 5 the flux leakage across the saturated path is less than

5% of the total magnet flux.

EXPERIMENTAL MEASUREMENTS

The prototype rotor is fitted into a standard low-cost six pole stator with a three-phase single-layer winding. The rotor is initially made oversize and subsequently turned down and finally shrunk into the non-magnetic can. To summarise the air gaps are as follows:

Stage 1 0.2 mm

Stage 2 0.8 mm

Stage 3 0.8 mm including the can thickness.

For each of these stages the machine performance is tested at different load conditions for various applied voltages and frequency levels. These voltages are chosen such that the machine operates around unity power factor, that is possibly at both leading and lagging power factor as the load varies. The level of the applied voltage also determines the pull-out torque and plays an important role since the magnet excitation cannot be controlled. Constant current tests are carried out to determine the maximum output torque of the machine. This value of the torque is used to compare the experimental results with those of the computation. The characteristics in Figure 6 show that the terminal voltage corresponding to the maximum torque increases with the load current which is not surprising. The synchronous performance of this prototype has been tested with different load conditions at frequencies of 30, 50, and 75 Hz. The obtained results indicate that the synchronous characteristics of this prototype are very similar to those of a high-field rotor. Except for the rotor leakage both machines show the same trend in operating at almost unity power factor and with high efficiency.

EFFECT OF A NON-MAGNETIC ROTOR SHAFT

The iron bridge between the magnets and a non-magnetic shaft, affects the mechanical strength of the machine. Since the six pole rotor, whose parameters are under investigation, is designed for possible high-speed applications, the mechanical strength becomes an important factor in determining the maximum speed at which the machine can be operated. With a smaller iron bridge the flux leakage around the magnet edges is reduced and as a result more flux is driven across the air gap. To give an idea of the changes in the flux levels inside the machine, computation is carried out for different values of the diameter of a non-magnetic shaft. Figure 7 shows the flux plot at full load where the magnets are attached to the non-magnetic shaft hence eliminating the leakage entirely while in Figure 8 the flux leakage under the magnets is illustrated very clearly. A comparison of these two figures indicates that though the operating point of the magnets has not changed (0.4< B <0.8), the flux density inside the machine with the non-magnetic shaft has risen significantly and the fundamental air gap flux density has increased by 22%.

The graph in Figure 9 represents the variation in the computed synchronous torque with the gradual reduction of the iron bridge. With maximum iron bridge width the saturated paths under the magnets have already formed a certain zone at the rotor centre where no flux is passing. The reduction in the iron-bridge, therefore, does not affect the torque values as long as the non-magnetic shaft diameter does not exceed this zone. Beyond this point any increase in the shaft diameter results in greater synchronous torque. The total increase of the torque is found to be around 23%.

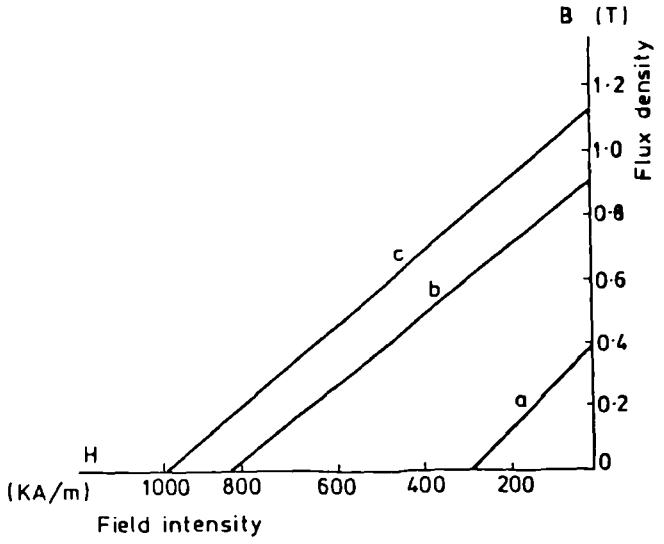

a ... ferrites
b ... $SmCo_5$
c ... NdFeB

Figure 1: Characteristics of NdFeB compared to samarium cobalt and ferrite magnets.

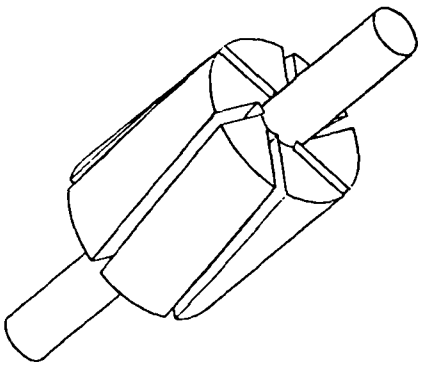

Figure 2: 3D-configuration of solid steel rotor with skewed magnets.

Table 2: Influence of the canning material on the machine performance.

	g=0.2mm	g=0.8mm inconel can	g=0.8mm ferromag. can
fundamental gap flux density	1.27	1.09	1.24
internal load angle	7.9	13.4	8.2
synch. torque	10.2	8.55	9.9

CONCLUSIONS

A prototype rotor of solid steel construction has been built and tested. The effect of skewing the rotor magnets is to reduce torque harmonics and noise-producing flux components. The effect of the rotor can is beneficial, in addition to increasing the operating speed of the machine. The solid canned rotor is very stable and easy to manufacture.

REFERENCES

1. Binns, K. J., Barnard, W. R. and Jabbar, M. A., 1978, 'Hybrid permanent magnet synchronous motors,' Proc. IEE, 125, No. 3, pp. 203-208.

2. Binns, K. J., and Low, T. S., 1983, 'Performance and application of multi-stacked imbricated permanent magnet generators,' Proc. IEE, 130, Pt. B, No. 6, pp. 407-414.

3. Binns, K. J. and Wong, T. M. 1984, 'Analysis and performance of a high-field permanent magnet synchronous machine,' Proc. IEE, 131, Pt. B, No. 6, pp. 252-258.

4. Binns, K. J., 1987, 'Handbook of electrical machines (edited by S. A. Nasar), 'Permanent Magnet Machines', chapter 9, McGraw-Hill.

5. Binns, K. J., Chaaban, F. B., Lisboa, P. J. G. and Mellor, P. H., 1987, 'The role of neodymium-iron-boron in relation to other materials for permanent magnet machines,' IEE Conf., EMD, London.

6. Hameed, A., Vandenput, A., Geysen, W. and Binns, K.J., 1984, 'Analysis of the magnetic field in a multipole permanent magnet machine by a finite element method', Proc. of ICEM, Lausanne, Switzerland, pp. 138-140.

7. Fitzgerald, A. E., 1961, 'Electric machinery,' 2nd Edition, McGraw-Hill Book Company.

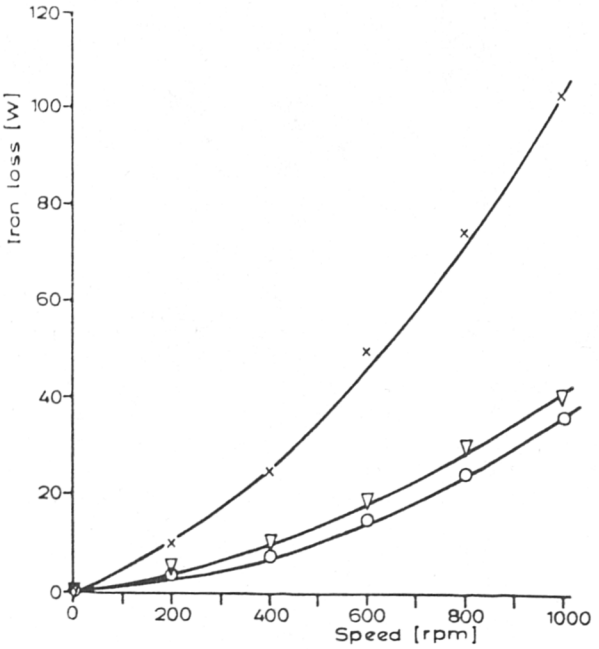

x... air gap = 0.2 mm
o... air gap = 0.8 mm
▽... air gap = 0.8 mm (canned rotor)

Figure 4: Iron loss as a function of speed.

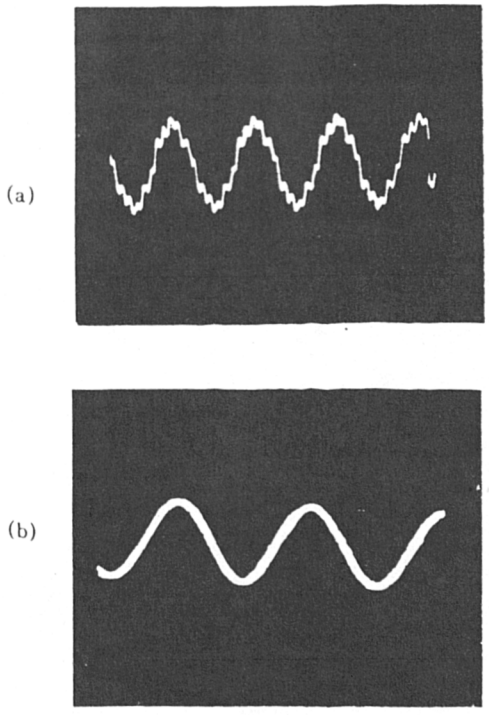

a... conventional PM rotor

b... rotor with skewed magnets

Figure 3: Open circuit generated voltage waveforms at f = 50 Hz

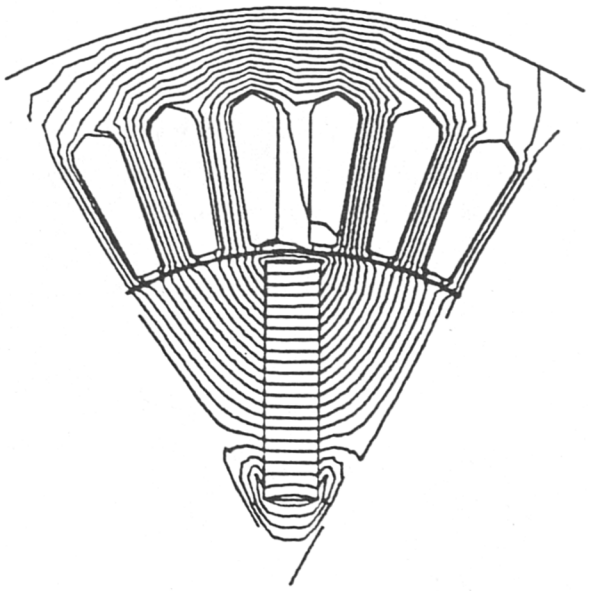

Figure 5: Flux distribution of the machine with ferromagnetic can at full load.

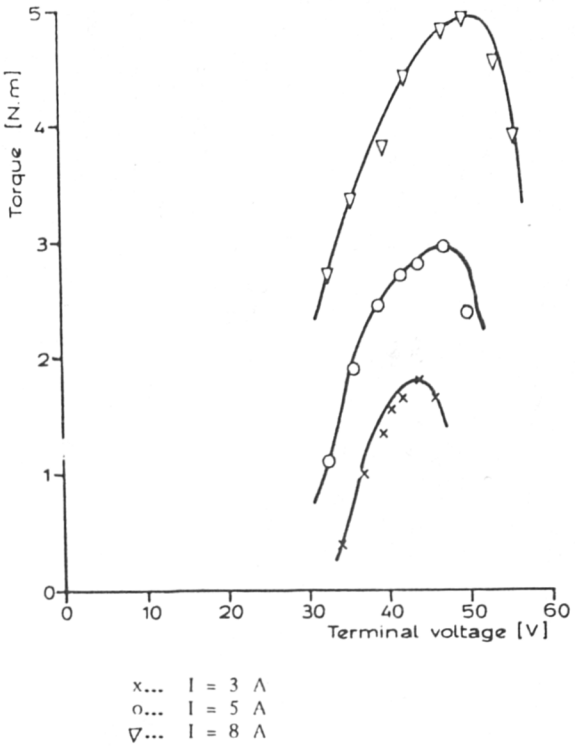

Figure 6: Variation of the torque as a function of the terminal voltage for different stator currents.

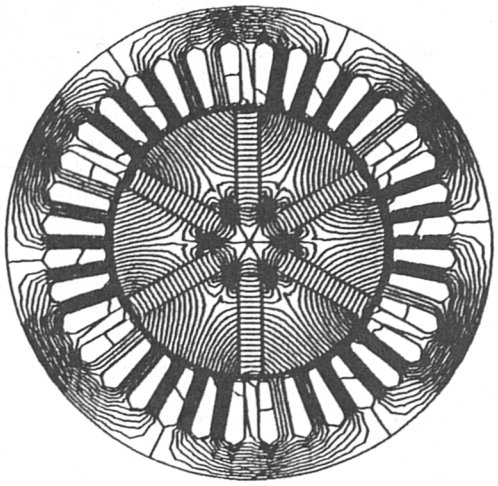

Figure 8: Illustration of the magnets flux leakage when ferromagnetic shaft is used.

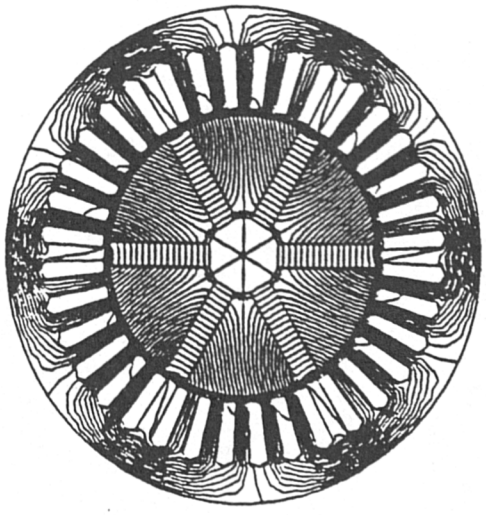

Figure 7: Flux distribution of the machine with magnets being attached to the non-magnetic shaft.

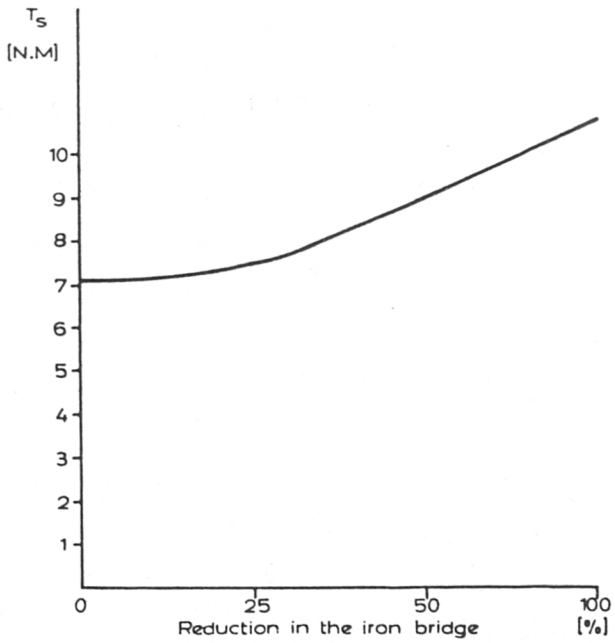

Figure 9: Effects of the bridge of magnetic material on the output torque.